



Morgan, Robert (2021) *Imaging alterations in the hemodynamic response in the SHRSP: A model of cerebral small vessel disease*. PhD thesis.

<http://theses.gla.ac.uk/82159/>

Copyright and moral rights for this work are retained by the author

A copy can be downloaded for personal non-commercial research or study, without prior permission or charge

This work cannot be reproduced or quoted extensively from without first obtaining permission in writing from the author

The content must not be changed in any way or sold commercially in any format or medium without the formal permission of the author

When referring to this work, full bibliographic details including the author, title, awarding institution and date of the thesis must be given

Enlighten: Theses
<https://theses.gla.ac.uk/>
research-enlighten@glasgow.ac.uk

Imaging alterations in the hemodynamic response in the SHRSP: A model of cerebral small vessel disease

Robert Morgan

B.Sc (Hons) Biomedical Science (Neuroscience)
Cardiff University

M.Sc Neuroimaging: Methods and Applications
Cardiff University

Submitted in fulfillment of the requirements for the
Degree of Doctor of Philosophy (Ph.D)

Institute of Neuroscience & Psychology
College of Medical, Veterinary & Life Sciences
University of Glasgow

May 2021

Acknowledgements

Firstly, I'd like to thank my supervisors for all their help and guidance through my PhD and for all the time and effort they have given me to help me on this journey. Jozien, thank you for all your help and support with all things pertaining to MRI and for all you have done to help me and other students overcome various hurdles encountered throughout this whole process. Chris, it was sad to see you leave before the end of my PhD, but you were always there to help me with any issues and for that I am grateful.

I'd also like to thank the technical staff of the WSI and GEMRIC. Lindsay, you were an enormous help throughout my PhD, helping me to optimise and set up various experiments. I am truly thankful for your help. Linda, thank you for all your help. I'll miss our chats while doing the tail cuff measurements. Jim, thank you for all your help with MRI and all the other various odds and ends you've helped me with over the years.

A huge thank you to all the PhD students that have been at the WSI over the course of my PhD. Your help and friendship over the past years has been overwhelming and will not be forgotten.

A special thank you to my beautiful wife and our three children. Your love, support, understanding and patience over the past 4 years have been unwavering and unrivalled.

I'd also like to thank the MRC, without which none of this would have been possible. I am grateful for the opportunity I have had over the past 4 years to engage in scientific research, for the experiences that have come with it and for all that will follow because of it.

Author's declaration

I hereby declare that this thesis is the result of my own work, except where stated otherwise in the text, and has not been submitted for any other degree at the University of Glasgow or any other institution.

Robert Morgan

Contents

Acknowledgements	2
Author's declaration	3
Contents.....	4
List of figures.....	10
List of tables.....	13
Abbreviations	14
Abstract	16
1. Introduction	19
1.1 Cerebral circulation.....	19
1.1.2 Blood vessel structure	20
1.1.3 Blood brain barrier	21
1.1.4 The neurovascular unit.....	22
1.1.5 Neurovascular coupling.....	24
1.1.6 Autoregulation	27
1.2 Cerebral small vessel disease	29
1.2.1 Pathogenesis	29
1.2.2 Features of cerebral small vessel disease.....	30
1.2.2.1 Lacunar ischemic stroke	30
1.2.2.2 Lacunes of presumed vascular origin.....	31
1.2.2.3 White matter hyperintensities	31
1.2.2.4 Perivascular spaces	31
1.2.2.5 Microbleeds.....	32
1.2.3 Functional MRI in patients with SVD	33
1.2.4 Sporadic and monogenic forms of cerebral SVD and associated risk factors.....	34
1.2.5 Animal models of cerebral small vessel disease	35
1.2.5.1 Hypertensive primate model	36
1.2.5.2 Chronic carotid occlusion	36
1.2.5.3 Middle cerebral artery occlusion	37
1.2.5.4 SHRSP.....	37
1.2.5.5 Transgenic mouse models.....	39
1.3 Principles of magnetic resonance imaging.....	41
1.3.1 Free induction decay	42

1.3.2 T ₁ relaxation	42
1.3.3 T ₂ and T ₂ *	42
1.3.4 Gradient coils	43
1.4 Functional MRI	43
1.4.1 BOLD.....	43
1.4.2 Physiological basis of the BOLD signal	45
1.4.3 Factors affecting the BOLD signal	45
1.4.3.1 Carbon dioxide.....	46
1.4.3.2 Anaesthesia.....	47
1.4.3.3 Ageing	48
1.4.3.4 Disease	49
1.5 Summary	50
2. Methods	52
2.1 Animals.....	52
2.2 Surgical preparation	53
2.2.1 Aseptic technique	53
2.2.2 Anaesthesia	53
2.2.3 Analgesia	54
2.3. Surgical procedures	54
2.3.1 Endotracheal intubation	54
2.3.2 Arterial and venous cannulation.....	55
2.3.3 Needle electrode placement	55
2.3.4 Laminectomy and craniotomy.....	58
2.3.5 Skull thinning	58
2.4 Magnetic resonance imaging.....	59
2.5 Laser Speckle Contrast Imaging.....	59
2.6 Recovery and post-operative care.....	60
2.6.1 Recovery following MRI.....	60
2.6.2 Perfusion fixation	61
2.7 Tail cuff plethysmography	62
2.7.1 Acclimatisation training	62
2.7.2 Systolic blood pressure measurements	63
3. Establishing non-invasive monitoring of PaCO₂ for functional imaging using micro-sampling side-stream capnography	64

3.1 Introduction	64
3.1.1 Carbon dioxide and the BOLD signal	64
3.1.2 Monitoring carbon dioxide	66
3.1.3 Mainstream capnography and side-stream capnography	66
3.1.4. Study aims	70
3.2 Methods	71
3.2.1 Study 1 - Non-invasive monitoring of PaCO ₂ using side-stream capnography to measure ETCO ₂	71
3.2.1.1 Animals	71
3.2.1.2 Anaesthesia	71
3.2.1.3 Side-stream capnography	71
3.2.1.4 Measuring ETCO ₂ and PaCO ₂	75
3.2.1.5 Data analysis	75
3.2.2 Study 2 - Evaluating the effects of varying PaCO ₂ on the stimulus- evoked BOLD signal	77
3.2.2.1 Animals	77
3.2.2.2 Stimulation parameters	78
3.2.2.3 Monitoring and varying PaCO ₂	78
3.2.1.4 Data analysis	78
3.3 Results	80
3.3.1 Study 1 - Non-invasive monitoring of PaCO ₂ using side-stream capnography to measure ETCO ₂	80
3.3.2 Study 2 - Evaluating the effects of PaCO ₂ on the stimulus-evoked BOLD signal	91
3.3.2.1 Inducing hypocapnia and hypercapnia	91
3.3.2.2 Assessing the effects of varying PaCO ₂ on the stimulus- evoked BOLD signal	93
3.4 Discussion	96
3.4.1 Non-invasive monitoring of PaCO ₂ using side-stream capnography to measure ETCO ₂	96
3.4.2 Evaluating the effects of varying PaCO ₂ on the stimulus-evoked BOLD signal	97
4. Assessing the effect of varying stimulation parameters on stimulus- evoked BOLD, neural and CBF responses	101
4.1 Introduction	101

4.1.1 Anaesthesia and neurovascular coupling	101
4.1.2 Optimal stimulation parameters.....	102
4.1.3 Medetomidine-isoflurane anaesthesia	103
4.1.4 Study Aims.....	104
4.2 Methods	105
4.2.1 Study 1 - Investigation and optimisation of stimulus parameters for BOLD fMRI using forelimb stimulation.....	105
4.2.1.1 fMRI preparation.....	105
4.2.1.2 fMRI forelimb stimulation.....	105
4.2.1.3 MRI experiments.....	106
4.2.1.4 Data analysis	106
4.2.2. Study 2 - Evaluating the effects of varying stimulus parameters on the somatosensory evoked potential.....	107
4.2.2.1 Animals.....	107
4.2.2.2 Laminectomy and craniotomy.....	107
4.2.2.3 Forelimb Stimulation	108
4.2.2.4 Recording CDPs and SEPs.....	109
4.2.1.5 Data Analysis	109
4.2.3. Study 3 - Evaluating the effects of varying stimulus parameters on cerebral blood flow as assessed by laser speckle contrast imaging...	113
4.2.3.1 Animals.....	113
4.2.3.1 Skull thinning	113
4.2.3.2 Recording of CBF	113
4.2.3.3 Forelimb stimulation.....	113
4.2.3.4 Data analysis	114
4.3 Results	115
4.3.1. Study 1 - Investigation and optimisation of stimulus parameters for BOLD fMRI using forelimb stimulation.....	115
4.3.1.1. Stimulus-evoked BOLD response	115
4.3.2. Study 2 - Investigation and optimisation of stimulus parameters for somatosensory evoked potentials using electrophysiology	122
4.3.2.1 Stimulus intensity	122
4.3.2.2 SEPs and stimulus frequency	130
4.3.3. Study 3 - Investigation and optimisation of stimulus parameters for CBF using laser speckle contrast imaging	139
4.3.3.1 Stimulus-evoked CBF response	139

4.3.3.2	Peak change in CBF	142
4.3.3.3	Integral of CBF	145
4.4	Discussion	150
4.4.1	The use of anaesthesia in rodent fMRI studies	150
4.4.2	Dependency of the BOLD response on stimulus parameters	152
4.4.3	Dependency of the SEPs on stimulus parameters	154
4.4.4	Dependency of CBF on stimulus parameters.....	156
4.4.5	Relationship between BOLD, SEP and CBF	158
4.4.6	Conclusion.....	159
5.	<i>Assessing the hemodynamic response in the SHRSP: A model of cerebral small vessel disease</i>	161
5.1	Introduction	161
5.1.1	Cerebral small vessel disease	161
5.1.2	SHRSP	161
5.1.3	Small vessel disease and BOLD.....	163
5.1.4	Study Aims and Hypothesis	165
5.2	Methods	166
5.2.1	Experimental Design	166
5.2.2	Experimental animals.....	166
5.2.3	Blood pressure measurements	167
5.2.4	Functional MRI	167
5.2.4.1	fMRI preparation.....	167
5.2.4.2	Forelimb stimulation.....	167
5.2.4.3	Monitoring of physiological variables	167
5.2.4.4	MRI protocol.....	168
5.2.4.4	Recovery following MRI.....	169
5.2.5	Laser speckle contrast Imaging experiments	169
5.2.5.1	LSCI preparation.....	169
5.2.5.2	Forelimb Stimulation	169
5.2.6	Data Analysis.....	169
5.2.6.1	fMRI	169
5.2.6.2	LSCI	170
5.2.6.3	Statistical Analysis	170
5.3	Results	171
5.3.1	Animals	171

3.3.2 Physiological Variables	173
3.3.2.1 Animal baseline physiology prior to scanning.....	173
5.3.2.2 Longitudinal blood pressure	177
5.3.2.3 Blood pressure and heart rate during MRI	179
5.3.2.4 Blood pressure and heart rate during LSCI	182
5.3.3 - Structural Characterisation of WKYs and SHRSPs	184
5.3.3.1 T ₂ Imaging	184
5.3.3.2 Brain volume measurements	191
5.3.4 Assessing the effect of acute and chronic hypertension on the stimulus-evoked BOLD response	193
5.3.5 Assessing the effect of acute and chronic hypertension on the stimulus-evoked CBF response using LSCI	198
5.4 Discussion.....	211
5.4.1 Characterising WKY and SHRSPs	211
5.4.1.1 Animal Physiology	211
5.4.1.2 Brain volume	212
5.4.1.3 T ₂ -weighted Imaging	213
5.4.2 Stimulus-evoked BOLD and CBF responses	214
5.4.3 Variation in hemodynamic responses	216
5.4.4 Effect of age on BOLD and CBF responses.....	217
5.4.5 Hypertension-induced neural alterations	217
5.4.6 Conclusion.....	218
6. General Discussion	219
6.1 Carbon dioxide and capnography	220
6.2 Assessment of stimulus parameters on BOLD, CBF and neural response.	221
6.3 The hemodynamic response and SHRSPs	222
6.4 The use of the hemodynamic response as a biomarker of cerebrovascular health and therapeutic response	223
Reference list.....	226

List of Figures

- Figure 1.1 Neurovascular unit
- Figure 2.1 Needle electrode placement figure
- Figure 3.1 Overview of two main types of capnography
- Figure 3.2 Overview of the sampling sites used with the MicroCapStar
- Figure 3.3 Agreement between PaCO₂ and ETCO with 1 m sample line sampling at recommended position
- Figure 3.4 Agreement between PaCO₂ and ETCO with 1 m sample line sampling from exhalation line
- Figure 3.5 Agreement between PaCO₂ and ETCO with 7 m sample line sampling at recommended position
- Figure 3.6 Agreement between PaCO₂ and ETCO with 7 m sample line sampling from exhalation line
- Figure 3.7 Agreement between PaCO₂ and ETCO with 1 m sample line sampling from exhalation line at a rate of 5 ml/min
- Figure 3.8 Agreement between PaCO₂ and ETCO with 5 m sample line sampling from exhalation line
- Figure 3.9 Overview of blood gas profiles
- Figure 3.10 Group-averaged times courses for stimulus-evoked BOLD under hypocapnic, normal and hypercapnic conditions
- Figure 3.11 Peak BOLD and integral of the BOLD response under hypocapnic, normal and hypercapnic conditions
- Figure 4.1 Measurement of individual SEP components using MATLAB.
- Figure 4.2 Anatomical RARE scans with the corresponding fMRI activation map
- Figure 4.3 Group averaged time courses of the BOLD response
- Figure 4.4 Effect of varying stimulus parameters on peak change in BOLD response
- Figure 4.5 Effect of varying stimulus parameters on integral of BOLD response
- Figure 4.6 Effect of varying stimulus parameters on the time to peak
- Figure 4.7 SEP traces at varying stimulus intensities
- Figure 4.8 Group averaged time course at varying stimulus intensities
- Figure 4.9 The effect of varying stimulus intensity on peak P1, N1 and P2

- components
- Figure 4.10 The effect of varying stimulus intensity on the sum of P1, N1 and P2 components
- Figure 4.11 The effect of varying stimulus intensity on the integral of P1, N1 and P2 components
- Figure 4.12 SEP traces at varying stimulus frequencies
- Figure 4.13 Group averaged time course at varying stimulus frequencies
- Figure 4.14 The effect of varying stimulus frequency on peak P1, N1 and P2 components
- Figure 4.15 The effect of varying stimulus frequency on the sum of P1, N1 and P2 components
- Figure 4.16 The effect of varying stimulus frequency on the integral of P1, N1 and P2 components
- Figure 4.17 Laser speckle view of brain
- Figure 4.18 Group-averaged time courses from S1FL area at varying stimulus intensities and stimulus frequencies
- Figure 4.19 The effect of varying stimulus frequency and stimulus intensity on peak change in CBF in contralateral S1FL area
- Figure 4.20 The effect of varying stimulus frequency and stimulus intensity on peak change in CBF in ipsilateral S1FL area and visual cortex
- Figure 4.21 The effect of varying stimulus frequency and stimulus intensity on the integral of the CBF response in contralateral S1FL area
- Figure 4.22 The effect of varying stimulus frequency and stimulus intensity on the integral of the CBF response in ipsilateral S1FL area and visual cortex
- Figure 5.1 An overview of animal ages for each experimental group
- Figure 5.2 Overview of animal body weight for each experimental groups
- Figure 5.3 Overview of blood pressure for each experimental group as assessed by tail cuff plethysmography.
- Figure 5.4 Longitudinal systolic BP measurements for aWKY and aSHRSPs at 3, 4, 5, 6, 7, 9 and 11 months
- Figure 5.5 Blood pressure and heart rate prior to and following medetomidine administration for aWKY and aSHRSPs
- Figure 5.6 MABP and HR measurements during scanning for all study groups

- Figure 5.7 MABP and mean HR during LSCI
- Figure 5.8 Overview of selected brain slices from a representative animal from each experiment group
- Figure 5.9: T₂-weighted scan of cSHRSP
- Figure 5.10 T₂-weighted scan of cSHRSP
- Figure 5.11 T₂-weighted scan of cSHRSP
- Figure 5.12 T₂-weighted scan of cSHRSP
- Figure 5.13 Brain and lateral ventricle volumes.
- Figure 5.14 Group-averaged %BOLD time courses in S1FL area
- Figure 5.15 Peak %BOLD and log of peak %BOLD in the S1FL area.
- Figure 5.16 Integrated BOLD and log of integrated BOLD measurements in the S1FL area.
- Figure 5.17 Raw and difference laser speckle images before and during stimulation for a representative aWKY and aSHRSP.
- Figure 5.18 Contralateral S1FL area group-averaged %CBF time course for all experimental groups
- Figure 5.19 Group-averaged CBF time courses for ipsilateral S1FL and ipsilateral visual cortex
- Figure 5.20 Peak %CBF in the contralateral S1FL area
- Figure 5.21 Integrated CBF and log of integrated CBF in the contralateral S1FL
- Figure 5.22 Peak % Δ CBF in the ipsilateral S1FL.
- Figure 5.23 Integrated CBF and log of integrated CBF measurements in the ipsilateral S1FL
- Figure 5.24 Peak % Δ CBF in the ipsilateral visual cortex
- Figure 5.25 Integrated CBF and log of integrated CBF in the ipsilateral visual cortex.

List of Tables

Table 3.1 Summary of mean bias, upper and lower limits of agreement, effective range and regression-based range

Table 4.1: A summary of the main results from each of the studies in Chapter 4

List of Abbreviations

AMP	adenosine monophosphate
AMPA	amino-3-hydroxy-5-methyl-4-isoxazolepropionic acid
ATP	adenosine triphosphate
BBB	blood brain barrier
BOLD	blood oxygenation level dependent
CBF	cerebral blood flow
CDP	cord dorsum potential
CNS	central nervous system
CO₂	carbon dioxide
COX	cyclooxygenase
CSF	cerebrospinal fluid
EETs	epoxyeicosatrienoic acids
ETCO₂	end-tidal carbon dioxide
FLASH	fast low angle shot
fMRI	functional magnetic resonance imaging
GLUT1	glucose transport type 1
LAT	large amino-acid transport type 1
LSCI	laser speckle contrast imaging
LOA	limits of agreement
MRI	magnetic resonance imaging
NMDA	N-methyl-D-aspartate
nNOS	neuronal nitric oxide synthase
PaCO₂	partial pressure of arterial carbon dioxide
PaO₂	partial pressure of arterial oxygen
ROI	region of interest
S1FL	primary forelimb somatosensory cortex
SEP	somatosensory evoked potential
SHR	spontaneously hypertensive rat
SHRSP	spontaneously hypertensive stroke-prone rat
SVD	small vessel disease
VRF	veterinary research facility
VSMCs	vascular smooth muscle cells

WMH white matter hyperintensity

Abstract

Cerebral small vessel disease (SVD) is associated with various pathological and neurological processes that affect perforating arterioles, capillaries and venules. The characteristic features of cerebral SVD include small lacunar subcortical infarcts, white matter hyperintensities, microbleeds and cortical microinfarcts. The underlying pathology of cerebral SVD is not fully known, owing to the difficulty of studying the disease in humans. Small lacunar infarcts are rarely fatal and often asymptomatic. In cases where death occurs, autopsy tissue is often difficult to interpret since multiple pathological changes have occurred at this late-stage in disease pathology.

Spontaneously hypertensive stroke prone rats (SHRSPs) are an accepted and validated model of cerebral SVD, demonstrating many of the features observed in the human condition. Arteriosclerosis, thickening of the vessel wall, narrowing of the arterial lumen, endothelial dysfunction and a loss of vessel reactivity have all been reported in SHRSPs. Given these pathologic cerebrovascular changes, the hemodynamic response in these animals may be sensitive to such changes and therefore provide a marker of cerebrovascular health and an indicator of therapeutic effect. Blunted BOLD responses have been observed in patients with SVD but no study has assessed whether SHRSPs demonstrate a similar reduction in the stimulus-evoked BOLD response. Therefore, the main aim of this thesis was to evaluate whether differences in the hemodynamic response could be detected in between SHRSPs compared to age-matched WKYs.

Prior to performing the study described above, we deemed it necessary to evaluate the ability to non-invasively monitor PaCO₂, by measuring end-tidal CO₂ using side-stream capnography. Baseline and stimulus-evoked cerebral blood flow (CBF) and blood oxygenation level dependent (BOLD) responses are sensitive to changes in the partial pressure of arterial carbon dioxide (PaCO₂). Therefore, it is important that PaCO₂ is monitored and kept within normal physiological values to avoid introducing confounds into the data. Blood gas analysis remains the gold standard for assessing PaCO₂ and other blood gases, however these measurements are invasive and discrete, only providing a measure of PaCO₂ for a short time following withdrawal and analysis of the

blood sample. The ability to continuously and non-invasively assess PaCO₂ using side-stream capnography would be beneficial for preclinical fMRI studies, particularly longitudinal studies, as it could minimise/eliminate any invasive surgery/procedure required to periodically take blood samples for blood gas analysis and provide a continuous measurement. However, the combination of the rat's small tidal volume, long sample lines, and large sample volumes required by most capnographs complicate the accurate assessment of PaCO₂ using ETCO₂ in these small animals. Therefore, an aim of this thesis was to assess the ability of micro-sampling side stream capnography to non-invasively assess PaCO₂ by comparing ETCO₂ measurements with PaCO₂ measurements obtained by blood gas analysis. Despite the smaller sample volumes required by micro sampling capnographs, our findings indicate that a large variability still exists between ETCO₂ and PaCO₂ values when long sampling lines are used, as would be required for use in an fMRI experiment. Therefore, side-stream capnography was not implemented in any of the other studies described in this thesis. However, the use of shorter lines for bench top experiments may hold promise with some optimisation.

It was also deemed necessary to explore the effects of varying forelimb stimulation parameters on stimulus-evoked BOLD, CBF and neural responses under combined medetomidine-isoflurane anaesthesia. Anaesthesia is known to have various effects on CBF and neural activity, depending on the anaesthetic being used, which can subsequently affect stimulus-evoked hemodynamic and neural responses. Therefore, there is a general consensus that stimulus parameters should be optimised to the anaesthetic being utilised, especially in cases where a novel anaesthetic is being used or if no stimulus optimisation is currently provided in the literature. Since no study has previously characterised the effects of varying stimulus parameters on the hemodynamic and neural responses under this anaesthetic protocol, the effect of varying the stimulus intensity, stimulus frequency and pulse duration on the stimulus-evoked BOLD, CBF and neural responses was subsequently investigated using fMRI, laser speckle contrast imaging and electrophysiology, respectively. The aim of these experiments was to identify the optimal stimulus parameters that evoked the largest response. Tested parameters were selected based on commonly used values in the literature. We observed that frequency had the largest impact on the resultant hemodynamic or neural measurements, with

higher frequencies generally evoking larger peak responses. However, analysis of the SEPs revealed that at higher frequencies there was a periodic loss of the SEP response and the overall amplitude of the SEPs declined over the course of stimulation. Stimulus intensity had a modest effect on the hemodynamic response with larger responses generally being observed >4 mA. Ultimately, the optimal parameters were selected as 6 mA, 0.3 ms and 3 Hz. These parameters were subsequently used for the fMRI study in SHRSPs.

The findings in this thesis represent one of the few preclinical studies assessing the hemodynamic response in SHRSPs. Several studies have assessed the hemodynamic response in patients with cerebral SVD and observed blunted BOLD responses to stimulation. However, to our knowledge, this has not been assessed in the SHRSP. Given the role of the endothelium in mediating the hemodynamic response, and that dysfunction of the endothelium has been reported in the SHRSP and patients with cerebral SVD, assessing the hemodynamic response may provide a biomarker of cerebrovascular health and therapeutic effect. Several clinical trials have already assessed cerebrovascular reactivity by evaluating changes in the BOLD response to a hypercapnic challenge as a primary endpoint, suggesting this assessment is clinically relevant. Characterising the hemodynamic response in SHRSPs could further support their use as a model of cerebral SVD and allow consistent assessments to be performed in preclinical and clinical stages, which could aid in drug identification and development. Therefore, the main aim of this study was to characterise any differences between the stimulus-evoked BOLD and CBF responses to forelimb stimulation in the SHRSP, including any differences between young and old animals and aged-matched WKYs. The hemodynamic response was found to differ between older SHRSPs and young and older WKYs, with the stimulus-evoked BOLD and CBF responses being larger in the old SHRSPs. This observation opposes the findings of other studies that assess the hemodynamic response in patients with SVD, but aligns with fMRI findings in the SHR parent strain. It will be important for future studies to characterise this difference of responses between preclinical and clinical populations to confirm whether it is underpinned by a biological and pathologic mechanism or whether it has been artificially created by some of the requirements for preclinical studies i.e. anaesthesia.

Introduction

1.1 Cerebral circulation

The brain is one of the most perfused organs within the human body, being supplied by a dense network of blood vessels. Blood is delivered to the brain via the internal carotid and vertebral arteries that provide anterior and posterior circulation, respectively. The right and left vertebral arteries join at the level of the pons to form the basilar artery. The basilar artery subsequently joins an arterial ring, known as the circle of Willis, that connects the basilar, internal carotid and posterior cerebral arteries via anterior and posterior communication arteries. Branches of the posterior cerebral, basilar and vertebral arteries supply the posterior cortex, midbrain, and brainstem, while branches from the internal carotid arteries supply the forebrain. Major branches of the internal carotid include the anterior and middle cerebral arteries, the latter of which gives rise to the lenticulostriate arteries that penetrate the basal surface of the brain to supply deep structures such as the basal ganglia. Branches of the anterior, middle and posterior cerebral arteries also run across the surface of the brain, within the pia-arachnoid. These pial arteries give rise to penetrating arterioles that enter the brain tissue and become parenchymal arterioles.

1.1.2 Blood vessel structure

Cerebral arteries consist of three concentric layers. The innermost layer, the *tunica intima*, consists of a single layer of endothelial cells that are arranged in continuous tubular formations, being ensheathed on the abluminal side by a layer of connective tissue known as the internal elastic lamina. The next layer, the *tunica media*, consists largely of vascular smooth muscle cells (VSMCs) with some elastin and collagen fibres. The number of VSMCs as well as the shape, size and orientation of individual cells varies depending on species, vessel size and position along the vessel (Todd et al. 1983; Ushiwata and Ushiki 1990). VSMCs express contractile proteins, such as actin and myosin, and play a crucial role in regulating vessel diameter (Hill et al. 2015). The outer most layer, the *tunica adventitia/tunica externa*, consists mostly of collagen fibres.

While the previously described structure generally relates to larger arteries, there are subsequent changes in vessel structure when progressing through the vascular tree from large arteries to capillaries, particularly in the *tunica media*. While large arteries may have as many as 20 VSMC layers within the *tunica media*, pial vessels may only have 2-3 layers of VSMCs and penetrating arteries that enter the brain parenchyma consist of an endothelial layer, a single layer of VSMC cells and the outer, *tunica adventitia*. In smaller arterioles and capillaries, VSMCs are replaced with a different type of mural cells known as pericytes. The role of pericytes in regulating vessel diameter has been questioned over the past decade. Pericytes were previously thought to play a critical role in regulating cerebral blood flow (CBF) in the microcirculation by driving changes in vessel diameter. However, it was later reported that pericytes lacked the contractile protein α -smooth muscle actin, thereby suggesting that they did not participate in capillary vasomodulation (Hill et al. 2015). However, recently it has been shown that pericytes do indeed contain the contractile protein α -smooth muscle actin (Alarcon-Martinez et al. 2018), with the authors attributing the inability to previously detect this protein due to the previously utilised tissue preservation technique and degradation of tissue samples. Pericytes have also been shown to play a role in maintaining the blood brain barrier (BBB; Armulik et al. 2010).

1.1.3 Blood brain barrier

The existence of the BBB was first postulated in the early 1900's following the observation that intravenously injected aniline dyes stained all organs in small animals, with the exception of the brain (Goldmann 1909). Later, when trypan blue dye was injected into the cerebrospinal fluid (CSF) of rabbits and dogs, the brain became readily stained but other organs did not (Goldmann 1913). Thus, early theories considered the BBB as an impermeable barrier, however years of subsequent research have shown that it is not impermeable and plays a more regulatory role.

The microvasculature of the central nervous system (CNS) is the foundation of the BBB and demonstrates unique properties to tightly regulate the entry and exit of substances from the brain. The two main components of the BBB are the brain capillary, formed from a single layer of endothelial cells, and the basement membrane that envelopes the capillary. Endothelial cells that comprise the BBB differ from those in the peripheral vasculature, having increased mitochondria, a lack of fenestrations and exhibiting minimal pinocytotic activity (Oldendorf et al. 1977; Fenstermacher et al. 1988; Sedlakova et al. 1999). The basement membrane comprises collagen type IV and extracellular matrix proteins, such as proteoglycans and laminin (Thomsen et al. 2017). Additionally, pericytes reside within the basement membrane and, as previously mentioned, play a role in regulating vessel diameter. Astrocytic end-feet processes also contact the basement membrane and encapsulate the entire structure.

In the BBB, endothelial cells are arranged in a continuous tubular formation and joined by tight junctions. Tight junctions are intermembranous strands that form a barrier between adjacent endothelial cells and are comprised of various proteins that include occludin, claudin and zona occludens (Anderson and Van Itallie 2009). As such, the brain endothelium forms a continuous barrier that restricts the paracellular exchange of molecules and cells. This limitation of movement between the periphery and central nervous system maintains an optimal chemical environment for neural activity and shields the brain from fluctuations in blood plasma composition and from circulating toxins or pathogens that could otherwise disturb the homeostatic chemical environment and injure the brain.

Despite the restrictions imposed by the presence of the BBB, the brain requires various molecules and substrates to sustain metabolic activity and requires the removal of metabolic waste products that could otherwise negatively alter the chemical environment and lead to cytotoxic damage. There are several mechanisms by which various molecules can cross the BBB. Firstly, passive diffusion in which a molecule follows a concentration gradient from high to low. Generally, only lipid soluble molecules with low molecular weight are able to cross the BBB by passive diffusion. These include gases such as oxygen and carbon dioxide. The majority of substances that cannot cross the BBB by diffusion are transported via carrier mediated and receptor mediated transport. The glucose transporter type 1 (GLUT1) enables the transport of glucose across the BBB and subsequently into the brain (Pardridge et al. 1990). Additionally, the large neutral amino-acid transport type 1 (LAT1) enables the transport of phenylalanine and other large neutral amino acids (Pardridge and Oldendorf 1975). Not all transport mechanisms result in an influx of molecules and substances into the brain and some also play a role in regulating homeostasis of the brain environment by removing substances from the brain. Receptor-mediated transport generally aid the transport of endogenous substances. One such example is the transport of insulin which is transported by binding to the endogenous insulin receptor (Pardridge et al. 1985). Efflux pumps such as P-glycoprotein and breast-cancer resistant protein are part of the adenosine triphosphate (ATP)-binding cassette family and actively remove exogenous compounds and drugs from the brain, which presents a challenge for drugs that target the central nervous system (Kooij et al. 2012).

1.1.4 The neurovascular unit

While the neuron is generally considered the fundamental unit of the brain and plays a critical role in signal transmission/processing throughout the nervous system, it is integrated with various other cell types such as astrocytes, microglia, pericytes and blood vessels to form the neurovascular unit. The concept of the neurovascular unit first emerged from the Stroke Progress Review meeting of the National Institute of Neurological Disorders and Stroke in 2001 to emphasise the relationship between brain cells and the cerebrovasculature (NINDS 2001). Prior to this time, there were some within the scientific community who assumed that there was generally little

interaction between neurons and the cerebrovasculature and similarly, that neurodegenerative diseases e.g. Alzheimer's disease and cerebrovascular diseases e.g. stroke were mutually exclusive and mechanistically unrelated (Iadecola 2017). Following the Stroke Progress Review group meeting, there was increasing interest in studying the neurovascular unit, as evidenced by the annual increase in the number of publications citing "neurovascular unit" in the years following the meeting (Iadecola 2017). Such research supported the concept that the components of the neurovascular unit were reciprocally connected with each other, both structurally and functionally, to enable cross-talk between the various cell types. This interdependence between the components of the neurovascular unit aids in its functions in brain development, the formation and maintenance of the BBB, signal transduction via the cerebrovascular matrix, clearance and immune surveillance through the perivascular compartment, and notably, neurovascular coupling (Iadecola 2017).

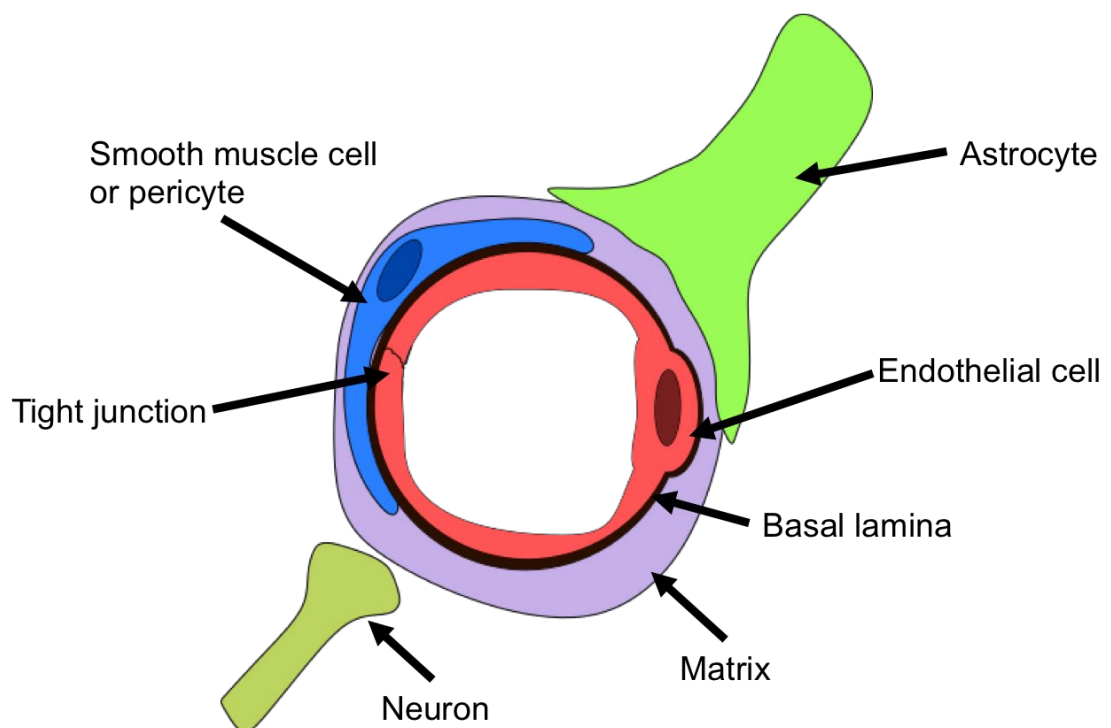


Figure 1.1: The neurovascular unit

1.1.5 Neurovascular coupling

While the brain only constitutes approximately 2% of the total body mass, it uses 20% of the total energy consumed by the body at rest. Of the total energy available to the brain, it is estimated that 50% is used to reverse glutamate-evoked ion fluxes (sodium and calcium), 21% on reversing ion gradients from induced action potentials, 20% on maintaining resting membrane potentials by actively pumping out sodium ions, 5% to reverse action potential-induced presynaptic calcium ion (Ca^{2+}) influx and 4% on neurotransmitter recycling (Howarth et al. 2012). Since there are no significant energy reserves within the brain, it depends on a continuous and adaptable blood supply to transport metabolic substrates, such as oxygen and glucose, to meet the dynamic metabolic changes associated with neural activity. Furthermore, the vascular system also enables the clearing of metabolic by-products that would otherwise build up and lead to cytotoxic damage.

Neurovascular coupling defines the close temporal and spatial relationship between neural activity and CBF; generally, an increase in neural activity is followed by a local increase in CBF. Such a relationship was first noted by the Italian physiologist Angelo Mosso, who observed increased blood pulsations over the right prefrontal cortex when a subject with a skull defect performed a mental arithmetic task (Mosso 1880). Later, Roy and Sherrington (1890) proposed that a metabolic feedback mechanism underpinned the coupling of cerebral blood flow to neural activity due to the observation that neural metabolic by-products, such as carbon dioxide (CO_2), could dilate cerebral vasculature. This subsequently led to the hypothesis that the local increase in cerebral blood flow observed with increased neural activity was generated due to a reduction in metabolic substrates, such as glucose and oxygen, and an increase in metabolic by-products such as CO_2 , adenosine and lactate (Kety 1950). Indeed such metabolic by-products are capable of inducing vasodilation of cerebral vessels (O'Regan 2005). However, local decreases in O_2 concentration at the site of neural activation are small and transient compared to the substantial increases in CBF that attend (Fox and Raichle 1986). Furthermore, these large CBF increases still occur under conditions of excess oxygen and glucose, and under hypoglycaemic conditions, suggesting that depletion of these substrates does not drive the observed increased CBF response (Powers et al. 1996; Wolf et al. 1997; Lindauer et al. 2010).

Therefore, such observations suggest that neurovascular coupling is unlikely driven by a metabolic 'feedback' mechanism.

An alternative feed-forward mechanism has been suggested to underpin neurovascular coupling, with increased neuronal activity initiating various signalling cascades that ultimately lead to vasodilation. In this model, neurons and astrocytes are thought to play key roles in mediating changes in CBF. In neurons, glutamate binding causes the influx of Ca^{2+} into postsynaptic terminals through activated N-methyl-D-aspartate (NMDA) and amino-3-hydroxy-5-methyl-4-isoxazolepropionic acid (AMPA) receptors, increasing intracellular Ca^{2+} and activating Ca^{2+} -dependent enzymes such as neuronal nitric oxide synthase (nNOS) and cyclooxygenase (COX) 2 which synthesise potent vasodilators (Iadecola 2017). Astrocytic end feet processes contact synapses exposing them to glutamate released from activated neurons. Here, glutamate acts on astrocyte metabotropic glutamate receptors and leads to the activation of phospholipase A_2 and the production of arachidonic acid from membrane phospholipids. Arachidonic acid is subsequently metabolised by COX and cytochrome p450 epoxygenase pathways to produce prostaglandins and epoxyeicosatrienoic acids (EETs), respectively, which can act on both smooth muscle cells and pericytes, leading to vasodilation of arteries and capillaries, respectively (Peng et al. 2002; Peng et al. 2004; Metea and Newman 2006; Gordon et al. 2008). The dominant prostaglandin in vasodilation is thought to be PGE_2 which has been shown to induce vasodilation by binding to the EP_2 and EP_4 prostaglandin receptors (Lacroix et al. 2015). Astrocytes have also previously been thought to mediate vasodilation through the siphoning of potassium ions (K^+), in which K^+ released from activated neurons depolarises nearby astrocytes resulting in the efflux of K^+ from astrocyte end feet contacting cerebral vessels (Paulson and Newman 1987). Indeed, modest increases in extracellular K^+ concentration can hyperpolarise smooth muscle cells which subsequently reduce the influx of Ca^{2+} through voltage-gated channels resulting in smooth muscle cell relaxation and dilation of the vessel (Knot et al. 1996).

The exact contributions of neurons and astrocytes in neurovascular coupling are not fully known. In a recent meta-analysis, blockade of nNOS was found to have the largest effect in reducing the magnitude of the neurovascular

response; an average reduction of 64% was observed across 11 *in vivo* studies (Hosford and Gourine 2019). Pharmacological inhibition and genetic deletion of nNOS result in a similar reduction of the hemodynamic response to stimulation (Ma et al. 1996; Yang et al. 2003), indicating that full inhibition of NO was likely achieved in these studies and therefore, the observed reduction of 64% was unlikely due to incomplete inhibition of nNOS. Interestingly, NO donors in nNOS-inhibited rats have been observed to restore the attenuated CBF response to non-nNOS-inhibited levels (Lindauer et al. 1999). Since NO donors provide a constant level of NO that does not vary with the level of neural activity, NO is likely to play a more permissive role in neurovascular coupling rather than mediate it. However, while nNOS signalling may account for the majority of the neurovascular response, a significant proportion of the response remains when this pathway is blocked, suggesting other signalling mechanisms are involved. Interestingly, blockade of COX or epoxygenase pathways results in an approximate 50% reduction in the hemodynamic response in animals and humans (Bruhn et al. 2001; Hosford and Gourine 2019). However, it should be noted that this observation may overestimate the contribution of these signalling pathways in neurovascular coupling since the non-specific COX inhibitor, indomethacin, was used. Indomethacin also inhibits cyclic AMP-dependent protein kinase activity, a critical component of vasomotor responses. Interestingly, blockade of NOS, COX and epoxygenase activity does not completely abolish the neurovascular response suggesting other mechanisms are involved (Leithner et al. 2010).

While neuron- and astrocyte-mediated signalling likely underpin the main pathways to induce CBF increases in neurovascular coupling, these are generally localised to the activated area. For flow to increase sufficiently, these vasodilatory signals need to be conveyed to upstream arterioles (Segal 2015). Indeed, several studies have shown that vasodilation is retrogradely propagated to upstream pial vessels (Dietrich et al. 1996; Iadecola et al. 1997; Silva and Koretsky 2002). The cellular origin of this retrograde vasodilation propagation has been attributed to the endothelium; lesion of the endothelium results in the failure of neural activation induced vasodilation to propagate beyond the local area of activity and alters the amplitude and temporal dynamics of the hemodynamic response (Chen et al. 2014).

1.1.6 Autoregulation

Cerebral autoregulation is the process whereby changes in cerebrovascular tone regulate blood flow and volume to ensure that a constant cerebral perfusion pressure (CPP) is maintained across a wide range of arterial blood pressures. The underlying mechanisms of cerebral autoregulation are not completely understood although myogenic, metabolic, neurogenic and endothelial mechanisms have been proposed (Armstead 2016). The myogenic component relates to the constriction or dilation of vessels through the actions of VSMCs that regulate vessel size and resistance, and has been suggested to play a dominant role in cerebral autoregulation (Hamner and Tan 2014). Additionally, metabolic by-products such as CO₂, H⁺ and adenosine are vasoactive and thereby may provide a metabolic component to autoregulation (Meng and Gelb 2015). Perivascular adrenergic nerves densely innervate the brain cerebrovasculature and VSMCs express alpha- and beta-adrenergic receptors (Edvinsson 1982), suggesting a neurogenic component to autoregulation. However, animal studies have reported both the abolishment and preservation of autoregulation in sympathetic and parasympathetic denervated animals (Sagawa and Guyton 1961), while in humans, the sympathetic and parasympathetic system have been shown to modulate cerebral autoregulation (Hamner et al. 2010; Hamner et al. 2012). Additionally, nNO has been shown to influence cerebral autoregulation in animal models (Talman and Nitschke Dragon 2007) while its role in human cerebral autoregulation remains unclear (White et al. 2000; Zhang et al. 2004). Such observations may be due to differences between species (Sándor 1999), however a definitive consensus concerning the involvement of a neurogenic component in cerebral autoregulation has yet to be achieved. Endothelial factors such as endothelial nitric oxide, endothelial derived hyperpolarisation factor, eicosanoids and endothelins may also be involved in regulating cerebral autoregulation due to their vasoactive properties (Peterson et al. 2011). In a normal adult, CBF is maintained at approximately 50 mL per 100 g of brain tissue per min, providing mean arterial pressure remains within the lower and upper limits of autoregulation (60–160 mmHg) (Phillips and Whisnant 1992). While CBF and vessel diameter are generally well maintained within these limits, increases in blood pressure above the upper limit (autoregulation breakthrough) results in forced dilation of the vessel, resulting in increased CBF, disruption of the BBB and increases in vascular permeability, all of which

may also contribute to the development of hypertensive encephalopathy (Lassen and Agnoli 1972; Strandgaard et al. 1974; MacKenzie et al. 1976; Kawamura et al. 1993; Tamaki et al. 1995). Conversely, below the lower limit of autoregulation, a cascade of deleterious events ensue as CBF declines below critical thresholds to sustain various metabolic processes; protein synthesis is first reduced then subsequently inhibited, anaerobic glycolysis and disruption to energy metabolism follow and finally anoxic depolarisation and cerebral ischemia (Hossmann 1994).

1.2 Cerebral small vessel disease

Cerebral small vessels refer to the arteries branching from the anterior, middle and posterior cerebral arteries that penetrate the brain and provide blood flow to deeper cerebral structures (Pantoni 2010). Cerebral small vessel disease (SVD) generally refers to various pathological and neurological processes that are characterised by structural changes within these perforating arterioles, capillaries, and venules, as well as the resultant changes occurring in deep white and grey matter structures. Cerebral SVD underlie lacunar strokes, a subtype of ischemic stroke that accounts for 20% of all strokes (25% of ischemic strokes), although the prevalence of lacunar infarction may be higher in some populations, such as the Chinese population, where epidemiological studies have indicated that lacunar infarction accounts for 38-46% of ischemic strokes (Fang et al. 2012; Tsai et al. 2013).

Lacunar strokes are characterised by small infarcts (2-20 mm in diameter) localised within deep brain structures that include cerebral white matter, basal ganglia and the pons (Bamford et al. 1988; Sudlow and Warlow 1997a; Wardlaw et al. 2013). While lacunar strokes can be symptomatically 'silent' and therefore go unnoticed, 25% of patients suffering a lacunar stroke are left with functional disabilities (Pantoni 2010). Symptoms of cerebral SVD include cognitive impairment, depression and gait problems. Additionally, a long term study in lacunar stroke patients reported that up to 25% of patients suffered a second stroke within 5 years of the first (Samuelsson et al. 1996).

1.2.1 Pathogenesis

The underlying mechanisms that lead to the development of cerebral SVD are not fully known. This is largely due to the difficulty of studying the disease in humans. Lacunar strokes are rarely fatal and can be 'silent' or 'mild' in regard to their clinical manifestation, and therefore often go unnoticed (Hainsworth and Markus 2008). In cases where death does occur from cerebral SVD, this may be long after lacunar stroke and other pathological changes have occurred. Therefore, there is limited autopsy tissue for analysis and identifying causative pathological mechanisms while assessing tissue from established or late-stage disease is difficult. However, it is generally thought that cerebral SVD arises from reduced CBF, impaired autoregulation and increased BBB

permeability. In recent years, evidence supporting a role of endothelial dysfunction in driving disease progression has also been observed (Quick et al. 2021).

1.2.2 Features of cerebral small vessel disease

The main features of cerebral SVD are typically identified by magnetic resonance imaging (MRI) and include small lacunar ischemic stroke or hemorrhage (typically sub-cortical), fluid-filled cavities known as lacunes of vascular origin (Vermeer et al. 2007; Shi and Wardlaw 2016), white matter hyperintensities (WMHs) (Rost et al. 2010; Kynast et al. 2018), visible perivascular spaces (Doubal et al. 2010), microbleeds (Cordonnier et al. 2007), brain atrophy (Aribisala et al. 2013) and cortical microinfarcts (Smith et al. 2012).

1.2.2.1 Lacunar ischemic stroke

Lacunar ischemic stroke is commonly observed in cerebral SVD and is defined as a stroke that causes small infarcts <15 mm (or sometimes <20 mm) in diameter in the white matter, basal ganglia, pons or brainstem (Wardlaw et al. 2013). These infarcts generally arise due to abnormalities, such as atherosclerosis, lipohyalinosis and fibrinoid necrosis, in a single small deep perforating or lenticulostriate artery (Fisher 1965). Of these, the most commonly described defect that leads to lacunar ischemic stroke is lipohyalinosis, characterised by thickening of the vessel wall, focal dilation and eventually, disintegration of the wall and development of an infarct (Wardlaw 2005). Unlike non-lacunar ischemic stroke, an embolism arising from the heart or large arteries does generally not cause lacunar stroke. However, that is not to say that lacunar strokes cannot be caused by embolism. Indeed, these have been observed to occur although the incidence of such is generally low, accounting for no more than 10-15% of all lacunar infarcts (Jackson et al. 2010). Lacunar ischemic strokes can normally be identified as rounded, ovoid or tubular hyperintense areas on diffusion-weighted, T₂-weighted and fluid-attenuated inversion recovery (FLAIR) images, hypointense on apparent diffusion coefficient (ADC) maps and T1-weighted images, or hypoattenuated on computed tomography (CT; Shi and Wardlaw 2016)

1.2.2.2 Lacunes of presumed vascular origin

Lacunes of presumed vascular origin are small round or ovoid cavities 3-15 mm in diameter that contain cerebrospinal fluid and are located in either the grey or white matter. Lacunes are usually recognised as a hypointense ‘hole’ surrounded by a hyperintense rim on FLAIR images, which aids in differentiating them from enlarged perivascular spaces (Shi and Wardlaw 2016). It is generally accepted that lacunes represent old infarcts that were asymptomatic and appeared ‘silently’ in the brain (Vermeer et al. 2007). However, large numbers of lacunes are associated with dementia, cognitive impairment, gait disturbance and increased risk of stroke (Snowdon 1997; Vermeer et al. 2003; Vermeer et al. 2007)

1.2.2.3 White matter hyperintensities

White matter hyperintensities (WMHs) are areas of increased signal intensity on T₂-weighted and FLAIR images that are typically distributed bilaterally and symmetrically in the white matter and deep grey matter. They are the hallmark of pathological change in cerebral SVD when assessed by MRI, and have been attributed to demyelination, axonal loss and gliosis (Frisoni et al. 2007). The underlying cause for WMHs is not clear, although incomplete infarction, chronic hypoperfusion and venous collagenous have all been proposed. In recent years, it has been observed that WMHs are heterogeneous and therefore may indicate different stages of lesion development. Attempts have been made to classify WMHs by size, contrast/“whiteness” and position to inform on the clinical risks associated with each class (Jung et al. 2021). The development of WMHs are preceded by a decline in the microstructural integrity of normal-appearing white matter, as evidenced by reduced fractional anisotropy (FA) and increased mean diffusivity (MD) being observed in the NAWM prior to the development of a WMH (Sam et al. 2016a; Van Leijssen et al. 2018). In a meta-analysis, WMHs were associated with an increased risk of stroke, dementia and death (Debette and Markus 2010).

1.2.2.4 Perivascular spaces

Perivascular spaces are fluid-filled spaces that surround perforating arterioles as they penetrate through deep grey and white matter structures. The visibility of some perivascular spaces is generally considered normal (Groeschel et al.

2006), however increased numbers of enlarged, visible perivascular spaces are associated with WMHs, hypertension, lacunar stroke and reduced cognitive function, suggesting that these may provide a marker of some underlying pathological processes (MacLulich et al. 2004; Hurford et al. 2014). Enlarged perivascular spaces appear as hyperintense punctuate areas of <3 mm in diameter on T2-weighted images, if viewed perpendicular to the vessel, or linear if viewed parallel to the vessel (Potter et al. 2015). It has been suggested that the number of visible perivascular spaces indicates active inflammation (Wuerfel et al. 2008), however the exact mechanisms underlying enlarged perivascular spaces are not well-known. Others have hypothesised that enlarged perivascular spaces may indicate impaired BBB or blockage in the draining of interstitial fluid due to the reduced pulsatility of hardened vessels to drive drainage (Shi and Wardlaw 2016).

1.2.2.5 Microbleeds

Cerebral microbleeds are generally observed as small (3-5 mm in diameter), homogenous hypointense foci on T₂-weighted images (Cordonnier et al. 2007). In symptomatic patients with cerebral SVD, microbleeds in the frontal, parietal and basal ganglia were independently associated with visuospatial/executive impairment suggesting that microbleeds may affect cognitive impairment, although their number and localisation likely plays a key role in determining any impact on cognition (Abdullah et al. 2020). However most cerebral microbleeds are asymptomatic and can be found in healthy adults, yet are often considered a marker of vascular risk factors (e.g. hypertension, diabetes) or amyloid deposition (Cordonnier et al. 2007). The underlying pathophysiology of cerebral microbleeds is not fully known but previous studies have shown that cerebral microbleeds are predominantly associated with perivascular hemosiderin-laden macrophages, although haematomas, intact erythrocytes, vascular pseudocalcification, microaneurysm and distended dissected vessels have also been observed (Shoamanesh et al. 2011). In a postmortem study, brains with the most extensive microbleeds had a higher Sclerosis Index, indicating an association between microbleeds and arteriolar injury (Wadi et al. 2020).

1.2.3 Functional MRI in patients with SVD

While the structural characteristics of cerebral SVD have received much attention, there is a growing interest in using functional MRI (fMRI) to characterise cerebrovascular reactivity and brain connectivity in patients with cerebral SVD. Abnormal changes and remote connectivity in the sensorimotor, frontoparietal and default mode networks have been associated with gait disorders, instability and aggravating factors in patient with cerebral SVD when assessed by resting-state fMRI (Zhou et al. 2020). Compared with controls, reduced stimulus-evoked BOLD responses in the visual cortex have been observed in patients with cerebral amyloid angiopathy (CAA), a small vessel disease (Dumas et al. 2012; Peca et al. 2013). Furthermore, it was noted that the reduction in the BOLD response occurred in the absence of any changes in the neural response, as assessed by comparing the visual-evoked potentials with controls, suggesting that this observation was underpinned by changes in the reactivity of the cerebrovasculature and not the neural response (Peca et al. 2013). Adults with severe-to-moderate WMHs have also demonstrated reduced task-related BOLD responses in the fronto-temporal and parietal cortices when performing an attention test (Atwi et al. 2018). In pre-symptomatic and symptomatic patients with a genetic form of CAA (hereditary cerebral haemorrhage with amyloidosis-Dutch type), the stimulus-evoked BOLD signal to visual stimulation was reduced (van Opstal et al. 2017). Several studies have used a hypercapnic challenge to assess cerebrovascular reactivity in patients with moderate-to-severe white matter disease and observed a reduced magnitude and speed of the hemodynamic response in normal-appearing white matter that later progressed to WMH (Sam et al. 2016a; Sam et al. 2016b). Collectively, the studies discussed in this section suggest that cerebrovascular reactivity is impaired in patients with cerebral SVD; both in those with established disease and those who are pre-symptomatic. Thus, the assessment of cerebrovascular reactivity in this patient population may provide a useful biomarker for early detection of cerebral SVD and a biomarker of the therapeutic efficacy.

1.2.4 Sporadic and monogenic forms of cerebral SVD and associated risk factors

Cerebral SVD can broadly be divided into two main categories, sporadic and monogenic. Most cases of cerebral SVD are sporadic and these can be further classified as non-amyloidal (most common sporadic form) or amyloidal. The sporadic non-amyloidal form of cerebral CVD generally describes disease with degenerative alterations in the cerebrovasculature (Charidimou et al. 2016), and is associated with traditional vascular risk factors that include hypertension, diabetes mellitus, hypercholesterolaemia and smoking. It is worth noting that such risk factors are equally as common in cortical atherothromboembolic stroke (Jackson et al. 2010) and some patients with cerebral SVD are not hypertensive or diabetic (Lammie et al. 1997). The brain-gut axis has also been implicated as a factor in the development of sporadic cerebral SVD. Improved BBB integrity was recently observed in SHRSPs who had been placed with WKY foster dams compared with those placed with SHRSP foster dams (Nelson et al. 2021). Environmental bacteria of the foster dam and nesting surroundings shape gut microbiomes suggesting that gut microbiota may contribute to the loss of BBB integrity often observed in early cerebral SVD. The amyloidal form of sporadic SVD is known as cerebral amyloid angiopathy (CAA) and describes a chronic degenerative disease characterised by progressive deposition of amyloid- β in the vessel wall of small arteries and arterioles which subsequently leads to fibrinoid necrosis, loss of smooth muscle cells, wall thickening, and formation of microaneurysms (Attems et al. 2011). Several familial forms of CAA also exist and include hereditary cerebral haemorrhage with amyloidosis Icelandic type (HCHWA-I) and hereditary cerebral haemorrhage with amyloidosis Dutch type (HCHWA-D; Revesz et al. 2002)

Monogenic forms of cerebral SVD arise from single-gene disorders and include cerebral autosomal dominant arteriopathy with subcortical infarcts and leukoencephalopathy (CADASIL), cerebral autosomal recessive arteriopathy with subcortical infarcts and leukoencephalopathy (CARASIL) cathepsin A-related with strokes and leukoencephalopathy (CARASAL), hereditary diffuse leukoencephalopathy with spheroids (HDLS), COL4A1/2-related cerebral SVD, autosomal-dominant retinal vasculopathy with cerebral leukodystrophy, and Fabry disease (FD; Giau et al. 2019). CADASIL is the most common monogenic

form of cerebral SVD and arises from mutations in the Notch Receptor 3 gene (NOTCH3) which encodes a transmembrane receptor expressed on vascular smooth muscle cells and pericytes. Distinct vulnerabilities in both grey and white matter have been observed in patients with typical CADASIL (Kim et al. 2019). Clinical symptoms of CADASIL may appear at younger ages or during adulthood and may include stroke, migraine, transient ischemic attack, cognitive impairment, dementia, mood disturbances or seizures (Giau et al. 2019). CARASIL is an extremely rare autosomal recessive disorder that has been linked to mutations in the HTRA1 gene which encodes HtrA serine peptidase/protease 1 (Hara et al. 2009; Verdura et al. 2015). Similar to CADASIL, CARASIL is radiologically characterised by diffuse white matter lesions and small infarcts in the basal ganglia. CARASAL is a rare, autosomal dominant small vessel disease linked to point mutations in CTSA, a gene encoding cathepsin-A, a carboxypeptidase associated with lysosomal enzymes (Finsterer et al. 2019). Symptoms of CARASAL include migraine, stroke, facial pain, cognitive dysfunction, sleep disorder and depression. HDLS is an autosomal dominant form of cerebral SVD clinically characterised by behavioural changes, dementia, depression, parkinsonism, and seizures (Rademakers et al. 2012). It has been linked with mutations in CSF1R, a receptor that has been observed to play a key role in microglial proliferation and differentiation. COL4A1/A2 related diseases are linked to mutations in COL4A1 and COL4A2 genes which encoded collagen type IV alpha chains (Giau et al. 2019). Clinically, COL4A1/A2 related diseases present with symptoms consistent with typical cerebral SVD. FD is a X-linked cerebral SVD attributed to mutations in the GLA gene that encodes lysosomal α -galactosidase A (Giau et al. 2019).

1.2.5 Animal models of cerebral small vessel disease

The ability to study cerebral SVD in humans is difficult, for reasons previously described. In such cases, animal models provide a useful tool to inform on disease pathology and progression and identify potential therapeutic targets. However, the lack of understanding of the pathological events that lead to cerebral SVD makes modelling this disease in animals difficult. Various models have been established for preclinical research, each mimicking certain features of cerebral SVD that may help to better understand the mechanisms underlying pathological changes in cerebral SVD.

1.2.5.1 Hypertensive primate model

Non-human primate models of disease are relatively rare in preclinical research, owing to cost and low public approval for their use. However, primates have large gyrencephalic brains similar to the human brain, exhibit complex behaviours resembling aspects of human cognition, and often mimic various disease features as seen in humans (Moss and Jonak 2007; Ndung'u et al. 2012; Camus et al. 2015). Chronically hypertensive macaque monkeys exhibit a progressive decline in cognitive functions such as memory, attention and executive functions similar to the human condition of cerebral SVD (Moss and Jonak 2007; Jiménez-Balado et al. 2019). Furthermore, microinfarcts of irregular shape and associated with local gliosis have been observed in the grey and white matter of these animals (Kemper et al. 1999; Kemper et al. 2001). However, these infarcts were smaller than those seen in human lacunar stroke, being less than 0.5 mm. Histological assessment also revealed a lack of white matter lesions or any changes occurring within the penetrating arteries in this model.

1.2.5.2 Chronic carotid occlusion

Cerebral hypoperfusion is thought to underlie cerebral SVD and therefore several different models have been developed to mirror this aspect of the disease. Bilateral occlusion of the common carotid arteries (two vessel occlusion, 2-VO) is the most commonly used hypoperfusion approach and results in chronic hypoperfusion in rats and results in cognitive impairment and the development of white matter lesions (Hainsworth et al. 2012). In rats, the bilateral occlusion approach is characterised by white matter degeneration, loss of oligodendrocytes, neuroinflammation and a loss of BBB integrity (Choi et al. 2016; Arena et al. 2019). Variations in this model include the 3-vessel occlusion (3-VO), 4-vessel occlusion (4-VO) and 2-vessel gradual occlusion (2-VGO) models. The 3-VO is achieved by performing both bilateral carotid artery occlusion and unilateral occlusion of a vertebral artery (de la Torre et al. 1992), while the 4-VO is achieved by performing unilateral occlusion of a carotid and a vertebral artery, and then occluding the remaining two arteries 7 days later (Pulsinelli and Buchan 1988). These severe chronic hypoperfusion models demonstrate spatial learning deficits, likely arising from neuronal loss

observed in CA1 pyramidal neurons in the hippocampus. The 2-VGO model is achieved by placing ameroid restrictor cuffs around each common carotid, which gradually swell and completely occlude the vessel after 3 days (Kitamura et al. 2012). This model develops spatial working memory impairment and white matter lesions but grey matter is relatively spared.

1.2.5.3 Middle cerebral artery occlusion

Changes in the structure of upstream large vessels, such as middle cerebral artery atheroma, have been shown to contribute to cerebral SVD pathology (Fisher 1979; Brisset et al. 2013; Xu 2014). Middle cerebral artery occlusion (MCAo) is a common method for the induction of ischemic stroke, of which the intraluminal filament model is the most widely used in preclinical rodent studies. The blockage of the MCA origin induces both cortical and subcortical ischemia, with lesions generally occurring in the cortex, hippocampus and striatum. However, tissue infarction is generally confined to subcortical structures in rat strains with good collateral blood supply to the cortex (Macrae 2011). However, this technique often suffers from frequent cases of early reperfusion, partial occlusion or subarachnoid haemorrhages (Braeuninger and Kleinschnitz 2009). Selective occlusion of the hypothalamic artery by advancing an intraluminal filament near to, but not occluding the origin of the MCA has also been shown to induce small infarcts in deep grey and white matter structures (He et al. 1999). Temporary MCAo in macaque monkeys for 30 mins - 4 hours has been observed to produce subcortical infarcts in grey matter structures (DeGirolami et al. 1984). However, these typically resembled striatocapsular infarcts, and there was relatively sparing of the white matter.

1.2.5.4 SHRSP

The spontaneously hypertensive rat family consists of both the spontaneously hypertensive rat (SHR) and the spontaneously hypertensive stroke prone rat (SHRSP). The SHR was developed first, being bred from Wistar rats demonstrating high blood pressure in a colony at Kyoto University (Okamoto and Aoki 1963). This model develops hypertension between 5-6 weeks of age which plateaus at approximately 8 weeks of age, with blood pressure reaching between 180-200 mmHg. However, this model does not generally develop stroke and is typically used as a model of hypertension. The SHRSP was

developed from 24th generation SHR, being selectively bred from parental animals who demonstrated spontaneous stroke (Okamoto et al. 1974). The established strain demonstrated severe hypertension (220–240 mmHg) and a high incidence of stroke (SHRSP, 80% vs SHR, 10%).

Cerebral pathology observed in the SHRSP includes cortical infarcts, enlarged perivascular spaces (Okamoto et al. 1974), microinfarcts, microaneurysms (Coyle 1987; Fredriksson et al. 1987), white matter lesions and BBB breakdown (Yamori et al. 1976; Takiguchi 1983; Minami et al. 1985; Chue et al. 1993), all of which are consistent with human cerebral SVD. Systematic reviews comparing several preclinical models of cerebral SVD with the human condition found that the SHRSP demonstrates many characteristics observed in human cerebral SVD and therefore represents a valid model of sporadic cerebral SVD (Hainsworth and Markus 2008; Bailey et al. 2009). The validity of the SHRSP as a model for cerebral SVD is further strengthened by observations that confirm similar underlying pathophysiological changes in the SHRSP and human patients with cerebral SVD. A higher number of proliferating endothelial cells (a sign of endothelial dysfunction) was observed in the brain tissue of 3-week SHRSPs and presymptomatic human patients with cerebral SVD when compared with controls (Rajani et al. 2018). Dysfunctional endothelial cells were subsequently noted to secrete factors, such as heat shock protein 90 α , that blocked oligodendrocyte maturation and proliferation, processes important in maintaining white matter integrity. A mutation in the *Atp11b* gene was identified in the SHRSP as the underlying cause of the observed endothelial dysfunctions, and seven single-nucleotide polymorphisms were subsequently identified in *ATP11B* in human patients which were significantly associated with WMHs (Rajani et al. 2018). Thus, in assessing the pathology of the SHRSP, early endothelial dysfunction was identified as an underlying mechanism of white matter pathology in both a model of cerebral SVD and in the human condition, and a mutation in *ATP11B* was identified as a potential contributor to SVD vulnerability.

SHRSPs <12 weeks old demonstrate vascular remodelling of large arteries due to increases in the number of VSMC layers (Fredriksson et al. 1988; Sironi et al. 2004). Such remodelling leads to an increase in the external diameter of large vessels as well as a decrease in the vessel lumen (Mangiarua and Lee 1992;

Kitazono et al. 1995a). Furthermore, vascular remodelling increases vessel stiffness with the resistance of large arteries being at least double in 1-year old SHRSPs compared to age-matched WKYs (Nordborg et al. 1985). Similar changes are observed within smaller vessels, which have shown decreases in lumen size (Thompson et al. 1988; Furspan and Bohr 1990; Furspan and Webb 1993). In 24-week old SHRSPs, internal and external diameters of third-order branches of the posterior cerebral artery were smaller to those in age-matched WKYs, in the absence of hypertrophy (Coyle 1987), suggesting that SHRSPs may have inherently smaller vessels compared to WKYs.

1.2.5.5 Transgenic mouse models

Transgenic mouse models have been developed for CADASIL and CAA. CADASIL is caused by mutations in *NOTCH3*, and ultimately results in accumulation and aggregation of the extracellular domain of Notch3 around vascular smooth muscle cells and pericytes of brain arteries and capillaries, in proximity to granular osmiophilic material (Chabriat et al. 2009). There are four mouse models that express common CADASIL mutations (*R90C*, *R169C*, *C428S* and *R142C*), all of which demonstrate accumulation of Notch3 and granular osmiophilic material, consistent with the human condition (Ayata 2010). Mouse models of CADASIL also display progressive white matter damage, reduced cerebral blood flow, decreased myogenic responses, impaired autoregulation during hypotension, and attenuated functional hyperaemia but an absence of pathological changes in cerebral artery structure and BBB breakdown (Joutel et al. 2010). There are also several models of CAA which are caused by mutations in amyloid precursor protein (APP). APPDutch mice overexpress human E693Q APP and subsequently demonstrate extensive amyloid angiopathy in the cerebrovascular, smooth muscle cell degeneration, hemorrhages and neuroinflammation (Herzig et al. 2004). Another model combines human Swedish, Dutch and Iowa APP mutations (Tg-SwDI) and demonstrate early onset deposition of amyloid- β in cerebral microvessels, decreased cerebral vascular densities, apoptotic cerebral vascular cell and cerebral vascular cell loss (Miao et al. 2005). Amyloid- β deposits are also associated with reactive astrocytes and activated microglia, and exaggerated by chronic hypoperfusion which can to increased amyloid angiopathy, microbleeds and haemorrhages (Salvadores et al. 2017; Shang et al. 2019).

1.3 Principles of magnetic resonance imaging

The atomic nucleus is at the centre of MRI. Although other nuclei are used for fMRI, hydrogen nuclei (protons) are the primary nuclei of interest in MRI. Atomic nuclei consist of protons and neutrons with a net positive charge and some atomic nuclei, such as hydrogen, possess 'spin'. The 'spinning' proton can be thought of as a moving electrical charge and as such generates a small magnetic field known as a magnetic moment. Under normal conditions, protons are orientated randomly within a sample and therefore it possesses no overall net magnetisation. However, when placed in a strong, external magnetic field (B_0), protons align either parallel with (low energy state) or antiparallel to (high energy state) the external field. The general preferred state of alignment is the one that requires the least energy, which results in an excess of protons aligning with the B_0 direction (z-axis), creating an overall net magnetisation vector (M_0) in that direction, referred to as longitudinal magnetisation. Given that each proton has angular momentum as a result of its 'spin', alignment with B_0 is not completely parallel but rather the proton precesses around the B_0 axis. The frequency with which a proton precesses within an external magnetic field is known as the Larmor frequency (ω), which can be calculated using the Larmor equation (Equation 1). The gyromagnetic ratio (γ) is a constant for a particular nuclear species and its value for protons is 42.6 MHz/T.

$$\omega = \gamma B_0 \tag{1}$$

The application of a radio frequency (RF) pulse results in the equalisation of the number of protons in the two energy levels (parallel and antiparallel to B_0) as well as induces phase coherence so that all protons subsequently precess in the same direction at the same time. However, this can only be done when the RF pulse matches the Larmor frequency of the nucleus of interest, referred to as resonance. The resultant transverse magnetisation, which now has a magnetisation vector in the xy-plane, precesses at the Larmor frequency, generating a rotating magnetic field that is capable of inducing an alternating voltage if a conductive receiver is placed nearby. Once the RF pulse is stopped, phase coherence is no longer maintained and protons begin to 'relax' back to a lower energy state and lose phase coherence by T_1 and T_2 relaxation.

1.3.1 Free induction decay

Once the RF pulse is stopped, both T_1 and T_2 relaxation occur. The protons continue to precess, but as they begin to re-align with the B_0 axis, the net magnetisation vector shrinks in the xy-plane and increases along the z-axis. With a receiver coil placed in the vicinity, the spiralling magnetisation vector generates an electrical signal known as the free induction decay.

1.3.2 T_1 relaxation

T_1 relaxation is associated with the restoration of longitudinal magnetisation and occurs as high energy state protons exchange energy with their surroundings to return to a lower energy state. T_1 is defined as the time taken for longitudinal magnetisation to return to 63% of its final value. The rate at which this occurs is dependent on the rate of motion of the molecules (tumbling rate) in which the proton resides. Energy exchange between protons and their surrounding molecules is more favourable when the tumbling rate matches the Larmor frequency of the proton. The tumbling rate is affected by the structure and size of a molecule and therefore different molecules have different tumbling rates, and therefore different T_1 relaxation times. Unrestricted water has a fast tumbling rate due to its small molecular size and as a result, energy transfer between protons and the surrounding molecules is not efficient. Therefore, longitudinal magnetisation takes a relatively long time to return and the T_1 of water is relatively long. Alternatively, fat molecules have a short T_1 because they are larger molecules with a tumble rate closer to the proton Larmor frequency. Given these inherent properties of various molecules, cerebrospinal fluid (CSF) is usually dark and white matter is usually brighter than gray matter in T_1 weighted images of the brain.

1.3.3 T_2 and T_2^*

T_2 and T_2^* relaxation are underpinned by the gradual loss of transverse magnetisation as protons lose phase coherence in the xy-plane. Other nuclei within a tissue possess their own magnetic field, thereby generating local inhomogeneities that can influence the magnetic spin of nearby protons. This causes individual protons to precess at different frequencies thereby leading to

a loss of phase coherence. This is known as T_2 relaxation or spin-spin relaxation since the 'spin' of neighbouring nuclei influences the 'spin' of nearby protons. T_2 is defined as the time for T_2 relaxation to decay to approximately 37% of its initial value.

T_2^* relaxation is also derived from magnetic field inhomogeneities however these arise due to inhomogeneities within the B_0 field. These may arise due to imperfections in the homogeneity of the magnet or due to susceptibility-induced distortions from tissue or other objects within the magnetic field. Given that the Larmor frequency is proportional to the magnetic field strength, inhomogeneities cause protons to precess at different frequencies within different locations of the magnetic field thereby resulting in a loss of phase coherence.

1.3.4 Gradient coils

Gradient coils controllably change the magnetic field and generate a gradient along a chosen axis. This subsequently results in protons having different Larmor frequencies along the gradient and therefore, specific precession frequencies will correspond to a spatial location along the gradient. Each gradient coil corresponds to an orthogonal direction (x, y, z). The three orthogonal directions that are used are, in standard imaging, referred to as slice selection, phase-encoding and frequency-encoding gradients and can be at oblique angles. The slice selection gradients induce a gradient along the z-axis. Then by applying a RF pulse across a range of frequencies, a slice the thickness of which can be varied by changing the upper and lower limits of the RF pulse frequency range or by altering the steepness of the gradient. Spatial localisation within the remaining x- and y-axis is similarly determined through the use of the frequency- and phase-encoding gradients.

1.4 Functional MRI

1.4.1 BOLD

Like many other neuroimaging techniques, fMRI takes advantage of neurovascular coupling by measuring changes associated with the local increase in CBF (hemodynamic response) to inform on changes in neural

activity. Specifically, the hemodynamic response elicited by increased neural activity alters the ratio of oxygenated and de-oxygenated haemoglobin, which subsequently alters the magnetic susceptibility of the blood.

Deoxyhaemoglobin is paramagnetic (Pauling and Coryell 1936) and causes local field inhomogeneities within the blood vessels, which subsequently shortens T_2^* . Thus the fMRI signal becomes dependent on the level of oxygenation of the blood and is therefore appropriately named the blood oxygenation level-dependent (BOLD) signal. Therefore, the BOLD signal provides an indirect measure of neuronal activity by measuring changes in the magnetic susceptibility of the blood associated with the coupled hemodynamic response.

The ability to use BOLD as an intrinsic contrast in MRI imaging was first identified by (Ogawa et al. 1990) who noted that changes in metabolic demand or blood flow induced by anaesthetics, hypoglycaemia or hypercapnia, resulted in changes to the BOLD contrast. Given that oxygen is extracted from the blood to support neural activity, it would be logical to assume that the T_2 signal decreases in an active brain area. However, as previously described in Section 1.1.5, the hemodynamic response that is coupled with increased neural activity is substantially surplus to the increased metabolic needs of the active brain area and therefore the concentration of deoxyhaemoglobin actually decreases, resulting in longer T_2 values and therefore the T_2 signal increases in active neural areas. The requirement for such a surplus increase in CBF in response to increased neural activity is not fully understood. Previous studies have suggested that this may be required to generate high gradients of oxygen to overcome the inefficient, passive diffusion of oxygen at high flow rates (Buxton and Frank 1997; Hyder et al. 1998). Others have suggested that the disproportionate increase in CBF is required to ensure tissue locations downstream of the activated area are still sufficiently oxygenated (Devor et al. 2011). Additionally, the increased CBF response may be required to remove heat generated during neural activity (Yablonskiy, Ackerman, and Raichle 2000). The relative delay in the hemodynamic response suggests that the additional substrates are not required for the initial needs of evoked neural activity.

The temporal profile of the BOLD response to a brief stimulus is well documented and referred to as the hemodynamic response function (HRF).

Following the presentation of a stimulus, the BOLD signal demonstrates a small decrease known as the initial dip, in which the increased metabolic demands of the stimulus-induced neural activity cause a local increase in oxygen metabolism and therefore an increase in deoxyhaemoglobin (Pauling and Coryell 1936). Following this, there is a rapid increase in the BOLD signal which generally starts 2-4 seconds post-stimulus and then peaks at approximately 6-9 seconds post-stimulus. The BOLD response then returns to baseline and in some instances a post-stimulus undershoot is observed. The underlying mechanism of the post-stimulus undershoot is not known, however delayed vascular compliance, sustained increases in $CMRO_2$ and post-activation reduction in CBF have all been suggested (van Zijl et al. 2012).

1.4.2 Physiological basis of the BOLD signal

The BOLD signal is an indirect measure of neural activity due to the phenomena of neurovascular coupling, however identifying the underlying mechanisms that link BOLD and neural activity has been a popular area of research since the discovery of the BOLD signal and is still ongoing. A substantial advancement in our understanding of the relationship between neural activity and BOLD came when simultaneous electrophysiology and fMRI were performed in the monkey visual cortex (Logothetis et al. 2001). When comparing several different electrophysiological measures, that included local field potentials (LFPs) and single- and multi-unit recordings, it was observed that LFPs highly correlated with the BOLD response while single- and multi-unit activity had lower correlations. LFPs are thought to provide a measure of synaptic activity, while single and multi-unit activity is indicative of neural spiking activity. Therefore, these findings suggested that the BOLD signal represented neural input and local processing within a local brain area as opposed to the spiking activity of a neuron.

1.4.3 Factors affecting the BOLD signal

The BOLD signal is the result of the interaction between neural activity and the cerebrovasculature and therefore any factors affecting either one or both of these measures can affect the resultant BOLD signal observed in fMRI and potential complicate interpretation of the data.

1.4.3.1 Carbon dioxide

CO₂ is known to be a potent vasodilator. Inhalation of 5-7% CO₂ has previously been shown to increase baseline CBF by 75% (Kety and Schmidt 1948). The underlying mechanism by which CO₂ mediates vasodilation is not completely understood. However, in the blood CO₂ and water diffuse into red blood cells where they are converted into carbonic acid (H₂CO₃) by carbonic anhydrase. Carbonic acid subsequently dissociates into hydrogen ions (H⁺) and bicarbonate (HCO₃⁻). H⁺ can activate voltage gated K⁺ channels, resulting in hyperpolarisation of the endothelial cells which reduces intracellular calcium and thereby induces vascular relaxation and increased CBF (Kety and Schmidt 1948). The increase in CBF induced under hypercapnic conditions results in an increase of oxyhaemoglobin and decreased deoxyhaemoglobin which results in a longer T₂^{*} (Kitazono et al. 1995; Kontos, Raper, and Patterson 1977). This subsequently leads to an increase in the baseline BOLD signal, which has been observed in both human and animal studies, where hypercapnia was induced by either breath-holding or breathing exogenous CO₂ concentrations (Kemna and Posse 2001).

The increase in baseline CBF and BOLD arising from the vasodilatory effects of CO₂ are associated with decreased stimulus-evoked CBF and BOLD responses (Sicard et al. 2005). Many studies assume that CO₂ challenges do not affect the underlying neural activity and therefore such observations relate solely to changes in the ability of the vasculature to respond. Indeed, early studies using MRI to assess oxygen consumption reported that CMRO₂ did not change under hypercapnic conditions (Posse et al. 1997), suggesting that neural activity was not affected by CO₂. However, later studies reported conflicting observations with some noting decreases in CMRO₂ (Kety and Schmidt 1948; Nilsson and Siesjö 1976) or neural activity (Kliefoth et al. 1979; Sicard and Duong 2005) in response to increased CO₂ while others reported increases (Balestrino and Somjen 1988; Zappe et al. 2008). The discrepancy in these observations may be underpinned by differences in methodologies and the species used, however an underlying mechanism for these observations has yet to be confirmed. In cases where neural activity was observed to increase under hypercapnic conditions, it has been suggested that the increased formation of carbonic acid

in response to increased CO₂ leads to a decrease in pH which reduces neural spiking and synaptic activity (Horvath et al. 1994; Jones et al. 2005). Indeed, mild acidosis has previously been reported to reduce neural activity in hippocampal cultures (Kliefoth et al. 1979; Balestrino and Somjen 1988). Collectively, these studies suggest CO₂ may affect neural activity as well as the hemodynamic response, however, given the various methodologies and species utilised in these studies, it is possible that such differences may have affected the results and therefore further investigation is required.

1.4.3.2 Anaesthesia

It is generally known that most anaesthesia exhibits a depressive effect on neural activity and CBF, which may introduce potential confounds interpreting the BOLD signal. Indeed, CBF responses to a hypercapnic challenge are larger in conscious animals compared to anaesthetised animals (Tombaugh and Sapolsky 1990). Additionally, NO inhibitors block the stimulus-evoked CBF response in anaesthetised animals but not in awake animals suggesting that the underlying mechanisms linking neural and hemodynamic responses may be affected by anaesthesia (Nakao et al. 2001). While most anaesthetics depress neural activity by affecting various components underlying neural transmission, their effects on the CBF response vary depending on the anaesthetic used. Commonly used anaesthetics in preclinical studies include α -chloralose, urethane, medetomidine, and volatile anaesthetics such as isoflurane. Generally, volatile anaesthetics are vasodilatory; isoflurane has been observed to dose-dependently dilate large cerebral and pial vessels (Brevard et al. 2003; Sicard et al. 2003). Additionally, baseline CBF is substantially lower in rats under isoflurane anaesthesia compared to pentobarbital or fentanyl (Iida et al. 1998). Such observations highlight the difficulty in comparing CBF and BOLD responses between studies utilising different anaesthetics as differences in response magnitude may be underpinned merely by differences in the anaesthetic used. Furthermore, the effect of various drugs on CBF may be confounded by the chosen anaesthetic. Cocaine administration was observed to cause a decrease in baseline CBF under isoflurane but an increase in baseline CBF under α -chloralose anaesthesia (Hendrich et al. 2001). Additionally, ethanol induced vasoconstriction in pial arteries under α -chloralose but vasodilation under halothane anaesthesia (Du et al. 2009). These observations

indicate various drugs can affect CBF differently, depending on the anaesthetic being used.

1.4.3.3 Ageing

Ageing is associated with various changes in the structure and functioning of the cerebral vasculature. Both human and animal studies have observed thickening of the vessel wall and basal membrane, narrowing of the arterial lumen (Nagasawa et al. 1979; Burns et al. 1981; Furuta et al. 1991; Alba et al. 2004), necrosis of medial smooth muscle cells (Knox et al. 1980; Masawa et al. 1994) and region-specific decreases in cerebral capillary density (Abernethy et al. 1993; Sonntag et al. 1997). Age-related alterations can also lead to the occlusion of venous structures (Moody et al. 1997). The development of blood vessel tortuosity has also been noted to occur with ageing, which can subsequently reduce or restrict blood flow to various areas of the brain, including deep white matter (Kawamura et al. 1993; Han 2012). Cerebral perfusion in frontal, temporal and parietal cortices is decreased in older, healthy individuals compared to younger individuals, an observation that was highly correlated with the development of leukoaraiosis around the anterior horns of the lateral ventricles (Kawamura et al. 1993). In addition to perfusion changes, mean blood flow velocity in anterior, middle and posterior cerebral vessels is also reduced in the older population (Krejza et al. 1999).

Given that the BOLD response largely arises from vasodilatory changes in cerebral vessels that increase CBF, it is unsurprising that structural changes that reduce vessel reactivity can impact functional responses. Indeed, reduced BOLD responses to visual and motor stimulation have been reported in older individuals compared to younger individuals (Hesselmann et al. 2001; Ances et al. 2009). Several studies have also reported decreased vessel reactivity to CO₂ in older individuals (Yamamoto et al. 1980; Ito et al. 2002; Leoni et al. 2017). Similarly, cerebral vessels excised from aged rats demonstrate reduced vasodilation to adenosine, acetylcholine and bradykinine (Mayhan et al. 1990; Jiang et al. 1992)..

Collectively, these studies show that age-related changes to the structure of the cerebrovasculature can affect functional responses and thereby introduce

potential confounds when using neuroimaging techniques that are dependent on the hemodynamic response as a measure of neural activity.

1.4.3.4 Disease

Alzheimer's disease

Alzheimer's disease (AD) is a chronic neurodegenerative disorder and the most prevalent form of dementia (Vinters 2015). The hallmark of AD is the accumulation of amyloid-beta (A β) in extracellular plaques and hyperphosphorylated tau protein in intracellular neurofibrillary tangles in the brain (De Strooper and Karran 2016). Traditionally, AD is considered to arise from neuronal and glial dysfunction, however, there is also substantial evidence that a vascular component contributes to AD pathology (Govindpani et al. 2019). A β is known to be vasoactive (Thomas et al. 1996) and mice overexpressing amyloid precursor protein (APP), the precursor to A β , demonstrate reduced baseline CBF and enhanced responses to vasoconstrictors (Niwa et al. 2001; Niwa et al. 2002). Furthermore, cerebral vessels in mice overexpressing APP demonstrate reduced vasodilation to acetylcholine and increased susceptibility to ischemic infarcts, an observation attributed to reduced endothelium-dependent vascular reactivity in ischemic areas at risk of infarct (Zhang et al. 1997). Attenuated stimulus-evoked CBF responses to somatosensory stimulation have also been observed in mice overexpressing APP and A β , with the level of attenuation reported to correlate with the concentration of A β (Niwa et al. 2000). Despite attenuation of the stimulus-evoked CBF response in this model, neuronal activity as assessed by glucose metabolism, was reported to remain similar to controls suggesting that the reduction in CBF response was due to vascular changes rather than neuronal (Niwa et al. 2000). Vascular changes in AD have also been shown to arise from the effect of A β on pericytes. A β has been observed to degrade pericytes and promote AD-like neurodegeneration (Sagare et al. 2013). Pericyte-deficient mice exhibit reduced microcirculation, baseline CBF and attenuated stimulus-evoked CBF responses to whisker stimulation (Bell et al. 2010). Collectively, these studies indicate that A β can affect the functioning of the cerebrovasculature and subsequently affect baseline CBF and stimulus-evoked responses. These could ultimately lead to the inaccurate assessment of fMRI measures, such as BOLD, in patients with AD. Indeed, resting state fMRI in AD patients has shown that the functional connectivity of BOLD fluctuations is

decreased compared to controls (Greicius et al. 2004; Sorg et al. 2007; Lim et al. 2014). However, such findings have been challenged by the observation that reductions in functional connectivity correlate with hypoperfusion and were independent from changes in glucose metabolism (Göttler et al. 2019).

Hypertension

It is well established that hypertension induces vascular changes that alter blood vessel structure. This vascular remodelling is generally classified as inward or outward remodelling to reflect decreases or increases in the lumen diameter, respectively (Mulvany 1999). Furthermore, remodelling can be hypertrophic (increase in cross-sectional area of vessel wall), eutrophic (no change in cross-sectional area of vessel wall) or hypotrophic (decrease in cross-sectional area of vessel wall). Generally, the effects of hypertension on the cerebral vasculature are similar to those observed with normal ageing, and observations are also similar between human and animal studies. Hypertrophy of smooth muscle cells and increases in collagen content lead to thickening of the arterial wall and narrowing of the vessel lumen in large cerebral arteries, resulting in an increase in vessel rigidity and vascular resistance (Baumbach and Heistad 1988; Pires et al. 2013). While this hypertension-induced vascular remodelling may be beneficial and reduce stress on the vessel wall and thereby protect downstream microvasculature (Heistad and Baumbach 1992), the loss of arterial elasticity can reduce the vasodilatory capability of the vessel. Indeed, blunted CBF responses to stimulation have been observed in hypertensive patients compared to normotensive controls (Jennings et al. 2005). Additionally, vessel reactivity to carbon dioxide is also reduced in hypertensive animals compared to normotensive controls (Tamaki et al. 1995; Nakajima et al. 2008). Collectively, these observations indicate that hypertension-induced vascular remodelling increases vessel stiffness and reduces vessel compliance, which subsequently reduces the ability of these vessels to dilate in response to appropriate stimuli.

1.5 Summary

The SHRSP is a valid model of cerebral SVD and demonstrates many disease characteristics observed in the human condition. However, to our knowledge, no study has yet evaluated the hemodynamic response in this animal model. Several fMRI studies in patients with cerebral small vessel disease have

observed blunted stimulus-evoked BOLD responses to visual and somatosensory stimuli, as well as vasodilatory stimuli (Pineiro et al. 2002; Dumas et al. 2012; Peca et al. 2013; van Opstal et al. 2017). This impaired hemodynamic response is likely attributed to dysfunctional endothelium which has been observed in SHRSPs and patients with cerebral SVD (Rajani et al. 2018). Furthermore, dysfunctional endothelium is associated with white matter pathology, and drugs that stabilise the endothelium have been shown to reverse the pathological endothelial cells and oligodendrocytes highlighting the endothelium as a therapeutic target. Therefore, assessing the BOLD response in animal models and patients with cerebral SVD may provide a marker of therapeutic efficacy. Indeed, several clinical trials have already used cerebrovascular reactivity with BOLD MRI as a primary endpoint to assess such efficacy (Lavallée et al. 2009; NCT01821118; NCT03082014). However, no study has yet evaluated the hemodynamic response in the SHRSP, a finding that could further strengthen the validity of this model and aid in the development and assessment of drug development in preclinical studies. Therefore, the main aim of the studies described in this thesis was to assess the hemodynamic response through the assessment of the stimulus-evoked BOLD and CBF responses. Given that the current monitoring of CO₂ in rodents relies on an invasive and discrete measure, we sought to establish a method of noninvasive and continuous monitoring through side-stream capnography to permit real-time recording of CO₂. Under a relatively, novel anaesthetic regime, we also sought to establish the optimal stimulation parameters for forelimb stimulation, given that such parameters should be optimised for different anaesthetic regimes, owing to their different effects on neural activity and the cerebrovasculature. Ultimately, these studies would then follow on to the assessment of the hemodynamic response in young and aged SHRSPs to evaluate whether the functional responses of this model align with those observed in the human condition.

Methods

2.1 Animals

In accordance with the Animals (Scientific Procedures) Act 1986, all experiments and procedures were carried out under license from the UK Home Office, working under Project Licenses 60/4449, P5A377AD5 and P6C83EF0 and personal license number I640B6D28. Surgical procedures pertaining to electrophysiology were carried out under Project License number 70/8163. Male SHRSP and WKY rats were obtained from inbred colonies in the Institute of Cardiovascular and Medical Sciences at the University of Glasgow. Male Sprague-Dawley rats were obtained from Harlan Laboratories, UK. All animals were allowed a 1-week acclimatisation period upon arrival before any experimentation. Animals were housed in standard laboratory cages with sawdust, sizzle nest and cardboard tubing. Animals were caged in maximum groups of 4. Food and water was available *ad libitum*. All animals were maintained on a 12 hour light/dark cycle. Surgical procedures were carried out by Robert Morgan, unless otherwise stated in the relevant study chapter methods section.

For all surgical procedures except those relating to electrophysiology (Section 4), rats were transferred from the animal housing unit in the veterinary research facility (VRF) to the surgical suites within the Wellcome Surgical Institute or the Glasgow Experimental MRI Centre (GEMRIC). For surgical procedures relating to electrophysiology, animals were transferred from the animal housing unit in the Cardiovascular Research Unit to the West Medical Building.

2.2 Surgical preparation

2.2.1 Aseptic technique

Aseptic techniques were adhered to for all surgical procedures as defined in the project license. Prior to surgery, surgical instruments were autoclaved along with other thermostable surgical consumables (e.g. swabs, gauze pads) and the bench top and corkboard were disinfected with 70% ethanol. The corkboard and sterile instruments were then set out on a sterile drape placed over the bench top. When multiple surgeries were performed in a single day, the surgical tools were scrubbed with Decon^R90, rinsed, dried and autoclaved again between surgeries. The corkboard and bench top were also disinfected and a new sterile drape was used. Clean gloves and a sterile gown were worn for all procedures.

Following induction of anaesthesia, the animal's hair at the intended surgical site(s) was shaved using electric clippers on a bench top distant to that intended for surgery. Prior to commencing any surgical procedure at the relevant surgical site, the skin was disinfected with a swab soaked in 0.5% w/v Chlorhexidine digluconate in 70% w/v ethanol solution (Hydrex^RClear, Ecolab)

2.2.2 Anaesthesia

Animals were initially placed in an anaesthetic chamber (Baxter Healthcare Ltd, UK) and anaesthesia was induced with 5% isoflurane in a mixture of oxygen and nitrous oxide at 30% and 70%, respectively. Sufficient depth of anaesthesia was assessed by lack of a withdrawal reflex when the footpad of the hindpaw was pinched. Following removal from the anaesthetic chamber, all animals underwent endotracheal intubation as described in Section 2.3.1. Ventilation parameters were generally set to 60-70 breaths/min with a stroke volume of 3-4 ml. Anaesthesia was maintained at 2% isoflurane in medical air (1L/min) supplemented with oxygen at 21 %.

The anaesthetic protocol followed in all surgical procedures was previously established in our lab (Hollyer 2016). Prior to the experiment, a stock solution of medetomidine (Domitor, Orion Pharma) was supplied at 1mg/ml and stored at room temperature. The animal was weighed and an aliquot of the stock solution was diluted in saline to 100 µg/kg/ml. A syringe containing 10 ml of

the medetomidine solution was then mounted onto a syringe pump (Fresenius Kabi, Injectomat MC Agilia®). For all non-MRI experiments, one end of a cannula was then attached to the mounted syringe and the other end to a butterfly needle. For all MRI experiments, the butterfly needle was replaced with a 16-gauge catheter.

Following all preparatory surgical procedures, the butterfly needle or catheter connected to the syringe pump was inserted into the subcutaneous space of the animal's shaved flank. A 0.5 ml bolus of medetomidine was administered. When blood pressure began to decrease (approx. 1-2 mins after bolus), the isoflurane was reduced to 1%. 15 minutes after the administration of the bolus, the subcutaneous infusion of medetomidine was started at 1 ml/hr and continued for the duration of the experiment.

2.2.3 Analgesia

For recovery experiments, buprenorphine was administered subcutaneously prior to the animal gaining consciousness, in addition to 2 ml of saline for hydration. Naropin was administered subcutaneously at the prepared surgical site prior to incision.

2.3. Surgical procedures

2.3.1 Endotracheal intubation

A loop of 2-0 suture thread was pinned to a corkboard and attached to the incisors of the anaesthetised rat. Once secured, the corkboard and the rat were lifted at a vertical angle so that the animal hung from its incisors with the mouth partially open. The tongue was pulled to one side using forceps and the oral cavity was dried using a cotton bud. A fibre optic light was positioned at the animal's neck to illuminate the larynx and upper trachea. A 16-gauge catheter attached to a guide wire was carefully advanced into the trachea before the guide wire was removed. The catheter was then connected to a volume-driven ventilator (Ugobasile, Harvard Bioscience). Correct placement of the catheter within the trachea was confirmed by observing synchronisation of chest expansion with the ventilator. In all non-recovery experiments, the catheter was secured in place by a 4-0 suture in the lip.

2.3.2 Arterial and venous cannulation

Arterial cannulation was required for physiological monitoring of an animal's blood pressure and heart rate using Biopac Acquisition software. It also enabled the sampling of arterial blood for analysis using a clinical blood gas analyser (RAPIDLab™ 248 System, Siemens). Venous cannulation was only required to administer a contrast agent in certain MRI experiments. Experiments involving venous cannulation have this noted in the relevant chapter methods section.

The procedure for carrying out arterial and venous cannulation is very similar for both respective vessel types. Therefore, unless otherwise stated, the reference to 'the vessel' in the following procedure will refer to both the femoral artery and femoral vein. The upper part of the animal's hindlimb was secured using stick tape and a small incision was made using blunt ended scissors in the inguinal area. After clearing connective tissue, the femoral artery, vein and nerve were carefully isolated from one another using forceps. Two 4-0 suture threads were loosely tied at the distal and proximal ends of the exposed vessel. The ligatures were pulled tight and secured to the corkboard using stick tape to restrict blood flow through the now raised area of the vessel. A small incision was made in the vessel using micro-scissors. A polythene catheter (0.93 mm internal diameter) connected to a 1 ml syringe containing heparinised saline was inserted into the vessel and advanced approximately 2 cm along the vessel. Both ligatures were then tightened and tied around the vessel and the catheter to secure it in place. Once secured, a small volume of blood was drawn back into the syringe to ensure that blood flow through the catheter was unobstructed. The catheter was then flushed with saline and connected to a transducer to enable real-time recording of blood pressure and heart rate. Excess thread from the suture was then removed and the incision closed using 4-0 suture thread to prevent the tissue drying out.

2.3.3 Needle electrode placement

Prior to placement of the electrodes, the animal's right forepaw was cleaned using a gauss pad soaked in 70% ethanol. The needle electrodes were then

inserted into the paw at the 2nd and 4th digits (Figure 2.1), and tape was then wrapped around the paw and electrode casing to secure in place.



Figure 2.1: Representation of a rat right forepaw. The red circles indicate the position at which the two needle electrodes were inserted.

2.3.4 Laminectomy and craniotomy

For electrophysiology experiments, a laminectomy and craniotomy were performed to expose the underlying spinal cord and brain for the placement of silver ball electrodes and subsequent recording of cord dorsal potentials (CDPs) and somatosensory evoked potentials (SEPs). The animal was placed on a corkboard and a rolled-up gauze pad was placed under the animal's chest thereby putting the animal in a hunched position, which allowed easier access to the spinal cord. A midline incision was made from upper cervical to upper thoracic regions and the skin retracted. The muscles overlaying the vertebral column were retracted or partially removed, if necessary, to expose the vertebral column. The posterior arches of C4-C6 vertebrae were carefully removed using small bone rongeurs to expose the underlying spinal cord.

Following the laminectomy, the animal was carefully transferred to a stereotaxic frame and secured using an incisor bar and ear bars. The rolled-up gauze pad was again placed under the animal's chest to maintain access to the spinal cord. Liquid paraffin was applied to the site of the laminectomy to prevent the cord from drying out.

A unilateral craniotomy of the left hemisphere was performed. A midline incision was made along the skull and using 4-0 suture thread, the skin was retracted and tension applied to raise the skin so that it would form a pool when liquid paraffin was later applied. The muscles overlying the skull were removed using a scalpel and forceps. A dental drill was used to thin a 5 x 5 mm area of skull until the surface vessels on the brain could be clearly seen. The area extended from -1 mm to 4 mm AP and 0 mm to 5 mm ML, relative to Bregma. Small bone rongeurs and watchmaker forceps were then used to remove the thinned area of skull, with care being taken to maintain the integrity of the dura. Liquid paraffin was applied to the surface of the brain.

2.3.5 Skull thinning

For laser speckling imaging, the skull was thinned prior to recording. The animal's head was secured in a stereotaxic frame using ear and tooth bars. A midline incision was made along the skull and the skin retracted and secured in place using 4-0 suture thread and sticky tape. The muscles overlying the skull

were removed using a scalpel and forceps. Using a dental drill, the frontal and parietal plates were thinned until the vessels on the surface of the brain were clearly visible and the skull flexed when light pressure was applied. Care was taken to ensure that the dura remained intact. During this process, saline was periodically applied to the exposed skull to clear away bone debris and to minimise any heating effect of drilling on the brain. Following skull thinning, a layer of paraffin oil (Johnson's baby oil, UK) was applied to the surface of the thinned skull to prevent it from drying out and ensure stable signal acquisition during imaging.

2.4 Magnetic resonance imaging

MRI experiments were performed using either a Bruker Biospec 7T, 30 cm system with a BGA12S2-HP 700 mT/m gradient insert or a Pharmascan 7T. Volume transmit coil with 4-channel phased array receive coil was used with both scanners. The scanner used in each study as well as details of the scanning protocol can be found in the relevant study chapter methods section.

Animals were anaesthetised, intubated and mechanically ventilated as described in Sections 2.2.2 and 2.3.1. The femoral artery was cannulated and if administration of a contrast agent was required, the femoral vein was also cannulated (Section 2.3.2). The animal was transferred to the MRI compatible Perspex cradle (Bruker Biospin) and placed prone, with the animal's head being secured using a tooth bar and ear bars. The animal's respiration rate was monitored using a pressure sensor (Graseby™) placed under the animal's chest, on the base of the cradle. Body temperature was monitored using a rectal probe and maintained using a water jacket placed over the dorsal surface of the animal connected to a closed circuit heated water system (Cole-Palmer Polystat). A four-channel phased array surface coil was placed over the animal's head and secured to the cradle. Respiration, heart rate and blood pressure were monitored using Biopac MP150 acquisition system and recorded using *AcqKnowledge* software.

2.5 Laser Speckle Contrast Imaging

Laser speckle contrast imaging (LSCI; PeriCam PSI HD system, Perimed, Stockholm, Sweden) was used to record real-time relative changes in cerebral

blood flow from the estimation of intravascular red blood cell movement. The penetration depth of the near infrared laser (785 nm) is approximately 500 μm below the thinned skull and therefore captures cerebral blood flow from cortical vessels located in the surface of the brain.

With the animal anaesthetised and secured in the stereotaxic frame, the laser speckle camera was positioned over the exposed and thinned skull at a distance of 10 cm. The camera's position was adjusted to ensure that the entire thinned skull was within the field of view and then secured in place. The temporal resolution was set to give an effective frame rate of 1 image per second, capturing 10 frames per second with averaging every 10 frames. The spatial resolution was set at 20 μm . Body temperature was monitored using a rectal probe and maintained using a thermo-coupled electric pad placed under the animals.

2.6 Recovery and post-operative care

2.6.1 Recovery following MRI

Only animals involved in the acute and chronic hypertensive studies were recovered (Chapter 5). As the following procedure applies to both the femoral artery and femoral vein, the term 'the vessel' will again be used to refer to both respective vessel types. Following surgery and scanning, the animal was removed from the MRI cradle and transferred back to the bench top.

Anaesthesia was maintained on 2% isoflurane in medical air (1 L/min) supplemented with oxygen at 21%. The suture thread holding the inguinal incision closed was cut to re-expose the underlying femoral vessels. The suture thread knots at the proximal and distal end of the vessel were loosened. The ligatures were pulled tight and secured in place using sticky tape. Using forceps to hold the vessel, the polythene catheter was carefully removed from the vessel. If necessary, the tension on the ligatures was re-adjusted as the polythene tubing was being removed to ensure there was no blood flow between the two ligatures. The incision in the vessel was sealed using diathermy forceps (Eschmann). The tension on the ligatures was slowly released to enable reperfusion of the hindlimb. Upon confirmation of successful reperfusion and the absence of any bleeding from the vessel, the ligatures around the proximal and distal ends of the vessel were removed and the inguinal incision was sutured closed using 4-0 thread.

Upon completion of the surgical procedure, 1 ml of Antisedan (Dosage, Brand) was administered subcutaneously and the isoflurane turned off. The ventilator was kept on until the animal showed signs of breathing on its own. At this point, the ventilator was switched off, the intubation tube removed and the animal was placed on a facemask with 21% oxygen only. The animal was then given a 1 ml subcutaneous bolus of saline (0.9%) and upon displaying additional signs of recovery (swallowing, blinking, pinch reflex), the animal was transferred to a cage lined with AD pads. The cage was placed in a designated recovery room and the animal was provided with softened food pellets in a plastic weighing boat. The animal was checked and weighed daily for the remainder of the recovery period (1 week). Softened food pellets were again provided on the day following surgery and the animal continued to have access to food and water *ad libitum*. If an animal's weight dropped by 25% of the pre-operative body weight, the Named Animal Care and Welfare Officer (NACWO) or Named Veterinary Officer (NVO) were to be notified and the animal's welfare and future assessed, as outlined in the Project license.

2.6.2 Perfusion fixation

At the end of the study, animals involved in the acute and chronic hypertension MRI studies were transcardially perfused with fixative for future histological analysis. Animals were transferred to a tray lined with absorbent pads, deeply anaesthetised with 5% isoflurane in a mixture of oxygen and nitrous oxide (30:70) and maintained on a facemask. The chest cavity was exposed by an initial incision at the sternum using blunt ended scissors. The diaphragm and ribcage were then cut and the ribcage retracted. The heart was loosely grasped with Halsted Mosquito forceps and a blunt 16 gauge needle attached to a perfusion-fixation set up was inserted into the apex of the heart and advanced into the aorta. During needle insertion, the perfusion-fixation set up was running heparinised saline (10 ml/l) at a pressure of 80-100 mmHg. Once satisfactory placement of the blunt needle tip in the aorta was achieved, the forceps were clamped to secure the needle in place and the right atrium cut to allow complete exsanguination. When saline draining from the cut atrium was clear of blood, paraformaldehyde (PAM; 4% in 50 mM phosphate buffer) was perfused at the same pressure and continued until spontaneous

movement ceases and tissue rigor were achieved (after approx. 200 - 300 ml). The animal was then decapitated and the head immersed in 4% PAM for a minimum of 24 hours. The brain was then removed and again immersed in 4% PAM until batch embedding.

2.7 Tail cuff plethysmography

To confirm the normotensive and hypertensive phenotypes in WKYs and SHRSPs, respectively, it was necessary to monitor systolic blood pressure in conscious animals. The tail cuff method use followed in the relevant study has previously been described (Tarr 2012). The tail cuff method to measure systolic blood pressure involves the placement of an inflatable cuff around the rat's tail which is inflated until the pressure matches that of the tail artery and transient occlusion of the vessel is achieved. A signal transducer placed around the rat's tail distal to the tail cuff, detects the absence of a pulse in the tail following occlusion and signals the central monitoring system connected to a laptop (Dell, UK). The pressure at which this occurs is recorded and displayed as the systolic blood pressure in mmHg. The cuff is then deflated.

2.7.1 Acclimatisation training

Prior to the recording of systolic blood pressure via tail cuff plethysmography, animals were subjected to a 2-day acclimatisation period to acclimatise them to the tail cuff procedure. On the first day, the animals were taken into the room where the tail cuff apparatus was kept and were removed from their cage and allowed to explore the table where tail cuff measurements would take place and where the apparatus was set up. After 5-10 mins, the animal was also wrapped in a towel and mildly restrained to mimic the tail cuff procedure. The animal was also placed in the heating box that would be used warm the animal to ensure maximal vasodilation of the tail artery. However, on this first instance, the animal was merely placed in the box and allowed to explore, without any heating. The animal was also handling throughout this session which generally lasted 20-25 minutes. On the second day, the same procedure was followed as described on the first day, however in this instance, the heating box was switched on and heated to approx. 34°C. The tail cuff and transducer were also positioned on the animals tail during mild restraint.

2.7.2 Systolic blood pressure measurements

Systolic blood pressure was measured 1-3 days prior to animals undergoing MRI scanning. Prior to transferring the animals into the room with the tail cuff apparatus, the heating box was switched on and warmed to approx. 34°C and the tail cuff apparatus set-up and laptop switched on. The tail cuff consisted the medial portion of a 5 ml syringe that had been cut to a length of 2 cm, in which a 6 cm length (1.5 cm width) of latex tubing was inserted. A 10-gauge catheter cut to a length of 4 cm was inserted and secured in the tubing by tying 5-0 thread. The opposite end of the tubing was folded over the outer surface of the syringe and secured in place using a plastic O-ring. The catheter was then connected to the central monitoring system that was also connected to a cylinder of medical air (BOC Gases, UK) via a hose, a piezoceramic transducer and a laptop (Dell, UK).

Prior to systolic blood pressure measurements, animals were placed in the pre-warmed heat box for 10-15 mins. Animals were checked periodically during this time. The rats were considered ready for blood pressure measurements when there was little spontaneous activity and the ears appeared pink. Once this was achieved, the animal was removed from the heating box, wrapped in the towel with the tail exposed, and the tail cuff and transducer positioned on the tail. The laptop was then used to control the inflation and deflation of the tail cuff in cycles and record the systolic blood pressure. In cases where a blood pressure reading could not be obtained, the animal was placed back into the heating box for 3-5 minutes. The cycles of inflation and deflation were repeated until 10 consistent measurements were acquired. Measurements recorded while the animal was visibly stressed were excluded. After the successful acquisition of 10 consistent measurements, the animal was returned to their home cage.

Establishing non-invasive monitoring of PaCO₂ for functional imaging using micro-sampling side-stream capnography

3.1 Introduction

The sensitivity of the BOLD signal to physiological variables, in particular CO₂, requires that these variables be monitored and maintained within normal physiological limits during fMRI experiments. The lack of careful monitoring risks introducing variability into the data which can reduce statistical power and thereby complicate interpretation of the BOLD signal. Furthermore, non-invasive monitoring of an animal's vitals is preferable for recovery experiments. In this chapter we investigated the ability of micro-sampling side-stream capnography to provide a non-invasive surrogate measure of the partial pressure of arterial CO₂ (PaCO₂) by analysing end-tidal CO₂ (ETCO₂) in the anaesthetised rat. We compare ETCO₂ with PaCO₂ to evaluate the side-stream capnography method and assess the effect of varying the PaCO₂ on the stimulus-evoked BOLD signal.

3.1.1 Carbon dioxide and the BOLD signal

It is well known that CO₂ is a potent vasodilator and that variation in the level of arterial CO₂ affects the baseline and stimulus-driven fMRI time series (Kety and Schmidt 1948). Exogenous CO₂ challenges and breath-holding challenges in animals and humans have clearly demonstrated that increases in PaCO₂ evoke an increase in the baseline BOLD signal intensity, an observation that is largely underpinned by CO₂-associated increases in CBF and CBV (Rostrup et al. 1994; Stillman et al. 1995; Kastrup et al. 1999; Li et al. 1999; Corfield et al. 2001;

Brevard et al. 2003; Sicard and Duong 2005). Alternatively, hyperventilation-induced hypocapnia has been observed to decrease the baseline BOLD signal intensity (Posse et al. 1997; Posse et al. 2001). Small fluctuations in PaCO₂ have also been observed to cause statistically significant low frequency BOLD signal fluctuations (Wise et al. 2004). This observation is especially important to consider for resting state fMRI, which probes temporally coherent low-frequency BOLD signal fluctuations to identify functional neural networks.

The stimulus-evoked BOLD response is also affected by variations in CO₂ with most studies observing an inverse relationship where increased PaCO₂ results in smaller stimulus-evoked responses (Wong and Bandettini 1997; Cohen et al. 2002; Stefanovic et al. 2006). However, it is unclear at what level of PaCO₂ the stimulus-evoked BOLD response is affected with some studies in rodents reporting changes only at severe hypocapnic and hypercapnic conditions (Weckesser et al. 1999; Kemna and Posse 2001; Posse et al. 2001; Sicard and Duong 2005). It is possible that differences in experiment methodologies, in particular the choice of anaesthetic, contribute to the lack of consensus in determining the level of PaCO₂ at which the BOLD response is affected. A systematic review of adults found that individual anesthetic agents differed in their degree of reactivity to hypercapnic and hypocapnic stimuli, with reactivity being highest under isoflurane and lowest under propofol (Mariappan et al. 2015). Given that the BOLD response is dependent on changes in the cerebrovasculature, any compounded effects of CO₂ and anaesthesia on vessel reactivity could affect the BOLD response.

Some human fMRI studies have also observed no difference in the stimulus-evoked BOLD response between normal and hypercapnic conditions (Corfield *et al.*, 2001; Whittaker *et al.*, 2016). However, such observations may arise due to the experiments being performed in conscious participants which can introduce potential confounds related to participant tolerance, sensitivity to hypercapnia and various involuntary changes to counteract CO₂ increases. Collectively, these findings highlight the importance of monitoring and maintaining PaCO₂ within normal physiological limits when performing fMRI.

3.1.2 Monitoring carbon dioxide

The current gold standard for monitoring PaCO₂ in animals is via blood gas analysis (Huttmann et al. 2014). This involves removing a small sample of arterial blood (50–100µL), which is then passed through a blood gas analyser to provide a measure of the current PaCO₂, as well as informing on the partial pressure of arterial oxygen (PaO₂), blood pH and several other parameters. However, these measurements are invasive and discrete, providing a blood gas profile only relevant for a short period of time after the sample is withdrawn. Therefore, over the course of a typical fMRI experiment, it may become necessary to take multiple blood samples for analysis to ensure that blood gases are within normal physiological limits and to avoid introducing confounds into the data. This is not ideal as there are limits to the amount of blood that can be withdrawn and withdrawing arterial blood is associated with increased risk of infection and thrombosis (Diehl et al. 2001).

Capnography overcomes the limitations of arterial blood gas analysis and provides a non-invasive method to continuously probe arterial CO₂ by analysing ETCO₂ as a surrogate measure. End-tidal CO₂ is the partial pressure of CO₂ expelled at the end of expiration and provides the closest representation of the expired gases coming from the alveoli and therefore the blood. Under normal conditions ETCO₂ and PaCO₂ are closely correlated, with ETCO₂ typically being 2 - 5 mmHg lower than PaCO₂. This difference between the two measures, known as the PaCO₂-ETCO₂ gradient, arises because not all inspired air participates in gas exchange due to physiologic dead space (Intagliata and Rizzo 2018). Physiologic dead space is defined as the sum of anatomical dead space, referring to the conducting airways that do not participate in gas exchange, and alveolar dead space that refers to ventilated alveoli that are not well perfused. In healthy adults, the alveolar dead space is generally considered negligible and therefore physiologic dead space is equivalent to anatomic dead space (Intagliata and Rizzo 2018).

3.1.3 Mainstream capnography and side-stream capnography

The foundation of capnography is based on the observation that CO₂ molecules strongly absorb infrared (IR) light at a wavelength of 4.3 µm. The amount of light absorbed is proportional to the CO₂ concentration. Therefore, by allowing

a sample of gas to pass between an IR source and a photodetector, the IR intensity before and after passing through the gas can be compared, and the partial pressure of CO₂ calculated.

There are two main types of capnography that are categorised based on the position of the CO₂ sensor in the ventilation pathway (Block and McDonald 1992). Mainstream capnography places the sensor at the airway in line with the respiratory gas stream, typically attaching between the breathing circuit and intubation tube in anaesthetised patients (Figure 3.1A). The proximity of the sensor to the airway permits real-time measurements of ETCO₂. The signal from the sensor is then passed to a unit where the ETCO₂ value and CO₂ waveform (capnogram) are displayed. Sidestream capnography places the CO₂ sensor in a unit remote to the participant, with a sample of the individual's respired gases being constantly diverted from the sampling site to the sensor through a sample tube (Figure 3.1B). Similar to mainstream capnography, the sample site is typically located between the breathing circuit and intubation tube in anaesthetised patients, with the sample line being connected using a T-piece adapter. In awake individuals, a nasal catheter can be used to sample expired gases. Due to the sensor being distant to the sample site in side-stream capnography, ETCO₂ measurements do not occur in real-time but rather suffer a time delay. This delay is dependent on several factors such as sample tube length and sample rate and may result in the displayed ETCO₂ value and capnogram being out of phase with respiration.

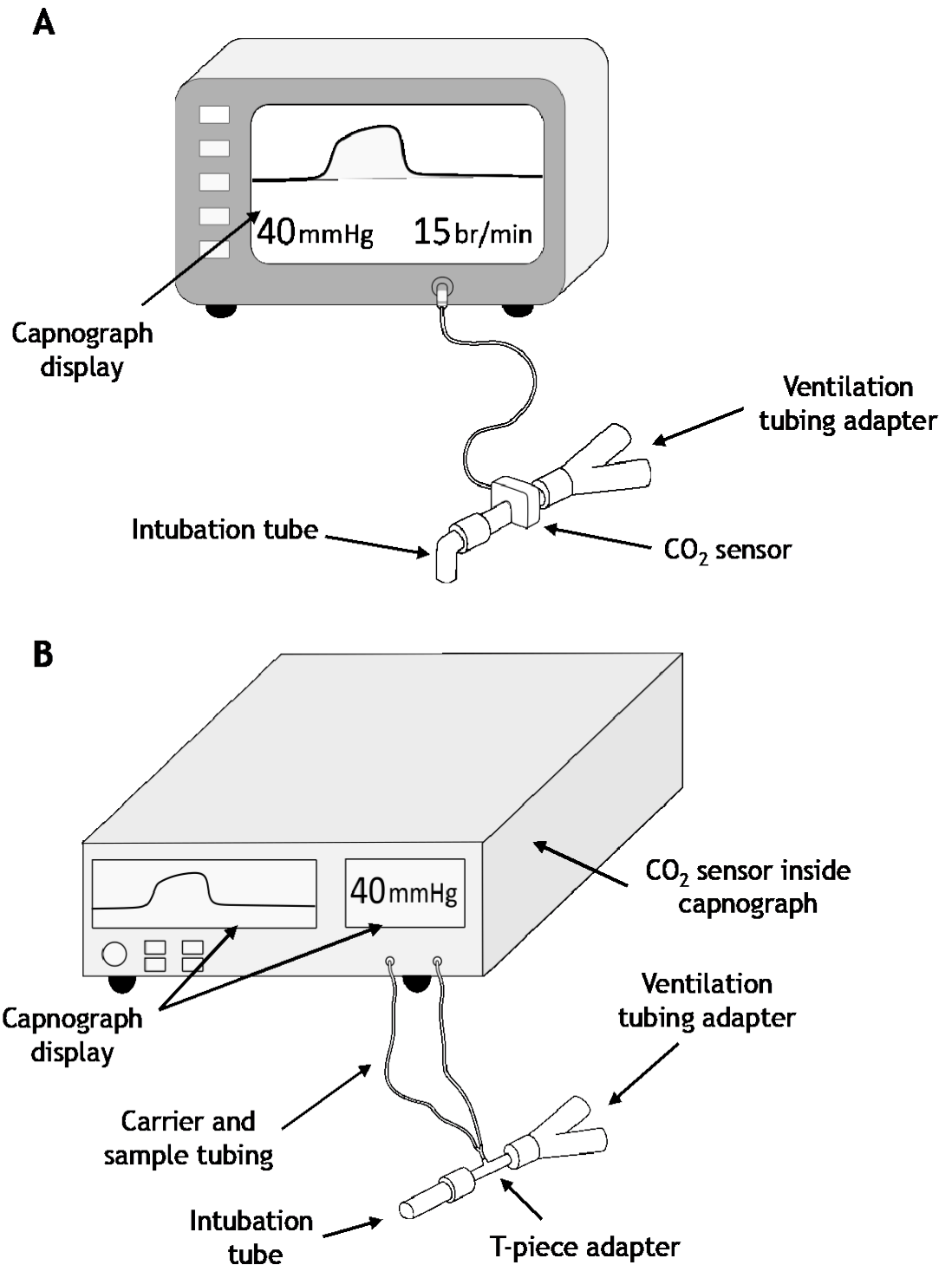


Figure 3.1: Overview of the two main types of capnography. In (A) mainstream capnography, the CO₂ sensor is placed in-line with the respiratory gas stream, between the intubation tube and breathing circuit. (B) Sidestream capnography continuously withdraws a sample of expired air and transports it back to the capnograph where it is analysed.

One significant advantage of sidestream capnography is that it can be used in an MRI setting. Due to components within the CO₂ sensor being MRI-incompatible, the sensor cannot be placed within a magnetic field as would be required when attempting to use mainstream capnography in an MRI experiment. However, a side-stream capnography set-up allows all MRI-incompatible components to be placed outside the magnetic field while maintaining the ability to divert expired air from the participant/animal through a long sample tube to the sensor. However, the fundamental design of side-stream capnographs introduces several issues that can lead to the observation of inaccurate and unreliable ETCO₂ values. Diffusion-driven dispersion of the sample gas as it travels through the sample tubing can lead to inaccurate ETCO₂ values (Epstein et al. 1980). Additionally, high sample rates and high flow rates of supplementary gases can lead to the dilution of the sample and result in the observation of low, false ETCO₂ values (Jaffe 2002; Marshall 2004). Loose fittings and cracks within the sample tubing and sample filter can also lead to the entrainment of ambient air and cause dilution of the expired gas sample, leading to the observation of low ETCO₂ values and abnormalities within the capnogram (Body et al. 2000; Tripathi and Pandey 2000; Zupan et al. 2006). Most of these issues are also exacerbated by long sample tube lengths and when used in animals with small tidal volumes.

Micro-sampling side-stream capnographs represent a sub-category of side-stream capnographs that are considered more appropriate for use in animals with small tidal volumes because they operate with smaller sample rates than standard capnographs. This minimises the sampling of supplementary gases and dilution of the expired gas sample that would otherwise occur with larger sample rates in mechanically ventilated small animals. However, establishing side-stream capnography in a preclinical MRI setting requires the use of long sample lines, which may still introduce challenges when attempting to accurately measure ETCO₂.

3.1.4. Study aims

The ability to accurately and non-invasively monitor PaCO₂ using ETCO₂ as a surrogate measure in rodents would benefit our planned fMRI study (Chapter 5) by minimising the amount of invasive preparatory surgery required to monitor blood gases and allowing continuous monitoring of PaCO₂. Given that cerebrovascular reactivity may vary depending on the type of anaesthetic used, and the current lack of studies assessing the effects of CO₂ on the BOLD signal under a combined medetomidine-isoflurane anesthesia, the aims of the studies included in this chapter were to:

- 1) Assess the ability of microsampling side-stream capnography to non-invasively monitor ETCO₂ as a surrogate measure for PaCO₂ in the anaesthetised rat
- 2) Assess the effect of varying the PaCO₂ on the stimulus-evoked BOLD response under combined medetomidine-isoflurane

3.2 Methods

3.2.1 Study 1 - Non-invasive monitoring of PaCO₂ using side-stream capnography to measure ETCO₂

3.2.1.1 Animals

Naïve, male Sprague Dawley rats weighing between 350–500g were used in this pilot experiment. Experiments were carried out on the benchtop with the animal lying prone to simulate the position of the animal when lying in the MRI cradle during scanning. All experiments were non-recovery.

3.2.1.2 Anaesthesia

Animals were anaesthetised as described in Section 2.2.2, and the femoral artery cannulated as outlined in Section 2.3.2.

3.2.1.3 Side-stream capnography

Two different capnographs were trialled in this experiment, the MicroCapStar (CWE Instruments) and the C1240 Micro Capnograph (Columbus Instruments).

MicroCapStar

ETCO₂ measurements using the MicroCapStar involved 4 different set ups using 2 different sample line lengths and 2 different sample sites within the ventilation pathway. These consisted of:

1. 1 m sample line sampling between the intubation tube and breathing circuit (n = 4)
2. 1 m sample line sampling from exhalation line only (n = 4)
3. 7 m sample line sampling between intubation tube and breathing circuit (n = 3)
4. 7 m sample line sampling from exhalation line only (n = 4)

The 1 m sample line is the standard length supplied with the capnograph and was used to confirm whether ETCO₂ could accurately monitor PaCO₂ in a benchtop experiment setting using a short sample line. It was assumed that any effects of line length would be minimised using this length of sample tubing and therefore act as a 'proof of concept' if accurate measurements were successfully recorded. The 7 m sample line was the required length for

use in an fMRI experiment, with the capnograph being placed outside the magnet room and the sample line reaching into the magnet and was therefore used to assess whether ETCO_2 could accurately monitor PaCO_2 in a MRI experiment. While sampling between the intubation tube and ventilation tubing is the recommended position as per the manufacturer's instruction, sampling from the exhalation line only was also investigated because when assessing the various set-ups in an MRI setting, it was noted that the design of our MRI cradle and position of the transmit/receiver coil when scanning would cause the sample tubing to kink and obstruct airflow when placed at the recommended sample site. However, sampling from the exhalation line would not encounter these issues. Therefore, if the ETCO_2 values achieved when sampling from the exhalation line were similar to those from the recommended sample site, then we could easily sample from the exhalation line and still achieve reliable and accurate ETCO_2 readings. If not, we would need to consider significant modifications to our MRI cradle to facilitate sampling from the recommended position.

When the sample site was located between the intubation tube and ventilation tubing, a T-piece adapter was used to connect the intubation tube, sample line Y-piece adapter and ventilation Y-piece adapter (Figure 3.2A). This is the recommended sampling position as it minimises the additional dead space and therefore, we will henceforth refer to this sampling site as the recommended sampling site. The distance between the end of the intubation tube and the sample line adapter in this set-up was approx. 10 mm. When the sample site was located in the exhalation line, the sample line Y-piece adapter was placed in a small hole in the exhalation line of the ventilation tubing (Figure 3.2B). A small amount of modelling clay (Plasticine, UK) was placed around the sample line adapter and secured in place, providing a seal to prevent the sampling of any ambient air. When secured in place, the distance between the end of the intubation tube and sample line adapter was approx. 22 mm. The measurements for the 1 m sample tubing were 0.79 mm internal diameter, 2.38 mm outer diameter with a wall thickness of 0.79 mm. When this tubing size was tested at a length of 7 m, the MicroCapStar was unable to maintain sufficient flow and encountered a pump error. Therefore we were unable to use this tubing size at a 7 m length but rather had to use tubing with an

internal diameter of 1.27 mm, an external diameter of 2.29 mm and a wall thickness of 0.51 mm.

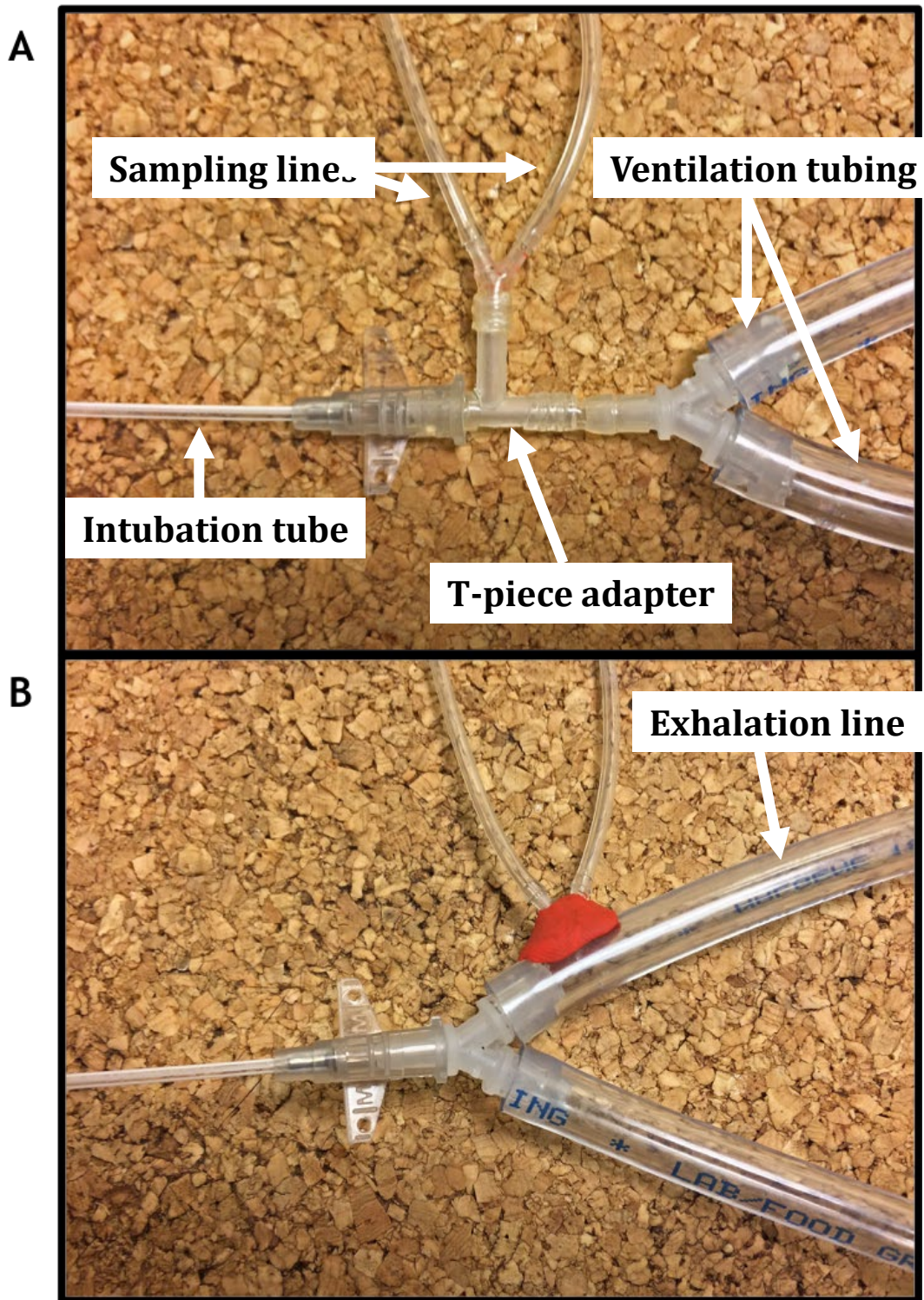


Figure 3.2: Overview of the two sampling sites used with the MicroCapStar. For the recommended sample site (A), the sampling line was integrated into the ventilation circuit via a T-piece connector joined to intubation tube and ventilation tubing. For the exhalation line only site, (B) the sampling tubing Y-piece was inserted into the exhalation line via a small hole and sealed via Plasticine.

At the start of each experiment, the sampling rate was set at 7.5 cc/min, which was recommended to be suitable for small animals according to the manufacturer's guidelines, with averaging set to every 4 breaths. The MicroCapStar zero value was set using room air and calibration was achieved using 5% CO₂ prior to the start of each experiment. Correct calibration was re-confirmed at the end of each experiment using 5% CO₂.

C1240 Micro Capnograph

Due to the design of the C1240 Micro Capnograph, ETCO₂ measurements were made using two different sample line lengths, each with a unique sample rate:

1. 1 m sample line sampling at 20 ml/min
2. 5 m sample line sampling at 5 ml/min

Due to the design of the C1240 Micro Capnograph sample line tubing, ETCO₂ measurements were only sampled from the expiration line. Animals that were monitored by the C1240 Micro Capnograph were trialled on both sample line lengths (n = 5). Prior to the start of each experiment, the Micro Capnograph zero value was set using room air and calibration was performed using 5% CO₂. The 1 m and 5 m sample tube lengths were chosen as these were the shortest and longest lengths available, respectively.

3.2.1.4 Measuring ETCO₂ and PaCO₂

ETCO₂ and PaCO₂ measurements were both taken every 15 minutes and 4 - 5 measurement pairs were taken in total for each animal. Prior to taking a blood sample for blood gas analysis, the ETCO₂ measurement displayed on the capnograph was recorded. A blood sample was then taken and passed through the blood gas analyser (RAPIDLab™248 System, Siemens) and the PaCO₂ measurement recorded.

3.2.1.5 Data analysis

The agreement between PaCO₂ and ETCO₂ measurements was assessed using the Bland-Altman comparison method (Bland and Altman 1999). Bland-Altman analysis is commonly used to assess agreement between two methods that typically measure the same variable. Generally, this analysis is used to

compare a novel measurement technique with a 'Gold Standard' technique that is known to acceptably measure the variable of interest. Since there will always be some difference between measurements by two different techniques, Bland-Altman analysis aims to quantify how much two methods differ on average (bias) and define boundaries within which most (95%) of those differences fall, referred to as the 95% limits of agreement (LOA). The user is then required to interpret whether the average difference and range of differences between the two methods are acceptable.

In our experiment we collected multiple measurement pairs for each animal. The standard Bland-Altman comparison method is appropriate when only one measurement from each method per participant/animal is collected (Bland and Altman 1999). Therefore, we adopted the Bland-Altman comparison method for multiple observations (Bland and Altman 2007). This method takes into consideration variances for the repeated difference between the two methods on a single subject and for the differences between the averages of the two methods across subjects.

Both the standard and multiple observations Bland-Altman comparison methods assume there is no correlation between the average of the two methods and the difference between those two methods. In cases where this is violated, proceeding with the analysis would result in the generation of LOA that are wider than the true LOA. The suggested method for analysing data that violates this assumption is to model the variance in the standard deviation using residuals from linear regression (Bland and Altman 1999). However, this approach assumes there is only one observation for each method per participant/animal. To our knowledge, there is currently no suggested approach for dealing with data that consists of multiple observations data and that violates the assumption of no correlation. Therefore, to analyse such data with a regression-based approach would require ignoring the multiple observations and treating each observation as if it were individual. This would generate LOA that are narrower than the true LOA. However, if both the multiple comparisons method and the regression-based approach are performed on any data that violated the assumption of no correlation, this would generate two sets of LOA, one that is narrower and another that is wider than the true LOA. From these limits, we could assess where the true LOA may

lie and come to an informed conclusion as to whether those limits would be acceptable. Therefore, in addition to using the Bland-Altman comparison method for multiple observations, a regression-based approach was also adopted in cases where the data both:

- Violated the assumption that there is no correlation between the average of the two methods and the difference between the two methods
- The correlation could not be removed by logarithmic transformation of the data

The regression-based approach does not provide a discrete upper and lower value for the LOA like those produced in the multiple comparisons approach. Rather, the LOA vary over the range of the measurements to accommodate the correlation within the data, thereby making it difficult to compare the LOAs between the two methods. However, we can calculate the difference between the upper and lower LOA to define the effective range of the LOA for both analysis approaches, which can then be compared.

Statistical advice for this study was sought from Dr J. McClure, Institute of Cardiovascular and Medical Sciences, University of Glasgow.

A power analysis was not performed for the Bland-Altman plot as it is generally accepted that the two measures being compared are different, the aim is to quantify by how much these two measures vary and whether this is clinically acceptable.

3.2.2 Study 2 - Evaluating the effects of varying PaCO₂ on the stimulus-evoked BOLD signal

3.2.2.1 Animals

In this pilot experiment naïve, male WKY rats (n=4) weighing between 250-360 g were used. Experiments were performed in a Bruker Biospec 7T/30 cm system with a BGA12 integrated 400 mT/m gradient (ID) system. The anaesthetic protocol followed in this experiment is outlined in Section 2.4. Once the animal was secured in the MRI cradle, two needle electrodes were inserted into the animal's right forepaw, as described in Section 2.3.3.

3.2.2.2 Stimulation parameters

Forepaw stimulation was achieved using a Grass S48 square pulse stimulator with output running through a constant current unit. The stimulation intensity was set at 6 mA, the pulse width at 0.3 ms and the pulse frequency at 3 Hz. These stimulation parameters were chosen based on the most commonly reported values in the literature that were most relevant to our anesthetic protocol (Gyngell et al. 1996; Silva et al. 1999; Keilholz et al. 2004; Liu et al. 2004; Sangannahalli et al. 2008; Zhao et al. 2008). The stimulation protocol consisted of a block design with 6 on-off blocks where the stimulus was on for 22 s and off for 38 s. There was a 10 s baseline period prior to the start of the first stimulus once scanning was started.

3.2.2.3 Monitoring and varying PaCO₂

PaCO₂, PaO₂ and blood pH levels were monitored using a blood gas analyser (RAPIDLab™248 System, Siemens). Hypocapnic, normal and hypercapnic conditions were induced by varying the ventilation frequency. Hypocapnia was defined as a PaCO₂ below 35 mmHg, the normal condition was defined as a PaCO₂ between 35 - 45 mmHg and hypercapnia was defined as a PaCO₂ above 45 mmHg. A small blood sample was withdrawn and analysed prior to each stimulus-evoked fMRI scan to ensure the blood gas profile was within the desired parameters. All animals were subjected to all three conditions and the order of the conditions was randomised. Following hypocapnic and hypercapnic conditions, the animal's blood gas profile was allowed to recover to within normal PaCO₂ limits for 5 mins before the next condition was started.

3.2.1.4 Data analysis

Functional MRI data was initially analysed in MATLAB using in-house scripts. Significantly activated voxels were calculated using a t-test thresholded at $p < 0.05$. A cluster threshold was applied to the resultant probability maps to remove single voxels of activation. The time courses for the remaining significant voxels were then extracted, normalised to the pre-stimulus baseline and averaged to produce a single time course for each run. The data was then imported to Graphpad Prism (Version 6) where the integral and peak BOLD responses for each condition were calculated and statistically analysed by one-

way repeated measures ANOVA. Pairwise comparisons between the 3 conditions were assessed using Tukey's multiple comparisons test.

A post-hoc power calculation indicated that there was a 30.0% probability of correctly rejecting the null hypothesis (Effect size f , 0.43; α error probability, 0.05; correlation, 0.5; nonsphericity, 1). To achieve a 95.0% probability of correctly rejecting the null hypothesis a sample size of 16 would be required.

3.3 Results

3.3.1 Study 1 - Non-invasive monitoring of PaCO₂ using side-stream capnography to measure ETCO₂

3.3.1.1 Agreement between ETCO₂ and PaCO₂ using the MicroCapStar

Agreement between PaCO₂ and ETCO₂ when assessed by the MicroCapStar with a 1 m sample line sampling between the intubation tube and breathing circuit produced a bias of 4.13 mmHg, indicating that on average PaCO₂ was 4.13 mmHg higher than ETCO₂. The 95% LOA were calculated to range from -1.98--10.25 mmHg (Figure 3.3A). This gave an effective range of 12.23 mmHg between the upper and lower limits. However, this data set violated the assumption of the absence of a correlation between the average and the difference of the two methods indicating that these LOA are wider than the true LOA. A regression-based analysis approach resulted in LOA with a slightly narrower range of 10.28 mmHg (Figure 3.3B), indicating the range between the true LOA lies between 10.28 and 12.23 mmHg.

When the 1 m sample line sampled from the exhalation line only, we observed a larger bias of 6.19 mmHg, compared to that observed when sampling from between the intubation tube and ventilation tubing. The 95% LOA were also wider, ranging from -5.33 to 17.71 mmHg and giving an effective range of 23.04 mmHg (Figure 3.4A). This data set also violated the assumption of the absence of a correlation. A regression-based analysis approach gave a narrower effective range of 14.03 mmHg (Figure 3.4B), indicating the range between the true LOA is between 14.03 and 23.04 mmHg.

Assessing the agreement between PaCO₂ and ETCO₂ when using the MicroCapStar with the longer 7 m sample line and sampling at the recommended sampling site resulted in a large bias of 17.18 mmHg. The 95% LOA were also considerably large and ranged from 2.97 to 31.39 mmHg, giving an effective range of 28.42 mmHg (Figure 3.5). This data set did not exhibit a correlation between the average and the difference between the two methods, and therefore a regression-based analysis was not conducted.

When the 7 m sample line length sampled from the exhalation line only, we observed a bias of 9.29 mmHg and LOA between -0.73 and 19.31 mmHg, giving an effective range of 20.04 mmHg (Figure 3.6A). This data set violated the

assumption of the absence of a correlation and therefore a regression-based analysis gave a slightly smaller effective range of 15.40 mmHg (Figure 3.6B)

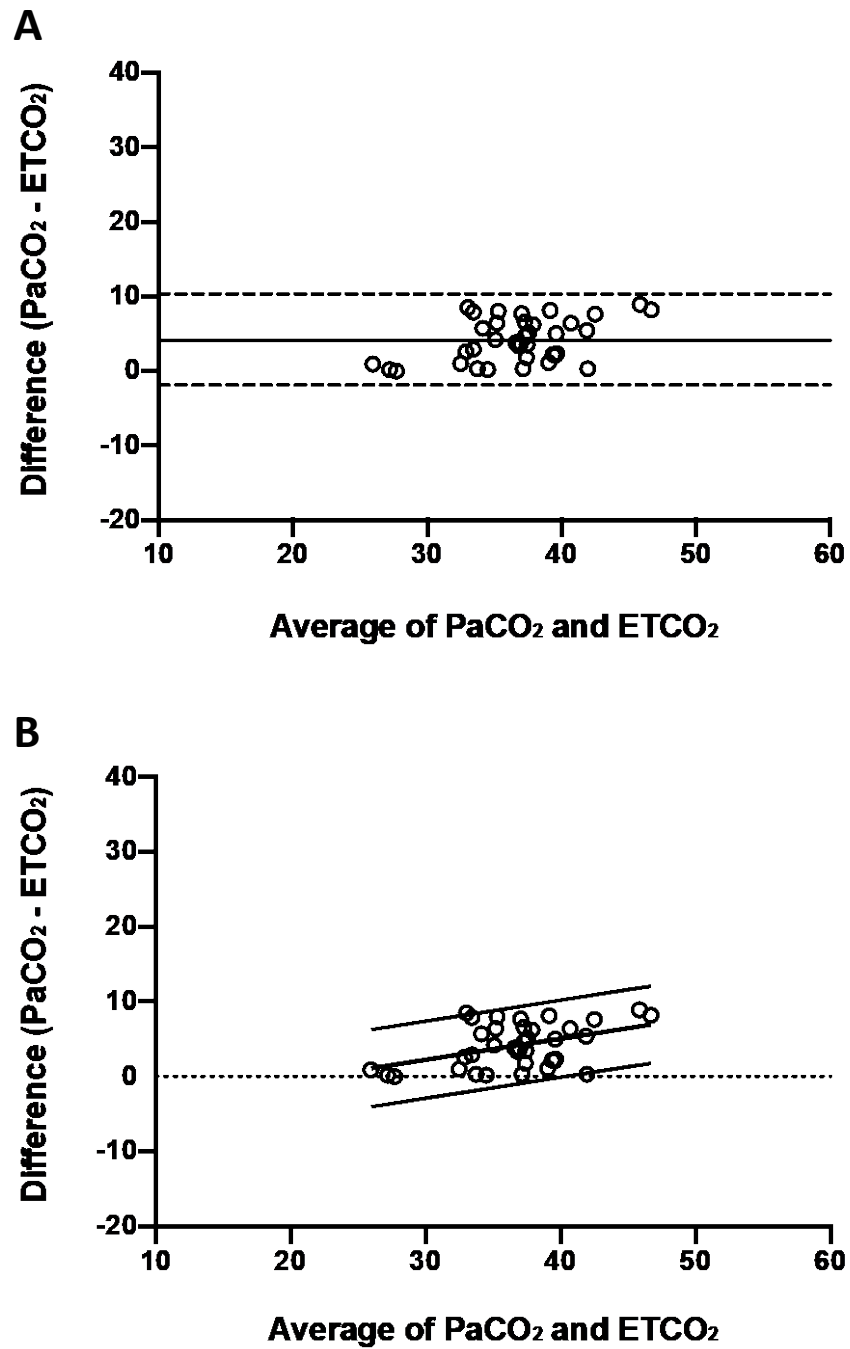


Figure 3.3: Bland-Altman plots comparing PaCO₂ and ETCO₂ measured by the MicroCapStar with 1 m sample line sampling at the recommended position. Data was analysed using a (A) multiple observation approach and (B) regression-based approach. A multiple observations analysis approach resulted in an effective range of 14.2 mmHg between upper and lower LOA while a regression-based analysis approach resulted in range of 10.3 mmHg. (A) Dashed lines indicate 95% limits of agreement; solid line indicates bias. (B) Upper and lower lines indicate 95% limits of agreement; midline indicates bias.

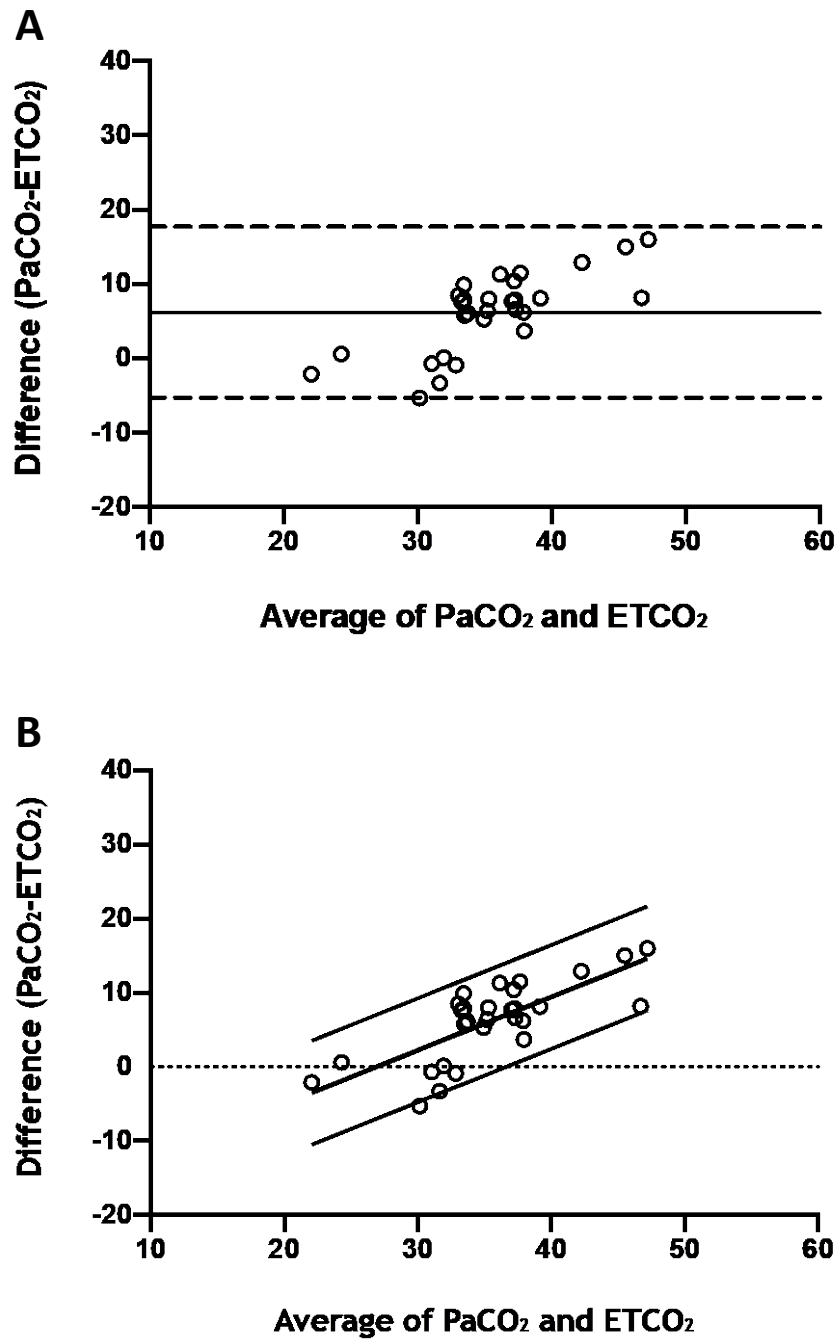


Figure 3.4: Bland-Altman plots assessing agreement between PaCO₂ and ETCO₂ measured by the MicroCapStar with a 1 m sample line sampling from the exhalation line only. (A) Multiple observations method resulted in an effective range of 22.04 mmHg between the upper and lower limits. (B) A regression-based approach produced an effective range of 14.03 mmHg. (A) Dashed lines indicate 95% limits of agreement; solid line indicates bias. (B) Upper and lower lines indicate 95% limits of agreement; midline indicates bias.

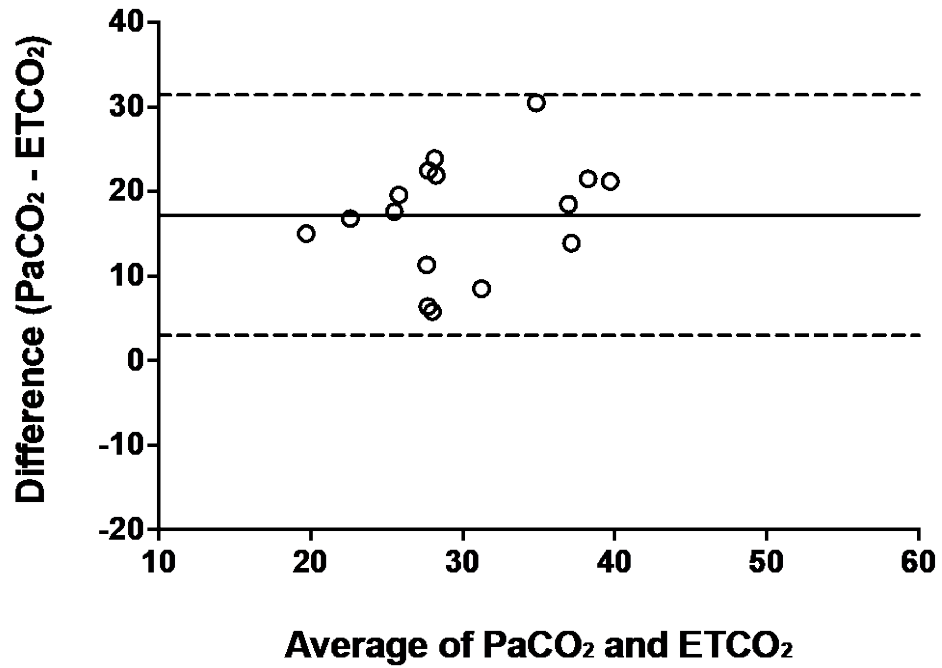


Figure 3.5: Bland-Altman plot showing agreement between PaCO₂ and ETCO₂ measured by the MicroCapStar with a 7 m sample line and sampling from between the intubation tub and ventilation tubing. The bias was 17.18 mmHg and 95% limits of agreement ranged from 2.97 to 31.39 mmHg, giving an effective range of 28.42 mmHg Dashed lines indicate 95% limits of agreement; solid line indicates bias.

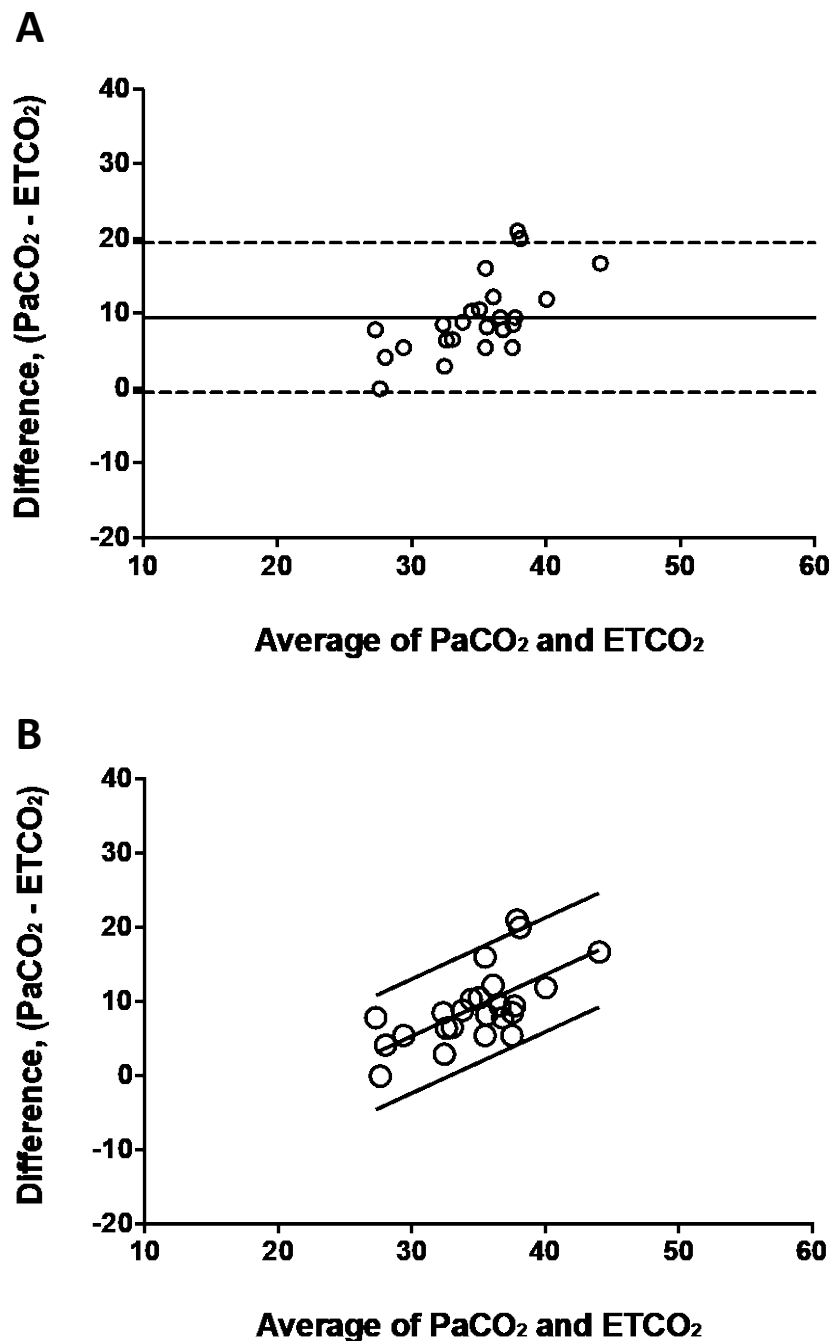


Figure 3.6: Bland-Altman plots showing agreement between PaCO₂ and ETCO₂ measured by the MicroCapStar with the 7 m sample line sampling from the exhalation line only. (A) Multiple comparisons approach resulted in an effective range of 20.04 mmHg between the upper and lower LOA. However, this data set violated the assumption of no correlation and therefore a regression-based analysis approach resulted in an effective range of 15.4 mmHg, as shown in B. (A) Dashed lines indicate 95% limits of agreement; solid line indicates bias. (B) Upper and lower lines indicate 95% limits of agreement; midline indicates bias.

3.3.1.2 Measuring agreement between ETCO_2 and PaCO_2 when using C1240 Micro Capnograph with various sample line lengths

The C1240 Micro Capnograph sampling lines had specific sampling rates unique to the sample line length and therefore we could not change the sample rate. When using the 1 m sample line with a sampling rate of 20 ml/min, we observed a relatively small bias of 5.96 mmHg but wide limits of agreement ranging from -9.30 to 21.25 mmHg, giving an effective range of 30.55 mmHg (Figure 3.7A). However, this data violated the assumption of the absence of a correlation and therefore a regression-based analysis resulted in a considerably smaller effective range of 14.75 mmHg (Figure 3.7B).

When using the longer 5 m sample line with a lower sampling rate of 5 ml/min, we observed a large bias of 13.87 mmHg and LOA ranging from -0.94 to 28.67 mmHg, giving an effective range of 29.91 mmHg (Figure 3.8). This data did not exhibit a correlation between the average and the difference of the two methods and so regression-based comparison was not conducted. The bias and LOA for each set-up is summarised in table 3.1.

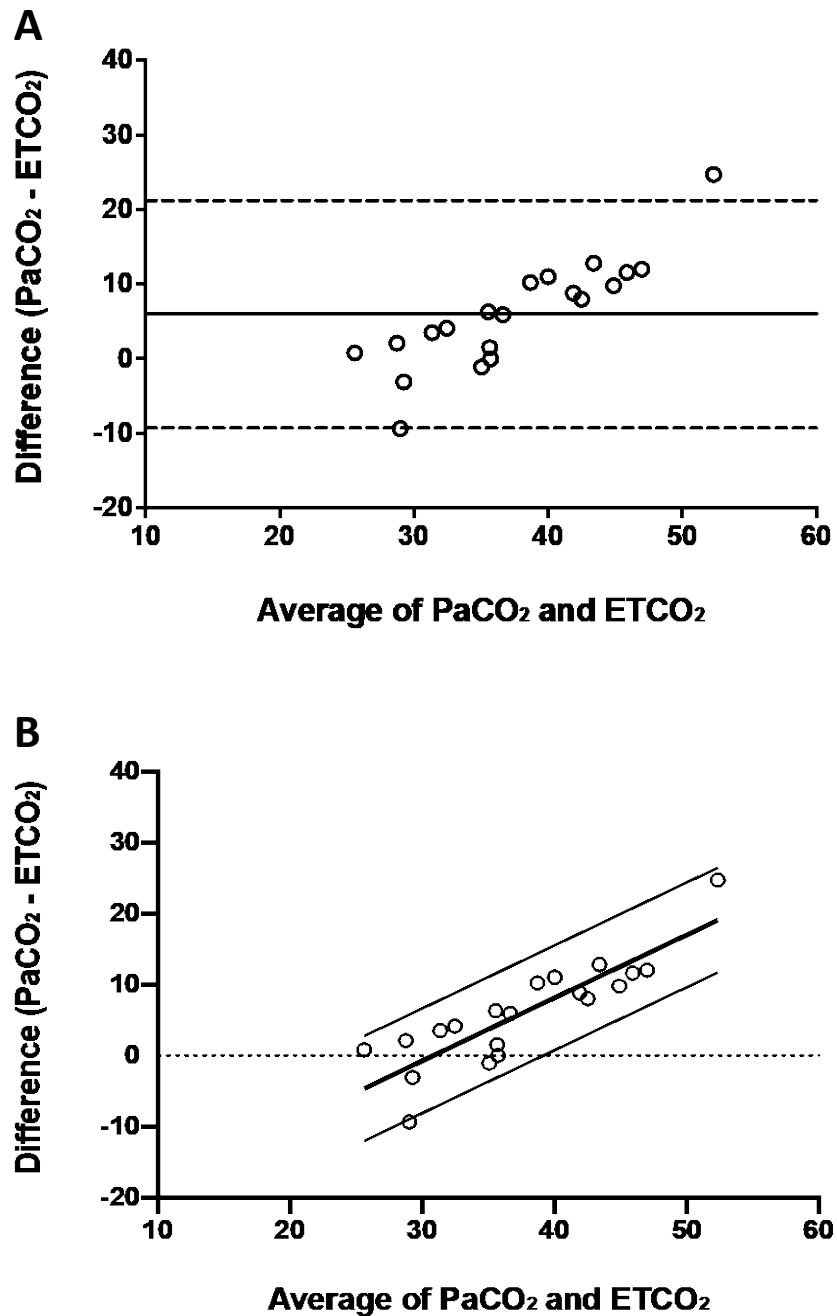


Figure 3.7: Bland-Altman plots showing agreement between PaCO₂ and ETCO₂ measured by the C1240 Micro Capnograph with the 1 m sample line sampling from the exhalation line with a sample rate of 5 ml/min. The data in A) was analysed with a multiple comparisons approach and resulted in an effective range of 30.55 mmHg between the upper and lower limits. This data set violated the assumption of no correlation and therefore a regression-based analysis approach resulted in an effective range of 14.75 mmHg, as shown in B. (A) Dashed lines indicate 95% limits of agreement; solid line indicates bias. (B) Upper and lower lines indicate 95% limits of agreement; midline indicates bias.

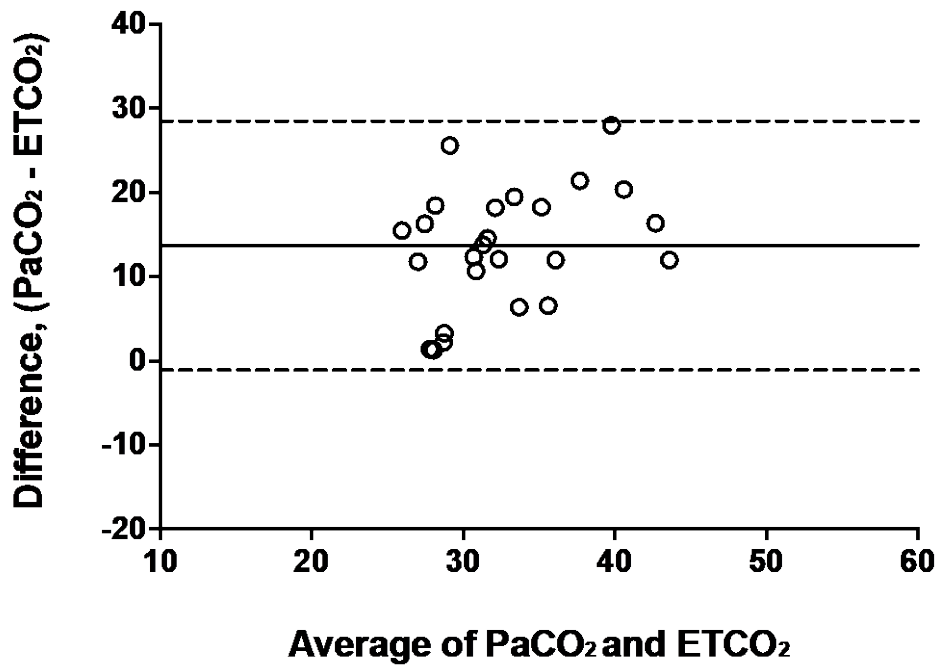


Figure 3.8: Bland-Altman plots showing agreement between PaCO₂ and ETCO₂ measured by the C1240 Micro Capnograph with the 5 m sample line sampling from the exhalation line with a sample rate of 20 ml/min. We observed a bias of 13.87 mmHg, with 95% LOA ranging from 0.94 to 29.91 mmHg. Dashed lines indicate 95% limits of agreement; solid line indicates bias.

	N	Bias	Lower L.O.A	Upper L.O.A	Effective range	Regression analysis required?	Regression-based range
MicroCapStar							
1 m (Recommended position)	4	4.13	-1.98	10.25	12.23	Yes	10.28
1 m (Exhale line)	4	6.19	-5.33	17.71	23.04	Yes	14.03
7 m (Recommended position)	3	17.18	2.97	31.39	28.42	No	
7 m (Exhale line)	4	9.29	-0.73	19.31	20.04	Yes	15.4
C1240 Micro Capnograph							
1 m (20 ml/min) ^a	5	5.98	-9.3	21.25	30.55	Yes	14.75
5 m (5 ml/min) ^a	5	13.87	0.94	28.67	29.91	No	

Table 3.1 - Summary showing the mean bias, upper and lower limits of agreement, effective range and regression-based range for each capnography set up. The recommended position sampled expired air from between the intubation tube and ventilation tubing.

^aMeasurements taken in the same animals. L.O.A, Limits of agreement

3.3.2 Study 2 - Evaluating the effects of PaCO₂ on the stimulus-evoked BOLD signal

3.3.2.1 Inducing hypocapnia and hypercapnia

PaCO₂ was modified by changing the ventilator stroke frequency; reducing the frequency induced hypercapnia and increasing the frequency-induced hypocapnia (Figure 3.9A). Hypocapnia was defined as a PaCO₂ <35 mmHg and the group average was 24.8 mmHg under this condition. The normal condition was defined as a PaCO₂ between 35-45 mmHg, with a group average of 40.38 mmHg being achieved. Hypercapnia was defined as a PaCO₂ >45 mmHg and the group average was 54.55 mmHg (Figure 3.9A). The PaCO₂ significantly differed between each of the hypocapnic, normocapnic and hypercapnic conditions (p<0.05).

The PaO₂ generally remained consistent under each manipulation with group averages of 110.18 mmHg, 99.03 mmHg and 103.45 mmHg for hypocapnic, normal and hypercapnic conditions, respectively (Figure 3.9B). Repeated measures ANOVA confirmed that PaO₂ did not statistically differ between any of the conditions (p=0.2242). Blood pH was found to be significantly different between conditions when assessed by repeated measures ANOVA (p=0.0019). A post-hoc Tukey test revealed there was no significant difference in blood pH between hypocapnic and normal conditions or between the normal and hypercapnic conditions. However, blood pH did significantly differ between hypocapnic and hypercapnic conditions (p<0.05; Figure 3.9C).

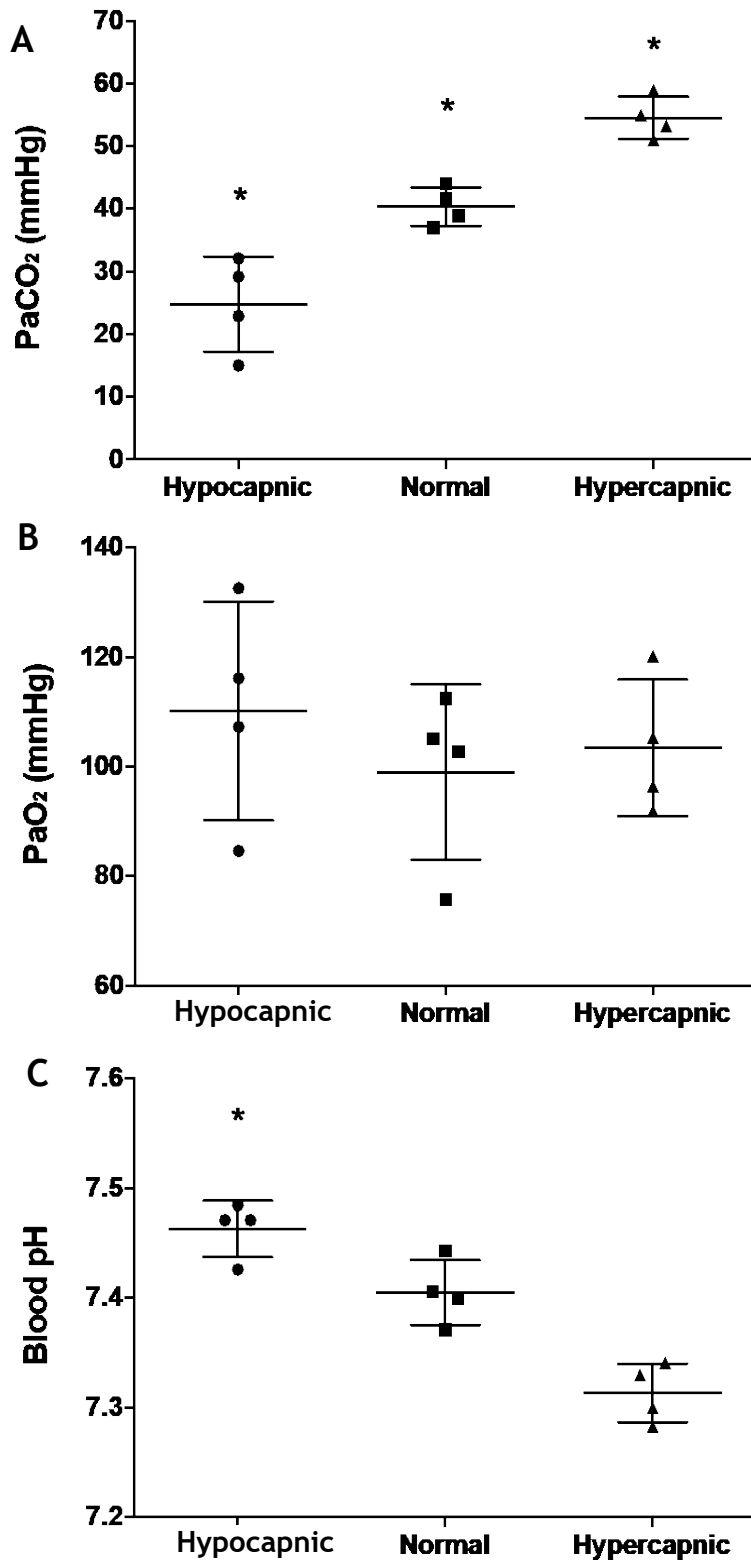


Figure 3.9: Overview of blood gas profiles. (A) PaCO₂ (B) PaO₂ and (C) blood pH under hypocapnic, normal and hypercapnic conditions. (A) *p<0.05 vs all other conditions (B) *p<0.05 vs hypercapnic condition only; RM one-way ANOVA with Tukey's multiple comparisons.

3.3.2.2 Assessing the effects of varying PaCO₂ on the stimulus-evoked BOLD signal

The effect of inducing hypocapnia and hypercapnia on the stimulus-evoked BOLD signal was assessed by measuring the peak BOLD response and the integral of the BOLD response (area under the curve) during stimulation (Figure 3.10). We observed group-averaged peak BOLD responses of 3.42%, 3.16% and 1.7% for hypocapnic, normal and hypercapnic conditions, respectively. The integrals of the BOLD responses for hypocapnic, normal and hypercapnic conditions were 41.7, 37.18 and 23.19, respectively. Repeated measures ANOVA revealed no significant difference for either the peak BOLD response ($p=0.1387$) or the integral of the BOLD response ($p=0.3367$), between any conditions tested (Figure 3.11)

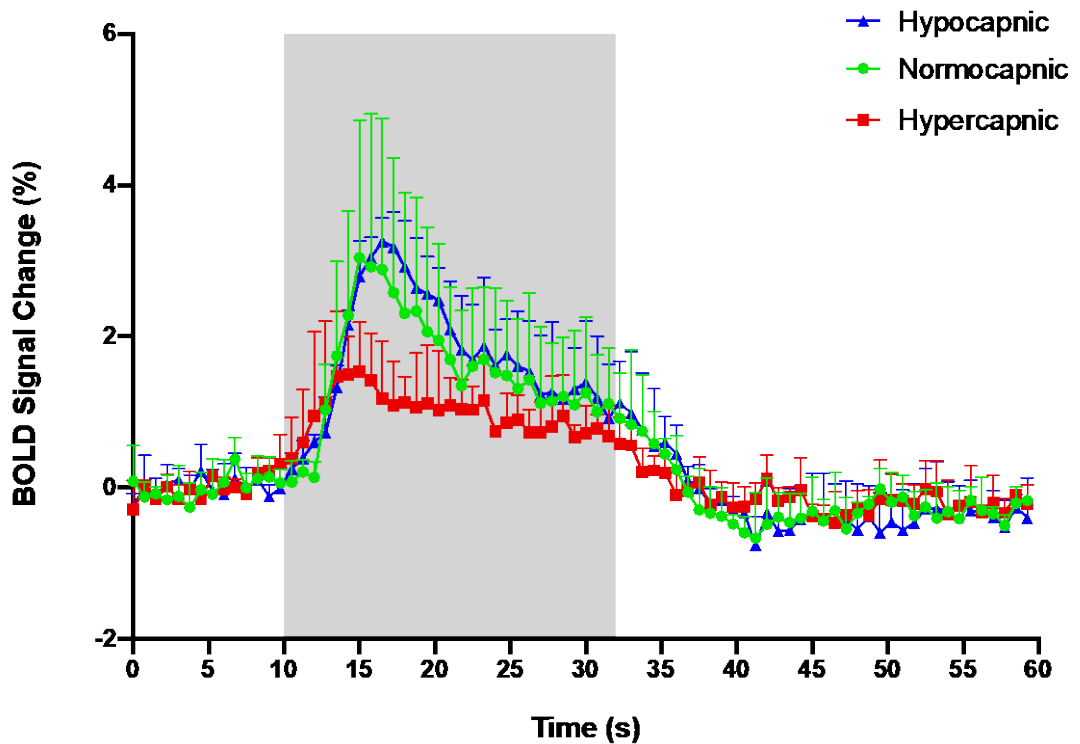


Figure 3.10: Group-averaged time courses for the stimulus-evoked BOLD signal in response to forelimb stimulation under hypocapnic, normal and hypercapnic conditions. N=4; all animals were assessed for each gas condition (i.e. hypocapnia, normocapnia and hypercapnic). Group averages for PaCO₂ under each condition were 24.8 mmHg, 40.38 mmHg and 54.55 mmHg for hypocapnic, normal and hypercapnic, respectively. Grey Section indicates when stimulation was applied. Error bars represent standard deviation. BOLD signal change calculated respective to baseline.

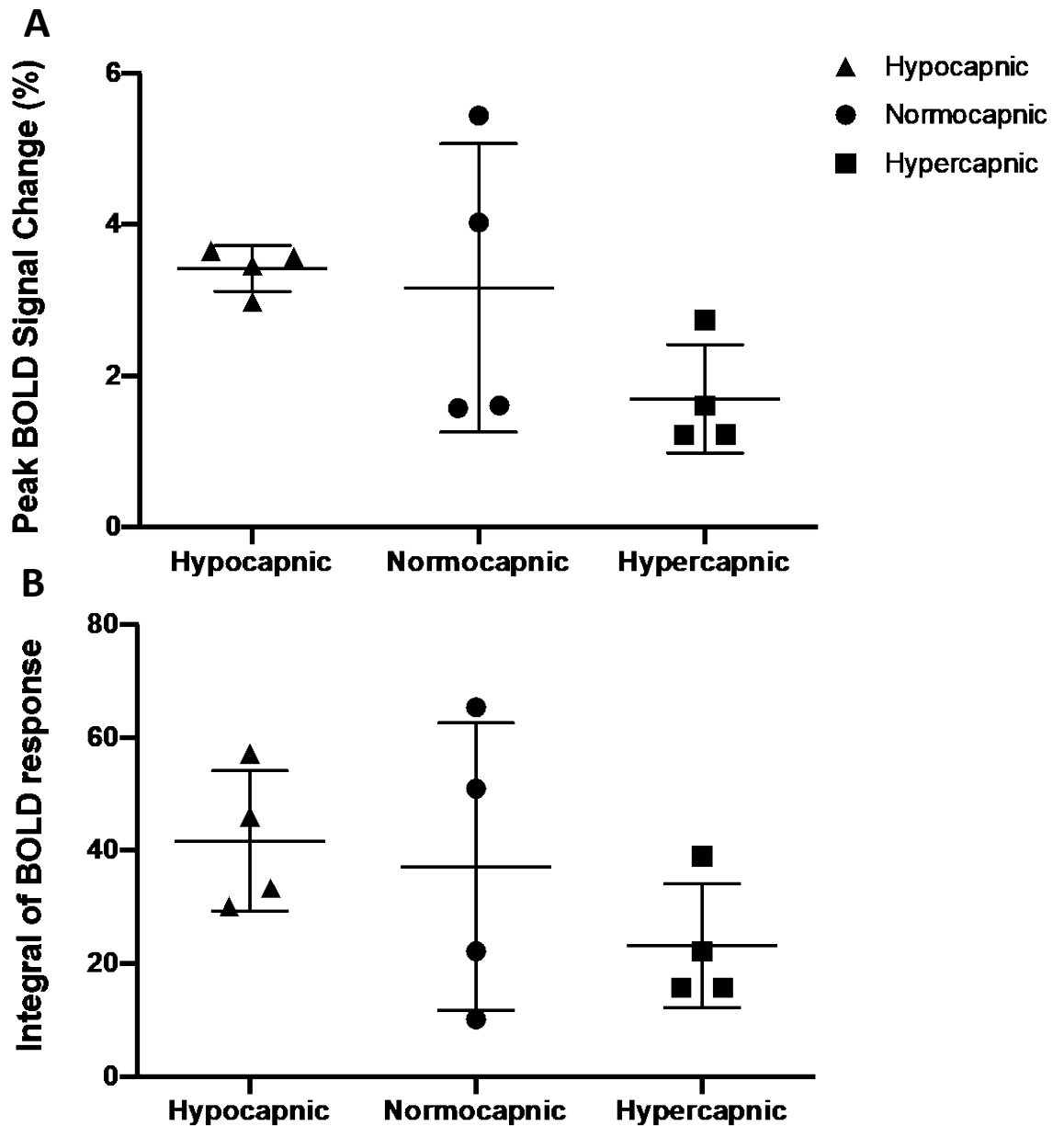


Figure 3.11: (A) Peak BOLD and (B) integral of the BOLD response under hypocapnic, normocapnic and hypercapnic conditions. No significant differences were observed in peak BOLD or integrated BOLD values between any condition when assessed by RM one-way ANOVA. Individual data points shown with mean and standard deviation overlaid.

3.4 Discussion

In our first study, we attempted to establish non-invasive monitoring of PaCO₂ in the anaesthetised rat by measuring ETCO₂ using two different micro-sampling side-stream capnographs. PaCO₂ values provided by blood gas analysis were compared with ETCO₂ values obtained from micro-sampling side-stream capnographs. Agreement between the two techniques was assessed and used to determine whether monitoring ETCO₂ via side-stream capnography could provide a practical and accurate method to monitor and maintain PaCO₂ values within normal physiological limits. We also assessed how hypocapnia and hypercapnia affected the stimulus-evoked BOLD signal.

3.4.1 Non-invasive monitoring of PaCO₂ using side-stream capnography to measure ETCO₂

When comparing blood gas analysis measurements with the MicroCapStar and C1240 Micro Capnograph measurements, we generally observed poor agreement between PaCO₂ and ETCO₂ under all configurations tested. The range between the lower and upper 95% LOA in all configurations was greater than 10 mmHg, indicating that the differences between PaCO₂ and ETCO₂ measurements were highly variable. This observation is clinically relevant since the range between the PaCO₂ physiological limits is 10 mmHg (35 - 45 mmHg). Therefore, this value represented the largest range between the 95% LOA that could theoretically be accepted to ensure PaCO₂ remained within normal physiological limits. However, this would require maintaining the ETCO₂ at an exact value throughout an experiment, which in our experience is highly unlikely. To be practically feasible, the range between the 95% LOA for any given side-stream configuration would need to be smaller than 10 mmHg. Given that PaCO₂ is known to be 2-5 mmHg higher than ETCO₂, these values represented the optimum lower and upper LOA that a given side-stream configuration could achieve. Under such circumstances, maintaining the ETCO₂ between 33-40 mmHg would ensure the corresponding PaCO₂ value is maintained within normal physiological limits, considering the difference between the two measures could vary by as little as 2 mmHg or as much as 5 mmHg. However, side-stream capnography is known to underestimate ETCO₂ (Schieber et al. 1985; Chan et al. 2003), and therefore larger bias values and wider LOA were expected in our experiment. The 1 m sample line sampling at

the recommended position demonstrated the smallest effective range between upper and lower LOA, with the range indicated to lie between 10.28-12.23 mmHg. Given that this range is marginally outside the theoretically acceptable 10 mmHg, it is possible that with further optimisation, this configuration could provide an acceptable method to non-invasively monitor PaCO₂ for bench top experiments where short sample lines can be used. Additionally, the range between upper and lower LOA when using the 7 m sampling line were generally larger than those observed when using the 1 m sampling line, suggesting that the variability in differences between PaCO₂ and ETCO₂ increases with line length. Therefore, a shorter sampling line, such as 0.75 m or 0.5 m, may be achievable in a bench top experiment and may provide narrower 95% LOA. Further studies could confirm this observation, however this was not achievable in the current study due to time constraints.

The large variation in differences between PaCO₂ and ETCO₂ measurements observed in our study are likely underpinned by several physical laws affecting the transport of a gas sample. As a sample of gas passes through a tube, it is subjected to dispersal by diffusion and convection which subsequently causes a loss of the lowest and highest concentration peaks (Scamman and Fishbaugh 1986; Pascucci et al. 1989). Dispersal is proportionate to the length of the tube and results in the underestimation of ETCO₂, especially when used in individuals or animals with small tidal volumes. Higher breathing frequencies (>31 breaths/min) and low sample flow rates can further contribute to the underestimation of ETCO₂ (From and Scamman 1988). Furthermore, a high flow of supplementary gases can lead to dilution of the expired CO₂ sample. Considering our experiment involved long sample line lengths, used high breathing frequencies (approx. 60 - 70 breaths/min) and involved small animals with small tidal volumes, it is likely that the combination of these factors contributed to the underestimation and variability of ETCO₂ values that we observed in all configurations.

3.4.2 Evaluating the effects of varying PaCO₂ on the stimulus-evoked BOLD signal

In the current study, we observed that the stimulus-evoked BOLD response did not significantly differ under hypocapnic (PaCO₂ = 25 mmHg), normal (PaCO₂ =

40 mmHg) or hypercapnic ($\text{PaCO}_2 = 55$ mmHg) conditions, when the peak BOLD response and integral of the BOLD response were assessed. However, it is worth noting that both measured characteristics of the BOLD response were numerically smaller during hypercapnia compared with normal and hypocapnic conditions, suggesting a trend for higher PaCO_2 values to reduce the stimulus-evoked BOLD response (Figure 3.10). In humans and rats, significant reductions in the stimulus-evoked BOLD signal have been observed under mild hypercapnic (PaCO_2 : 50-55 mmHg) and severe hypercapnic conditions (PaCO_2 approx. 70 mmHg), with the stimulus-evoked BOLD signal being virtually absent under severe hypercapnic conditions (Posse et al. 2001; Cohen et al. 2002; Sicard and Duong 2005; Nasrallah et al. 2015). Such severe hypercapnia is generally induced with breathing 10% CO_2 and it has previously been observed that baseline CBF is similar between 10-15% CO_2 (Sicard and Duong 2005). The lack of increased baseline CBF suggests that cerebral blood vessels are maximally dilated which likely underpins the severely attenuated/virtually absent stimulus-evoked BOLD response at these levels of hypercapnia. However, the lack of a statistically significant reduction in the current study under mild hypercapnia is likely a result of the considerable intersubject variability within our normal group (Figure 3.11) and the small study sample size. However, it is also important to note that the use of anaesthesia, in particular isoflurane, may also introduce confounds in to such preclinical studies. Isoflurane is a known vasodilator previously been shown to suppress neural activity and cerebral reactivity to CO_2 (Kety and Schmidt 1948; Brevard et al. 2003; Sicard et al. 2003). Therefore, this may have also contributed to the lack of significant differences between normocapnic and hypercapnic conditions.

Interestingly, our observation during hypocapnia opposes that reported by Sicard *et al.* (2005) who observed a significantly attenuated stimulus-evoked BOLD response (0.7% ΔBOLD) during hypocapnia ($\text{PaCO}_2 = 26$ mmHg) when animals were exposed to a 9% O_2 challenge. Under a similar hypocapnic condition ($\text{PaCO}_2 = 25$ mmHg), we observed a larger group-averaged BOLD signal change of 3.42%, which was found to not significantly differ from the responses observed under our normal and hypercapnic conditions. The discrepancy between our observations and those observed by Sicard *et al.* (2005) is likely due to differences in PaO_2 levels. PaO_2 was maintained around normal values within all our conditions however, under 9% O_2 , Sicard *et al.*

(2005) reported a PaO₂ of approximately 33 mmHg. Since CMRO₂ was observed to be similar under both the normal (21% O₂) and 9% O₂ condition, it is likely that the reduced BOLD signal change observed at 9% O₂ is due to hypoxia-induced attenuation of neurovascular coupling, as the author suggests.

The effects of PaCO₂ on baseline global blood flow are well established with many studies observing non-linear increases in baseline BOLD, CBF and MRI signals at various PaCO₂ intervals between 20 - 70 mmHg (Posse et al. 2001; Brevard et al. 2003; Sicard et al. 2003; Sicard and Duong 2005). While reduced stimulus-evoked BOLD responses have generally been reported under hypercapnic conditions, some studies have reported contradictory findings. We observed no difference in the stimulus-evoked BOLD response between PaCO₂ values of 25 - 55 mmHg, although as previously stated, there were several limitations to our study but we observed a trend towards a smaller stimulus-evoked response at higher PaCO₂ values. Various human fMRI studies have observed consistent stimulus-evoked BOLD and CBF responses between normocapnic and hypercapnic conditions suggesting that stimulus-evoked BOLD and CBF responses are independent of baseline blood flow (Hoge et al. 1999; Corfield et al. 2001; Uludag et al. 2004; Whittaker et al. 2016). However, these findings are opposed by observations that an inverse relationship exists between baseline CBF and stimulus-evoked BOLD responses (Wong and Bandettini 1997; Cohen et al. 2002; Stefanovic et al. 2006). Conversely, other studies have observed a non-linear relationship between baseline CBF and stimulus-evoked responses, with reduced BOLD responses only being observed at severe hypocapnic and hypercapnic conditions (Sicard and Duong 2005). The discrepancies between these results likely arise from differences in study methodologies, such as different CO₂ concentrations being used and for varying durations, the use of anaesthesia and whether free-breathing or mechanical ventilation is used. Furthermore, few of these studies report PaCO₂ or ETCO₂ values with some only reporting the percentage of CO₂ being administered to the breathing gases, which in cases of free breathing, may result in different PaCO₂ values being achieved between studies due to differences in individual tolerance to CO₂ and various compensatory effects. The inclusion of either PaCO₂ or ETCO₂ in such studies may provide more insight into understanding the relationship between PaCO₂, baseline CBF and stimulus-evoked responses. Additionally, the matter is further complicated within the pre-clinical research

field as these studies typically involve the use of anaesthesia which provides another variable that could confound the data. Therefore, to elucidate the relationship between PaCO₂, baseline CBF and stimulus-evoked responses, further studies that use consistent variables and control for potential confounds are required.

In conclusion, we observed that the microsampling side-stream capnographs assessed under the current experimental set-ups did not provide an accurate and reliable surrogate marker of PaCO₂ for use in an MRI setting, although there could be potential for use in a bench top setting with further optimisation of the 1 m sample line length. We also observed that hypocapnia (PaCO₂ = approx. 25 mmHg) and hypercapnia (PaCO₂ = approx. 55 mmHg) did not significantly affect the peak or integral of the BOLD response suggesting that the acceptable physiological range of PaCO₂ could be widened without affecting the BOLD response in fMRI experiments using medetomidine-isoflurane anaesthesia. However, given the large variability and low sample size of this study, further study is warranted. Ultimately, given the lack of accuracy and reliability between ETCO₂ and PaCO₂ in the current study, we did not implement side-stream capnography as a non-invasive measure of PaCO₂ and therefore retained the arterial blood gas analysis method for the assessment of the blood gas profile in all future studies.

Assessing the effect of varying stimulation parameters on stimulus-evoked BOLD, neural and CBF responses

4.1 Introduction

Pre-clinical fMRI studies often use anaesthesia to minimise the movement and stress of the animal during scanning, which could otherwise lead to the generation of artefacts and non-specific activations (Lahti et al. 1998; Peeters et al. 2001; Sicard et al. 2003). However, any anaesthetic used in a fMRI study must be carefully considered since different anaesthetics can have various effects on the underlying neural activity, hemodynamic response and the coupling mechanisms that link them, thereby also affecting the BOLD signal. Therefore, in studies assessing the stimulus-evoked BOLD or CBF response under anaesthesia, it is often necessary to characterise and optimise stimulus parameters in cases where the anaesthetic protocol is not currently represented within the literature. Additionally, assessing BOLD, CBF and neural responses under a specific anaesthetic protocol may inform on its effect on neurovascular coupling. In this chapter, data are presented to characterise the effects of varying forelimb electrical stimulation parameters on stimulus-evoked BOLD, CBF and neural responses.

4.1.1 Anaesthesia and neurovascular coupling

Alpha-chloralose (α -chloralose) has previously been favoured for preclinical fMRI studies since it exhibits minimal effects on respiratory and reflex functions and preserves neurovascular coupling (Lees 1972; Ueki et al. 1992; Austin et al. 2005; Franceschini et al. 2010). However, α -chloralose can cause acidosis, seizure-like activity and a prolonged and poor recovery, and therefore cannot be used for longitudinal studies. Isoflurane is a commonly used volatile anaesthetic often favoured for its ease of use, that has also been used in fMRI

experiments (Liu et al. 2004; Sicard and Duong 2005; Kim et al. 2010; Nasrallah et al. 2015). However, isoflurane is a potent vasodilator that has been shown to increase resting CBF at doses >1%, as well as suppress neural activity (Eger 1984; Masamoto et al. 2007). It has been noted that at concentrations <1%, isoflurane does not strongly affect baseline CBF or CBV, and hemodynamic responses are only marginally smaller than those evoked under α -chloralose (Franceschini et al. 2010). However, at these concentrations, animals are inadequately anaesthetised and have been reported to exhibit reflex responses and unintentional limb movements which can interfere with recordings (Franceschini et al. 2010; Kortelainen et al. 2016). Medetomidine is an injectable anaesthetic that has gained some popularity in recent years with several fMRI studies reporting robust stimulus-evoked BOLD responses under this anaesthetic (Weber et al. 2006; Zhao et al. 2008; Pawela et al. 2009). However, the dosage of medetomidine needs to be periodically increased for longer experiments due to pharmacokinetic changes over time which would otherwise result in the animal regaining consciousness after 3 - 4 hours (Pawela et al. 2008; Zhao et al. 2008).

4.1.2 Optimal stimulation parameters

Due to the varying effects of different anaesthetics on neurovascular coupling, there is a great variation within the preclinical literature concerning stimulus parameters for optimal BOLD, CBF and neural responses. Studies using α -chloralose have demonstrated maximal responses at stimulus frequencies of 1 and 3 Hz with stimulus intensities as low as 0.5 mA (Gyngell et al. 1996; Silva et al. 1999; Keilholz et al. 2004; Sanganahalli et al. 2008), while other studies using isoflurane have observed maximal responses at 12 Hz with stimulus intensities of 1.4 - 1.5 mA (Masamoto et al. 2007; Kim et al. 2010). Maximal responses under medetomidine have also been demonstrated at stimulus frequencies of 9 Hz with stimulus intensities as low as 1 mA (Zhao et al. 2008). It is important to note that under α -chloralose, BOLD, CBF and neural responses decline as stimulus frequency increases, becoming completely abolished at 9-10 Hz. Therefore, if the optimal stimulus frequency for maximal responses under isoflurane (12 Hz) was applied in a study using α -chloralose, little to no responses would be observed. Collectively, these observations indicate that optimal stimulus parameters for one anaesthetic should not be

applied to a different anaesthetic and therefore, optimal stimulus parameters should be determined specifically for each protocol, if no optimisation has been previously performed in the literature.

4.1.3 Medetomidine-isoflurane anaesthesia

Previously, a novel anaesthetic protocol combining dexmedetomidine (an active enantiomer of medetomidine) and isoflurane was observed to provide stable anaesthesia for several hours and enable the acquisition of robust resting state networks and stimulus-evoked BOLD responses in the rat (Lu et al. 2012). These observations were also confirmed in our own lab, as well as the ability of animals to recover well from this anaesthesia, thereby confirming its potential for longitudinal fMRI experiments (Hollyer 2016). However, to our knowledge, no study has yet characterised the effects of varying stimulus parameters on stimulus-evoked BOLD, CBF or neural responses under this adapted anaesthetic protocol. Such observations would not only prove helpful in establishing the optimum stimulus parameters under this anaesthesia, but would also develop our understanding of how neurovascular coupling may be affected.

4.1.4 Study Aims

Given the lack of studies in the literature characterising the effects of varying forelimb stimulation parameters on BOLD, CBF and neural responses in rodents under a combined medetomidine-isoflurane anaesthesia, it was important to perform the following experiments to characterise how these responses were affected and to identify the optimal stimulation parameters for this anesthetic protocol that could be used in future studies. The aims of the experiments described in this chapter were to:

1. Characterise the effects of varying stimulus frequency, stimulus intensity and pulse duration on the stimulus-evoked BOLD signal using fMRI and identify the optimal stimulation parameters
2. Characterise the effects of varying stimulus frequency and stimulus intensity on neural activity by measuring various components of the somatosensory-evoked potential (SEP) and identify the optimal stimulation parameters
3. Characterise the effects of varying stimulus frequency and stimulus intensity on the stimulus-evoked CBF response using laser speckle contrast imaging (LSCI) and identify the optimal stimulation parameters

4.2 Methods

4.2.1 Study 1 - Investigation and optimisation of stimulus parameters for BOLD fMRI using forelimb stimulation

4.2.1.1 fMRI preparation

Wistar Kyoto (WKY) rats (n=9) weighing between 275 - 370 g were anaesthetised as outlined in Section 2.2.2. The femoral artery was cannulated as detailed in Section 2.3.2 to allow continuous monitoring of blood pressure, heart rate, and to allow periodic arterial blood sampling for the analysis of blood gas and pH levels. The animal was then transferred to the MRI cradle and secured, according to Section 2.4. Body temperature was monitored using a rectal probe and maintained at $37^{\circ}\text{C} \pm 0.5$ using a heated water jacket. One animal was excluded from the study due to complications with the arterial line that prevented monitoring of the animal's blood pressure, heart rate and blood gas profile.

4.2.1.2 fMRI forelimb stimulation

Two needle electrodes were inserted subcutaneously in the right forepaw at the second and fourth digits, as described in Section 2.3.3. Forepaw stimulation was achieved using a Grass S48 square pulse stimulator with output running through a constant current unit. For each stimulus run, either the stimulus frequency, pulse duration or stimulus intensity was systematically varied in reference to a set of baseline parameters. When one stimulus parameter was changed, the other parameters were maintained at a standard set of values. The standard reference parameter values were 3 Hz for stimulus frequency, 0.3 ms for pulse duration and 6 mA for stimulus intensity.

Additional variation in the stimulus parameters were investigated as follows:

- (1) **Stimulus intensity:** the intensity of the stimulus was varied at 2 and 4 mA with the stimulus frequency set at 3 Hz and the pulse duration at 0.3 ms
- (2) **Stimulus frequency:** the frequency of the stimulus was varied at 6, 9 and 12 Hz with the stimulus intensity set at 6 mA and the pulse duration at 0.3 ms
- (3) **Pulse duration:** the pulse duration was varied at 0.6 and 1 ms while the stimulus frequency was set at 3 Hz and the stimulus intensity at 6 mA

Only these three stimulation parameters were assessed as these are the parameters that are typically modified in rodent fMRI forelimb stimulation studies (Gyngell et al. 1996; Silva et al. 1999; Keilholz et al. 2004; Sangahalli et al. 2008). The values investigated for each parameter were generally identified based on those assessed in these studies. The reference parameter values were chosen based on the most commonly used. However, it should be noted that while low stimulus intensities were commonly assessed and used (i.e. <2 mA), these studies were often performed under α -chloralose. Other studies using isoflurane or medetomidine have investigated higher stimulus intensities and observed larger BOLD responses at higher intensities (Liu et al. 2004; Zhao et al. 2008). Therefore, stimulus intensities of 2 mA, 4 mA and 6 mA were investigated, and 6 mA chosen as the reference value based on these studies, given they were more appropriate to our own.

Each run of the experiment consisted of a block design with 6 on-off periods where the stimulus was on for 22 seconds and off for 38 seconds. The start of each run was also preceded by a 10 second baseline period. The order at which the stimulus parameters were tested was randomised for all animals.

4.2.1.3 MRI experiments

MRI experiments were performed using a Bruker Biospec 7T, as detailed in Section 2.4. A fast low angle shot (FLASH) sequence was used to verify correct positioning of the animal within the scanner as well as coil positioning. Local shimming was performed using a fieldmap-based algorithm ('MAPSHIM'). Functional echo planar image (EPI) series were acquired during the forelimb stimulation paradigm to assess the stimulus-evoked BOLD (TR 750 ms, TE 20 ms, FOV 3.2 x 2.4 cm², matrix 64 x 48, 15 slices of 1mm thickness, in-plane spatial resolution 500 μ m²). A 320 x 240 μ m² rapid acquisition with relaxation enhancement (RARE) T₂ sequence was used for anatomical reference.

4.2.1.4 Data analysis

Data analysis was initially performed in MATLAB using in-house scripts. Significantly activated voxels were calculated using a t-test thresholded at $p < 0.05$. A cluster threshold was applied to the resultant probability maps to remove single voxels of activation. The time courses for the remaining

significant voxels were then extracted, normalised to the pre-stimulus baseline and averaged to produce a single time course for each run. Each run was then averaged across the 6 on-off blocks to produce a single event-related average for each stimulus condition for each animal. The single event-related time courses from all animals were then grouped by stimulus parameter and used to extract the peak %BOLD for each animal. The single event-related time course values were then exported to Prism 6 where the integral of the BOLD response was calculated (area-under-curve, AUC). A threshold was applied during AUC calculation so that only positive peaks larger than 10% of the maximal Y value were measured. Additionally, only peaks that had a start point within the stimulus time period (i.e. 10 - 32 seconds) were included in the calculation. Peak %BOLD data for all stimulus conditions were analysed using a repeated measures one-way ANOVA (RM one-way ANOVA). Multiple comparisons between datasets within their respective stimulus category were made using a Tukey's multiple comparisons test (e.g. 2 mA vs 4 mA vs 6 mA (reference), 3 Hz (reference) vs 6 Hz vs 9 Hz vs 12 Hz, 0.3 ms (reference) vs 0.6 ms vs 1 ms). The integrals of the BOLD response were analysed using a Friedman test.

A post-hoc power analysis revealed that the current study had an 89.6% probability of correctly rejecting the null hypothesis (Effect size f , 0.40; α error probability, 0.05; correlation, 0.5; nonsphericity, 1).

4.2.2. Study 2 - Evaluating the effects of varying stimulus parameters on the somatosensory evoked potential

4.2.2.1 Animals

Wistar Kyoto (WKY) rats ($n=6$) were anaesthetised according to Section 2.2.2. The femoral artery was cannulated to enable the monitoring of blood pressure and heart rate, as outlined in Section 2.3.2. Body temperature was monitored using a rectal probe and was maintained at $37^{\circ}\text{C} \pm 0.5$ using a heating pad and radiant heat lamp.

4.2.2.2 Laminectomy and craniotomy

A laminectomy was performed to remove C4-C6 vertebra and expose the underlying spinal cord for the recording of cord dorsum potentials (CDPs). A

craniotomy was performed to create a cranial window over the S1FL area for the recording of SEPs. Both procedures are outlined in Section 2.3.4 and were performed by Mrs Lindsay Gallagher.

4.2.2.3 Forelimb Stimulation

Two needle electrodes were inserted into the right forepaw at the 2nd and 4th digits, as outlined in Section 2.3.3. Forelimb stimulation was achieved using a custom Grass stimulator with output running through a constant current unit. For each stimulus run, the stimulus frequency or the stimulus intensity were systemically varied while other stimulus parameters were kept constant. To maintain consistency and allow comparisons with the fMRI experiment, the same stimulus intensities and frequencies were assessed. The effect of varying the pulse duration on the SEP was not investigated, as the same pulse durations could not be replicated with the different stimulus equipment.

Variation in the stimulus parameters were investigated as follows:

- (1) Stimulus intensity: the intensity of the stimulus was varied at 2, 4 and 6 mA with the stimulus frequency set at 3 Hz and the pulse duration at 0.2 ms
- (2) Stimulus frequency: the frequency of the stimulus was varied at 3, 6, 9 and 12 Hz with the stimulus intensity set at 6 mA and the pulse duration at 0.2 ms

Due to pre-set pulse duration configurations in the stimulator, we were unable to replicate the 0.3 ms pulse duration as used in the fMRI study, with the closest available option being 0.2 ms. When assessing the effect of stimulus frequency on the SEP, the stimulus paradigm followed that as previously described in Section 4.2.1.2. Briefly, each run consisted of 6 on-off blocks where the stimulus was on for 22 seconds and off for 38 seconds. When assessing the effect of stimulus intensity on SEPs, each run consisted of a single on-off block where the stimulus was on for 22 seconds and off for 38 seconds. For all conditions, the first stimulation block was preceded by a 10 second baseline period. Total run time for each stimulus frequency run was 6 minutes and 10 seconds, while total run time for each stimulus intensity run was 1 minute and 10 seconds. The order at which the stimulus parameters were tested was randomised.

4.2.2.4 Recording CDPs and SEPs

To confirm the activation of ascending somatosensory white matter tracts in the dorsal column, CDPs were recorded from the surface of the ipsilateral dorsal column at approximately C5. Recordings were made using silver ball electrodes with the indifferent electrode being placed on nearby back muscles. SEPs were recorded from the surface of the contralateral somatosensory cortex at the stereotaxic co-ordinates 0 mm AP, -4 mm ML relative to bregma. The indifferent electrode was placed on scalp muscles located under the retracted skin. The amplitude of the first positive deflection, first negative deflection and second positive deflection of the SEP were measured. We use the terms P1, N1 and P2 to refer to these components of the SEP, respectively. Responses were recorded using Spike2 Software (Cambridge Electronic Design Limited, UK).

4.2.1.5 Data Analysis

Spike2 acquisition files (.csg) were exported to MATLAB using the Spike2 software. In-house scripts were used to measure the amplitude of the individual components of the SEP in MATLAB. Briefly, for each animal and condition, segments of the SEP data trace were sequentially isolated at frequency-defined intervals (e.g. every 0.333 ms from baseline start time for 3 Hz runs). Within the isolated data segments, boundaries were defined to identify the expected positions of P1, N1 and P2. All isolated data segments were then displayed in a grid and visually checked to ensure that the frequency-defined intervals correctly captured SEPs along the data trace, where applicable, and that the individual components fell within the relevant boundaries (Figure 4.1A). Due to the lack of any responses during the stimulus 'off' period, only data segments containing SEPs from the stimulus 'on' period could be used to visually confirm correct positioning. Upon visual confirmation, all isolated data segments were displayed individually with the measured P1, N1 and P2 amplitude values to ensure that correct measurements had been obtained (Figure 4.1B). The subsequent P1, N1 and P2 values were normalised to the first pre-stimulus baseline period and a correction factor, obtained by measuring a 100 μ A calibration pulse after each experimental session, was applied.

For runs relating to variations in stimulus frequency, acquired amplitude values for P1, N1 and P2 were individually averaged across the 6 on-off stimulation blocks to produce a single event-related amplitude plot for each animal and each condition. For runs relating to variations in stimulus intensity, SEP amplitude values from the single on-off block were used. From these single event-related amplitude plots, the first peak amplitude for each SEP component (P1, N1, P2) was measured. While informative, these amplitude SEP measurements represent the mean neuronal response to each stimulus pulse whereas BOLD and CBF data represent integrated responses, which are a function of stimulus number and neural activity per stimulus. Therefore, we also calculated the individual sum of the SEP (Σ SEP) for P1, N1 and P2 as an index of integrated neuronal activity by summing the amplitude values evoked after each stimulus pulse. The data was then imported to Prism GraphPad 6 where the integral of the amplitude plots (AUC) was calculated for each animal and each stimulus condition. AUC was calculated as previously described in Section 4.2.1.4, with the exception that for N1 measurements, only negative peaks were included in the calculation. Data within the respective stimulus parameter category for each component was then analysed by a repeated measures one-way ANOVA.

A post-hoc power calculation indicated that there was a 50.8% probability of correctly rejecting the null hypothesis (Effect size f , 0.43; α error probability, 0.05; correlation, 0.5; nonsphericity, 1).

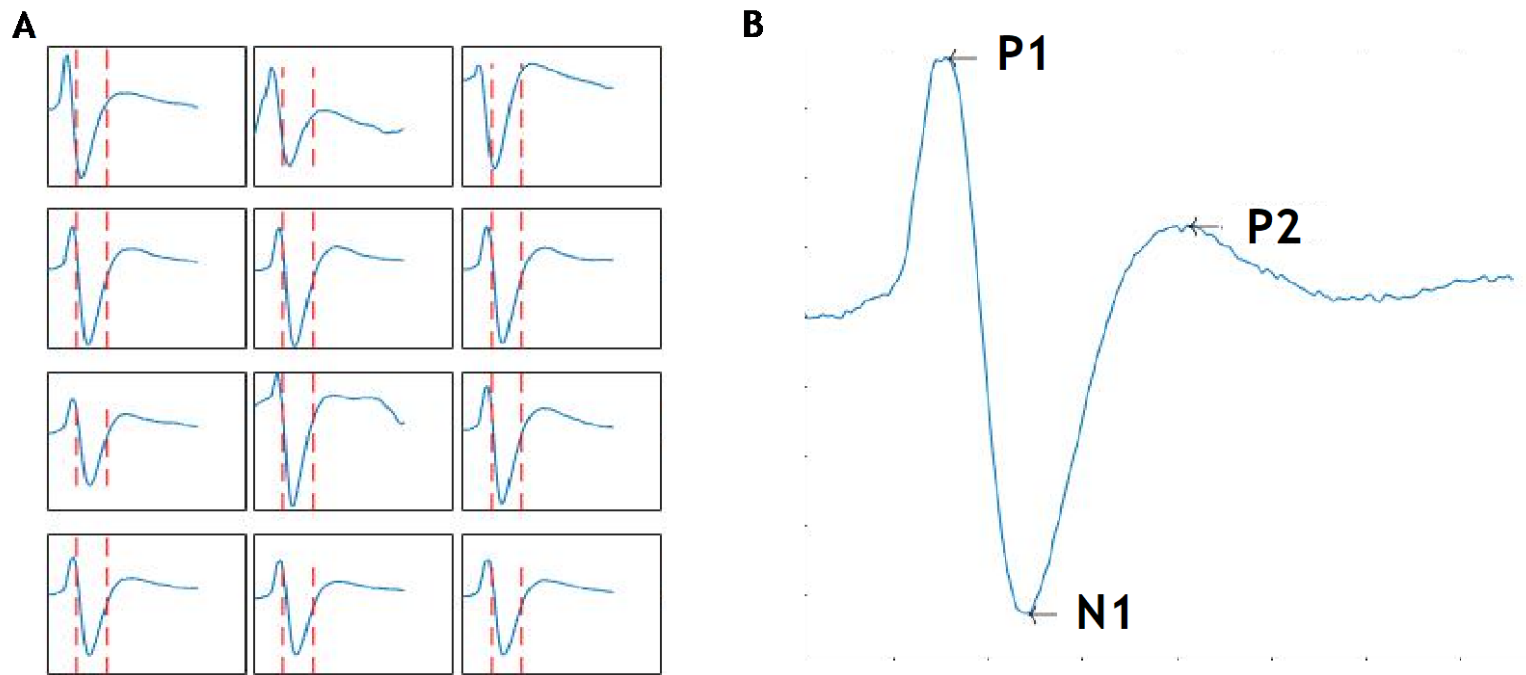


Figure 4.1: Measurement of individual SEP components using MATLAB. (A) A representative section of the grid containing isolated data segments. N1 was measured as the minimum value between the two dashed lines, with P1 and P2 being measured as the maximum values to the left of the first dashed line or right of the second dashed line, respectively. (B) Upon visual confirmation of correct

positioning within the relevant boundaries, SEPs were displayed individually with the measured amplitude values to ensure correct measurement of the relevant components.

4.2.3. Study 3 - Evaluating the effects of varying stimulus parameters on cerebral blood flow as assessed by laser speckle contrast imaging

4.2.3.1 Animals

In a separate cohort, WKY rats (n=6) weighing 315g - 400g were anaesthetised as outlined in Section 2.2.2. The femoral artery was cannulated as detailed in Section 2.3.2 to allow continuous monitoring of blood pressure and heart rate and to enable periodic blood sampling for analysis of blood gases. Body temperature was monitored using a rectal probe and was maintained at 37°C ± 0.5 using a heating blanket and radiant heat lamp.

4.2.3.1 Skull thinning

The animal was secured in a stereotaxic frame and skull thinning performed as outlined in Section 2.3.5.

4.2.3.2 Recording of CBF

Laser speckle contrast imaging was performed to measure stimulus-evoked CBF responses using PIMSoft Software (Perimed, Stockholm, Sweden). ROIs were drawn over the ipsilateral and contralateral somatosensory cortices to monitor and inform on blood flow changes within these areas during the course of the experiment. Given that unilateral stimulation may evoke bilateral responses in the relevant brain areas, an additional ROI was drawn over the ipsilateral visual cortex as a control area.

4.2.3.3 Forelimb stimulation

Needle electrodes were inserted at the 2nd and 4th digits of the right forepaw as detailed in the Section 2.3.3. Similar to the fMRI forelimb stimulation study, for each stimulus run, either the stimulus frequency or stimulus intensity was systematically varied in regard to a reference set of stimulus parameters. To maintain consistency and allow comparisons with the fMRI and electrophysiology experiments, the same stimulus intensities and frequencies were investigated. The effect of varying the pulse duration on the SEP was not investigated. The reference parameters were 3 Hz for stimulus frequency, 6 mA for stimulus

intensity and 0.3 ms for pulse duration. Variation in the stimulus parameters were then investigated as follows:

- (1) **Stimulus intensity:** the intensity of the stimulus was varied at 2 and 4 mA with the stimulus frequency set at 3 Hz and the pulse duration at 0.3 ms
- (2) **Stimulus frequency:** the frequency of the stimulus was varied at 6, 9 and 12 Hz with the stimulus intensity set at 6 mA and the pulse duration at 0.2 ms

Each run consisted of 3 on-off blocks where the stimulus was on for 22 seconds and off for 38 seconds. For all conditions, the first stimulation block was preceded by a 10 second baseline period. Each run was separated by 5 mins to allow any stimulus-induced effects to return to baseline and to reduce any effects of habituation between runs. The order at which the stimulus parameters were tested was randomised.

4.2.3.4 Data analysis

Analysis was initially carried out using PIMSoft. ROIs were established over the contralateral and ipsilateral S1FL areas, as well as over the ipsilateral visual cortex. The position and size of the ROIs were defined based on the Paxinos and Watson rat atlas (Paxinos and Watson 1998). For the contralateral S1FL ROI, a 3 x 2 mm oval was centred at 0 mm AP and -4 mm ML to Bregma and another centred at 0 mm AP and 4 mm ML to Bregma for the ipsilateral S1FL area. For the visual cortex ROI, a 3 x 2 mm oval was centred at -6 mm AP and 4 mm ML to bregma. The time course of each ROI was then separated according to stimulus condition and normalised to the first pre-stimulus baseline for each condition. The data was then averaged across the 3 on-off blocks to produce a single event-related average for each stimulus condition for each animal. The single event-related time courses for all animals were then grouped by stimulus condition and used to extract the peak $\% \Delta \text{CBF}$. The data were then imported to Prism 6 and the AUC for each stimulus condition for every animal was calculated, as previously described in Section 4.2.1.4. The data were then analysed using a repeated measures one-way ANOVA.

A post-hoc power calculation indicated that there was a 99.0% probability of correctly rejecting the null hypothesis (Effect size f , 0.82; α error probability, 0.05; correlation, 0.5; nonsphericity, 1).

4.3 Results

4.3.1. Study 1 - Investigation and optimisation of stimulus parameters for BOLD fMRI using forelimb stimulation

4.3.1.1. Stimulus-evoked BOLD response

To assess the effect of varying stimulus parameters on the stimulus-evoked BOLD response, we systematically varied either the stimulus frequency, pulse duration or stimulus intensity in regard to a reference set of stimulus values. For each condition tested, we observed a consistent activation cluster within the left S1FL area, being contralateral to the stimulated forelimb (Figure 4.2). The group-averaged time courses for most stimulus conditions produced a similar temporal profile, showing an increase in the BOLD signal shortly after stimulus onset, which gradually declined and plateaued over the course of stimulation and then returned to baseline shortly after stimulation was stopped (Figure 4.3). Higher frequencies of 6 Hz and above demonstrated a more pronounced peak in the BOLD response following stimulus onset, which declined rapidly after peaking but eventually plateaued similar to the responses during other stimulus conditions.

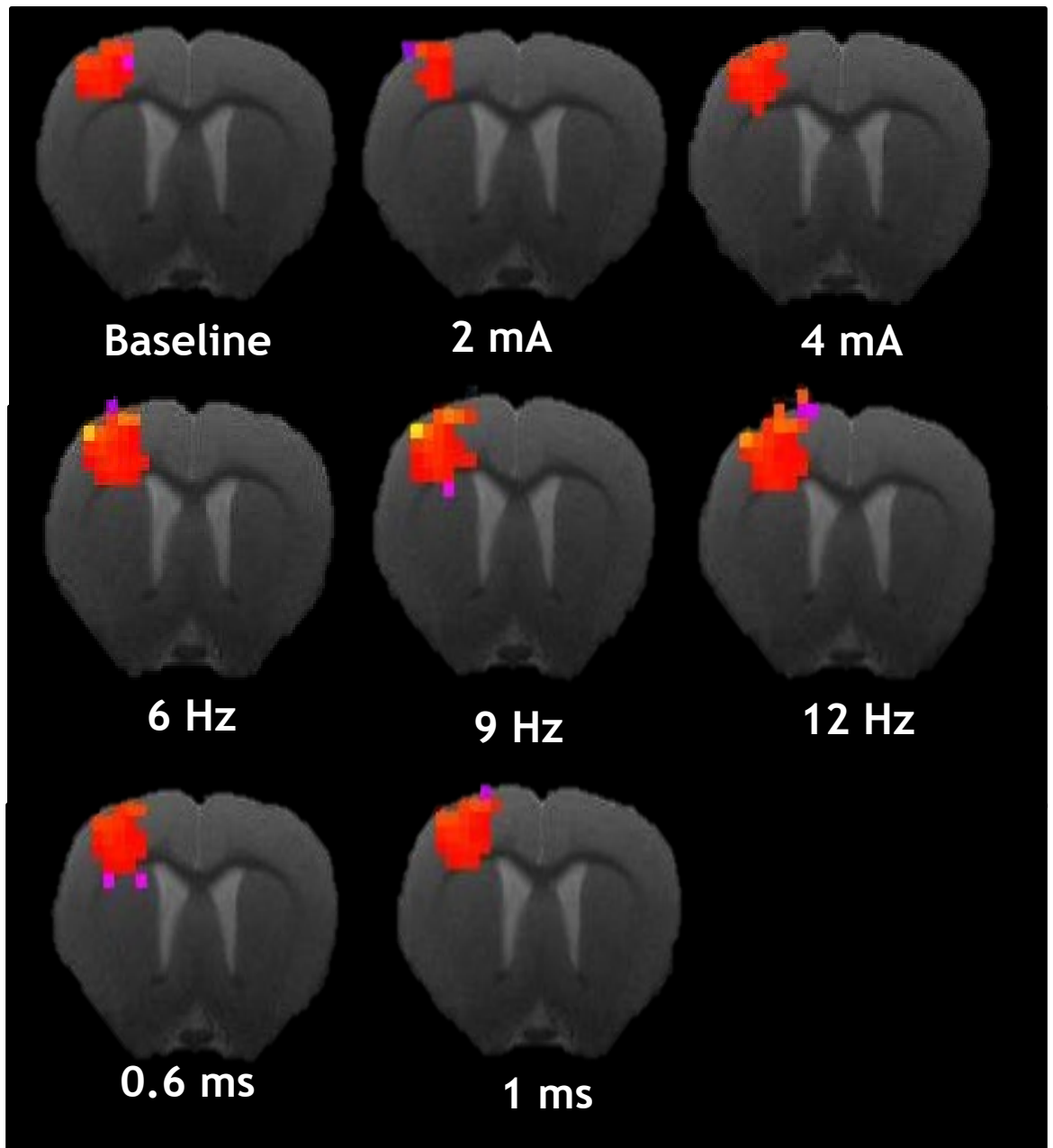


Figure 4.2: Anatomical RARE scans with the corresponding fMRI activation map overlaid for a representative animal. All variations in the stimulus parameters elicited an increased BOLD response within the contralateral somatosensory cortex for all animals.

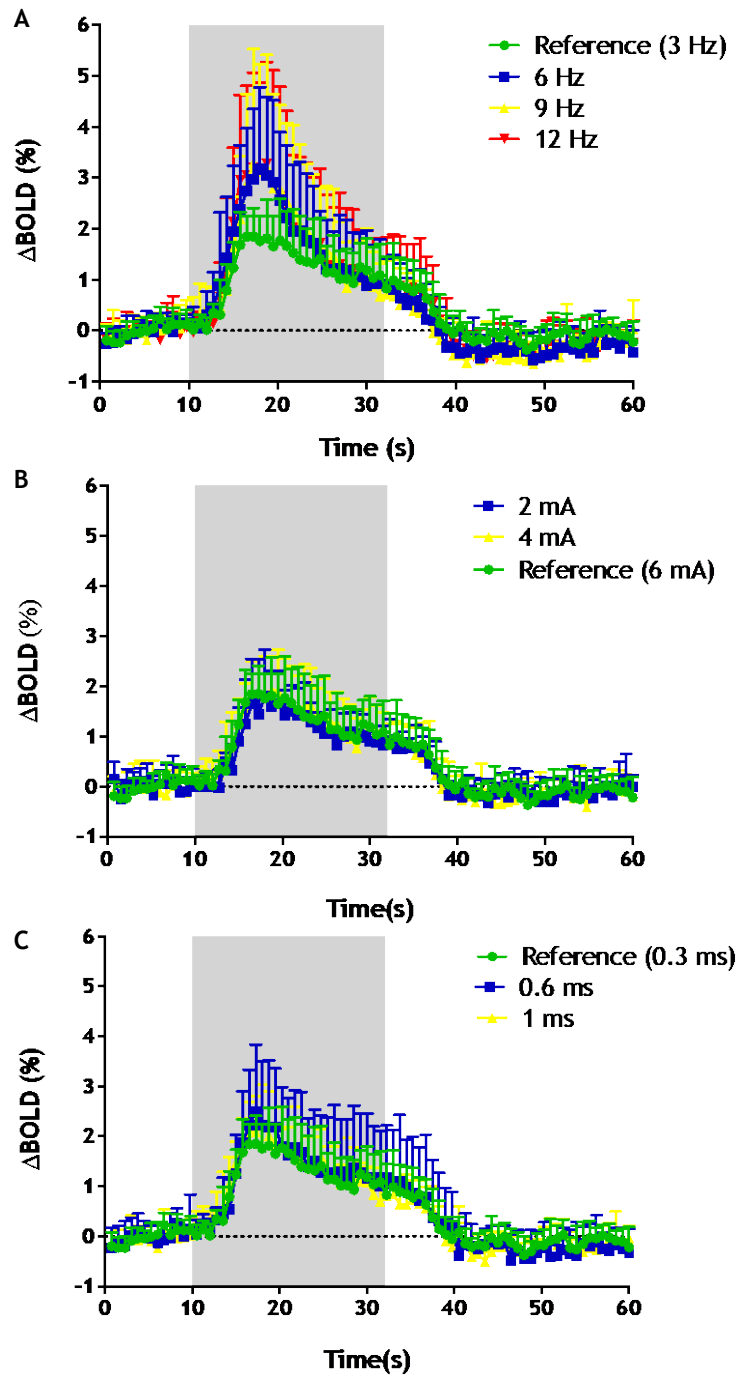


Figure 4.3: Group-averaged time courses showing the effects of varying (A) stimulus frequency, (B) stimulus intensity and (C) pulse duration on the Δ BOLD signal. Shaded area indicates stimulation. Data presented as mean \pm standard deviation.

We observed a significant effect of varying the stimulus parameters on the peak Δ BOLD signal (RM one-way ANOVA, $p = 0.0335$). However, no significant pairwise comparisons were observed when stimulus conditions were compared within their respective stimulus category (Figure 4.4). The group-averaged BOLD time courses were similar in size and shape for the reference, stimulus intensity (2 mA, 4 mA) and pulse duration conditions (0.6 ms, 1 ms), indicating that the stimulus-evoked BOLD responses remained consistent between these tested parameters. However, mean peak amplitude demonstrated a trend to increase with stimulus frequency, peaking at 9 Hz with a marginally smaller mean peak amplitude observed at 12 Hz (Figure 4.4). While this trend is clearly demonstrated when observing the mean peak amplitude values for each stimulus frequency, we observed a large variation in the peak amplitude values between individual animals for higher frequencies (≥ 6 Hz), which was generally not observed in any of the other stimulus conditions.

We did not observe a significant effect of varying the stimulus parameters on the integral of the BOLD response (Figure 4.5) or the TTP (Figure 4.6). The TTP for most conditions varied between 6 - 6.7 seconds on average, however, for the lower stimulus intensities of 2 mA and 4 mA, we observed an averaged TTP of 7.8 seconds and 7.3 seconds, respectively.

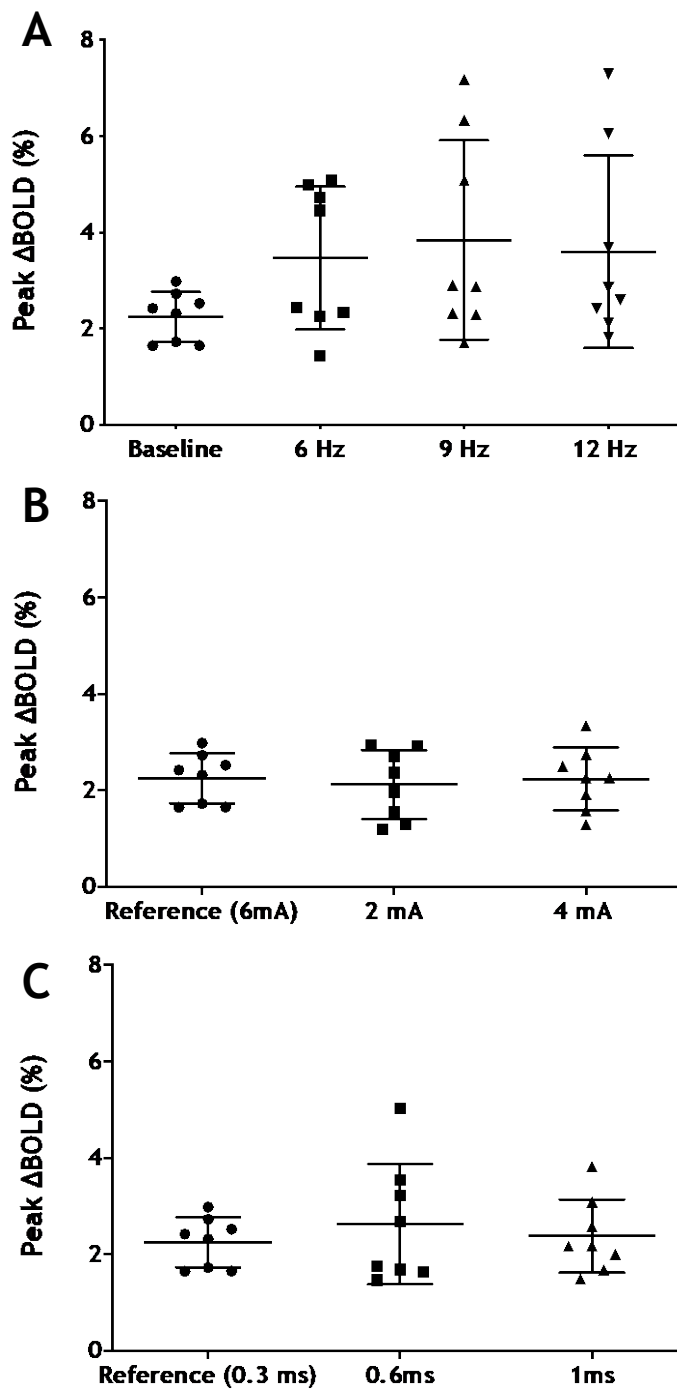


Figure 4.4: Peak Δ BOLD for variations in (A) stimulus frequency, (B) stimulus intensity and (C) pulse duration. A significant effect was observed when data were analysed using RM one-way ANOVA ($p=0.036$), however no significant pairwise comparisons were observed within each stimulus category when using Tukey multiple comparison test. Data presented as mean \pm standard deviation.

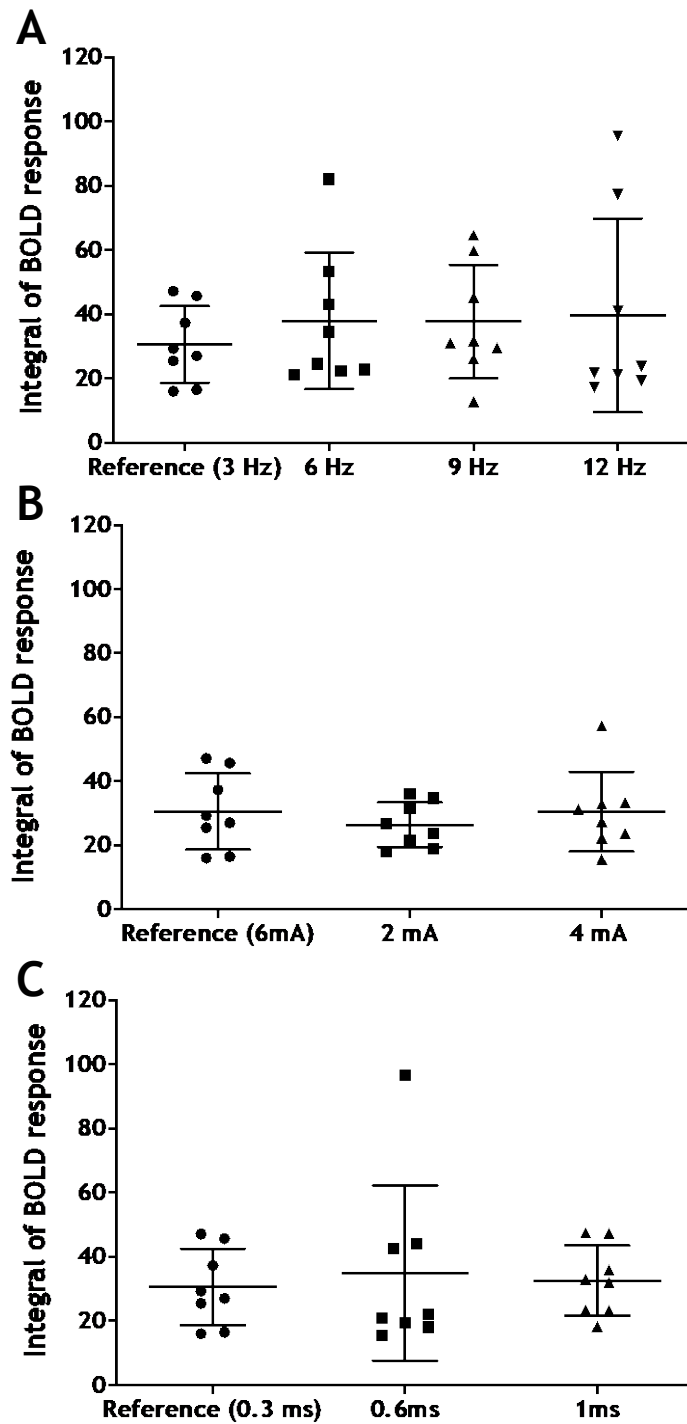


Figure 4.5: The effect of varying (A) stimulus frequency, (B) stimulus intensity and (C) pulse duration on the integral of the BOLD response. No significant effect was observed for any stimulus condition tested (Friedman test, $p=0.49$). Data presented as mean \pm standard deviation. Data organised into stimulus condition categories for display purposes only.

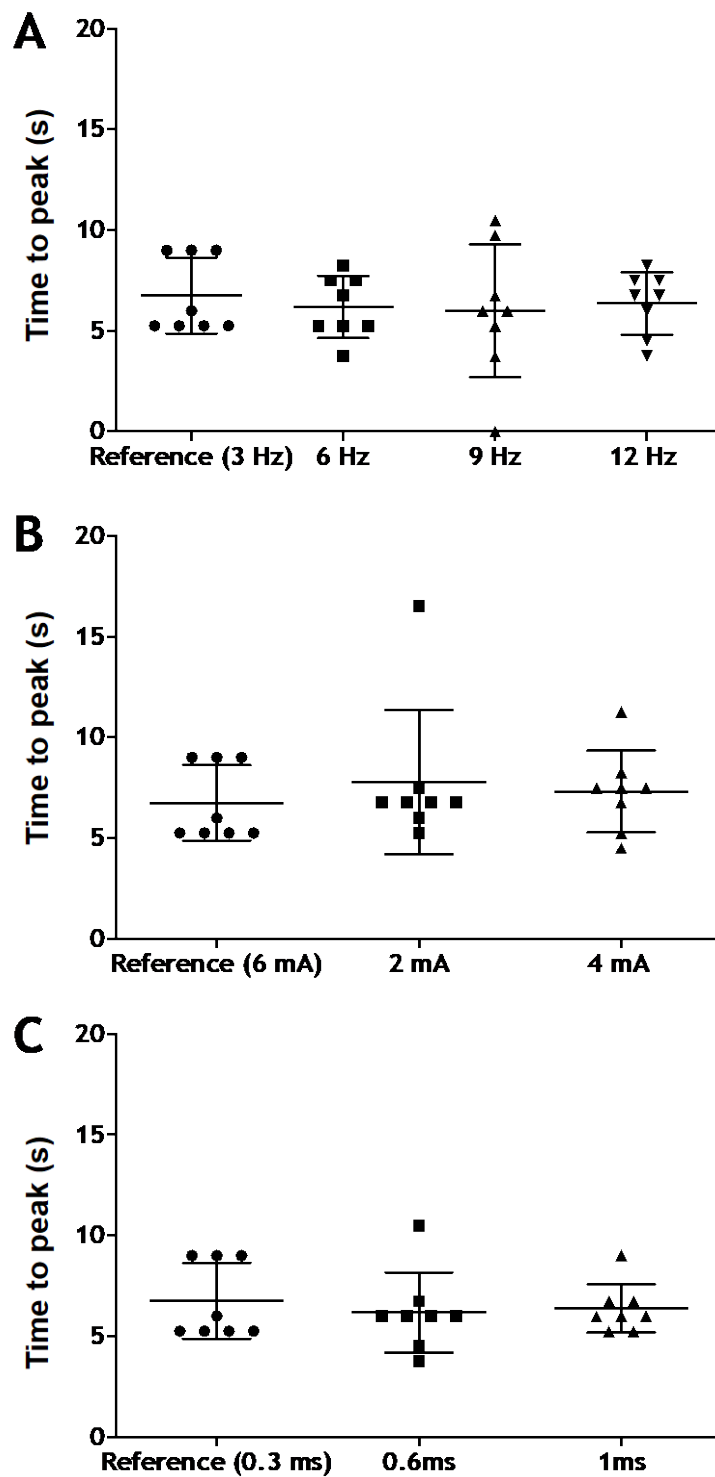


Figure 4.6: The effect of varying (A) stimulus frequency, (B) stimulus intensity and (C) pulse duration on the time-to-peak. No significant effect of any stimulus variation on the time-to-peak was observed (Friedman test, $p=0.78$). Data presented as mean \pm standard deviation.

4.3.2. Study 2 - Investigation and optimisation of stimulus parameters for somatosensory evoked potentials using electrophysiology

4.3.2.1 Stimulus intensity

To assess the effect of varying the stimulus parameters on the various components of the SEP, we varied either the stimulus intensity or stimulus frequency while keeping all other stimulus parameters constant. All stimulus variations produced observable cord dorsum potentials (CDPs) in the ipsilateral dorsal column and measurable SEPs in the left somatosensory cortex, being contralateral to the site of stimulation. Figure 4.7 shows the SEP traces from a representative animal for the first 10 seconds of stimulation during the 2 mA, 4 mA and 6 mA conditions. For all stimulus intensities tested, each stimulus pulse typically evoked a corresponding SEP. However, during recording sessions for all animals, we observed bursts of spontaneous activity within the SEP trace that either distorted or entirely abolished the SEP. Therefore in some instances, we did not observe a corresponding SEP to the stimulus pulse due to the on-going spontaneous activity. These bursts of activity were observed to occur during both stimulus 'off' and stimulus 'on' periods and were only observed in the SEP trace and not the CDP trace.

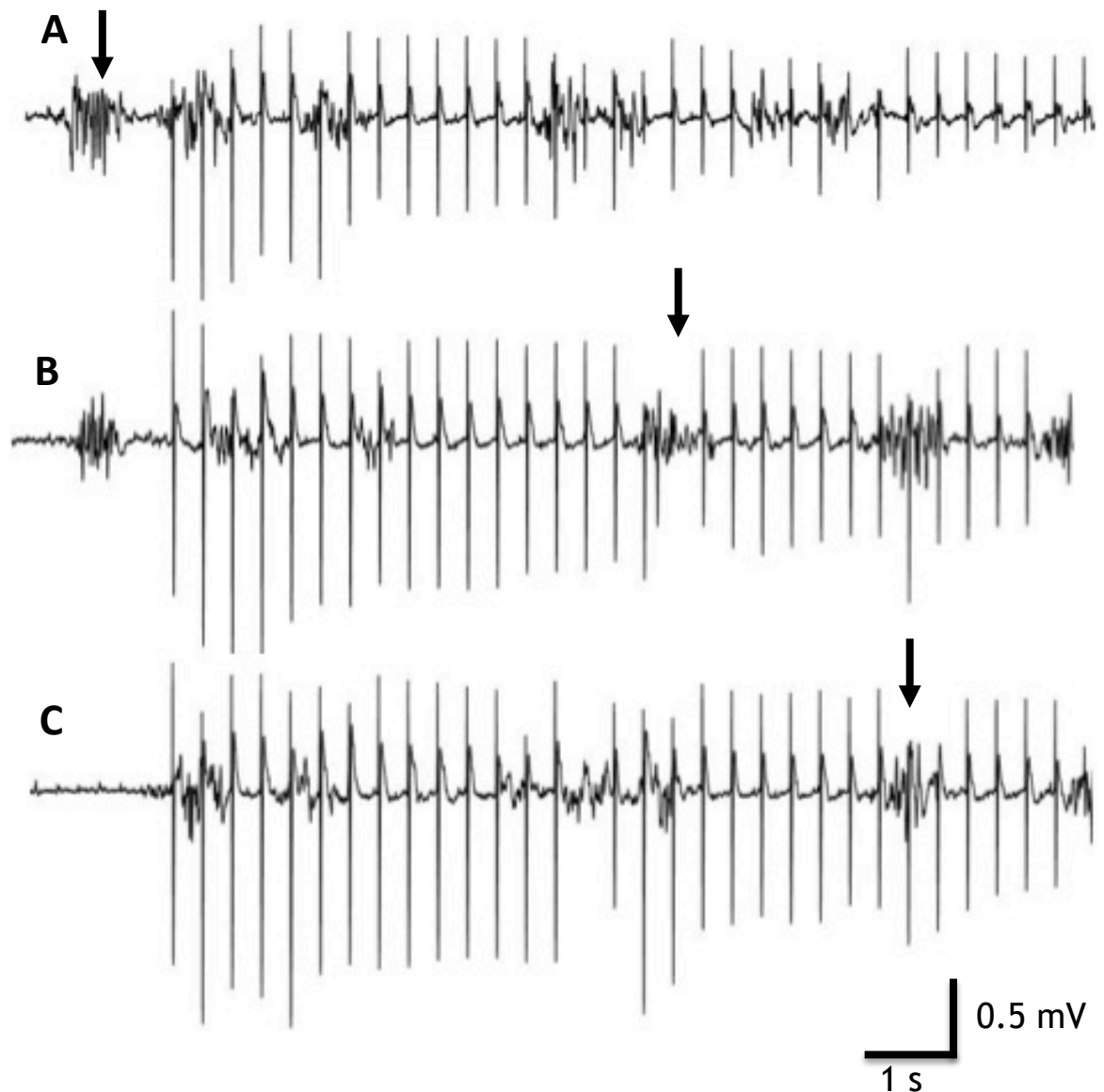


Figure 4.7: SEPs traces showing 2 seconds of pre-stimulus baseline and the first 10 seconds of stimulation at 2 mA (A), 4 mA (B) and 6 mA (C). Stimulus frequency was 3 Hz and pulse duration 0.3 ms. Spontaneous activity can be seen at various instances during all traces. In trace A, the arrow indicates spontaneous activity prior to stimulus onset. In trace B, the arrow indicates an absent SEP that has been abolished by the on-going spontaneous activity. In trace C, the arrow identifies modest distortion of the SEP.

When the amplitudes of P1, N1 and P2 were measured, we observed that the shape of the amplitude plot remained relatively consistent between all components of the SEP (Figure 4.8). For all components examined, the amplitude rapidly increased from baseline values with the appearance of the SEP following stimulus onset. Peak amplitudes were generally observed within the first few pulses, however once the peak amplitude was achieved, there was a decline in amplitude over the remaining duration of the stimulation period. The downward slope of the amplitude decline over the course of stimulation appeared to differ between the positive and negative components. Group-averaged P1 and P2 amplitudes demonstrated a gradual decline over the course of stimulation while group-averaged N1 amplitudes demonstrated a much more pronounced and sharper decline over the course of stimulation, almost returning to baseline values at the end of the stimulation period (Figure 4.8).

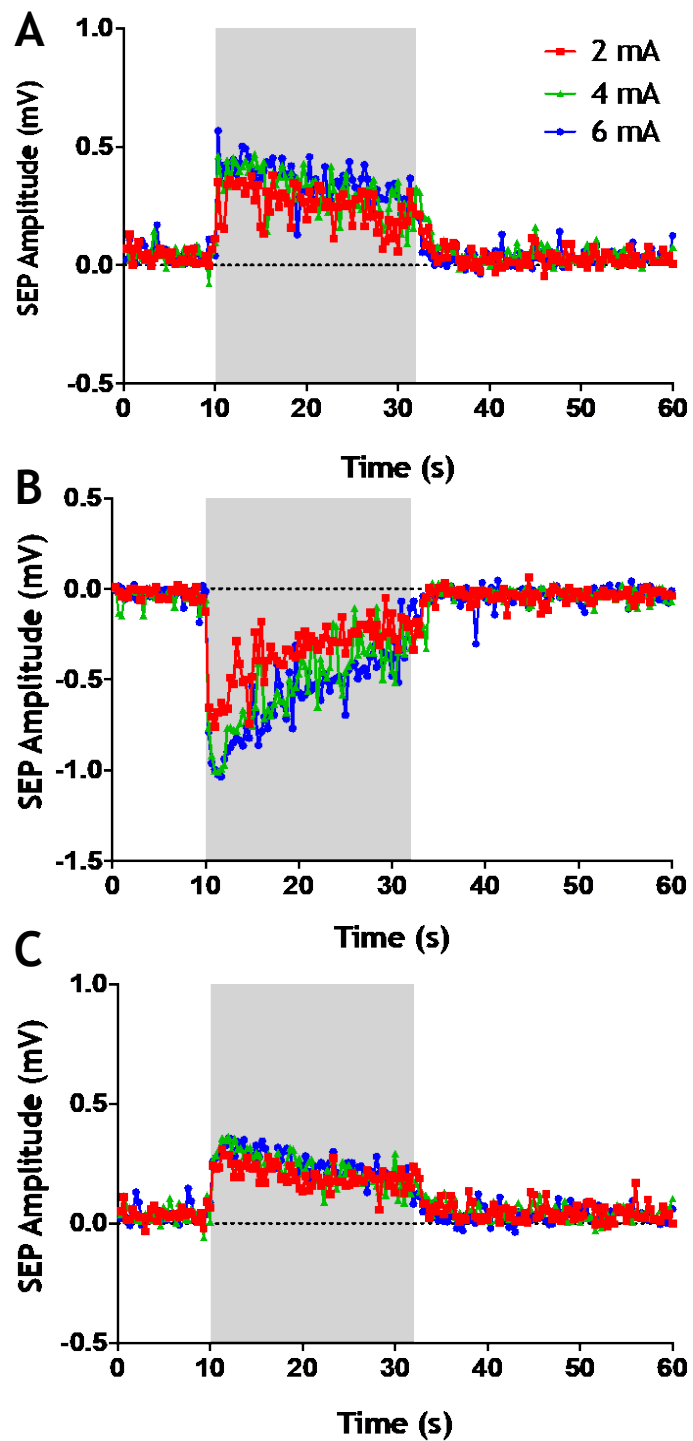


Figure 4.8: Group-averaged stimulus intensity time courses for (A) P1, (B) N1 and (C) P2 waveform components at 2, 4 and 6 mA. Stimulus frequency was 3 Hz and pulse duration was 0.3 ms. Shaded area indicates stimulation.

When comparing the characteristics of P1, N1 and P2, we observed that the peak amplitude did not significantly differ between any of the stimulus intensities tested (Figure 4.9). There was a significant effect of stimulus intensity on $\Sigma P1$ ($p=0.04$), with values increasing with stimulus intensity, however no significant pairwise comparisons were observed (11.57 mV vs. 14.48 mV vs. 15.55 mV; 2mA vs. 4mA vs. 6mA). The lack of any significant comparisons is likely underpinned by the low sample size and large variability observed in our data. A significant effect of stimulus intensity was also observed on the $\Sigma N1$ values, (-16.67 mV vs. -25.05 mV vs. -26.60 mV; 2mA vs. 4mA vs. 6mA, $p = 0.02$) with $\Sigma N1$ at 4 mA being significantly larger than that at 2 mA (adjusted $p=0.04$). There was also a trend for $\Sigma N1$ at 6 mA to be larger than that at 2 mA (adjusted $p=0.05$). $\Sigma P2$ was also significantly affected by stimulus intensity (8.90 mV vs. 11.01 mV vs. 11.30 mV; 2mA vs. 4mA vs. 6mA, $p=0.01$) with $\Sigma P2$ values at both 4 mA and 6 mA being significantly larger than those observed at 2 mA ($p<0.05$ for both). A summary of $\Sigma P1$, $\Sigma N1$ and $\Sigma P2$ is shown in Figure 4.10.

There was a significant effect of varying the stimulus intensity on the amplitude of N1 ($p=0.02$) and P2 ($p=0.01$) components over the course of the stimulation period, with the integrals of N1 and P2 being significantly larger at 4 mA and 6 mA (adjusted $p<0.05$ for both), respectively, compared with 2 mA (Figure 4.11). No significant effect of stimulus intensity on the integral of P1 was observed however there was a trend for values to increase with stimulus intensity ($p=0.06$). Collectively our findings indicate that larger individual components of the SEP and therefore, larger SEPs in general, are evoked and maintained at the higher stimulus intensities of 4 mA and 6 mA. However, it is worth noting that for all measured characteristics (e.g. peak, sum and integral) of the SEP, the increase in each measure with increasing stimulus intensity appears to be non-linear, as mean increases were numerically larger between 2 mA and 4 mA than between 4 mA and 6 mA. Therefore, while higher intensities evoked larger SEPs at the stimulus intensities investigated, it is likely that there is a limit to which increasing the stimulus intensity will result in an increased SEP.

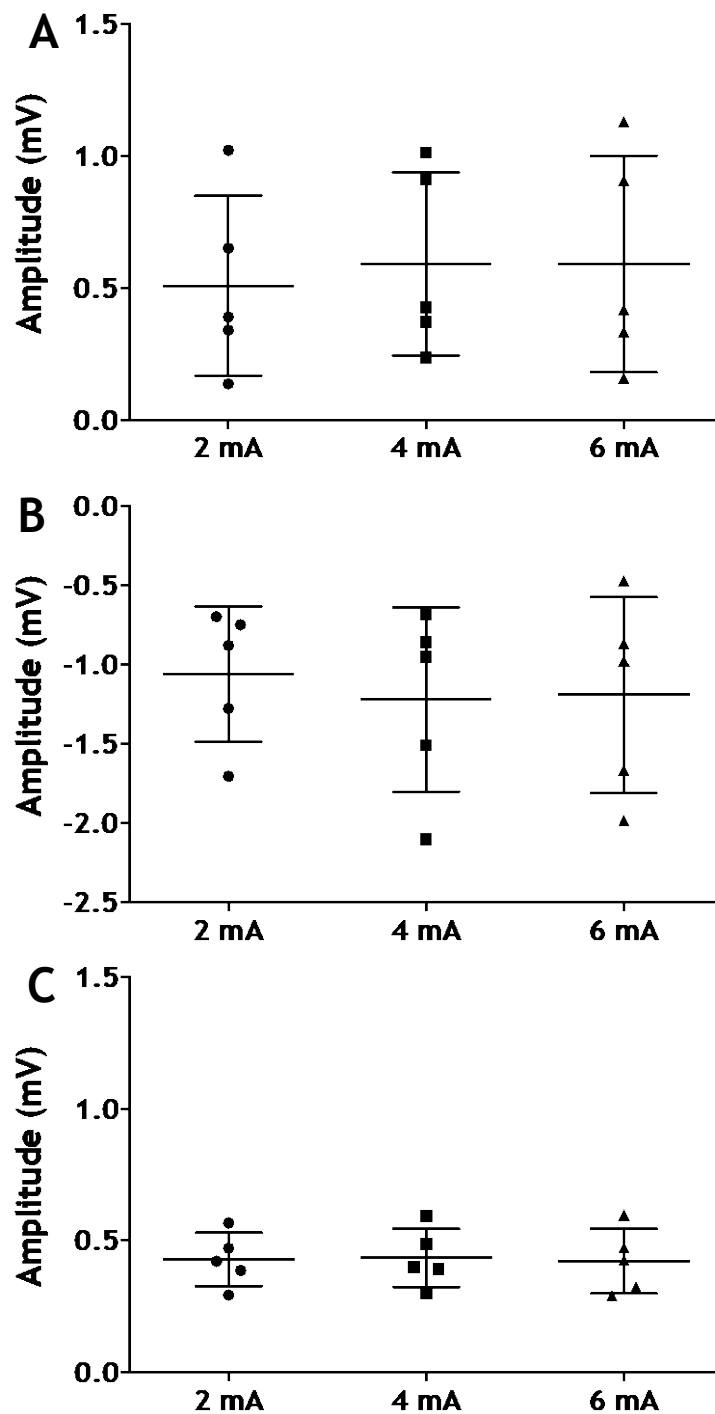


Figure 4.9: Peak amplitude values for (A) P1, (B) N1 and (C) P2 waveform components at 2, 4 and 6 mA. No significant effect of varying the stimulus intensity on the peak amplitude of P1 (RM one-way ANOVA, $p=0.16$), N1 (RM one-way ANOVA, $p=0.27$) or P2 (RM one-way ANOVA, $p=0.84$) at any stimulus intensity tested. Individual data points shown with mean \pm standard deviation overlaid.

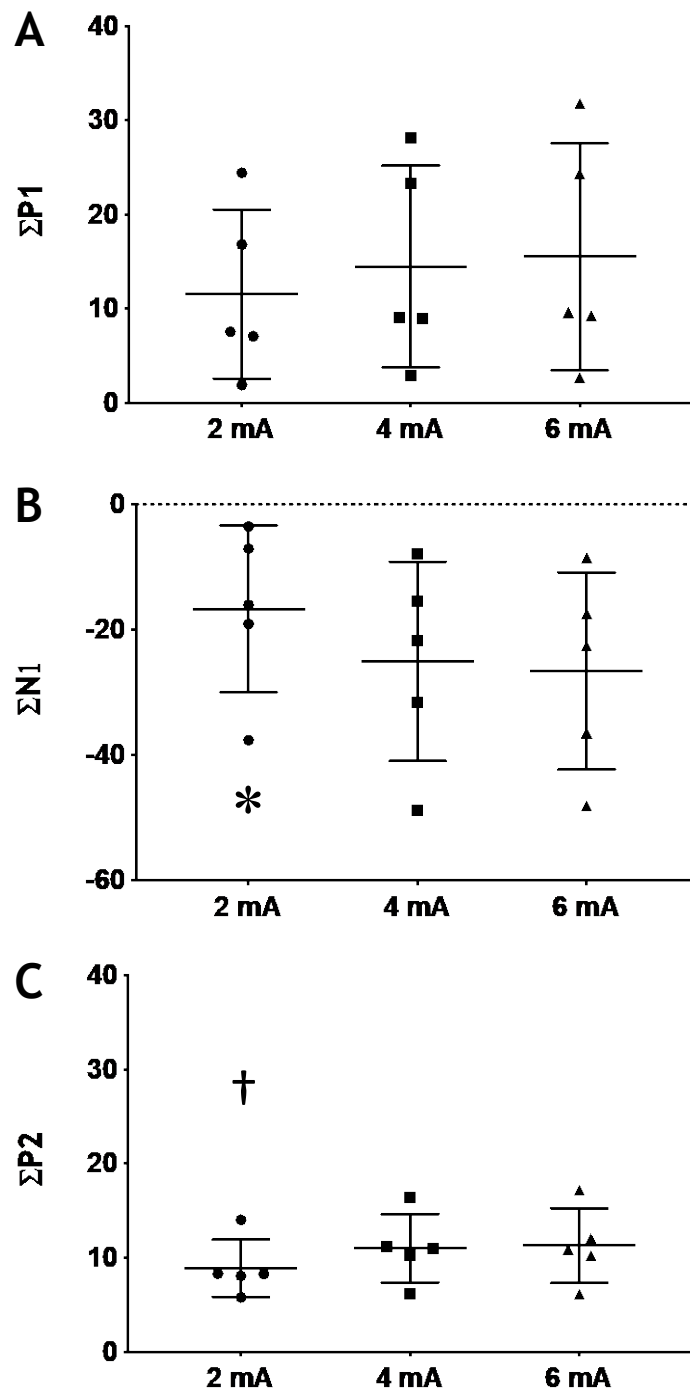


Figure 4.10: The effect of varying stimulus intensity on (A) $\Sigma P1$, (B) $\Sigma N1$ and (C) $\Sigma P2$. All SEP components demonstrated a trend to increase with stimulus intensity. $\Sigma N1$ at 2 mA was significantly smaller compared to 4 mA ($p=0.02$). $\Sigma P2$ at 2 mA was significant smaller compared to 4 mA and 6 mA ($p<0.01$). A significant effect of stimulus intensity on $\Sigma P1$ was observed ($p = 0.04$) but no significant pairwise comparisons. Data analysed using RM one-way ANOVA with Tukey's multiple comparisons test. * $p<0.05$ vs 4 mA; † $p<0.05$ vs 4 mA and 6 mA. Individual data points shown with mean \pm standard deviation overlaid.

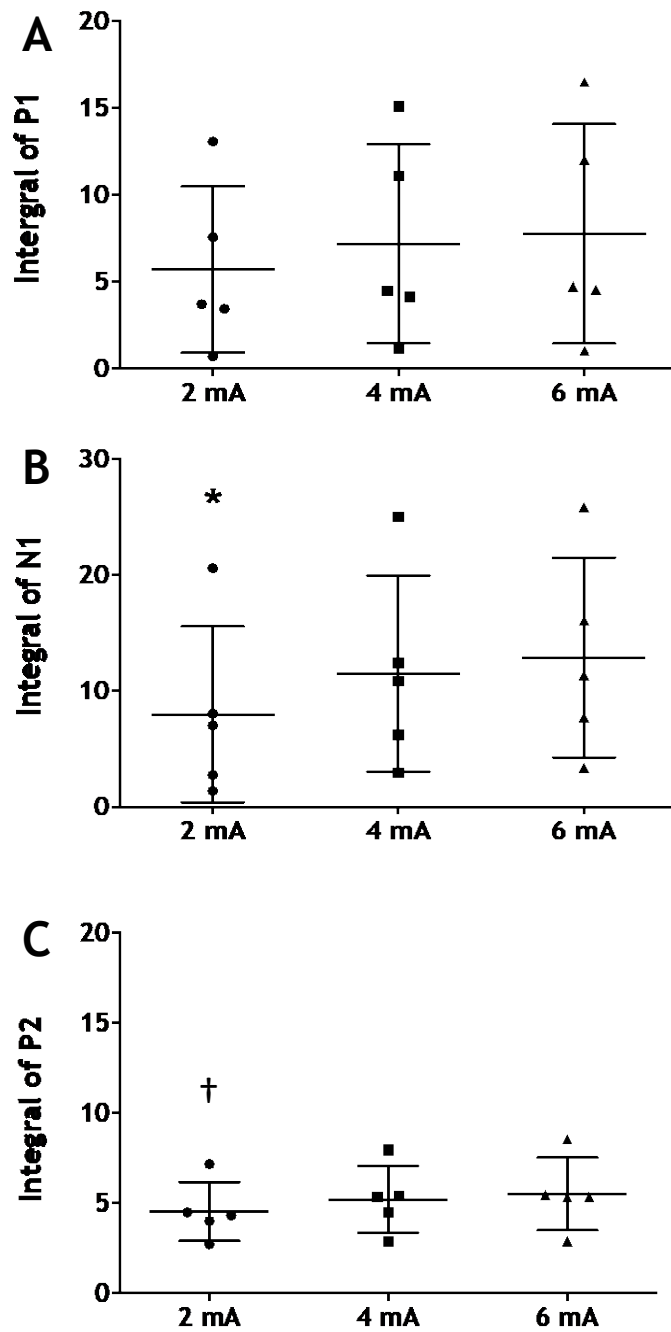


Figure 4.11: The effect of varying stimulus intensity on the integral of (A) P1, (B) N1 and (C) P2. Larger responses were generally maintained at higher stimulus intensities (≥ 4 mA) compared to 2 mA. N1 at 2 mA was significantly smaller compared to 4 mA ($p=0.02$). $\Sigma P2$ at 2 mA was significant smaller compared to 6 mA ($p=0.01$). No significant effect of stimulus intensity on $\Sigma P1$ was observed ($p = 0.0574$). Data analysed using RM one-way ANOVA with Tukey's multiple comparisons test. * $p < 0.05$ vs 4 mA; † $p < 0.05$ vs 6 mA. Individual data points shown with mean \pm standard deviation overlaid.

4.3.2.2 SEPs and stimulus frequency

Changing the stimulus frequency between 3, 6, 9 and 12 Hz had varying effects on the resultant SEPs over the course of stimulation. Examples of SEP traces during the first 10 seconds of the first stimulation period for a representative animal are shown in Figure 4.12. During 3 Hz stimulation, each stimulus pulse generally evoked an SEP, however as previously noted, there were instances of spontaneous activity that in some cases abolished the SEP. When the stimulus frequency was 6 Hz, we observed a one-to-one ratio of stimulus pulse-to-SEP for most animals. However in 3 animals, after an initial period of stable, consistent responses, the amplitude of N1 exhibited an oscillatory pattern of amplitude changes, noticeably increasing and decreasing periodically over the course of stimulation. This can be seen in the SEP trace shown for the representative animal in Figure 4.12B. Interestingly, this oscillatory pattern of activity was most prominent in the N1 waveform for 3 animals but was also demonstrated by 2 animals for the P2 waveform. None of the examined animals exhibited this oscillatory pattern of amplitude change for the P1 waveform, which maintained a stable presence with only a gradual reduction in amplitude over the course of stimulation. During 9 Hz stimulation, we again observed an oscillatory pattern of amplitude changes over the course of stimulation, however, at this stimulus frequency all animals and all components demonstrated this pattern of response. Interestingly, N1 demonstrated this effect most notably and exhibited clear periodic bursts of SEP activity interspersed with periods where N1 was abolished. These bursts of activity typically demonstrated a gradual increase in SEP amplitude with subsequent stimulus pulses, building towards a peak amplitude and then gradually declining in amplitude. While P1 and P2 demonstrated this oscillatory change in amplitude, both components maintained a stable presence even during the 'quiescent' oscillatory periods, although during these periods their amplitude was severely attenuated. During 12 Hz stimulation, we observed an initial burst of SEPs with relatively large amplitude immediately following stimulus onset. However, this burst of activity was quickly attenuated and remained very low for the remaining duration of stimulation.

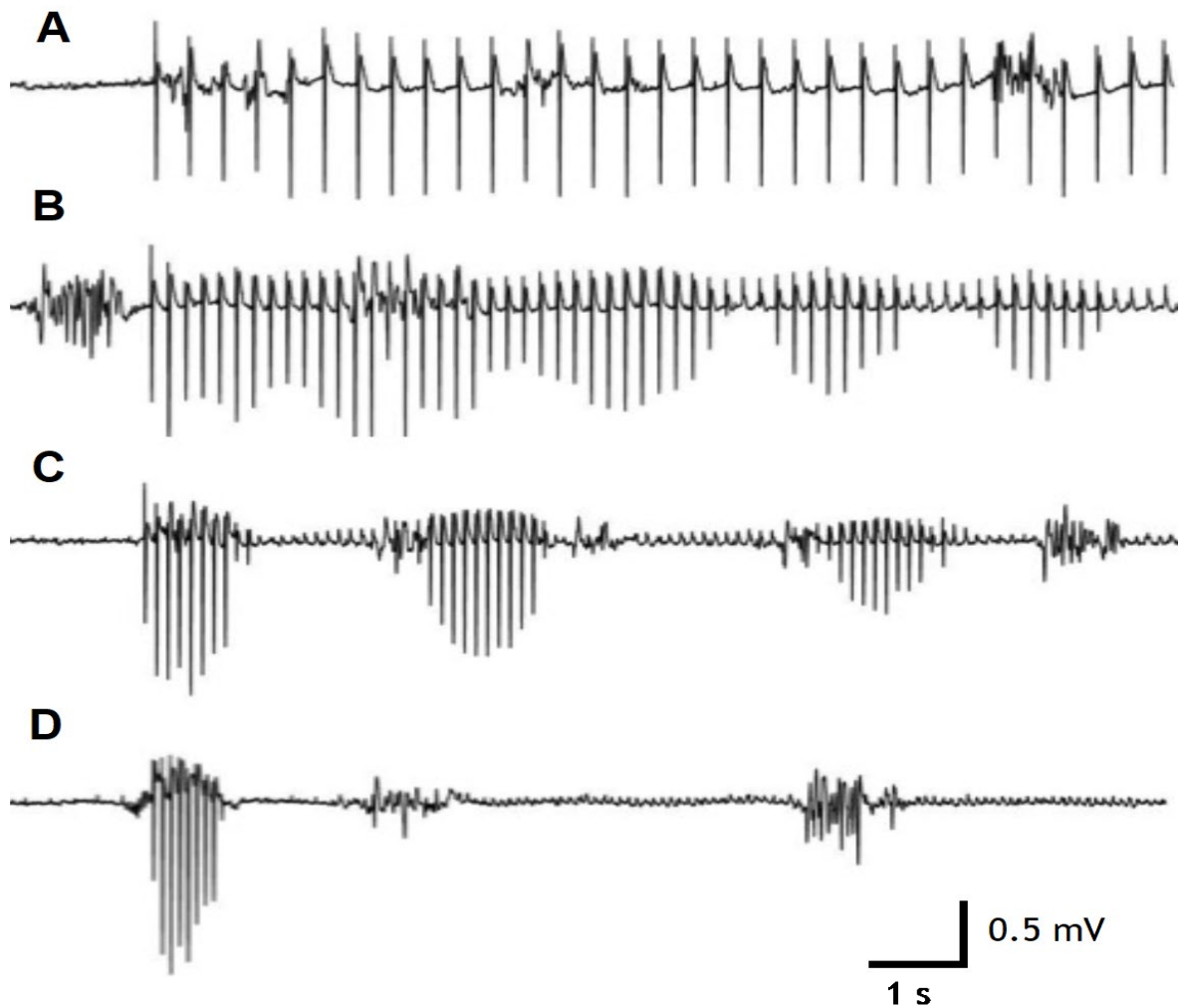


Figure 4.12: SEP data traces for the first 10 seconds of stimulation at (A) 3 Hz, (B) 6 Hz, (C) 9 Hz and (D) 12 Hz. 3 Hz stimulation generally maintained a consistent stimulus pulse to SEP. SEPs during 6 Hz stimulation demonstrated an oscillatory pattern in amplitude with a gradual decline over the course of stimulation. 9 Hz stimulation demonstrated a strong oscillatory effect of amplitude changes of the SEPs which periodically appeared and disappeared. 12 Hz stimulation resulted in a short burst of SEP activity at the beginning of stimulation that quickly disappeared and remained absent for the remainder of the stimulation period.

The shape of the amplitude plot for each frequency generally reflects the pattern of SEP activity described above. At 3 Hz, amplitude values demonstrated a rapid increase after stimulus onset with the appearance of the SEP, which remained elevated but demonstrated a gradual decline over the course of stimulation. The values quickly returned to baseline following cessation of the stimulus and absence of the SEP (Figure 4.13A). Stimulus frequencies above 3 Hz exhibited a more profound effect on the components of the SEP over the course of stimulation. During 6 Hz, group-averaged measurements revealed that all SEP components exhibited an initial amplitude peak shortly after stimulus onset, which declined more noticeably over the course of stimulation, almost returning to baseline values at the end of the stimulation period (Figure 4.13B). During the 9 Hz stimulus condition, we initially observed a large peak in amplitude values after stimulus onset that rapidly returned to baseline and then exhibited an oscillatory pattern of changes, with the amplitude increasing and decreasing as bursts of SEPs periodically appeared and disappeared for the remaining duration of stimulation (Figure 4.13C). This effect was observed for all SEP components in all animals during the 9 Hz stimulation but was most noticeable in the N1 component. During the 12 Hz stimulus condition, we again observed a large peak in amplitude values following stimulus onset that rapidly returned to baseline and then remained very low for the remainder of the stimulation period as the SEPs remained virtually absent (Figure 4.13D)

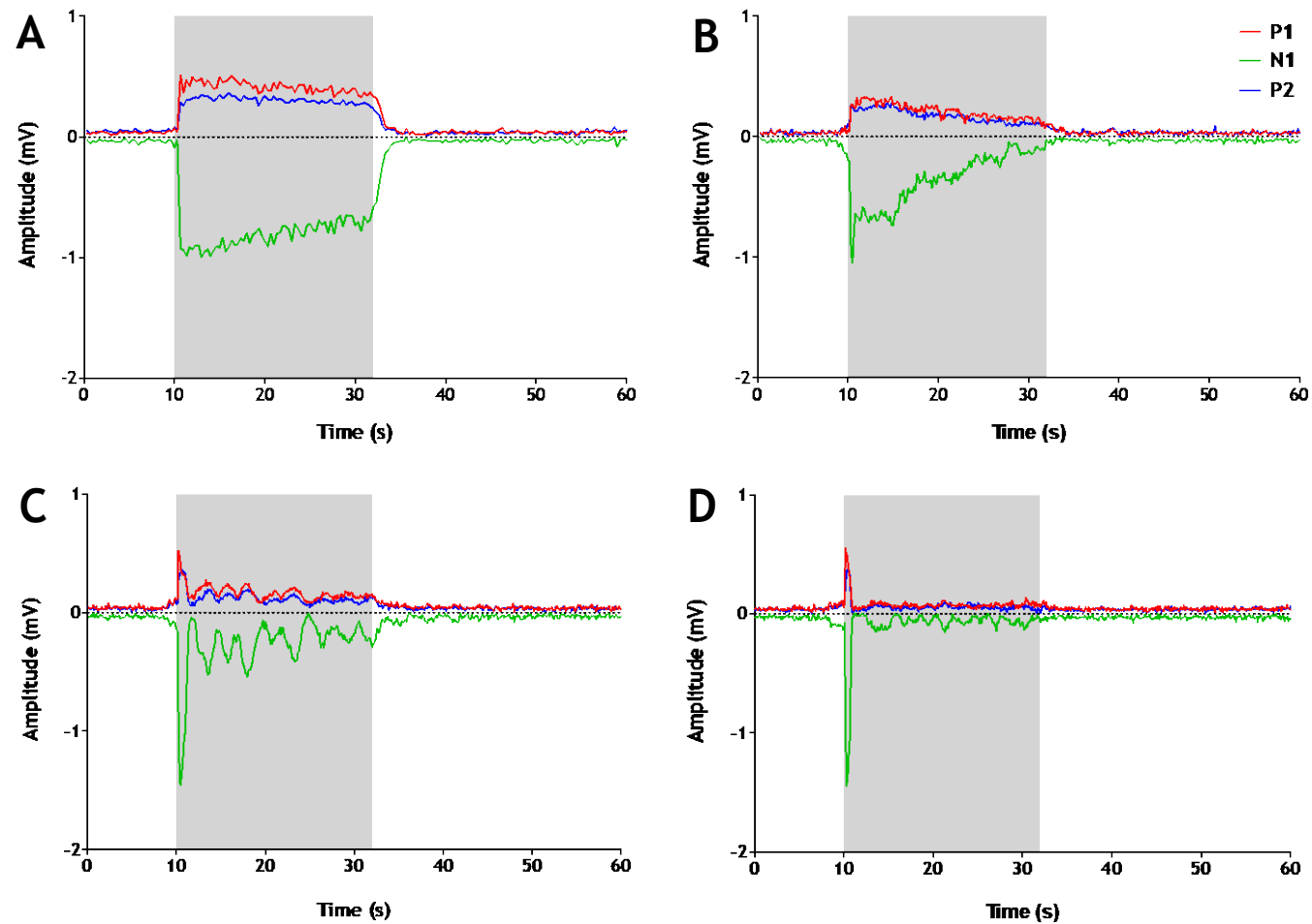


Figure 4.13: Group-averaged amplitude plots for (A) 3 Hz, (B) 6 Hz, (C) 9 Hz and (D) 12 Hz stimulation. 3 Hz maintained the most stable amplitudes during stimulation for each waveform component while higher frequencies resulted in a suppression of the SEP response. 9 Hz stimulation revealed an oscillatory pattern of activity with SEPs ‘waxing and waning’ throughout the stimulation.

Figure 4.14 shows the individual peak amplitude values for all measured components of the SEP at each stimulus frequency tested. We observed that varying the stimulus frequency did not have a significant effect on either the P1 peak amplitude (0.6179 mV vs. 0.5019 mV vs. 0.5602 mV vs. 0.5941 mV, 3 Hz vs. 6 Hz vs. 9 Hz vs. 12Hz; $p = 0.15$) or the peak P2 amplitude (0.3934 mV vs. 0.3617 mV vs. 0.3914 mV vs. 0.3950 mV, 3 Hz vs. 6 Hz vs. 9 Hz vs. 12Hz; $p = 0.31$). However, there was a significant effect of stimulus frequency on the peak N1 amplitude (-1.170 mV vs. -1.113 mV vs. -1.486 mV vs. -1.466 mV, 3 Hz vs. 6 Hz vs. 9 Hz vs. 12Hz; $p = 0.0006$), with 9 Hz evoking a larger N1 peak amplitude than that observed at 3 Hz and 6 Hz (adjusted $p < 0.05$ and $p < 0.01$, respectively). 12 Hz was also observed to evoke a larger peak N1 amplitude compared that that evoked at 6 Hz (adjusted $p < 0.05$).

Both $\Sigma P1$ and $\Sigma P2$ demonstrated a trend to increase with stimulus frequency but only until 9 Hz (Figure 4.15). The mean values observed at 12 Hz for both $\Sigma P1$ and $\Sigma P2$ were notably smaller than those observed at all other test frequencies ($\Sigma P1$, 27.2 mV vs. 31.9 mV vs. 33.3 mV vs. 22.2 mV; $\Sigma P2$, 19.9 mV vs. 22.7 mV vs. 24.5 mV vs. 16.4 mV; 3 Hz vs. 6 Hz vs. 9 Hz vs. 12 Hz). However, we did not observe a significant effect of stimulus frequency on these measurements ($\Sigma P1$, $p = 0.11$ and $\Sigma P2$, $p = 0.07$, Friedman test). Unlike the positive SEP components, $\Sigma N1$ did not demonstrate a clear trend to increase with stimulus frequency. However, there was a significant effect of varying the frequency on $\Sigma N1$ with the $\Sigma N1$ observed at 12 Hz being significantly smaller than that observed at the lower stimulus frequencies of 3 Hz and 6 Hz (adjusted $p < 0.05$).

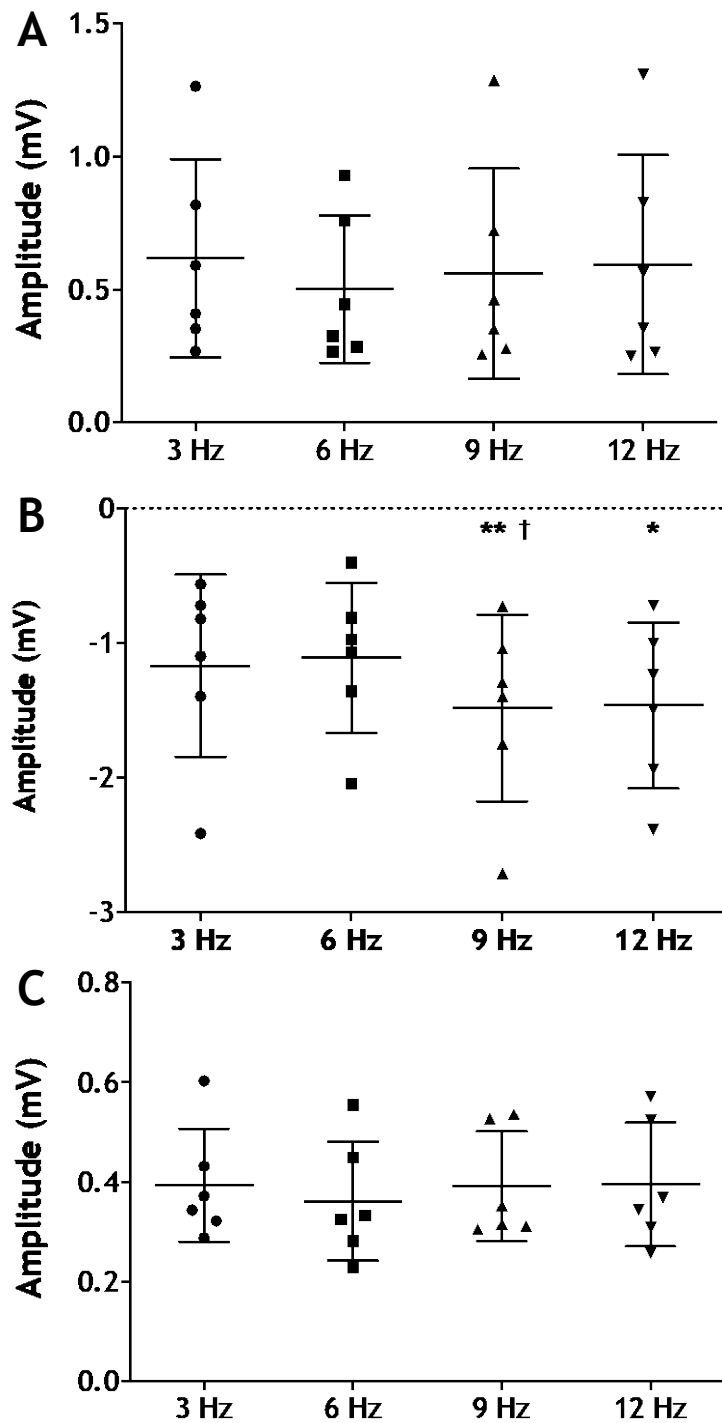


Figure 4.14: The effect of varying stimulus frequency on the peak amplitudes of (A) P1, (B) N1 and (C) P2. Peak amplitudes remained consistent for P1 and P2 waveforms but 9 and 12 Hz evoked significantly larger peak amplitudes than those observed at the lower stimulus frequencies. Individual responses with mean and standard deviation shown. * $p < 0.05$ vs 6 Hz; ** $p < 0.01$ vs 6 Hz; † $p < 0.05$ vs 3 Hz.

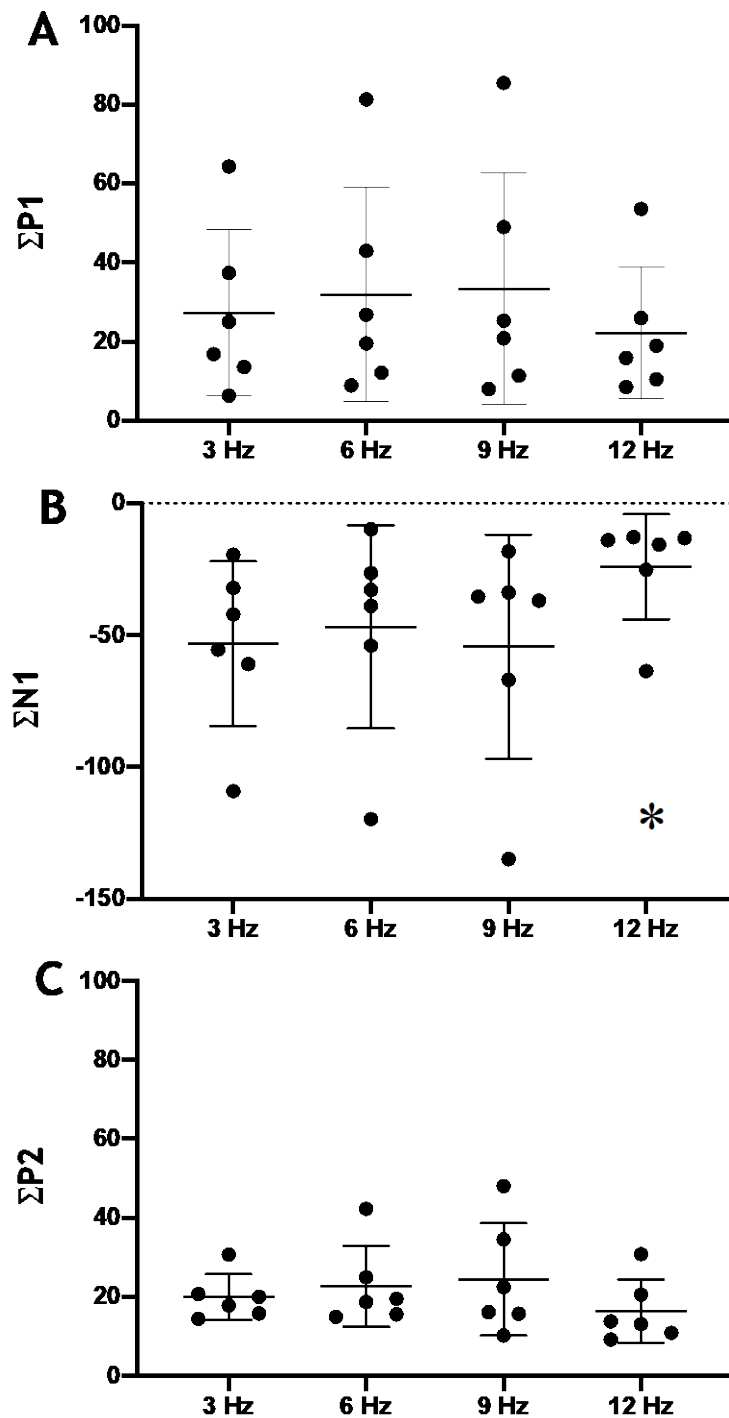


Figure 4.15: Effect of varying stimulus frequency on (A) $\Sigma P1$, (B) $\Sigma N1$ and (C) $\Sigma P2$ values. Both positive components demonstrated a trend to increase with stimulus intensity, peaking at 9 Hz and then declining at 12 Hz. N1 at examined frequencies ≤ 9 Hz remained similar but N1 at 12 Hz was significantly lower than that at 3 Hz and 9 Hz. Data analysed using Friedman test. Individual responses with mean and standard deviation shown. * $p < 0.05$ vs 3 Hz and 6 Hz.

Given that higher frequencies will contain more stimulus pulses than lower frequencies, it is difficult to separate the effect of frequency from stimulus number when calculating Σ SEP. Therefore, we also assessed the integral of P1, N1 and P2 responses by calculating the AUC of the individual amplitude plots, to better isolate the effects of frequency on amplitude over the course of stimulation (Figure 4.16). There was a significant effect of varying stimulus frequency on the integrated measurements for all SEP components (P1, $p=0.03$, N1, $p<0.01$, P2, $p<0.0001$, RM one-way ANOVA) with higher frequencies of 6 Hz and above demonstrating smaller values than that observed at 3 Hz. Collectively, our observations indicate that higher frequencies of 9 and 12 Hz evoke larger peak amplitudes in the N1 waveform than those evoked at 3 Hz and 6 Hz. However, these high amplitudes are not maintained over the course of stimulation but become attenuated, either periodically in the case of 9 Hz or completely in the case of 12 Hz.

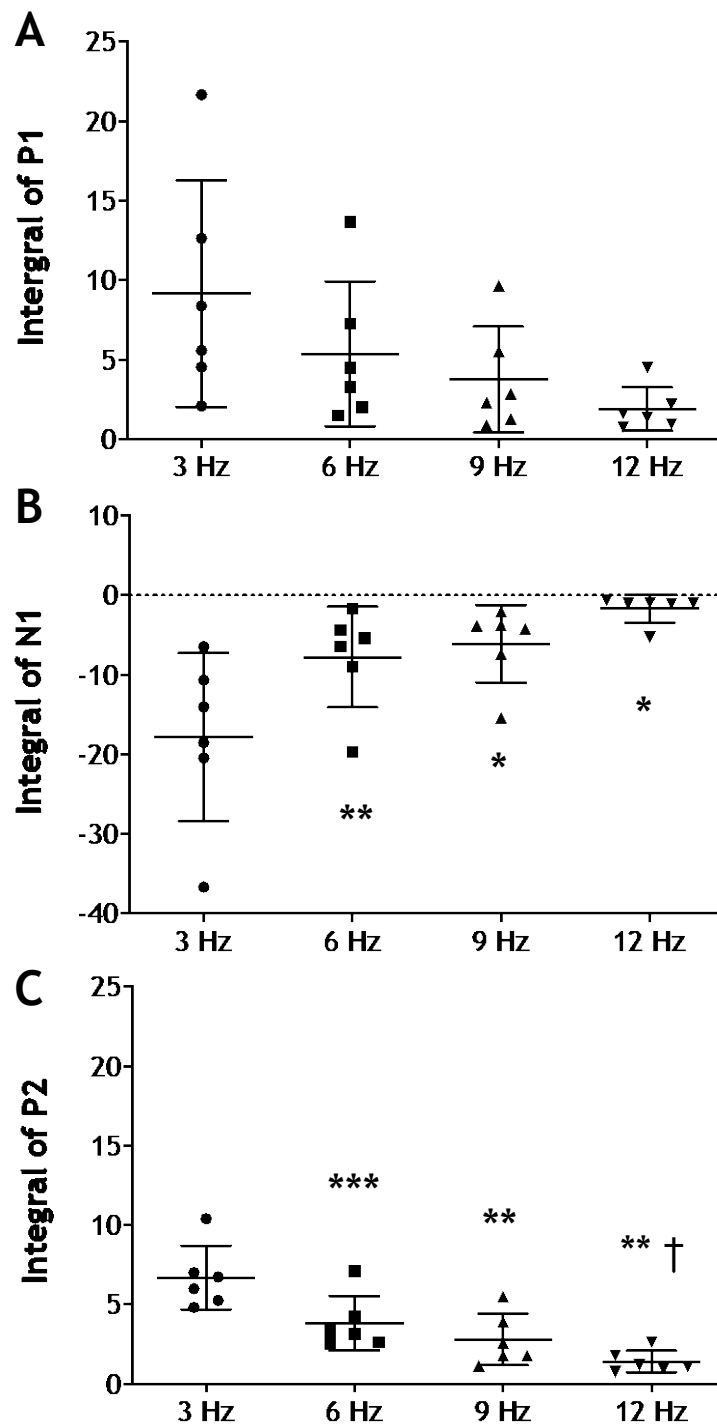


Figure 4.16: The effect of stimulus frequency on the integral of the SEP for (A) P1, (B) N1, and (C) P2 waveforms. A significant effect of varying stimulus frequency was observed on P1 ($p=0.03$), N1 ($p<0.01$), and P2, ($p<0.0001$). The integrals of N1 and P2 were significantly larger at 3 Hz compared to other stimulus frequencies. Individual responses with mean and standard deviation shown. * $p<0.05$ vs 3 Hz; ** $p<0.01$ vs 3 Hz; *** $p<0.001$ vs 3 Hz; † $p<0.05$ vs 6 Hz.

4.3.3. Study 3 - Investigation and optimisation of stimulus parameters for CBF using laser speckle contrast imaging

4.3.3.1 Stimulus-evoked CBF response

To assess the effect of varying stimulus parameters on the rCBF response to forepaw stimulation, we systematically varied either the stimulus frequency or the stimulus intensity with regard to a reference set of stimulus parameters. For each stimulus condition tested, we observed an increased blood flow response on the surface of the cortex within the somatosensory area (Figure 4.17). The group-averaged time courses for most stimulus conditions showed a similar response shape with the CBF peaking shortly following stimulus onset, gradually declining over the course of stimulation and then returning to baseline following cessation of the stimulus (Figure 4.18). Group-averaged responses for the higher frequencies of 9 Hz and 12 Hz demonstrated a noticeable delay in the CBF response returning to baseline following the end of stimulation. However, this observation is underpinned by responses from 3 animals during the 9 Hz condition, and one animal during 12 Hz condition that demonstrated considerably large rCBF responses that were slow to return to baseline. The group-averaged rCBF response for the 12 Hz condition demonstrates a sharp and clear peak following stimulus onset followed by a plateau for the remainder of the stimulation period. This effect was observed in all animals during the 12 Hz run. We generally did not observe stimulus-induced responses in the ipsilateral S1FL area or the ipsilateral visual cortex ROIs, however 2 animals during the 9 Hz condition and 1 animal during the 12 Hz condition exhibited stimulus-induced CBF increases in the ipsilateral S1FL area of a similar shape to that observed in the contralateral S1FL, however at a notably smaller amplitude.

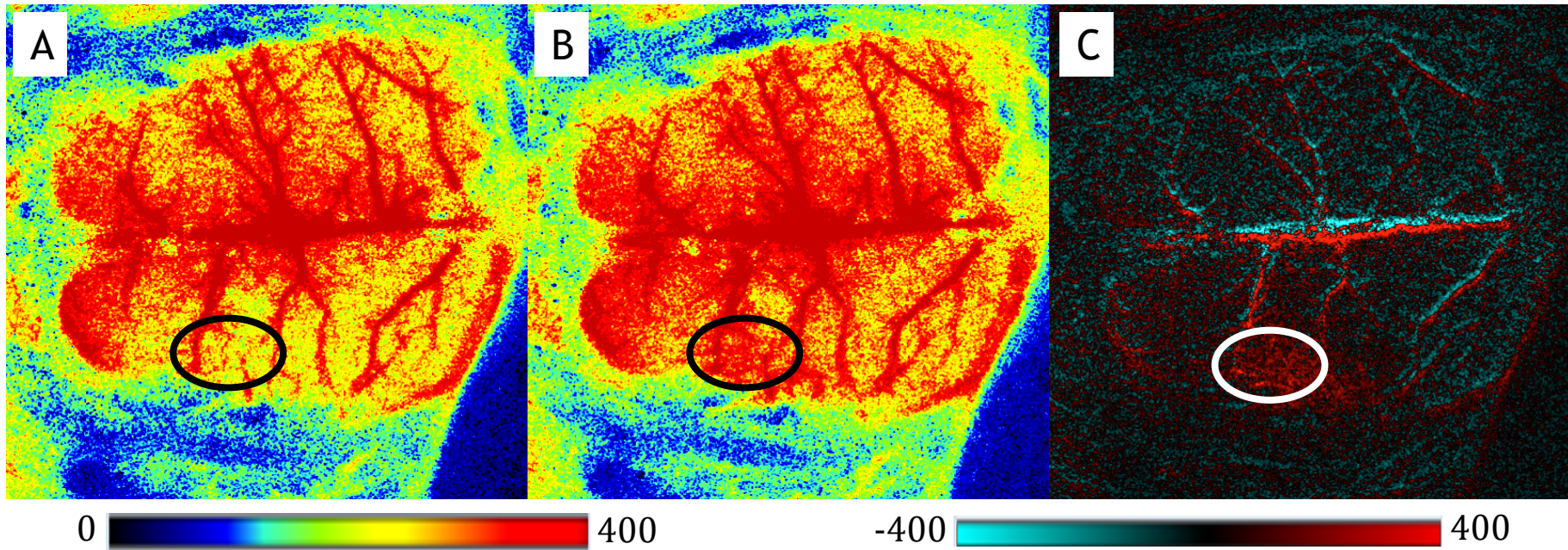


Figure 4.17: Laser speckle images showing top-down view of the brain. (A) An averaged image of 10 raw images during the pre-stimulus baseline period. (B) An averaged image during stimulation. (C) The difference image, created by subtracting pre-stimulus baseline and stimulation images. The contralateral S1FL ROI boundary is outlined in black/white. Scale bar indicates arbitrary units.

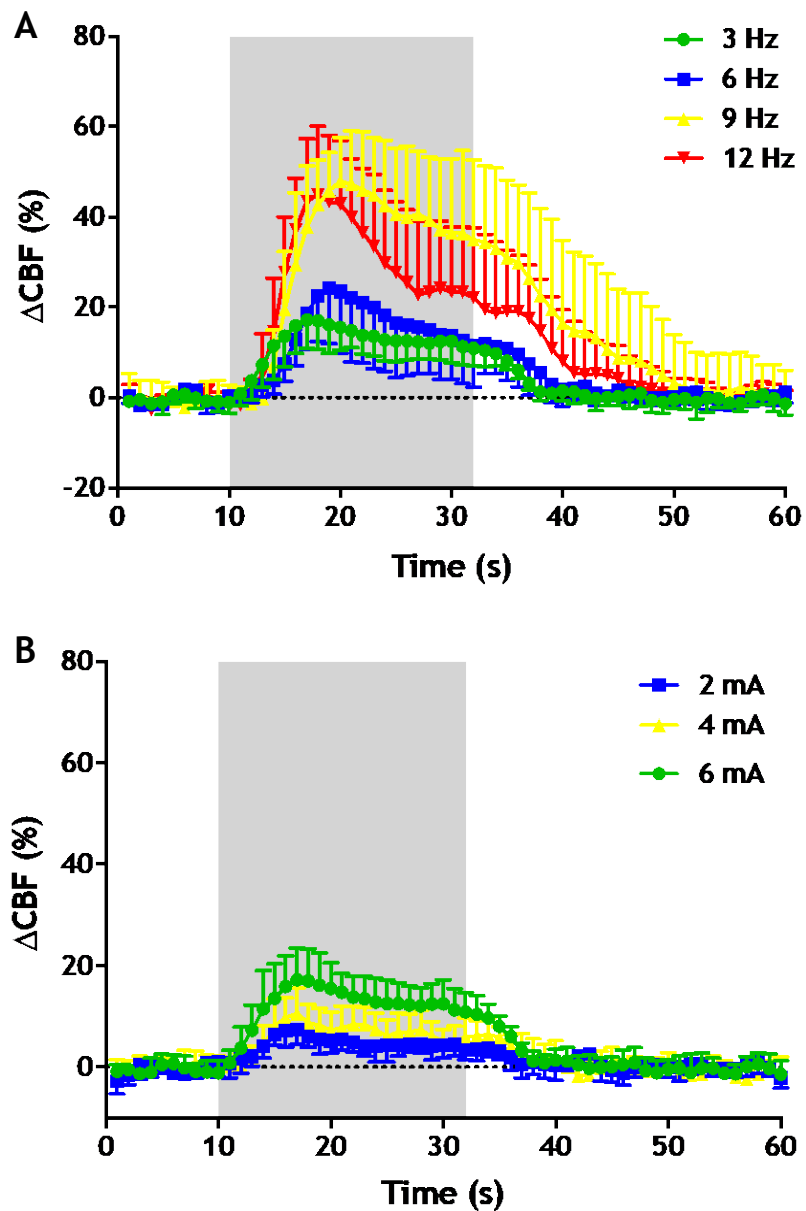


Figure 4.18: Group-averaged time courses from the S1FL area ROI showing ΔCBF under different (A) stimulus frequencies and (B) stimulus intensities. Data was normalised to the pre-stimulus baseline. Data shown in mean \pm standard deviation.

4.3.3.2 Peak change in CBF

Assessment of the peak Δ CBF revealed a significant effect of frequency and intensity in the contralateral S1FL area ($p < 0.001$). We observed a trend for the peak Δ CBF to increase with stimulus frequency, peaking at 9 Hz and then plateauing at 12 Hz (Figure 4.19A). Indeed, the peak Δ CBF evoked at 9 Hz and 12 Hz was found to be significantly larger than that evoked at 3 Hz ($p < 0.01$ and $p < 0.05$, respectively). Similarly, we observed that the peak Δ CBF increased with stimulus intensity (Figure 4.19B), with peak Δ CBF at 6 mA being significantly larger than that at 4 mA ($p < 0.05$). The peak Δ CBF values remained consistent between all the tested stimulus intensity and stimulus frequency conditions when ipsilateral S1FL and ipsilateral visual cortex ROIs were assessed (Figure 4.20).

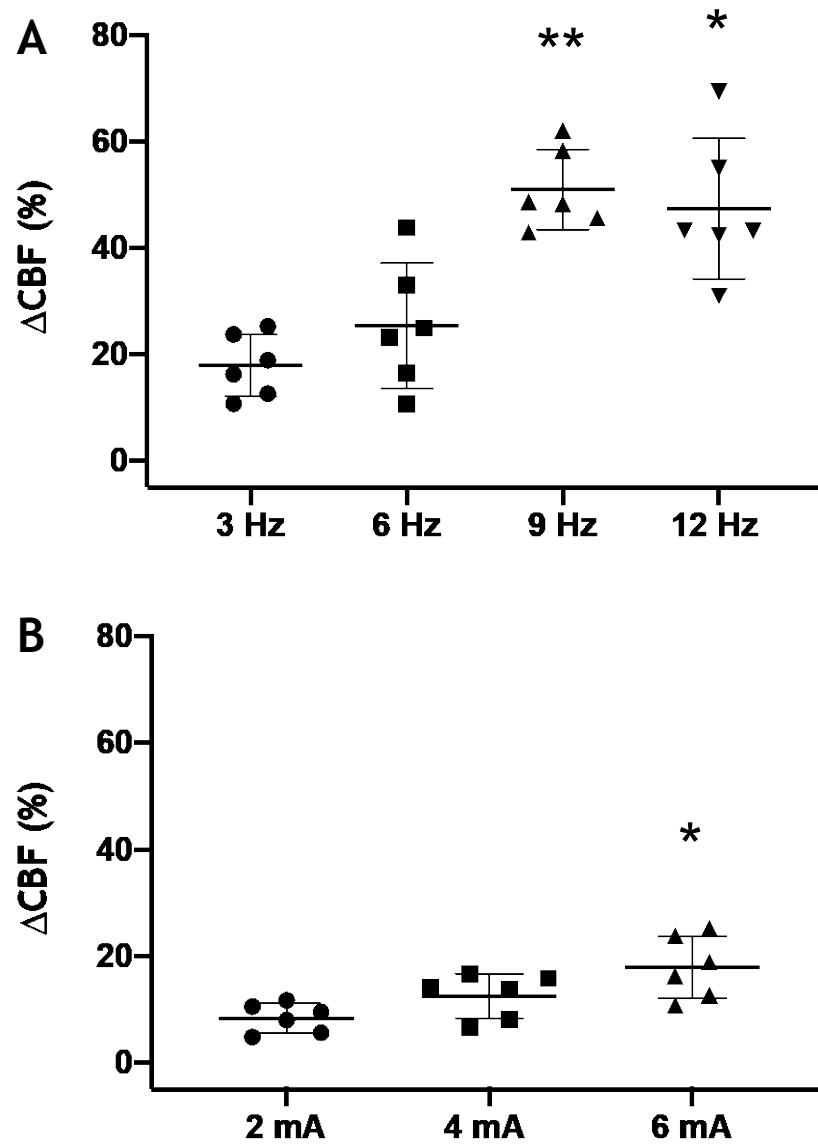


Figure 4.19: The effect of varying (A) stimulus frequency and (B) stimulus intensity on peak Δ CBF in the contralateral S1FL area. A significant effect of varying stimulus parameters was observed on peak CBF ($p < 0.001$) with larger increases observed at 9 Hz ($p < 0.01$) and 12 Hz ($p < 0.05$) compared to 3 Hz, as well as 6 mA compared to 4 mA ($p < 0.05$). 3 Hz and 6 mA data represent the same reference dataset. Individual data with mean \pm standard deviation shown. (A) ** $p < 0.01$ vs 3 Hz; * $p < 0.05$ vs 3 Hz. (B) * $p < 0.05$ vs 4 mA.

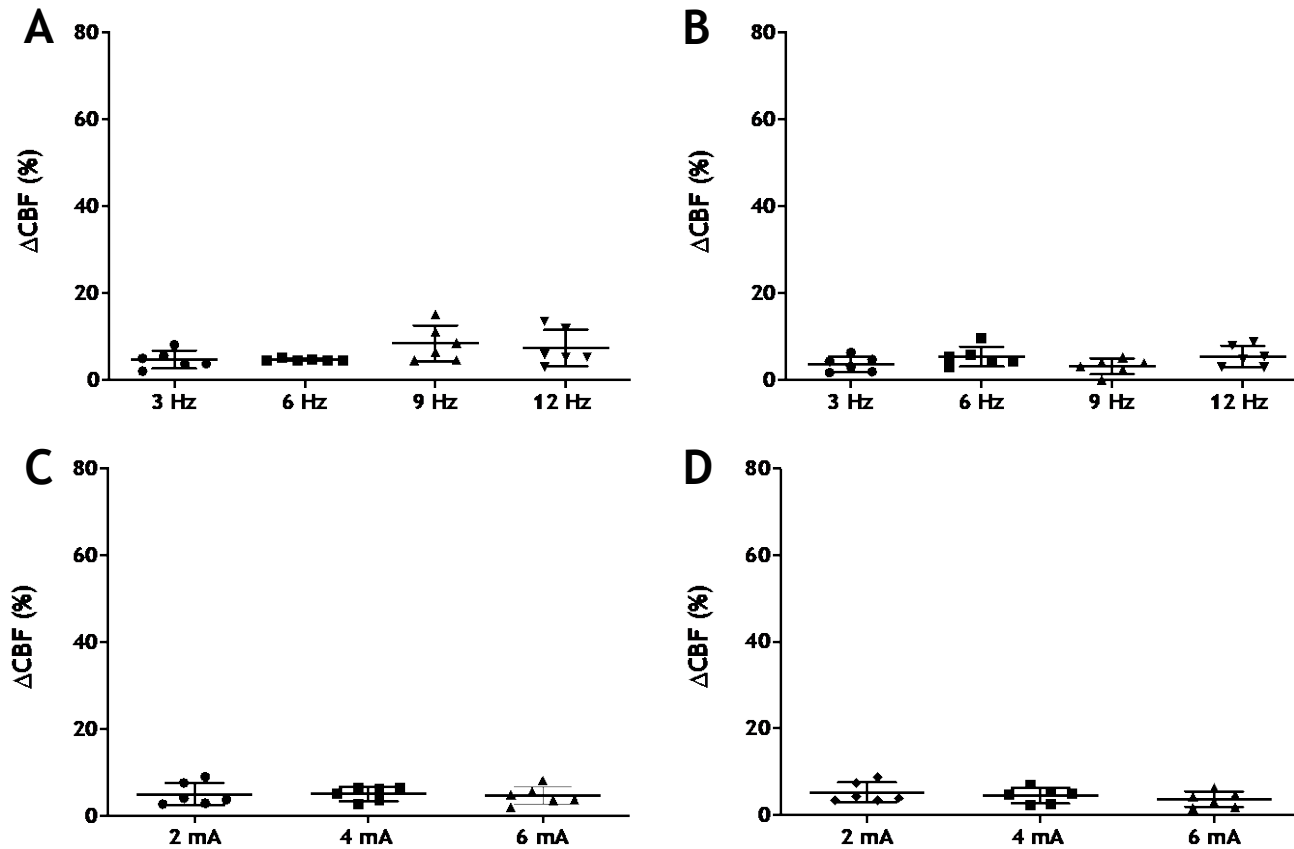


Figure 4.20: The effects of varying stimulus frequency on peak ΔCBF in the (A) ipsilateral S1FL area and (B) ipsilateral visual cortex, as well as the effects of varying stimulus intensity on the (C) ipsilateral S1FL area and (D) ipsilateral visual cortex. (Ipsilateral S1FL, $p=0.18$; Ipsilateral visual cortex, $p=0.26$; RM one-way ANOVA). 3 Hz and 6 mA data represent the same reference dataset. Individual data with mean \pm standard deviation shown.

4.3.3.3 Integral of CBF

Analysis of the integral of the CBF response for the contralateral S1FL area also revealed a significant effect of frequency and intensity (Figure 4.21; $p < 0.01$, RM one-way ANOVA). The group-averaged integral values of the CBF response demonstrated a trend to increase with stimulus intensity (111.5% vs. 173.7% vs. 289.8%; 2 mA vs. 4 mA vs. 6 mA) and stimulus frequency, peaking at 9 Hz and notably declining at 12 Hz (289.8 vs. 381.2 vs. 1081.0 vs. 764.5; 3 Hz vs. 6 Hz vs. 9 Hz vs. 12 Hz). However, no significant pairwise comparisons were observed (Tukey's multiple comparison test, $\alpha = 0.05$). The integral of CBF responses for ipsilateral S1FL and ipsilateral visual cortex were consistent between all conditions tested ($p = 0.24$, $p = 0.11$, RM one-way ANOVA; Figure 4.22).

The main results from each of the previously described studies in this chapter have been summarised in Table 4.1.

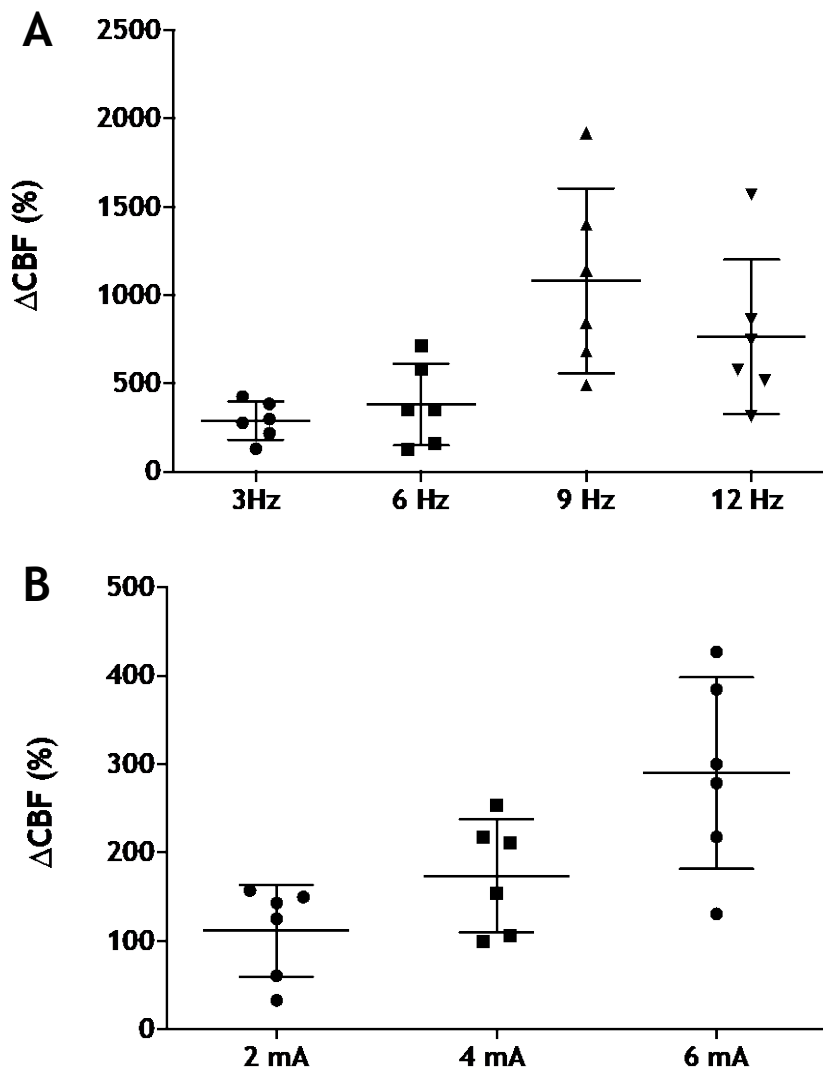


Figure 4.21: The effect of varying (A) stimulus frequency and (B) stimulus intensity on the integral of the CBF response in the contralateral S1FL area. There was a significant effect of varying stimulus frequency and intensity on the integral of the CBF response ($p < 0.01$) but no significant pairwise comparisons were observed when data were compared within their respective stimulus category e.g. frequency or intensity. 3 Hz and 6 mA data represent the same reference dataset. Individual data with mean \pm standard deviation shown.

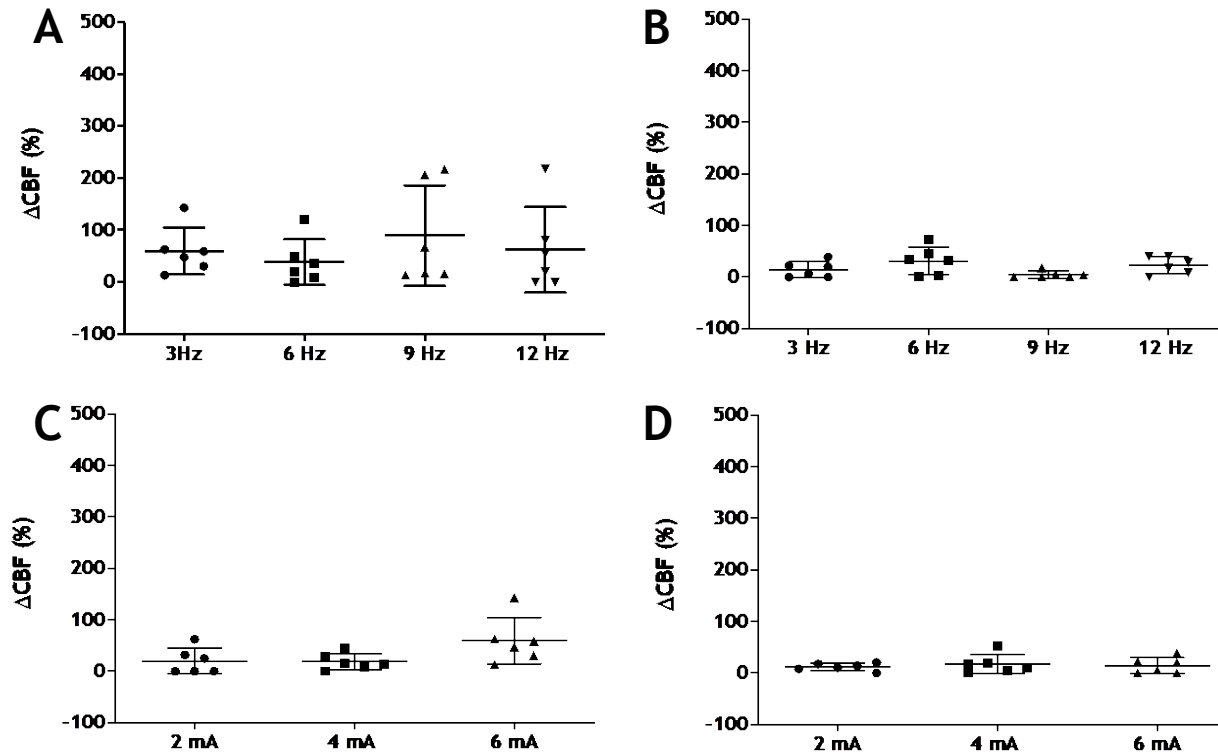


Figure 4.22: The effects of varying stimulus frequency on the integral of the CBF response in the (A) ipsilateral S1FL area and (B) ipsilateral visual cortex, as well as the effects of varying stimulus intensity in the (C) ipsilateral S1FL area and (D) ipsilateral visual cortex. There was no significant effect of varying stimulus frequency or stimulus intensity on the integral of the CBF response at either the ipsilateral S1FL ($p=0.24$) or visual cortex ($p=0.11$). 3 Hz and 6 mA data represent the same reference dataset for their respective ROI. Individual data with mean \pm standard deviation shown.

	Stimulus Frequency				Stimulus intensity			Pulse duration		
	3 Hz*	6 Hz	9 Hz	12 Hz	2 mA	4 mA	6 mA*	0.3 ms	0.6 ms	1 ms
MRI measurements										
Peak Δ BOLD (%)	2.25 (0.52)	3.47 (1.49)	3.84 (2.07)	3.60 (2.00)	2.12 (0.72)	2.24 (0.65)	2.25 (0.52)	2.25 (0.52)	2.63 (1.25)	2.38 (0.76)
Integral of BOLD	30.59 (11.94)	37.96 (21.21)	37.66 (17.62)	39.67 (30.14)	26.45 (6.98)	30.49 (12.44)	30.59 (11.94)	30.59 (11.94)	34.92 (27.26)	32.61 (10.90)
Time-to-peak (s)	6.75 (1.88)	6.19 (1.54)	6.00 (3.31)	6.38 (1.56)	7.78 (3.58)	7.31 (2.03)	6.75 (1.88)	6.75 (1.88)	6.19 (1.99)	6.38 (1.20)
Electrophysiology measurements										
Peak P1	0.62 (0.37)	0.50 (0.28)	0.56 (0.40)	0.59 (0.41)	0.51 (0.35)	0.63 (0.42)	0.62 (0.37)
Peak N1	-1.17 (0.68)	-1.11 (0.56)	-1.49 (0.69)	-1.47 (0.62)	-1.06 (0.42)	-1.22 (0.58)	-1.19 (0.62)
Peak P2	0.39 (0.11)	0.36 (0.12)	0.39 (0.11)	0.40 (0.12)	0.43 (0.10)	0.44 (0.11)	0.42 (0.12)
Σ P1	27.24 (21.06)	31.93 (27.10)	33.33 (29.38)	22.22 (16.60)	11.57 (8.98)	14.48 (10.71)	15.55 (12.05)
Σ N1	-53.21 (31.32)	-46.96 (38.48)	-54.37 (42.53)	-24.06 (19.91)	-16.67 (13.31)	-25.05 (15.88)	-26.60 (15.70)
Σ P2	19.93 (5.82)	22.68 (10.25)	24.51 (14.24)	16.41 (8.07)	8.89 (3.06)	11.01 (3.64)	11.11 (4.56)
Integral of P1	9.16 (7.12)	5.37 (4.55)	3.77 (3.31)	1.90 (1.37)	5.70 (4.78)	7.19 (5.70)	7.76 (6.30)
Integral of N1	-17.81 (10.56)	-7.77 (6.34)	-6.12 (4.89)	-1.66 (1.79)	7.95 (7.59)	11.47 (8.44)	12.87 (8.60)
Integral of P2	6.70 (2.0)	3.82 (1.72)	2.79 (1.62)	1.41 (0.68)	4.52 (1.62)	5.18 (1.85)	5.49 (2.01)

LSCI measurements										
Peak Δ CBF (%)	17.96 (5.86)	25.39 (11.80)	51.06 (7.53)	47.42 (13.21)	8.36 (2.74)	12.53 (4.18)	17.96 (5.86)
Integral of CBF response	294.3 (108.5)	390.1 (226.6)	1084 (525.0)	764.5 (437.6)	114.4 (46.92)	180.4 (67.00)	294.3 (108.5)

Table 4.1: A summary of the main results from each of the studies in this chapter. Data presented are mean (standard deviation). Pulse duration not assessed for electrophysiology and laser speckle studies. *3 Hz and 6 mA measurements were from the same run for MRI and laser speckle experiments.

4.4 Discussion

In this chapter, data are presented demonstrating how SEPs and stimulus-evoked BOLD and CBF responses are affected by varying the stimulus parameters during forelimb stimulation under combined medetomidine-isoflurane anaesthesia.

4.4.1 The use of anaesthesia in rodent fMRI studies

Most pre-clinical fMRI studies in rodents use anaesthesia to minimise movement and stress in the animal during scanning, which could otherwise lead to the generation of artefacts and non-specific activations (Lahti et al. 1998; Peeters et al. 2001; Sicard et al. 2003). While protocols for assessing awake animals have been introduced, and have demonstrated larger hemodynamic and neural responses when compared with anaesthetised animals (Brevard et al. 2003; Sicard et al. 2003; Aksenov et al. 2015), these are more labour-intensive and time-consuming. Furthermore, spontaneous movement and stress responses may still occur despite the animal undergoing extensive acclimatisation training (Paasonen et al. 2018). The use of anaesthesia overcomes these potential confounds but there are several different anaesthetics that are often used in preclinical fMRI studies, each with their own advantages and potential confounds. In general, anaesthetics can depress neuronal activity and cerebral metabolism, and alter vascular reactivity and dynamics, thereby affecting neurovascular coupling (Masamoto and Kanno 2012; Aksenov et al. 2015). Such effects are often produced by suppression of excitatory synaptic activity or enhancement of inhibitory activity (Richards 2002). However, the degree of these effects is often determined by the type and dosage of the anaesthetic used. Given the variety of anaesthetics used in preclinical fMRI studies and that such studies may further vary in their dosage, route of administration and set-up, it is difficult to compare findings between studies, even when the same anaesthetic is used.

In a systematic review assessing the effects of anaesthetic regime on the BOLD response, the most commonly used anaesthetics in rat fMRI studies were isoflurane, dex-medetomidine/medetomidine and α -chloralose, with isoflurane being the most popular (Steiner et al. 2021). Other anaesthetics used included

urethane, propofol, isoflurane-medetomidine and ketamine. It is unsurprising that isoflurane is the most commonly used anaesthetic in rat fMRI studies given its ease of use and fast induction and recovery times (Liu et al. 2004; Sicard and Duong 2005; Kim et al. 2010; Nasrallah et al. 2015). However, as previously described, isoflurane is a potent vasodilator that could confound the fMRI readout due to its effects on baseline BOLD and CBF at doses >1% (Eger 1984; Masamoto et al. 2007; Steiner et al. 2021). Few studies identified in the systematic review used isoflurane-medetomidine, yet this is the anaesthetic protocol used in the current study and all studies described throughout.

The medetomidine-isoflurane anaesthetic protocol described throughout this thesis was previously established in our lab (Hollyer 2016), and was based on the original protocol first introduced by Weber et al. 2006 and a subsequent adaptation by Lu et al. 2012. The use of combined isoflurane-medetomidine has previously been shown to sedate rats for several hours without the need to increase the dose of medetomidine (a potential limitation of using medetomidine alone), produce robust stimulus-evoked responses and allow imaging of resting-state networks in rats (Lu et al. 2012; Hollyer 2016). However consistent, robust BOLD responses under this anaesthetic protocol are only observed after 90 mins following anaesthetic induction, with responses before this time being variably smaller (Lu et al. 2012). This temporal variability of the BOLD response has also been observed under a medetomidine-only protocol, with responses within the first 2 hours following medetomidine administration being variably smaller when compared with responses measured during 2-4 and 4-6 hours post-medetomidine (Simpilatz et al. 2019). Of note, this observed temporal evolution of the BOLD response was dependent on the route of administration as well as the dose. Temporal variability was observed when medetomidine was continuously infused subcutaneously and a pre-dose bolus given, when infused intravenously without a pre-dose bolus, and when administered intravenously with a lower dose bolus and infusion than that described in the original protocol by Weber et al. 2006. Consistent, robust BOLD responses were observed at all assessed time windows when medetomidine was infused intravenously with a pre-dose bolus at the same dosage described in the original protocol. The difference in the timing of the temporal variability of the BOLD response between these two studies (90 mins vs. 2 hours) may be due to several factors such as the use of a lower dose

of medetomidine, a different route of administration (intramuscular) and the addition of isoflurane in the Lu et al. 2012 study. However collectively, these two studies indicate that temporal variability of the stimulus-evoked BOLD response may occur when medetomidine is used and therefore this should be factored into the study design to ensure consistent BOLD responses are recorded and measured.

Based on the observations of Lu et al. 2012, no recordings in the current study or in any study described in this thesis were made until at least 90 mins had passed following the administration of the medetomidine bolus. Given that the findings of Sirmipilatzte et al. 2019 were not published until after completion of the studies in this thesis, we were not aware that the temporal variability of the BOLD response may extend within the first 2 hours following medetomidine administration. However, as the current study used medetomidine-isoflurane and not medetomidine-only, it is possible that the timing of the temporal variation of the BOLD signal described by Lu et al. 2012 may be more comparable to our own study. Yet, it is worth noting that the anaesthetic protocol followed in all experiments in this thesis used a higher dose of medetomidine (0.05 mg/kg bolus; 0.1 mg/kg/hr infusion), a different route of administration (subcutaneous) and a higher dose of isoflurane (1%) compared with the study by Lu et al. 2012. Therefore, given that our anaesthetic protocols do not exactly match, it is unclear whether the timing of the temporal variation of the stimulus-evoked BOLD signal is the same and therefore we cannot completely rule out that this may have led to some variation within our results. Future work should assess the temporal evolution of the BOLD response under this specific anaesthetic protocol to confirm such.

4.4.2 Dependency of the BOLD response on stimulus parameters

In our study we observed a trend for the peak BOLD amplitude to increase with stimulus frequency, evoking the largest peak amplitude at 9 Hz and then plateauing at 12 Hz. The peak BOLD response at 12 Hz while statistically similar to 9 Hz was numerically lower, suggesting that the peak response may begin to decline above a stimulus frequency of 12 Hz. These findings are consistent with previous rodent forepaw stimulation studies that observed

maximal peak BOLD amplitudes at 9 Hz and 12 Hz when using medetomidine and isoflurane respectively (Zhao et al. 2008; Kim et al. 2010).

Similar to previous studies using these anaesthetics, we did not observe a significant effect of stimulus frequency on the integrated BOLD values. While an increase in stimulus frequency up to 9 Hz evoked a larger peak in the BOLD response, the overall size of the response, as measured by the integral of the response, remained consistent between the stimulus frequencies. However, this observation is likely dependent on the stimulus duration. Both BOLD and CBF responses to stimulus durations of 15 seconds or more have been observed to peak within the first 10 seconds of stimulation, and then plateau for the remainder of the stimulation period, similar to our own observations (Ureshi et al. 2004; Zhao et al. 2008; Kim et al. 2010). When integrated BOLD values were calculated for each 10-second period during 30 seconds of stimulation, Kim et al. (2010) observed a significant effect of frequency for the first 10 seconds, with the largest signal change occurring at 12 Hz. However, there was no significant effect of frequency on integrated BOLD values for the second (11 - 20 seconds) or third periods (21 - 30 seconds), when the response had plateaued, and the largest signal change was observed to occur at 6 Hz (Kim et al. 2010). Collectively, these observations indicate that stimulus duration should also be considered when assessing the optimum stimulus parameters for integrated BOLD.

While we identified 9 Hz as the optimum stimulus frequency for achieving the maximal peak BOLD amplitude, it is considerably higher than the optimum stimulus frequencies observed under α -chloralose anaesthesia, which have been observed to range between 1.5 - 5 Hz (Brinker et al. 1999; Silva et al. 1999; Keilholz et al. 2004; Sanganahalli et al. 2008). Both isoflurane and medetomidine have been observed to depress excitatory synaptic transmission (Larsen et al. 1997; Larsen and Langmoen 1998; Richards 2002; Sinclair 2003; Sandstrom 2004; Angenstein et al. 2010), while α -chloralose enhances inhibitory activity by potentiating GABA_A receptor activity (Garrett and Gan 1998). Furthermore, α -chloralose has been observed to prolong neural refractory periods while isoflurane maintains short refractory periods (Masamoto et al. 2007; Masamoto et al. 2009; Kim et al. 2010). The different

target sites and mechanisms of action of these anaesthetics likely underpin the differences in the required stimulus frequency to evoke a maximal response.

Peak and integrated BOLD values remained consistent at all stimulus intensities examined. Peak BOLD responses have previously been observed to monotonically increase at stimulus intensities of 1, 2 and 4 mA in medetomidine-sedated rats, with higher stimulus intensities of 6 and 8 mA exhibiting no further increases (Zhao et al. 2008). However, aside from using a different anaesthetic protocol, Zhao et al. (2008) assessed the various stimulus intensities at 9 Hz while in our study, the various stimulus intensities were assessed at a stimulus frequency of 3 Hz. This observation introduces the possibility of an interaction between stimulus intensity and stimulus frequency, where a combination of a higher stimulus intensity and higher frequency may evoke larger peak amplitudes. Most fMRI studies assessing optimal stimulus parameters typically assess variations in one parameter category at a time, as is the case with our own study. However, few assess all possible comparisons to determine whether interactions between parameters may exist. While this may be due to various reasons, including time-constraints for scanning, future studies could focus on assessing multiple combinations between a small number of commonly used stimulus parameters to assess any interactions between them.

4.4.3 Dependency of the SEPs on stimulus parameters

In our study we assessed the effects of varying stimulus parameters on cortical neural activity by measuring the individual SEP components. P1, N1 and P2 were separated and measured individually because these waveforms originate from different subpopulations of pyramidal cells (Kulics and Cauler 1986; Di and Barth 1991; Staba et al. 2003; Jellema et al. 2004), and as such, respond differently under various experimental conditions, stimulus paradigms and drugs (Kublik et al. 2001; Staba et al. 2003; Stienen et al. 2004; McElhone et al. 2006). We observed that peak P1, N1, and P2 values remained invariable under all stimulus intensities tested. However, the individual Σ SEP and integral values demonstrated a trend to increase with stimulus intensity.

Electrophysiological studies examining stimulus-evoked field potentials (FP) have reported that peak amplitude increases with stimulus intensity, with the Σ FP also demonstrating a non-linear increase with intensity (Ureshi et al. 2005; Franceschini et al. 2008). However, these studies were performed under α -chloralose and assessed at stimulus intensities at various increments below 2.5 mA. It is possible that in our study, a ceiling effect was achieved, with the response at 2 mA representing a maximal or near-maximal peak response. Assessing stimulus intensities at various increments below 2 mA may have revealed an effect of intensity on peak SEP amplitude. However, data from individual animals, as shown in Figure 4.9, demonstrates a wide variability between animals. This variability may mask any effect of stimulus intensity on peak amplitude within our study. Therefore, a larger sample size with smaller variability in the data may reveal an underlying relationship between stimulus intensity and peak SEP amplitudes.

Peak amplitude values for both positive waveforms also remained consistent when the stimulus frequency was varied, however higher N1 peak amplitudes were observed at 9 Hz and 12 Hz compared with lower frequencies. Both Σ P1 and Σ P2 demonstrated a clear trend to increase with frequency, peaking at 9 Hz and then declining at 12 Hz, while Σ N1 remained consistent at stimulus frequencies of 3, 6 and 9 Hz, but declined at 12 Hz. Previous studies have shown that P1 originates from thalamo-cortical input-derived excitatory postsynaptic activity in cortical neurons of layer IV, while N1 and P2 generally arise from cortico-cortical activity in the more superficial layers I-III (Kulics and Cauller 1986; Di and Barth 1991). Given the shared origin of N1 and P2, similar response patterns have been reported for both waveforms to various stimulus parameters (Franceschini et al. 2008). Our findings do not mimic this observation, but rather we observed similar response patterns between both P1 and P2 components, that typically differed from N1. It is possible that this discrepancy is underpinned by the difference in our anaesthetic protocols and the variability within our data. Therefore, further investigation would be required to verify our observation.

We observed that each stimulus pulse generally evoked a corresponding SEP at 3 and 6 Hz, however SEPs were periodically abolished at 9 Hz and quickly abolished at 12 Hz. Several electrophysiology studies using α -chloralose have

also observed that the one-to-one response of stimulus pulse-to-FP remains intact until 5 Hz and breaks down at higher stimulus frequencies (Matsuura and Kanno 2001; Ureshi et al. 2005). However, the next stimulus frequency assessed after 5 Hz in both these studies was 10 Hz. Therefore, it is possible that the one-to-one relationship remains intact at frequencies higher than 5 Hz but lower than 10 Hz. The similar range at which the one-to-one relationship breaks down between our study and previous α -chloralose studies suggests that this observation may arise from a common underlying mechanism that is robust to different anaesthetics.

4.4.4 Dependency of CBF on stimulus parameters

Using LSCI to measure stimulus-evoked CBF changes on the S1FL cortical surface, we observed that peak amplitude and integrated CBF values increased with both stimulus intensity, up to 6 mA, and stimulus frequency, peaking at 9 Hz and declining at 12 Hz. Previous LSCI studies in the rat have also observed that the peak CBF response to forelimb stimulation increases with stimulus intensity, however these studies were performed under α -chloralose and only stimulus intensities of up to 2 mA were assessed (Durduran et al. 2004; Dunn et al. 2005; Royle et al. 2006). While there were slight differences in the stimulus frequency (3-4 Hz), pulse duration (0.3-0.4 ms) and dose of α -chloralose between these studies, the CBF responses were generally similar, with peak changes of approximately 10-15% and 20-25% being observed at 1 mA and 2 mA, respectively. In the current study, the mean peak change in the CBF response was 8.36% at 2 mA, 12.53% at 4 mA and 17.96% at 6 mA, when stimulus frequency was 3 Hz and pulse duration 0.3 ms. Thus, under the current anaesthetic protocol, the peak CBF at 2 mA was substantially smaller to that observed in studies using α -chloralose. This difference is to be expected given the different mechanisms of action of these anaesthetics. A previous study observed that the peak CBF response to forelimb stimulation, as assessed by fMRI, was 84% lower under isoflurane compared with α -chloralose (Masamoto et al. 2007). The strong reduction in the peak amplitude of the CBF response was attributed to the change in baseline CBF, which increased by 54% under isoflurane compared with α -chloralose. Therefore, it is likely that the use of isoflurane in the current study underpins the substantially smaller BOLD response when compared with

responses observed under α -chloralose. Collectively, these studies further support that stimulus parameters should be optimised to the individual anaesthetic protocol and also indicate that comparisons between studies using different anaesthetic protocols should be interpreted with caution.

The effects of changing stimulation parameters on the stimulus-evoked CBF response to forelimb stimulation in the rat somatosensory cortex have also been investigated using laser-Doppler flowmetry. Under α -chloralose anaesthesia, a trend for the peak and integrated CBF response to increase with stimulus intensity up to 2.5 mA has been observed (Detre et al. 1998; Silva et al. 1999; Ureshi et al. 2005). Interestingly, Detre et al. 1998 observed that the CBF response at 2.5 mA was accompanied with an increase in MABP, while Silva et al. 1999 observed an increase in MABP at 2.0 mA. The difference between the two studies as to the stimulus intensity at which increase in MABP were observed may be due to the difference in the dose of anaesthetic used; a lower dose of α -chloralose was used by Detre et al. 1998. These increases in MABP suggest that the stimulus had become noxious, which can confound neuroimaging measures as a result of global changes in CBF and neurovascular coupling (Jeffrey-Gauthier et al. 2013; Uchida et al. 2017). Similar observations have been made under isoflurane anaesthesia, with CBF responses increasing with stimulus intensity up to 8 mA, but eliciting increases in MABP at this higher stimulus intensity (Liu et al. 2004). Collectively, these studies indicate that stimulus-evoked CBF responses increase with stimulus intensity, however higher stimulus intensities, which are likely relative to the dose and type of anaesthetic being used, can become noxious and induce changes in MABP and global CBF.

While we did not analyse the effects of stimulation on MABP, we did not observe any spikes or increases in the MABP trace during stimulation. We also observed that CBF increases with stimulus intensity between 2 mA and 6 mA, with no indication of the response plateauing at the latter stimulus intensity. Therefore, it is likely that increasing the stimulus intensity above 6 mA could have resulted in a further increase in stimulus-evoked CBF response. However, this current study did not assess stimulus intensities >6 mA given that such high intensities are rarely used in the literature and changes in MABP and global CBF

have been observed at 8 mA in rats anaesthetised with 1.1-1.2% isoflurane (Liu et al. 2004).

When assessing the effect of stimulus frequency on the CBF response, we observed that integrated and peak CBF increased with stimulus frequency, peaking at 9 Hz and declining at 12 Hz. To our knowledge, there are no LSCI studies that have assessed the effects of changing stimulus frequency on the stimulus-evoked CBF response in the rat somatosensory cortex. However, several studies have used laser-Doppler flowmetry to investigate such changes in rats under α -chloralose. Such studies have observed both peak and integrated CBF values increase with frequency, peaking at an optimal frequency typically dependent on the anaesthetic, then declining at above-optimal frequencies (Detre et al. 1998; Ngai et al. 1999; Silva et al. 1999; Ureshi et al. 2004; Masamoto et al. 2007). Collectively, these studies highlight that different anaesthetic protocols do not affect the general pattern of CBF response to variations in stimulus frequency, as all show a tendency for CBF measures to peak at an optimal frequency and then decline at higher frequencies. However, the chosen anaesthetic does appear to influence the optimal frequency, with each unique anaesthetic protocol demonstrating a different optimal frequency.

4.4.5 Relationship between BOLD, SEP and CBF

To accurately characterise the relationship between BOLD, SEPs and CBF, it is typically favourable to measure these components simultaneously under similar conditions. Due to experimental constraints, we did not acquire these measurements simultaneously and while efforts were made to ensure most aspects of the experiments were consistent, there were some differences that may have introduced additional variability into the data. These included different invasive surgical preparations e.g. intact skull for fMRI, craniotomy for electrophysiology and skull thinning for LSCI, and the use of different cohorts between studies with differing sample sizes. In our case, the latter restricts our ability to statistically assess correlations between the data since observations are not related between measures of interest. Additionally, the sample sizes within our experiments were relatively small and therefore this may also affect variability and statistical significance within our study.

However, measuring these key components of neurovascular coupling individually can still provide useful insights, if interpreted with caution.

Several studies have previously shown that neural responses, as measured by Σ SEP or Σ FP, are highly correlated with CBF increases (Ngai et al. 1999; Kim et al. 2010). The summed neural measure is typically used when assessing the correlation between neural and hemodynamic responses as it is generally accepted that hemodynamic responses are underpinned by integrated neural activity, rather than average or peak activity. Indeed, when the effect of stimulus frequency on mean peak amplitude was studied, an inverse relationship between peak neural and peak CBF values has been observed (Ngai et al. 1999; Kim et al. 2010). While we cannot report on the correlation between changes in frequency-dependent Σ SEP and integrated CBF responses in our study, we speculate that one does exist between these measures, owing to the observation that both demonstrate a similar trend to increase with frequency, peak at 9 Hz and then decline at 12 Hz. Previous studies that report a high correlation between CBF and neural measures observed similar patterns of responses, however, since most of these studies were performed under alpha-chloralose, the peak occurred at a lower stimulus frequency of 5 Hz.

Since the stimulus-evoked BOLD response is generally underpinned by a local increase in CBF, it is reasonable to assume that the frequency-dependent integrated BOLD responses would exhibit a similar pattern to the integrated CBF responses. However, we observed that integrated BOLD values remained relatively constant at stimulus frequencies of 6 Hz and above, and did not demonstrate the previously seen 9 Hz peak and subsequent decline at 12 Hz. This discrepancy likely arises from our small sample size and high variability within the data and therefore further investigation is required.

4.4.6 Conclusion

In conclusion, we observed that the largest stimulus-evoked BOLD and CBF responses were evoked at a stimulus frequency of 9 Hz. While the largest summed responses of the SEP components were also observed at this frequency, we observed that the amplitude of the overall neural response decreases with increasing stimulus frequency and there is a loss of the one-to-

one stimulus to SEP ratio when higher frequencies are used. While the stimulus-evoked BOLD response evoked at 3 Hz was generally smaller than those evoked at higher frequencies, there was less variation in the size of the BOLD responses at this frequency and SEPs were generally consistent in amplitude and maintained throughout the course of stimulation. Thus, 3 Hz was selected as the optimum stimulus frequency after considering the data from all modalities. Larger CBF responses were generally observed at a stimulus intensity of 6 mA, however there was no statistical difference between any of the stimulus intensities when measuring the stimulus-evoked BOLD response or any components of the SEP, although there was a general trend for the summed and integral of the SEP components to increase with stimulus intensity. Therefore, 6 mA was chosen as the optimal stimulus intensity. Stimulus pulse duration was only assessed in the fMRI study and we observed no effect of varying the pulse duration on the stimulus-evoked BOLD response. Therefore, 0.3 ms was selected as the optimum pulse duration given that this is also commonly used in the literature. These optimum parameters were subsequently used in the fMRI study described in Chapter 5.

Assessing the hemodynamic response in the SHRSP: A model of cerebral small vessel disease

5.1 Introduction

The SHRSP is a model of malignant hypertension, stroke and cerebral SVD. The aim of this study was to assess whether changes in the hemodynamic response (BOLD, CBF) can be detected in this model of cerebral SVD and therefore could provide a biomarker of endothelial function and an indicator of therapeutic response.

5.1.1 Cerebral small vessel disease

Lacunar stroke infarcts are common in cerebral SVD and account for approximately 20% of all strokes (Sudlow and Warlow 1997b). Lacunar strokes are characterised by small infarcts (<20 mm in diameter) in deep brain structures that include cerebral white matter, basal ganglia or pons (Bamford et al. 1988). Additionally, cerebral SVD is characterised by WMHs (Kynast et al. 2018), lacunes of vascular origin (Vermeer et al. 2007), microbleeds (Cordonnier et al. 2007) and cortical microinfarcts (Smith et al. 2012). The cause of cerebral SVD and resultant pathology is unclear, owing to the difficulty of studying the disease in humans; lacunar strokes are rarely fatal and pathological changes, which include small focal infarctions in the brain, can be mild and go unnoticed (Hainsworth and Markus 2008). Furthermore, death may occur long after stroke and other pathological changes, leading to limited tissue for analysis that is difficult to interpret.

5.1.2 SHRSP

The SHRSP is a model of cerebral SVD that demonstrates similarities to human SVD pathology (Bailey et al. 2011a). Interestingly, WMHs are commonly

observed and regarded as a typical sign of cerebral SVD in human patients, (Shi and Wardlaw 2016), yet a MRI study of 10-month old SHRSPs did not observe any WMHs in a stroke-free cohort (Brittain et al. 2013). However, SHRSPs and patients with cerebral SVD have both demonstrated dysfunctional endothelial cells and BBB leakage, both of which contribute to many of the pathological features of cerebral SVD (Quick et al. 2021). Compared with WKYs, SHRSPs exhibit reduced claudin-5, an endothelial tight junction protein, from 5 weeks of age indicating that BBB dysfunction in these animals precedes the onset of hypertension and may be an initial driver of disease (Bailey et al. 2011a). Furthermore, the expression of tight junction proteins, including claudin-5, has previously been observed to remain consistent in SHRs, compared with WKYs, following 4-hour middle cerebral artery occlusion (Hom et al. 2007). While the use of surgical intervention to induce ischemic stroke may complicate interpretation of this observation, such findings suggest that the reduced expression of claudin-5 observed in SHRSPs compared with SHRs may underlie the 'stroke prone' phenotype of these animals.

The assessment of pathological changes in the SHRSP occurring at later, chronic stages of this disease are rare. A systematic review showed that the majority of the studies assess SHRSPs between 9-16 weeks of age, during the acute stages of hypertension and SVD progression (Bailey et al. 2011a). Furthermore, almost a quarter of studies fed animals a Japanese diet or added salt ('salt-loading') to the drinking water to accelerate the hypertensive pathology (Bailey et al. 2011b; Di Nicolantonio and Silvapulle 1988). Severe hypertension is established at a younger age in salt-loaded animals, which subsequently do not typically live beyond 28-weeks of age (Bailey et al. 2011b). One study compared salt-loaded WKYs and SHRSPs and observed changes in gene and protein expression in networks affecting inflammatory pathways, vascular structure and myelin integrity that, in the case of the salt-loaded WKY, were observed in the absence of an increase in blood pressure (Bailey et al. 2018). Furthermore, expression of *CLDN11*, a gene that encodes the tight junction protein Claudin-11, was significantly down-regulated in salt-loaded SHRSPs compared with non-salt-loaded SHRSPs. This observation, coupled with the reduced claudin-5 expression previously observed in SHRSPs (Bailey et al. 2018), suggest that salt-loading in SHRSPs may further compromise the integrity of the BBB compared with non-salt-loaded SHRSPs.

Whether these changes reflect an accelerated disease pathology or a potentially different pathology to salt-naïve SHRSPs is not clear. The difficulty in evaluating this lies in part to the lack of studies assessing pathological changes in SHRSPs occurring later in SVD progression and in the absence of potential confounds, such as salt loading. Therefore, assessing the normal pathological development in these animals at this later time point may better inform on disease progression and further support how SHRSPs can model human disease pathology, which is typically associated with older individuals over the age of 65 years (Pantoni 2010).

5.1.3 Small vessel disease and BOLD

Most neuroimaging studies in patients with SVD assess structural characteristics associated with the disease, such as small infarcts, lacunes of vascular origin, WMHs, microbleeds and brain atrophy (Wardlaw et al. 2013). However, there is a growing interest in using functional MRI to probe cerebrovascular reactivity in patients with cerebral SVD for use as a biomarker of cerebrovascular health and therapeutic response (Blair et al. 2015; Sleight et al. 2021; Stringer et al. 2021). Given that endothelial dysfunction has previously been observed in young SHRSPs and presymptomatic patients with cerebral SVD (Bailey et al. 2011a; Rajani et al. 2018), and that the endothelium plays a key role in controlling blood flow (Quick et al. 2021), assessing cerebrovascular reactivity may provide an early indicator of tissue at risk.

A loss of vessel reactivity has previously been observed in cerebral SVD patients (Saji et al. 2016). Reduced stimulus-evoked BOLD responses have been observed in the visual cortex of patients with CAA (Dumas et al. 2012; Peca et al. 2013; van Opstal et al. 2017), and in the frontal-temporal and parietal cortices of patients with moderate-to-severe WMHs when performing an attention task (Atwi et al. 2018). Several studies have used a hypercapnic challenge to assess cerebrovascular reactivity in patients with moderate-to-severe white matter disease and observed a reduced magnitude and speed of the vascular response in normal-appearing white matter that later progressed to WMH (Sam et al. 2016a; Sam et al. 2016b). Furthermore, age and hypertension are strong indicators of WMHs and cognitive decline in cerebral SVD (Khan et al. 2007; Abraham et al. 2016). These risk factors are known to

induce pathological stiffening of arterial vessels, which may precede the development of other features of cerebral SVD. In another study, a significant decrease in the BOLD response to a hand-tapping task was observed in the somatosensory cortex of patients with SVD who had previously suffered a lacunar stroke (Pineiro et al. 2002). Therefore, it is possible that the assessment of the hemodynamic response to stimulation may provide a biomarker of cerebrovascular health and an indicator of therapeutic response to therapies targeting the endothelium or cerebrovasculature in cerebral SVD. However, there has been a lag in the assessment of cerebrovascular reactivity in animal models of cerebral SVD and, to our knowledge, no study has yet assessed cerebrovascular reactivity using functional MRI in the SHRSP. Therefore, the assessment of stimulus-evoked BOLD and CBF responses in SHRSPs could provide insight on how the hemodynamic response, and thus cerebrovascular reactivity, is affected in this model of SVD.

5.1.4 Study Aims and Hypothesis

To assess the potential of the stimulus-evoked BOLD response as a biomarker of cerebrovascular health and a potential marker of therapeutic response in the SHRSP, it was important to establish whether significant differences in the BOLD response could be observed between WKYs and SHRSPs. Furthermore, given that endothelial dysfunction occurs early in disease and cerebrovascular reactivity is known to decline with age, such changes were assessed in young and aged WKY and SHRSP cohorts to assess whether differences exist. As the BOLD response is not only dependent on changes in CBF, we also used LSCI to more directly assess any changes in the stimulus-evoked CBF response. Given the lack of studies accessing aged SHRSPs, and in the absence of salt-loading, we also aimed to acquire and assess structural MRI images to characterise any pathological changes. Therefore, in summary, the aims of this study were to:

1. Evaluate any differences in the stimulus-evoked BOLD response to forelimb stimulation between WKYs and SHRSPs, and assess whether any differences exist between young and aged cohorts
2. Evaluate any changes in the stimulus-evoked CBF response to forelimb stimulation, as assessed by LSCI, and assess whether any differences exist between young and aged cohorts
3. Characterise any structural differences between young and old WKYs and SHRSPs using T₂-weighted imaging, including the assessment of brain atrophy and the presence of WMHs

Based on previous studies demonstrating endothelial dysfunction and reduced cerebrovascular reactivity and hemodynamic responses in patients with cerebral SVD and considering the SHRSP to be a valid model of this disease, the main hypothesis of this study was that SHRSPs would demonstrate reduced stimulus-evoked BOLD and CBF responses, compared with WKYs.

5.2 Methods

5.2.1 Experimental Design

A 2x2 experimental design was utilised in this study to assess the effects of both age and disease on stimulus-evoked BOLD and CBF responses. The 4 groups consisted of acute WKYs (aWKYs), chronic WKYs (cWKYs), acute SHRSPs (aSHRSPs) and chronic SHRSPs (cSHRSPs). Experiments were conducted on animals in the acute groups at 3-4 months of age, shortly after the onset of hypertension in SHRSPs, and aimed to provide insight into any changes occurring during the acute stages of disease. Animals assigned to the chronic groups were assessed at 11-12 months of age. At this age, SHRSPs are at an increased risk of suffering a spontaneous stroke.

At the indicated ages, functional MRI with forelimb stimulation was used to assess changes to the stimulus-evoked BOLD response. While several fMRI studies in human patients with cerebral SVD have assessed BOLD responses to visual stimulation (Dumas et al. 2012; Peca et al. 2013; van Opstal et al. 2017), somatosensory stimulation was chosen for the current experiment due to the ease of setting up and implementing this stimulation method in the rat in an MRI setting. Furthermore, somatosensory stimulation can be replicated in human patients and blunted stimulus-evoked BOLD responses in the somatosensory cortex have been observed in patients with cerebral SVD during a hand tapping task (Pineiro et al. 2002). Thus, this method is appropriate and could easily translate for clinical assessment.

Following fMRI scanning, animals were recovered and one week later, LSCI was conducted to measure the stimulus-evoked CBF response. Following LSCI, animals were perfused and fixated for future histological analysis, the scope of which is beyond this thesis due to time constraints.

5.2.2 Experimental animals

Animals were obtained from breeding colonies of WKYs and SHRSPs in the Institute of Cardiovascular and Medical Sciences, University of Glasgow. Shortly after weaning, animals were transferred to the Veterinary Research Facility (VRF) where they were kept until they were required for experiments at the appropriate age. WKYs and SHRSPs were fed on standard rat chow with food

and water available *ad libitum*. For the acute time point, 12 WKYs and 13 SHRSPs were assigned while 12 WKYs and 20 SHRSPs were assigned to the chronic time point. Each experimental cohort was an independent group; none of the animals assigned to the acute time point were used in the chronic experiments.

5.2.3 Blood pressure measurements

To confirm the hypertensive and non-hypertensive phenotypes of SHRSPs and WKYs, respectively, systolic blood pressure was measured 1-3 days prior to fMRI scanning using tail cuff plethysmography while animals were conscious, as previously described in Section 2.6. The mean systolic blood pressure for each animal was calculated from 10 individual blood pressure measurements, which were compiled for each experimental group.

In a subgroup of cWKYs (n=5) and cSHRSPs (n=7), systolic blood pressure was measured at 3, 4, 5, 6, 7, 9 and 11 months of age to inform on any longitudinal changes in blood pressure.

5.2.4 Functional MRI

5.2.4.1 fMRI preparation

Animals were anaesthetised, intubated and the femoral artery cannulated for blood pressure monitoring and blood gas measurements. The animals were then transferred and secured in the MRI cradle, as described in Section 2.4.

5.2.4.2 Forelimb stimulation

Needle electrodes were inserted in the right forepaw as detailed in Section 2.3.3. Stimulation parameters were set at 3 Hz, 6 mA, and 0.3 ms for stimulus frequency, stimulus intensity and pulse duration, respectively. The stimulus paradigm consisted of 6 on-off blocks where the stimulus was on for 22 seconds and off for 38 seconds. The first stimulation block was preceded by a 10 second baseline period.

5.2.4.3 Monitoring of physiological variables

During the experiment, the following variables were monitored and, where applicable, maintained within normal limits:

- Body temperature - maintained at $37^{\circ}\text{C} \pm 0.5$
- Arterial paO_2 - normal range: 80-100 mmHg
- Arterial paCO_2 - normal range: 35-45 mmHg
- Arterial pH - normal range: 7.45-7.55
- Mean arterial blood pressure
- Heart rate
- Breathing rate

PaO_2 was generally higher (110 mmHg-130 mmHg) than the upper normal limit as additional O_2 was supplemented in the inhalation gas mixture during anaesthesia at 30%. Blood gas measurements were assessed in arterial blood samples withdrawn via the arterial cannula (approx. 80 μl). Between 3 and 6 blood samples were taken for each animal during the scanning session, the total number depending on the ability to maintain physiological variables within normal limits. If blood gas measurements fell outside of the normal physiological limits, the ventilator settings were adjusted to return blood gas levels back within normal range. Stimulus-evoked BOLD runs were only performed when physiological variables were all within normal limits, with the exception of PaO_2 as previous mentioned.

5.2.4.4 MRI protocol

MRI experiments were carried out using a Bruker Pharmascan 7T. A FLASH sequence was used to verify correct positioning of the animal in the scanner and correct positioning of the coil. Local shimming was performed using a fieldmap-based algorithm ('MAPSHIM'). Functional echo planar image (EPI) series were acquired during the forelimb stimulation paradigm to assess the stimulus-evoked BOLD (TR 750 ms, TE 20 ms, FOV $3.2 \times 2.4 \text{ cm}^2$, matrix 64×48 , 15 slices of 1 mm thickness, in-plane spatial resolution $500 \mu\text{m}^2$).

A $320 \times 240 \mu\text{m}^2$ RARE T_2 sequence was acquired for structural analysis. T_2 scans were visually assessed to detect any vascular lesions. These were defined as regions of hyperintense signal with or without a hypointense region. T_2 scans were also imported into ImageJ where the whole brain volume (excluding ventricles) and the volume of the lateral ventricle were measured. The boundaries of the 'whole brain' measurement were limited between the cerebellum and the interrhinal fissure.

5.2.4.4 Recovery following MRI

Following scanning, animals were removed from the MRI cradle and transferred back to the surgical theatre bench top. The arterial cannula was removed, the artery sealed and the animal recovered from anaesthesia as described in Section 2.6.1. This procedure was performed by Mrs. Lindsay Gallagher.

5.2.5 Laser speckle contrast Imaging experiments

5.2.5.1 LSCI preparation

Animals were anaesthetised, intubated and the femoral artery was cannulated (opposite femoral artery to that previously cannulated in the fMRI experiment). Animals were secured in a stereotaxic frame and the skull was exposed and thinned as described in Section 2.3.5. The laser speckle camera was subsequently set up as detailed in Section 2.5.

5.2.5.2 Forelimb Stimulation

Forelimb stimulation was carried out similar to that described in the fMRI experiment (Section 4.2.4.2), except that only 3 on-off stimulation blocks were performed.

5.2.6 Data Analysis

5.2.6.1 fMRI

Data analysis was performed in MATLAB using custom-written scripts, SPM12 (<https://www.fil.ion.ucl.ac.uk/spm/>) and AFNI. All MRI datasets were first converted from Paravision to NiftI format. A 6-parameter rigid body spatial transformation was then applied to each dataset to realign all images to the first in the series to correct for scanner drift during the functional scans (SPM). A structural image from a WKY was chosen as a target reference space to which all other WKY structural scans were registered (SPM) and then averaged to produce a structural reference image. The image was re-sliced to match the resolution of the functional datasets and fMRI scans from all animals were subsequently registered to this reference image. A high pass filter of 0.01 Hz was applied to all functional datasets (AFNI).

Using the structural reference image, a ROI was drawn in the forelimb area of the somatosensory cortex as defined in the Paxinos and Watson atlas (Paxinos and Watson 1998). This was then applied to all functional dataset sets to extract the BOLD time course from the S1FL area. The 6 on-off stimulation blocks were averaged to produce a single stimulus-event from which the peak BOLD and integrated BOLD (AUC) values were calculated. Integrated values were calculated in Prism Graphpad 8. Only positive peaks were included in the AUC measurement and any peaks with a start time outside of the stimulation period were excluded from the calculation.

5.2.6.2 LSCI

Analysis was initially carried out using PIMSoft (Perimed, Stockholm, Sweden). ROIs were established over the contralateral and ipsilateral S1FL areas, as well as over the ipsilateral visual cortex. The position and size of the ROIs were defined based on the Paxinos and Watson rat atlas (Paxinos and Watson 1998). For the contralateral S1FL ROI, a 3 x 2 mm² oval was centred at 0 mm AP and -4 mm ML to bregma and another centred at 0 mm AP and 4 mm ML to bregma for the ipsilateral S1FL area. For the visual cortex ROI, a 3 x 2 mm² oval was centred at -6 mm AP and 4 mm ML to bregma. Relative CBF time courses from each ROI were then extracted and normalised to the respective baseline period for each ROI. The ROI dataset was averaged across the 3 on-off blocks to produce a single event-related average for each animal. The single event-related time courses for all animals were used to extract the peak %CBF. The data was then organised by experimental group and imported to Prism 8 where the integral of CBF response (AUC) for every animal was calculated, as previously described (Section 4.2.6.1).

5.2.6.3 Statistical Analysis

All statistical analysis was performed in Prism Graphpad v8.1. Animal physiology (e.g. body weight, blood pressure) was assessed by two-way ANOVA with the measured variable as the dependent variable and age (acute vs chronic) and strain (WKY vs SHRSP) as independent variables. Animal age, blood pressure and heart rate data during experiments were assessed by one-way ANOVA.

Functional MRI data and laser speckle data were assessed using a two-way ANOVA with the measured characteristic (e.g. peak value or AUC) as the dependent variable and strain (WKY or SHRSP) and age (acute or chronic) as independent variables. Where applicable, additional pairwise comparisons were assessed using Tukey's multiple comparison's test, unless otherwise stated. Due to the violation of homoscedasticity for two-way ANOVA, both BOLD and CBF data were log transformed and subsequent statistical analysis performed on the transformed data. Log transformation was chosen as this has been previously recommended for fMRI data sets (Lewis et al. 2005). Both log transformed and back transformed data values are reported.

Assessment of the main effect of strain on the BOLD and CBF response and whether a significant difference could be observed between the two strains was the main interest of this study. Based on previous fMRI data in SHRs and patients with cerebral SVD, a total sample size of 42 animals across the 4 groups was required to achieve 0.95 β error probability (effect size f , 0.577; α , 0.05). Due to exclusions and deaths, this was not achieved in the study and based on the actual sample size of the study, there was an 83% probability of correctly rejecting the null hypothesis of no difference in the stimulus-evoked BOLD response in the MRI study and a 76% probability of correctly rejecting the null hypothesis of no difference in the stimulus-evoked BOLD response in the MRI study.

5.3 Results

5.3.1 Animals

For the acute time point, 3/13 SHRSPs were excluded from fMRI analysis due to technical issues that affected the stimulator and prevented reliable stimulation of the forelimb. No animals were excluded from the WKY population at this time point. Therefore, the total numbers of animals included in the fMRI analysis for the acute time point were 12/12 WKYs and 10/13 SHRSPs.

For the acute follow-up laser speckle experiment, 1/12 WKYs and 2/13 SHRSPs were not included in the analysis group. The SHRSPs previously excluded from the fMRI analysis ($n=3$) were included in the laser speckle experiment since

they were only excluded for technical issues and had recovered well following the fMRI experiment. One (1) WKY and one (1) SHRSP did not recover well following the MRI experiment and were subsequently culled. Another SHRSP (1) died during surgery due to complications with the arterial line. Therefore, the final sample size of the laser speckle analysis group at the acute time point was 11/12 WKYs and 11/13 SHRSPs.

For the chronic time point, 3/12 WKYs and 13/20 SHRSPs were not included in fMRI analysis. 2 WKYs sustained severe injuries and were subsequently culled prior to reaching the designated scanning time point, and 1 WKY was excluded due to technical issues that prevented accurate monitoring of body temperature. 7 SHRSPs died from spontaneous stroke prior to reaching the designated scanning time point and 4 SHRSPs were excluded following scanning due to the presence of stroke within the somatosensory cortex. One (1) animal showed a hyperintense region in the posterior cortex of the ipsilateral hemisphere to stimulation. Since this was only observed in a few slices and did not intrude on the S1FL, this animal was included in the analysis. One (1) SHRSP did not respond well to anaesthetic induction and was subsequently terminated without any scanning. One (1) SHRSP was excluded due to a technical error that prevented the stimulation of the forelimb. Therefore, the final sample sizes for the chronic fMRI study were 9/12 WKYs and 7/20 SHRSPs.

For the chronic laser speckle follow-up experiment, any animal previously excluded from fMRI analysis due to technical issues could again be included in the laser speckle study population. Therefore, the total numbers of animals available were 10/12 WKYs and 8/20 SHRSPs. However, 1/10 WKY and 2/10 SHRSPs were not included in laser speckle analysis due to complications during surgery that either prevented the acquisition of robust and reliable data or resulted in the death of the animal prior to data acquisition. Therefore, the total numbers of animals included in the laser speckle analysis group for the chronic time point is 9/10 WKYs and 6/10 SHRSPs.

3.3.2 Physiological Variables

3.3.2.1 Animal baseline physiology prior to scanning

For the acute time point, animals were scanned at an average age of 20 and 18 weeks for WKYs and SHRSPs, respectively. For the chronic time point, animals were scanned at an average age of 54 and 51 weeks for WKYs and SHRSPs, respectively (Figure 5.1). As expected, WKYs and SHRSPs at their respective acute or chronic time points did not significantly differ in age, however both strains at the chronic time point were significantly older compared to the both acute groups ($p < 0.0001$ for all comparisons).

Two-way ANOVA revealed a significant effect of strain on body weight ($p < 0.0001$), with SHRSPs generally demonstrating a lower body weight than WKYs at both acute and chronic time points (aWKY, 384.6 g; aSHRSP, 290.0 g; cWKY, 425.6 g; cSHRSP, 330.0 g; Figure 5.2). Significantly lower body weights were observed in aSHRSPs compared to aWKYs ($p = 0.0017$) and cWKYs ($p < 0.0001$), while cSHRSPs demonstrated significantly smaller body weights compared to cWKYs only ($p = 0.0006$). A significant effect of age was also observed ($p = 0.0012$) with older animals generally weighing more than their younger counterparts. However, this was only significant between aWKYs and cWKYs ($p = 0.0170$). While cSHRSPs body weight was higher than aSHRSPs, this was not found to be statistically significant ($p = 0.3447$).

A summary of systolic blood pressure, as assessed by tail cuff plethysmography, is shown in Figure 5.3. Acute and chronic SHRSPs had similar systolic blood pressures as no difference was found between the two groups ($p = 0.99$). The average systolic blood pressure was 213.3 mmHg and 208.7 mmHg for aSHRSPs and cSHRSPs, respectively. Both acute and chronic SHRSPs had significantly higher systolic blood pressure than aWKYs (149.4 mmHg; $p < 0.0001$ for both) and cWKYs (130.5 mmHg; $p < 0.0001$ for both). Interestingly, cWKYs displayed significantly lower blood pressure than their acute counterparts ($p = 0.04$).

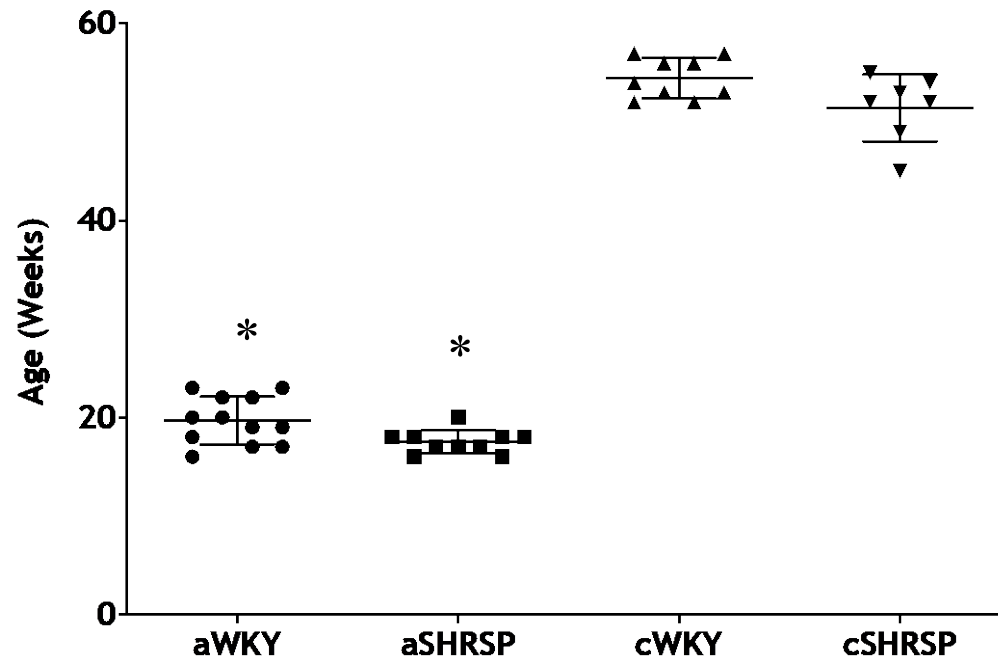


Figure 5.1: An overview of animal ages for each experimental group. aWKY and aSHRSP animals were similar in age ($p=0.1458$) but both groups were significantly younger than cWKY and cSHRSP ($p<0.0001$). cSHRSP and cWKY animals were also similar in age ($p=0.0637$). Statistical comparisons performed with one-way ANOVA with Tukey's multiple comparison's test. Individual data points for each animal shown with mean and standard deviation. * $p<0.0001$ vs cWKY and cSHRSP.

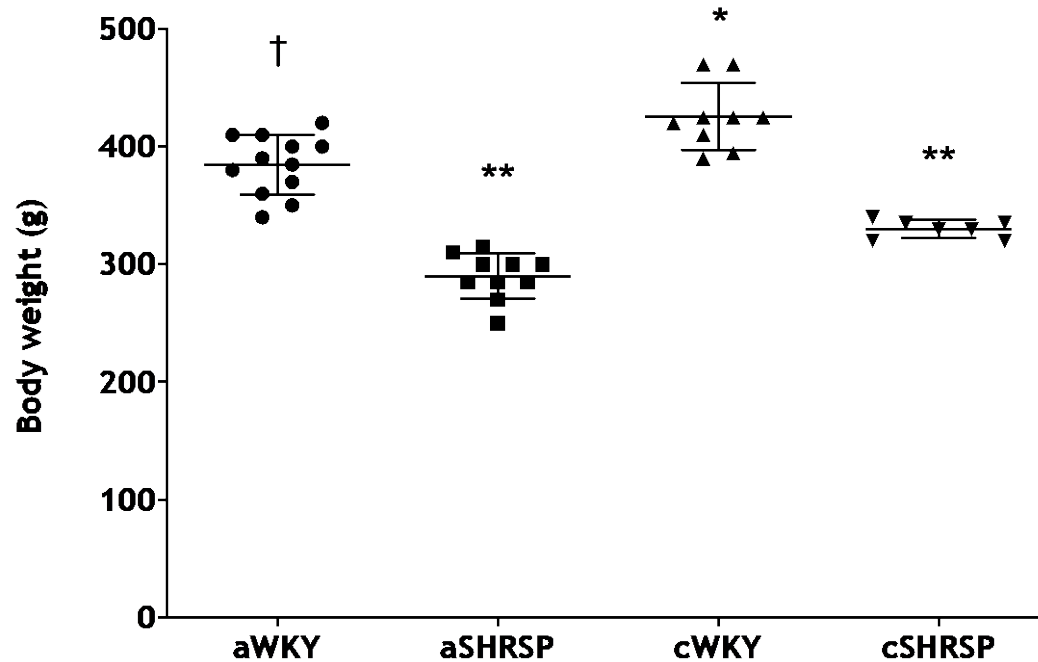


Figure 5.2: Overview of animal body weight for each experimental group prior to scanning. A significant effect of age ($p=0.0012$) and strain ($p<0.0001$) on weight was observed but no interaction ($p=0.4648$, two-way ANOVA). aWKYs weighed significantly more than aSHRSPs ($p<0.0017$) and cWKYs weighed significantly more than aWKYs ($p=0.0170$), aSHRSPs ($p<0.0001$) and cSHRSPs ($p=0.0006$; Tukey's multiple comparison test). cSHRSPs did not significantly differ from aWKYs or aSHRSPs. Individual data points for each animal shown with mean and standard deviation. * $p<0.05$ vs aWKY; ** $p<0.001$; *** $p<0.0001$ vs cWKY; † $p<0.01$ vs aSHRSP.

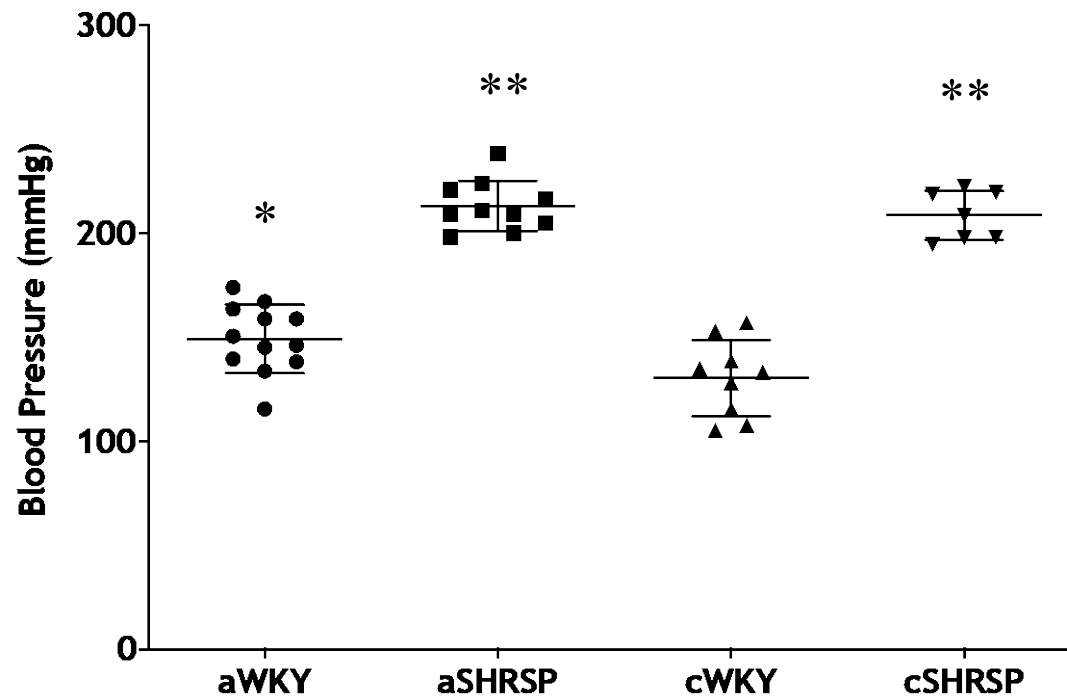


Figure 5.3: Overview of blood pressure for each experimental group prior to scanning as assessed by tail cuff plethysmography. A significant effect of strain ($p < 0.0001$) and age ($p < 0.0428$) on blood pressure was observed but no interaction ($p = 0.1120$). Both aSHRSPs and cSHRSPs exhibited significantly higher blood pressures than aWKYs and cWKYs ($p < 0.0001$) but did not significantly differ from each other ($p = 0.9885$). cWKYs also exhibited significantly lower blood pressure than aWKYs ($p < 0.0417$). * $p < 0.05$ vs cWKY; ** $p < 0.0001$ vs aWKY and cWKY.

5.3.2.2 Longitudinal blood pressure

In a subset of WKYs (n=5) and SHRSPs (n=7) allocated to the chronic time point, systolic BP was monitored periodically from 3 months of age until 11 months of age. Systolic BP was significantly higher in SHRSPs compared to WKYs at all time points investigated (Figure 5.4). Systolic BP measurements in the cSHRSP groups were generally above 200 mmHg for all time points, with a mean of 215 mmHg being observed throughout. The group-averaged MABP measurements for SHRSPs were 209.7 mmHg at 3 months and 210.8 mmHg at 11 months. A mean of 160 mmHg was observed for WKYs throughout all studied time points however, a gradual decrease in systolic BP was observed over time with the first group averaged measurement at 3 months showing 171 mmHg and the final measurement at 11 months showing 144 mmHg.

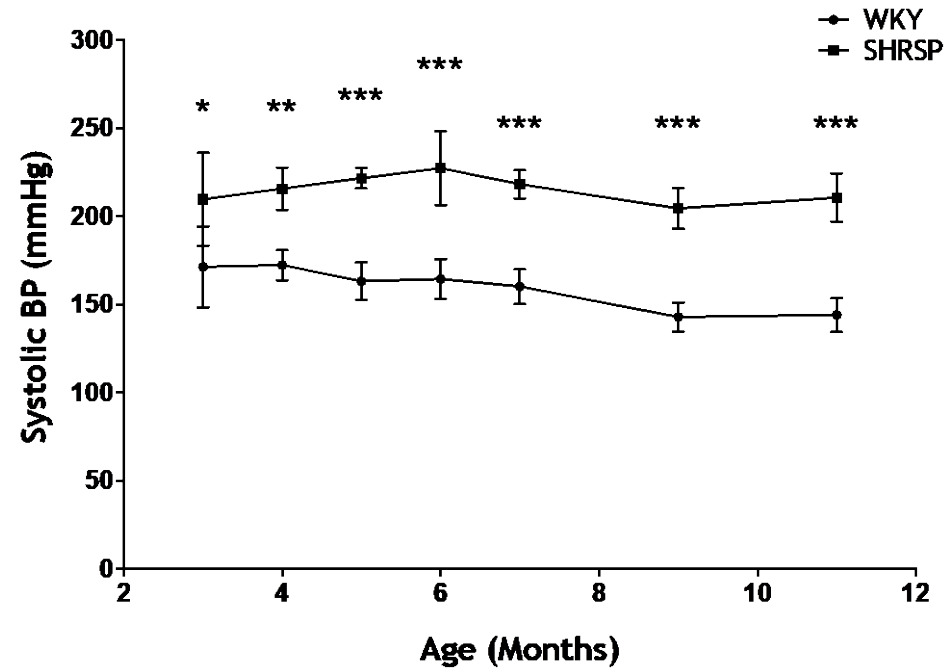


Figure 5.4: Longitudinal systolic BP measurements for aWKY and aSHRSPs at 3, 4, 5, 6, 7, 9 and 11 months. Systolic BP measurements were significantly higher in SHRSPs compared to WKYs at all time points investigated. Data was analysed using multiple t-tests with statistical significance being determined by the Holm-Sidak method to correct for multiple comparisons. Data presented as mean \pm standard deviation. * $p < 0.05$; ** $p < 0.01$; *** $p < 0.0001$.

5.3.2.3 Blood pressure and heart rate during MRI

Medetomidine is known to affect heart rate and blood pressure (Hollyer 2016). Therefore, to inform on such changes following medetomidine administration, MABP and HR measurements over a 1-minute period were averaged at 2 minutes prior to and 5 minutes after medetomidine bolus administration in a subgroup of aWKYs (n = 10) and aSHRSPs (n = 7).

An overview of MABP and HR prior to and following medetomidine administration is shown in Figure 5.5. Prior to medetomidine administration, animals were maintained on 1.5% isoflurane in medical air supplemented with 30% oxygen. Under this initial anaesthesia, group-averaged MABP measurements were 145.8 mmHg and 196.3 mmHg for aWKYs and aSHRSPs, respectively. Following administration of the medetomidine bolus, a significant decrease in MABP was observed for both aWKYs (81.7 mmHg, $p < 0.0001$, paired t-test) and aSHRSPs (106.5 mmHg, $p = 0.0008$, paired t-test). A similar response pattern was observed for HR with group-averaged values of 303 bpm and 335 bpm being observed prior to medetomidine administration and 234 bpm and 192 bpm being observed 5 mins following medetomidine administration for aWKY and aSHRSP, respectively. MABP measurements before medetomidine bolus administration were not recorded for cWKYs and cSHRSPs. Therefore a comparison of MABP before and after medetomidine in these chronic experimental groups is not possible, although similar decreases in MABP and HR were generally observed following the bolus during the scanning sessions.

MABP was monitored for all groups throughout the scanning session. Due to technical issues, MABP and HR measurements from 3 aSHRSPs and 1 cSHRSP were not recorded. Under combined medetomidine-isoflurane anaesthesia, MABP was similar between aWKYs, cWKYs and cSHRSPs (aWKY, 92.38 mmHg; cWKY, 88.1 mmHg; cSHRSP, 98.1 mmHg), while aSHRSPs (111.3 mmHg) demonstrated a significantly higher MABP than cSHRSPs ($p = 0.0069$) and cWKYs ($p = 0.0017$; Figure 5.6A). Heart rate measurements between aWKY, cWKY and cSHRSP were also similar with aSHRSPs demonstrating higher HR measurements compared to aWKY, cWKY and cSHRSPs (Figure 5.6B; aWKY, 207 bpm; aSHRSP, 251 bpm; cWKY, 217 bpm; cSHRSP, 224 bpm).

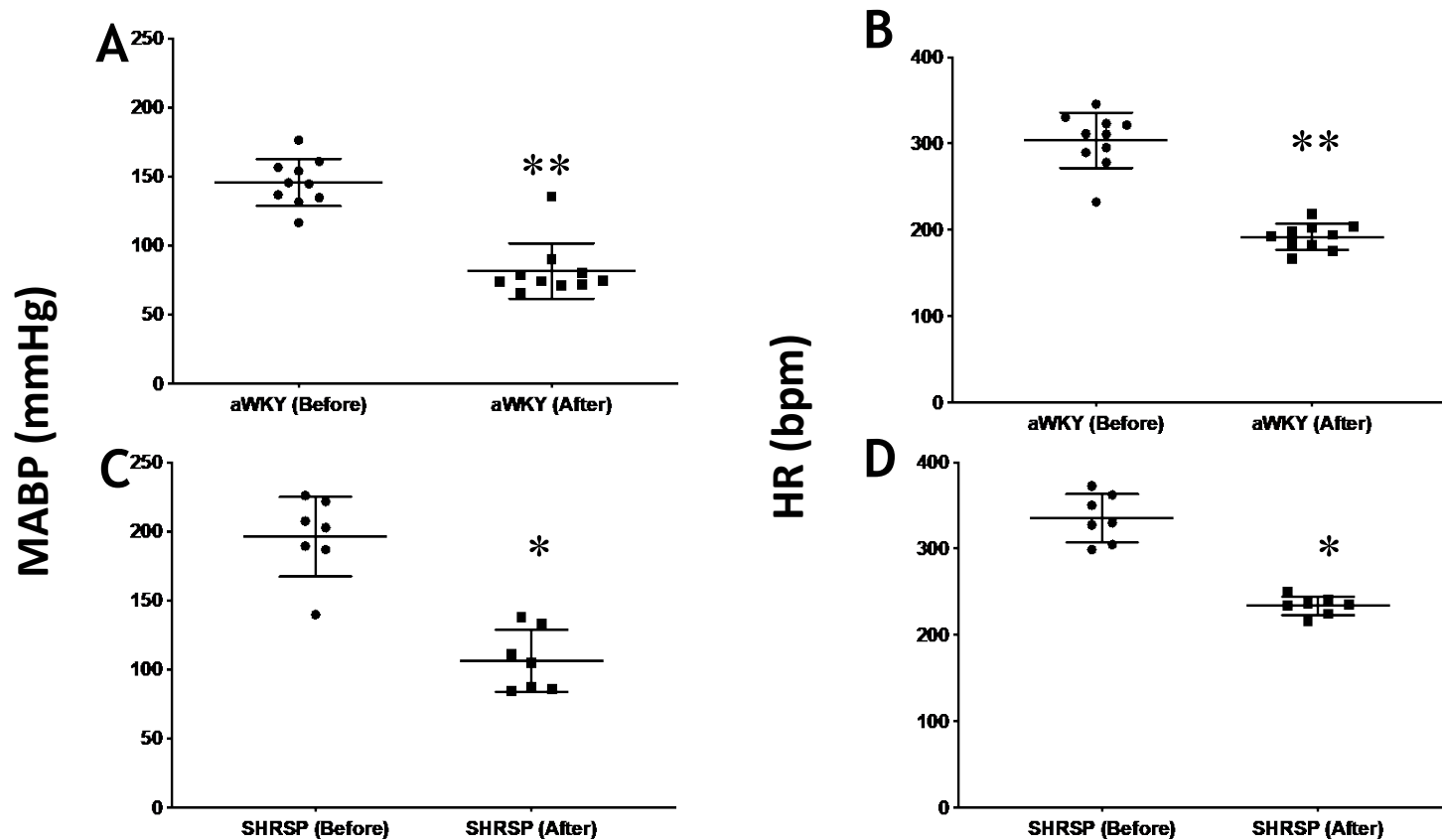


Figure 5.5: Blood pressure (A, C) and heart rate (B, D) prior to and following medetomidine administration for aWKY (A, B) and aSHRSPs (C, D). Blood pressure was significantly lower following medetomidine administration in both aWKY ($p < 0.0001$, paired t-test) and aSHRSP ($p < 0.001$, paired t-test). Heart rate was also significantly lower following medetomidine administration in aWKY ($p < 0.0001$, paired t-test) and aSHRSP ($p < 0.001$, paired t-test). * $p < 0.001$, ** $p < 0.0001$. HR, heart rate; MABP, mean arterial blood pressure.

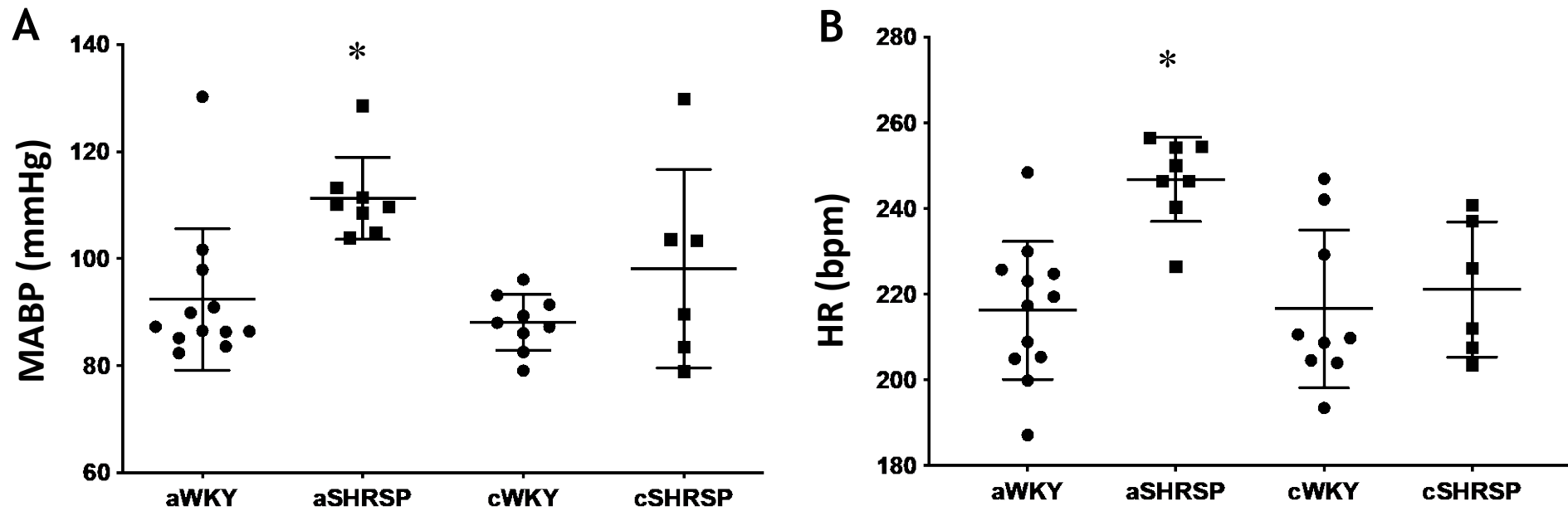


Figure 5.6: MABP (A) and HR (B) measurements during scanning for all study groups. Both MABP and HR significantly differed between experimental groups ($p=0.0018$ and $p=0.0007$, respectively). Under medetomidine-isoflurane anaesthesia, MABP was similar for aWKY, cWKY and cSHRSP groups. aSHRSPs demonstrated significantly higher MABP values compared to aWKY ($p=0.0069$) and cWKYs ($p=0.0017$). Similarly, HR s similar between aWKY, cWKY and cSHRSPs but aSHRSPs demonstrated significantly higher HR compared to aWKY ($p=0.0008$), cWKY ($p=0.002$) and cSHRSP ($p=0.0222$). Data was analysed using one-way ANOVA with Tukey's multiple comparisons test. Adjusted p-values are indicated. Individual data shown with mean \pm standard deviation. HR, heart rate; MABP, mean arterial blood pressure.

5.3.2.4 Blood pressure and heart rate during LSCI

MABP and HR were monitored during LSCI (Figure 5.7). Data was not collected for 1 aWKY, 2 aSHRSPs, 1 aWKY and 1 cSHRSP. Similar to previous findings during MRI, there was a significant difference in MABP between the experimental groups ($p < 0.0001$, one-way ANOVA). Under combined medetomidine-isoflurane anaesthesia, MABP did not significantly differ between aWKYs, cWKYs, and cSHRSPs (aWKY, 85.81 mmHg; cWKY, 75.79 mmHg; cSHRSP, 87.05 mmHg), however MABP was significantly higher in aSHRSPs (108.5 mmHg) compared to aWKYs and cWKYs ($p < 0.01$ and $p < 0.0001$, respectively). Similar to MABP, mean HR over the duration of the experiment was observed to significantly differ between the experimental groups ($p < 0.01$, one-way ANOVA). Mean HR did not differ between aWKYs, cWKYs, and cSHRSPs (aWKY, 225 bpm; cWKY, 232 bpm; cSHRSP, 254 bpm), however HR was significantly higher in aSHRSPs (265 bpm) compared to aWKYs and cWKYs ($p = 0.0028$ and $p = 0.0213$, respectively, Tukey's multiple comparisons test).

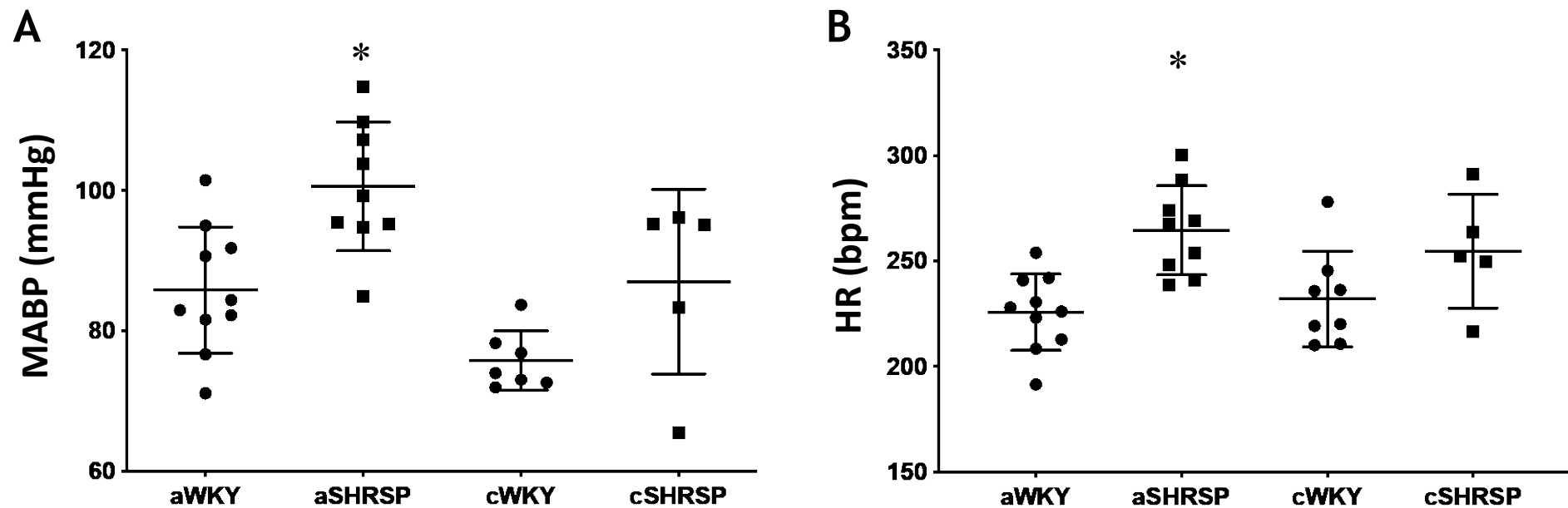


Figure 5.7: MABP (A) and mean HR (b) during LSCI. Both MABP and HR significantly differed between experimental groups ($p < 0.0001$ and $p < 0.01$, respectively, one-way ANOVA). MABP was similar for aWKY, cWKY and cSHRSP groups. aSHRSPs demonstrated significantly higher MABP values compared to aWKY ($p < 0.01$) and cWKYs ($p < 0.001$). Similarly, no significant differences in HR were observed between aWKY, cWKY or cSHRSP but aSHRSPs demonstrated significantly higher HR compared to aWKY ($p < 0.001$), cWKY ($p < 0.01$) and cSHRSP ($p < 0.05$). Data was analysed using one-way ANOVA with Tukey's multiple comparisons test. Adjusted p-values are indicated. Individual data shown with mean \pm standard deviation. * $p < 0.05$ compared to other groups.

5.3.3 - Structural Characterisation of WKYs and SHRSPs

5.3.3.1 T₂ Imaging

T₂ imaging was used to detect any vascular lesions. Ischemic lesions showed as areas of hyperintense signal (oedema) with or without a localised hypointense region. Vascular lesions were not observed in any aWKY, aSHRSP or cWKY animals (Figure 5.8). However, in 5 cSHRSPs various vascular lesions were identified, 4 of which were located caudally in the left hemisphere and 1 of which was located in the right hemisphere. All infarcts were generally confined to the cortex. In 1 cSHRSP, a large hyperintense cyst-like structure, indicative of a recent infarct, was identified in the left hemisphere and was present throughout most of the imaged brain (Figures 5.9). Interestingly, this large infarct was generally confined within the cortex, although substantial tissue compression was observed. Two animals also demonstrated evidence of recent haemorrhages in penetrating cortical arteries, identified by hypointense areas (Figure 5.11). Another cSHRSP demonstrated small hypointense 'spots' within the striatum, indicative of small infarcts (Figure 5.12). In 3 of the 5 cSHRSPs, hyperintense areas were clearly defined in the cortex with localised hypointense cores (Figures 5.10–5.12). In these animals, hyperintensities were also observed in the around the corpus callosum of the affected hemisphere.

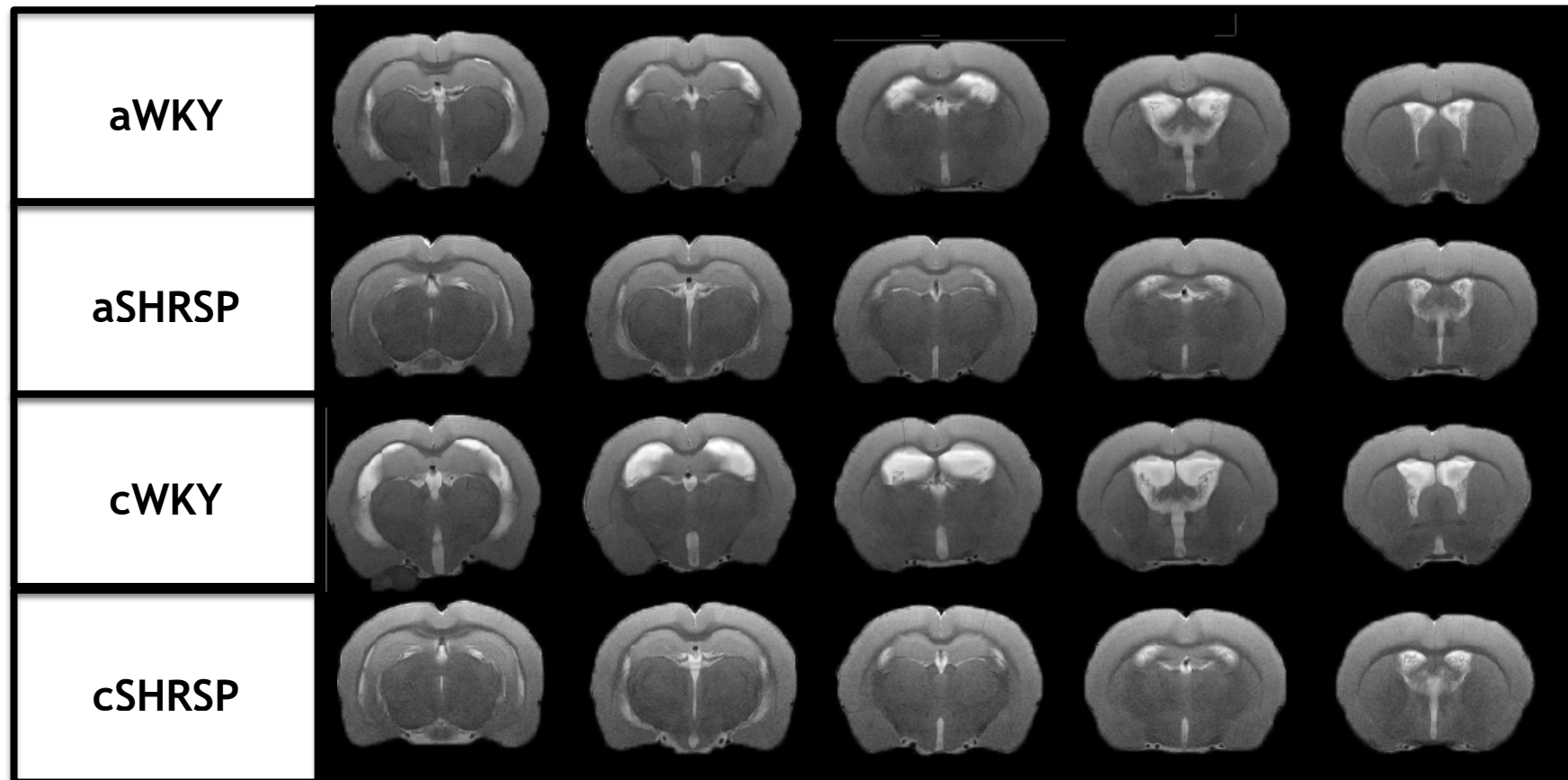
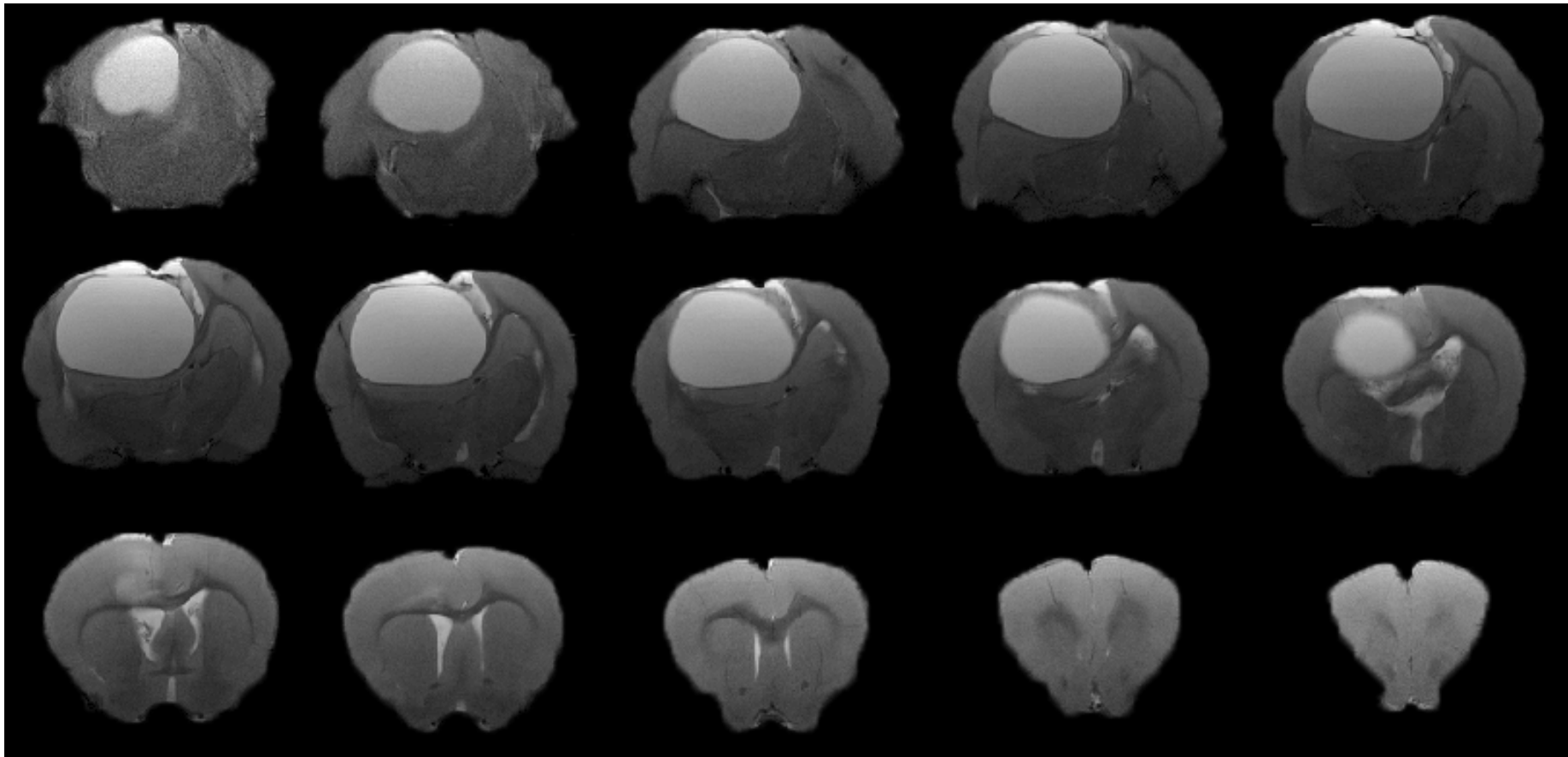


Figure 5.8: Overview of selected brain slices from a representative animal from each experiment group. For the cSHRSP group, one of the seven animals that had not suffered a stroke was selected.

Figure 5.9: T₂-weighted scan of cSHRSP. Animal had previously suffered a substantial stroke in the left hemisphere that had subsequently become a cyst, as indicated by the large hyperintense region.



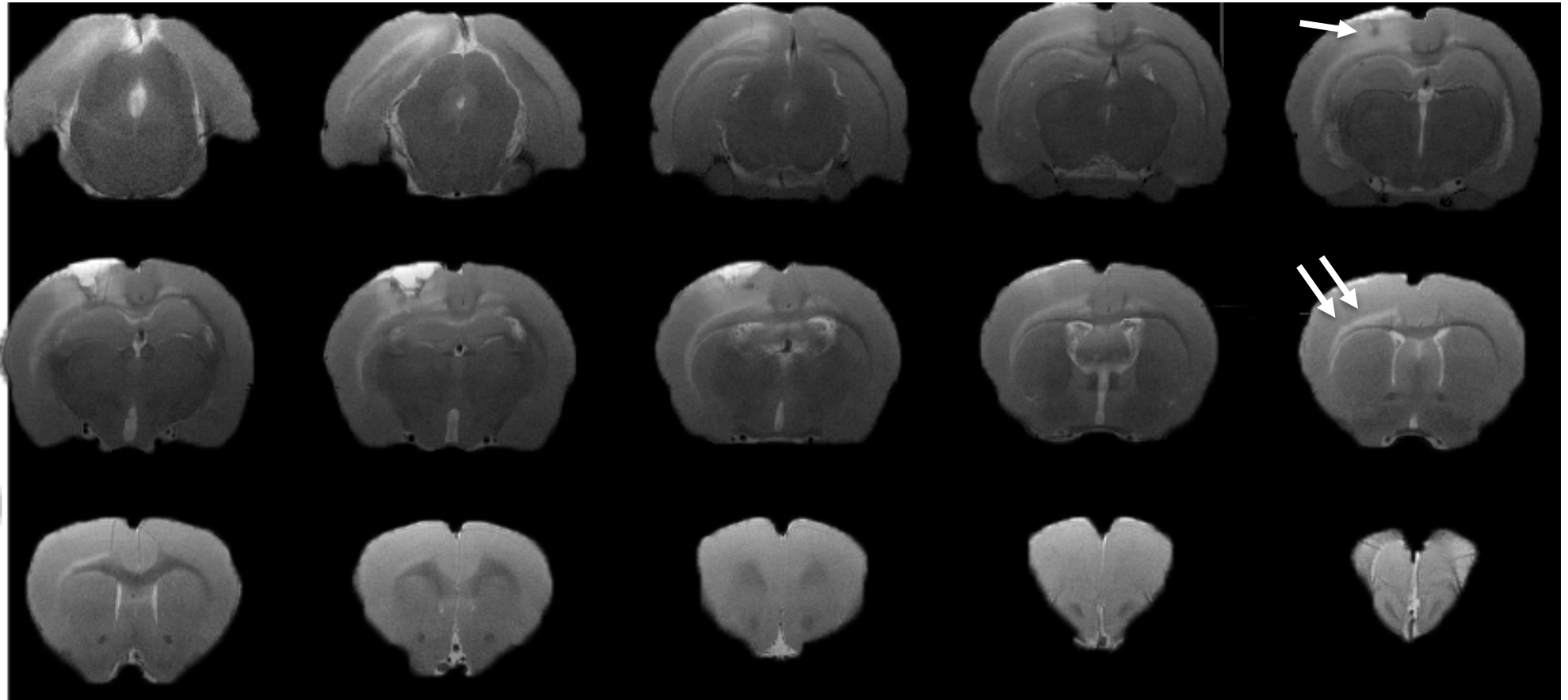


Figure 5.10: T₂-weighted scan of cSHRSP. Evidence of a stroke can be observed in the left hemisphere. Single arrow indicates a hypointense core within a hyperintense region. Double arrows indicate hyperintensity near the corpus callosum of the affected hemisphere.

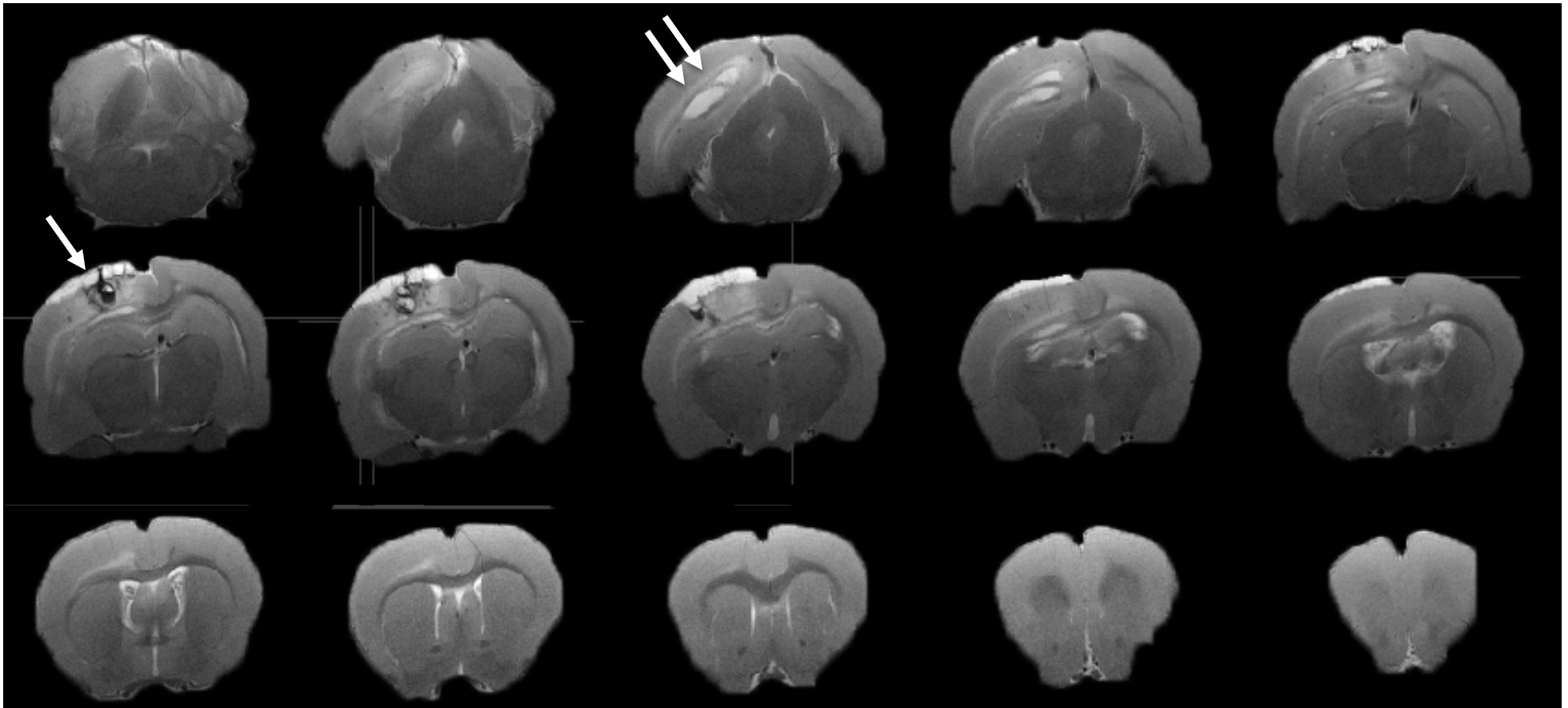


Figure 5.11: T₂-weighted scan of cSHRSP. Stroke had occurred in the left hemisphere. Single area indicates a hypointense haemorrhage from a penetrating cortical vessel. Double arrows indicate hyperintensity in the corpus callosum of the affected hemisphere.

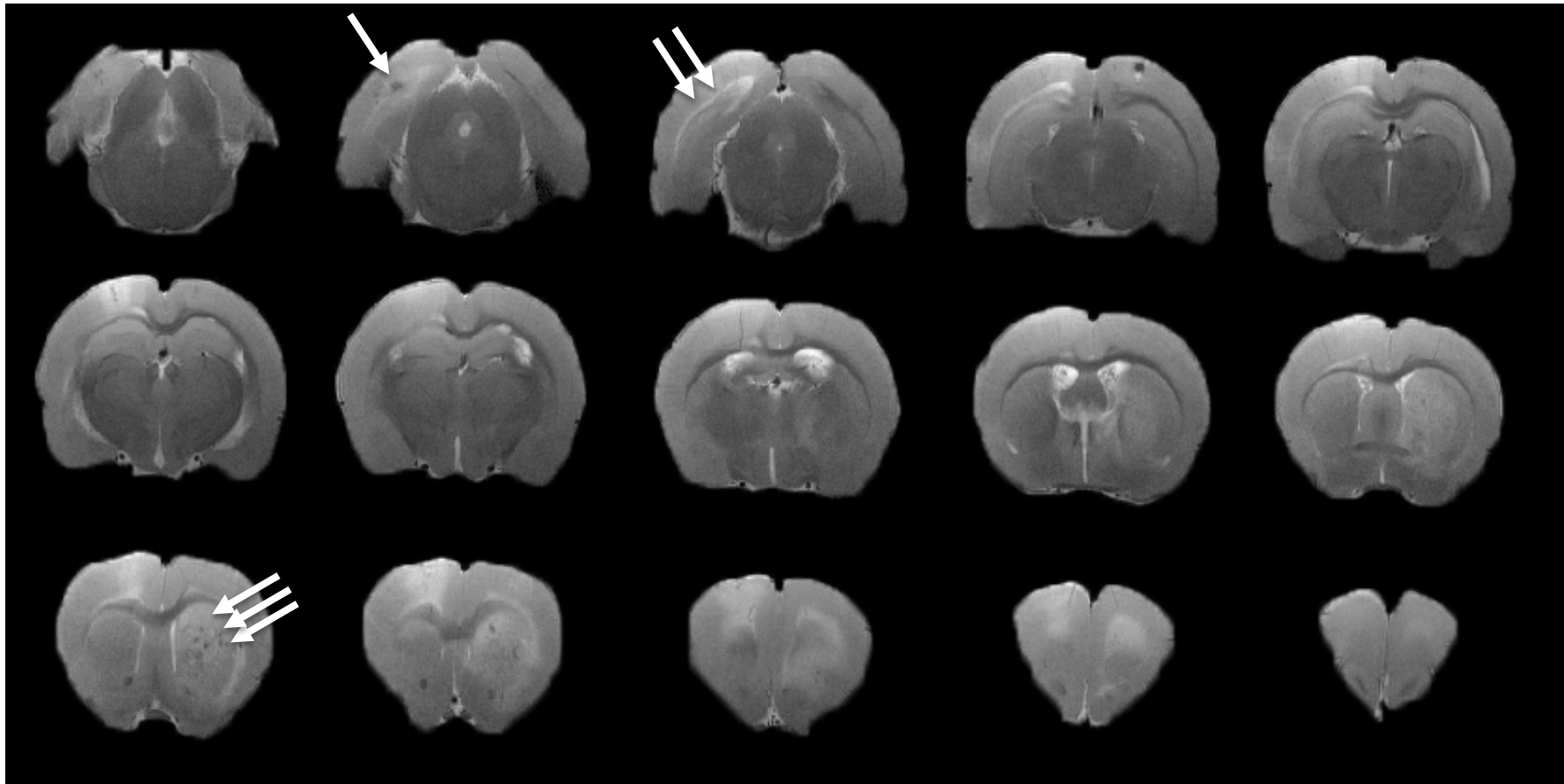


Figure 5.12: T₂-weighted scan of a cSHRSP. Stroke in the left hemisphere. Single arrow indicates a hypointense region from a previous infarct. Double arrows indicate hyperintensity around the corpus callosum of the affected hemisphere. Three arrows indicate small hypointense 'spots' within the striatum due to infarct.

5.3.3.2 Brain volume measurements

Brain and ventricle volumes were calculated for each experimental group. Two-way ANOVA found a significant effect of strain ($p < 0.0001$) on brain volume but no effect of age ($p = 0.36$) or any interaction ($p = 0.81$). Mean brain volumes for aWKYs (1462 mm^3) and cWKYs (1487 mm^3) were generally larger than both aSHRSPs (1350 mm^3) and cSHRSPs (1365 mm^3 ; Figure 5.13A). Brain volumes between aWKYs and cWKYs, as well as aSHRSPs and cSHRSPs did not significantly differ ($p = 0.94$ and $p = 0.99$, respectively). However, aWKYs had significantly larger brain volumes compared to aSHRSPs ($p = 0.002$) and cSHRSPs ($p = 0.02$). Brain volumes for cWKYs were also significantly larger compared to aSHRSP and cSHRSPs ($p < 0.001$ and $p = 0.004$, respectively).

Lateral ventricle volume followed a similar pattern to that observed in the brain volume measurements. Mean lateral volume measurements were generally larger in aWKYs (47.28 mm^3) and cWKYs (67.56 mm^3) compared to both aSHRSPs (14.76 mm^3) and cSHRSPs (26.11 mm^3 ; Figure 5.13B). Two-way ANOVA revealed a significant effect of strain ($p < 0.0001$) and age ($p = 0.0324$) on lateral ventricle volume with WKYs generally demonstrating larger ventricle volumes than SHRSPs and older animals demonstrating larger ventricle volumes compared to younger animals. However, no interaction was observed ($p = 0.8708$). Lateral ventricle volumes were significantly larger in aWKYs compared to aSHRSP ($p < 0.0001$) and cSHRSP ($p = 0.0003$). Similarly, cWKYs demonstrated significantly larger lateral ventricle volume compared to aSHRSP and cSHRSP ($p < 0.0001$ for both). Despite being larger in both chronic WKYs and SHRSPs, compared to their acute counterparts, lateral ventricle volume was not found to significantly differ between acute and chronic WKYs ($p = 0.57$) or between acute and chronic SHRSPs ($p = 0.53$) groups.

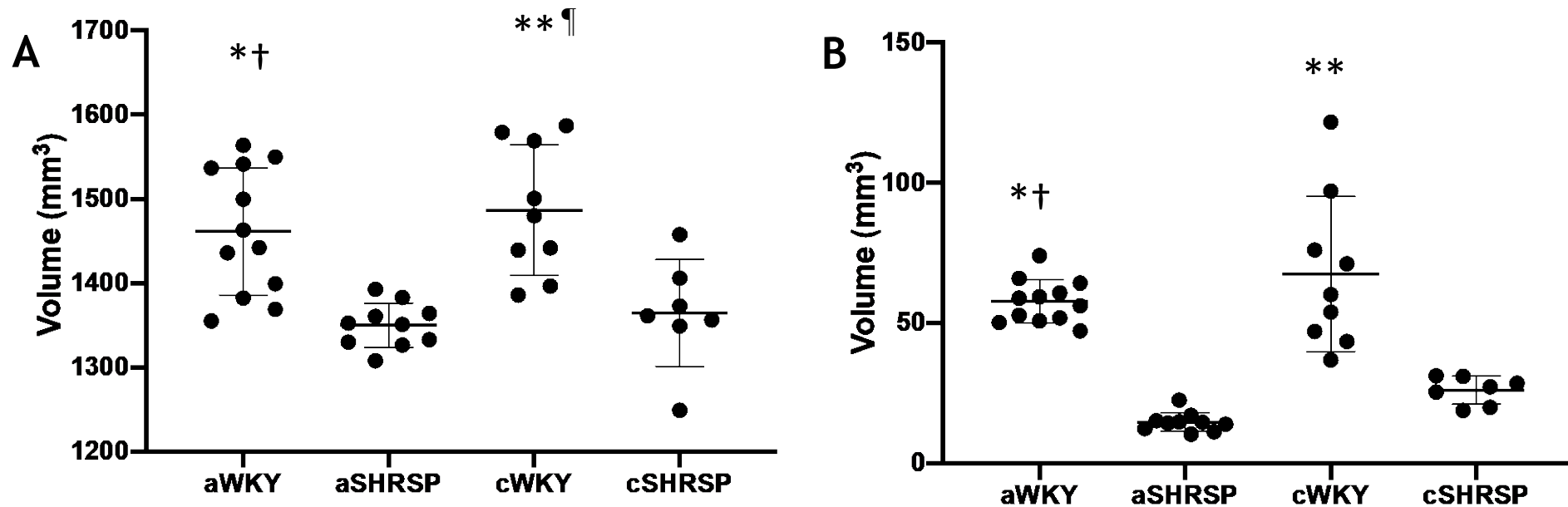


Figure 5.13: Brain and lateral ventricle volumes. (A) Both aWKY and cWKYs had significantly larger brain volumes than aSHRSPs and cSHRSPs. A significant effect of strain ($p < 0.0001$) on brain volume was observed but no effect of age ($p = 0.1525$) or interaction ($p = 0.8285$; Two-way ANOVA). (B) A significant effect of strain ($p < 0.0001$) and age ($p = 0.0324$) on lateral ventricle volume was observed but no interaction ($p = 0.8708$). Both aWKYs and cWKYs had significantly larger lateral ventricle volumes compared to aSHRSPs and cSHRSPs. Older animals exhibited numerically larger lateral ventricle volumes but these were not found to significantly differ. (A) * $p < 0.01$ vs aSHRSP; † $p < 0.05$ vs cSHRSP; ** $p < 0.001$ vs aSHRSP; †† $p < 0.01$ vs cSHRSP. (B) * $p < 0.001$ vs cSHRSP; † $p < 0.0001$ vs aSHRSP; ** $p < 0.0001$ vs aSHRSP and cSHRSP.

5.3.4 Assessing the effect of acute and chronic hypertension on the stimulus-evoked BOLD response

Electrical forelimb stimulation was used to assess the effects of acute and chronic disease duration on the stimulus-evoked BOLD signal in young and aged WKYs and SHRSPs. Group-averaged BOLD responses are shown in Figure 5.14. Both aWKY and cWKY group-average BOLD responses demonstrated a similar temporal profile, slowly increasing following stimulus onset to achieve a plateau that persisted for the remainder of stimulation and for several seconds once stimulation was switched off, but then declined back to baseline. In the aSHRSP group, a gradual increase in BOLD peaked shortly following the onset of stimulation, declined slightly and then achieved a plateau that was generally maintained for the remainder of the stimulation period and then gradually declined back to baseline once the stimulus was switched off. The group-averaged BOLD response for cSHRSPs shows a large increase in the BOLD response following stimulus onset, that peaks approximately half-way through the stimulation period, and then exhibits a gradual decline for the remainder of stimulation, and returns to baseline shortly following the end of stimulation.

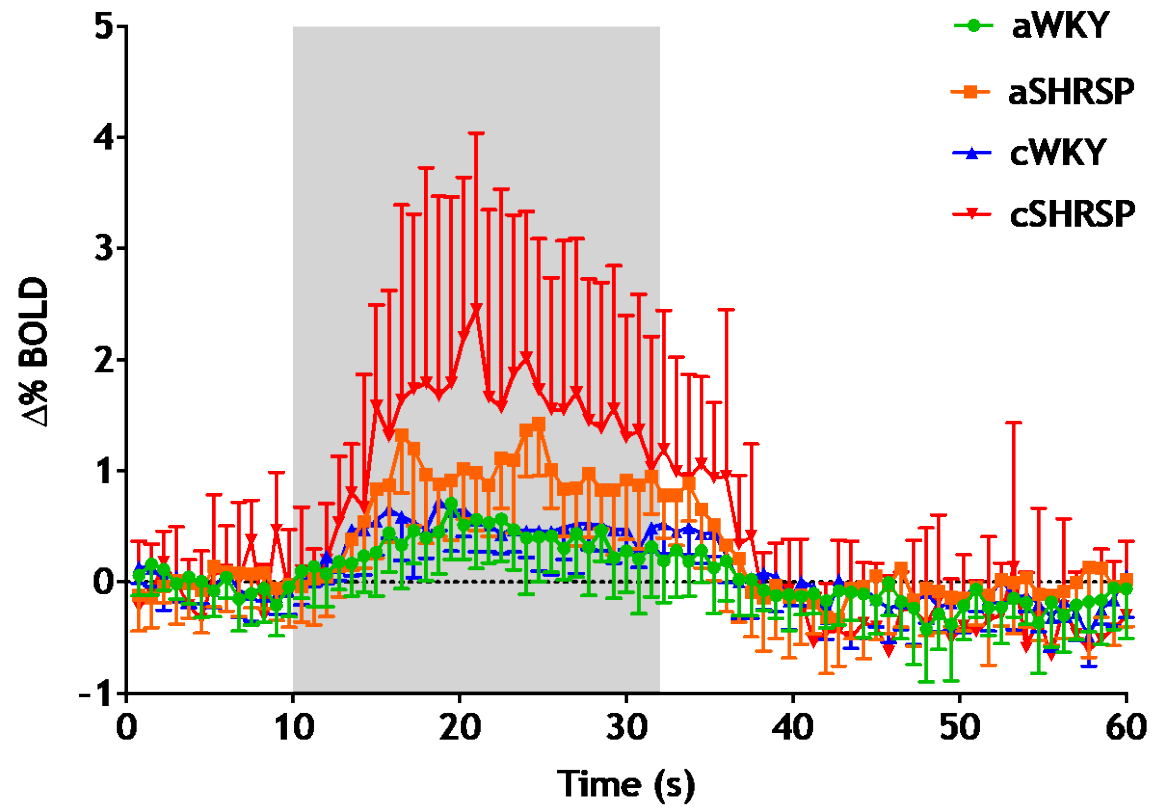


Figure 5.14: Group-averaged %BOLD time courses in S1FL area. Shaded area indicates stimulation period. Data presented as mean \pm standard deviation.

When the characteristics of the BOLD response were assessed, SHRSPs generally demonstrated larger BOLD responses, exhibiting larger peak %BOLD and larger integrated BOLD values. Both aSHRSPs and cSHRSPs demonstrated significantly larger peak %BOLD values than those observed in the aWKY group (Figure 5.15). While the mean peak %BOLD observed in the cWKY (0.9%) group was lower than both aSHRSPs (1.8%) and cSHRSPs (2.1%), and marginally higher than the aWKY group (0.7%), it was only observed to be significantly smaller than the cSHRSP group and did not significantly differ from the aSHRSP group.

The integrals of BOLD responses were also found to be significantly higher in the aSHRSP (23.5%) and cSHRSP (34.5%) groups compared aWKY (8.5%), indicating that a larger BOLD response was maintained over the course of stimulation for these groups (Figure 5.16). Integrated BOLD measurements for the cWKY (12.4%) group were again lower than both SHRSP groups and only marginally higher than aWKYs, however no significant difference was observed between cWKY and SHRSP groups. While both peak Δ BOLD and integrated BOLD measurements demonstrated an effect of strain, no effect of age or any interaction between age and strain for either measurement was observed when assessed by two-way ANOVA.

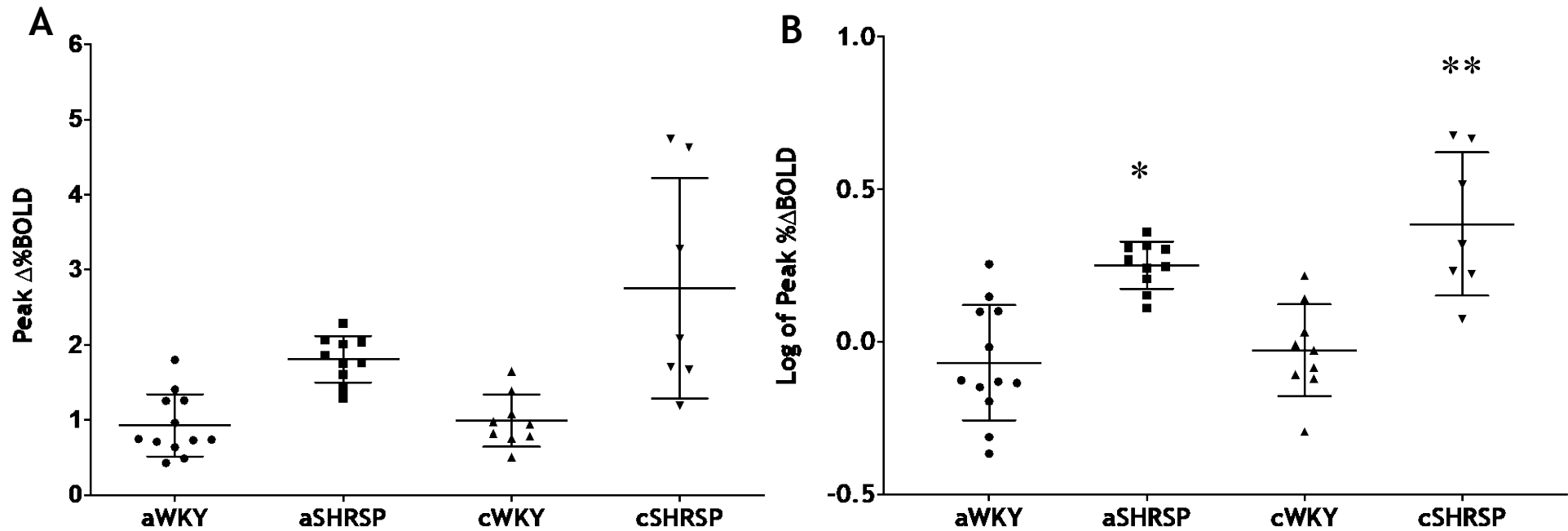


Figure 5.15: (A) peak %BOLD and (B) log of peak %BOLD in the S1FL area. A two-way ANOVA revealed a significant effect of strain on peak %BOLD ($p < 0.0001$) but no significant effect of age ($p = 0.0998$) and no interaction ($p = 0.1623$). Significantly higher peak responses were observed in aSHRSPs compared aWKY ($p = 0.0005$) and cWKYs ($p = 0.0051$). Significantly higher peak BOLD values were also observed in cSHRSPs compared to aWKY ($p < 0.0001$) and cWKY ($p = 0.0001$). Adjusted p-values are indicated. Individual data points presents with mean \pm standard deviation overlaid. Statistical analysis was performed on log-transformed values only. * $p < 0.01$, ** $p < 0.001$.

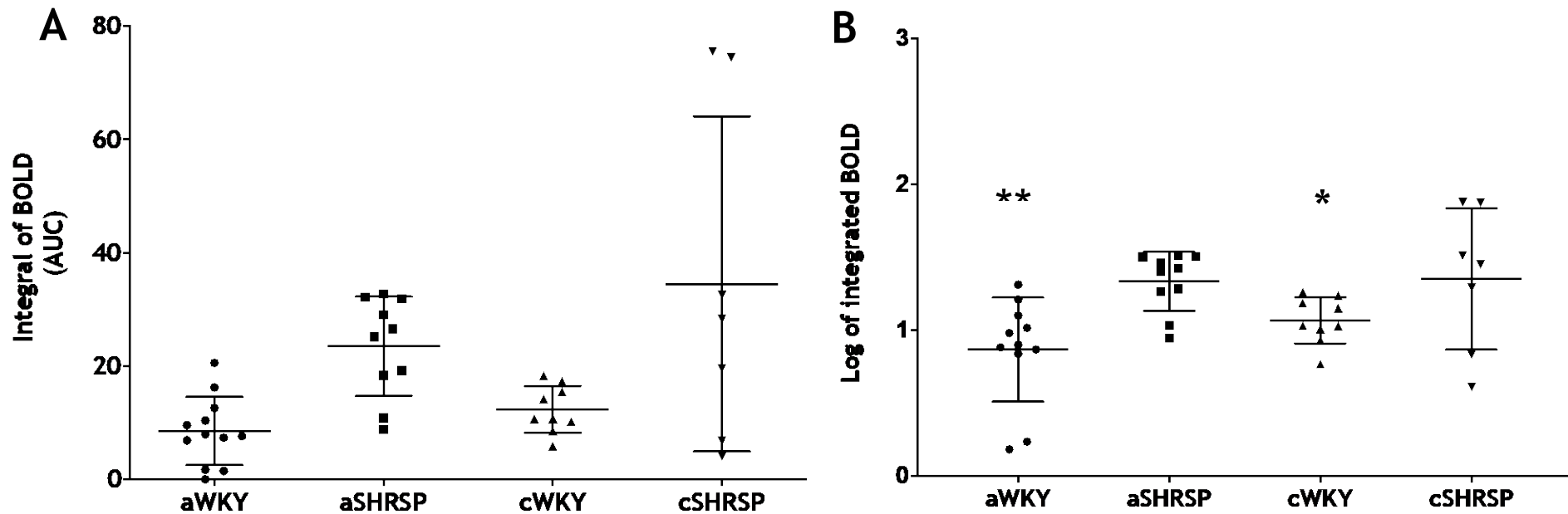


Figure 5.16: Integrated (A) BOLD and (B) log of integrated BOLD measurements in the S1FL area. Two-way ANOVA revealed a significant effect of strain on integrated BOLD measurements ($p=0.0003$) but no significant effect of age ($p=0.1131$) and no interaction ($p=0.4357$). Integrated BOLD measurements were significantly larger in cSHRSPs compared to aWKY ($p=0.0020$) and cWKY ($p=0.0157$) when assessed by Tukey's multiple comparisons test. Adjusted p-values are indicated. Individual data points are shown with mean \pm standard deviation overlaid. Statistical analysis was performed on log-transformed values only. * $p<0.05$ vs cSHRSP; ** $p<0.01$ vs cSHRSP

5.3.5 Assessing the effect of acute and chronic hypertension on the stimulus-evoked CBF response using LSCI

In a follow-up experiment one week after MRI scanning, we assessed the effects of acute and chronic disease duration on the stimulus-evoked CBF response in young and aged WKYs and SHRSPs using LSCI. Electrical stimulation of the right forepaw evoked a CBF response in the contralateral S1FL area for all animals. Raw laser speckle and difference images for a representative aWKY and aSHRSP are shown in Figure 5.17. The responses for all experimental groups demonstrated a similar temporal profile, peaking shortly after stimulus onset, declining slightly over the course of stimulation, and then exhibiting a delayed and gradual decline back to baseline once stimulation was stopped (Figure 5.18). The ipsilateral S1FL and ipsilateral visual cortex were also monitored as control areas to assess any non-specific changes in CBF, however most animals did not exhibit responses in these areas during forelimb stimulation (Figure 5.19).

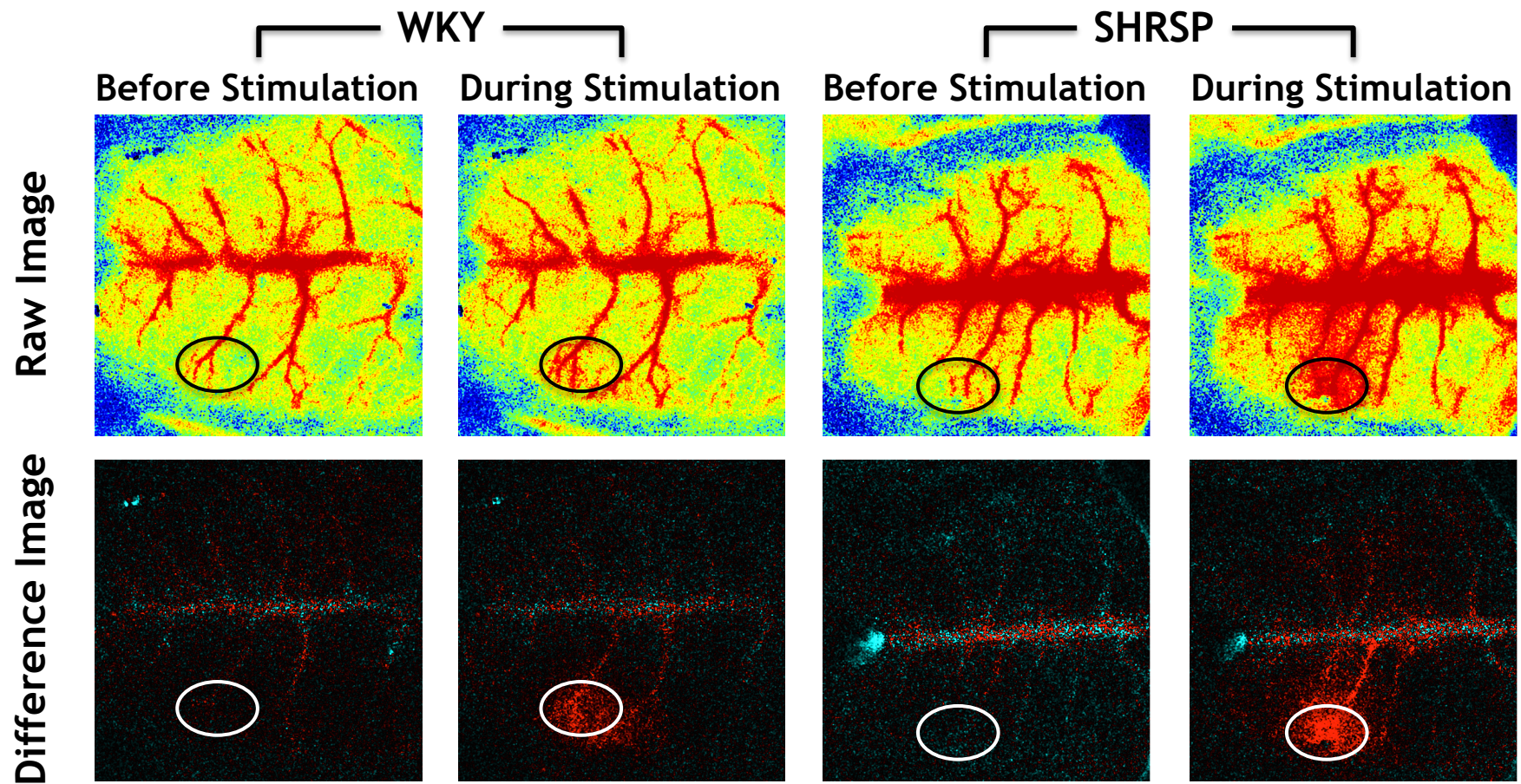


Figure 5.17: Raw (top row) and difference (bottom row) laser speckle images before and during stimulation for a representative aWKY and aSHRSP. Black and white ROIs indicates contralateral S1FL. Raw images were captured at 10 frames per second, with averaging every 10 frames giving an effective frame rate of 1 frame per second.

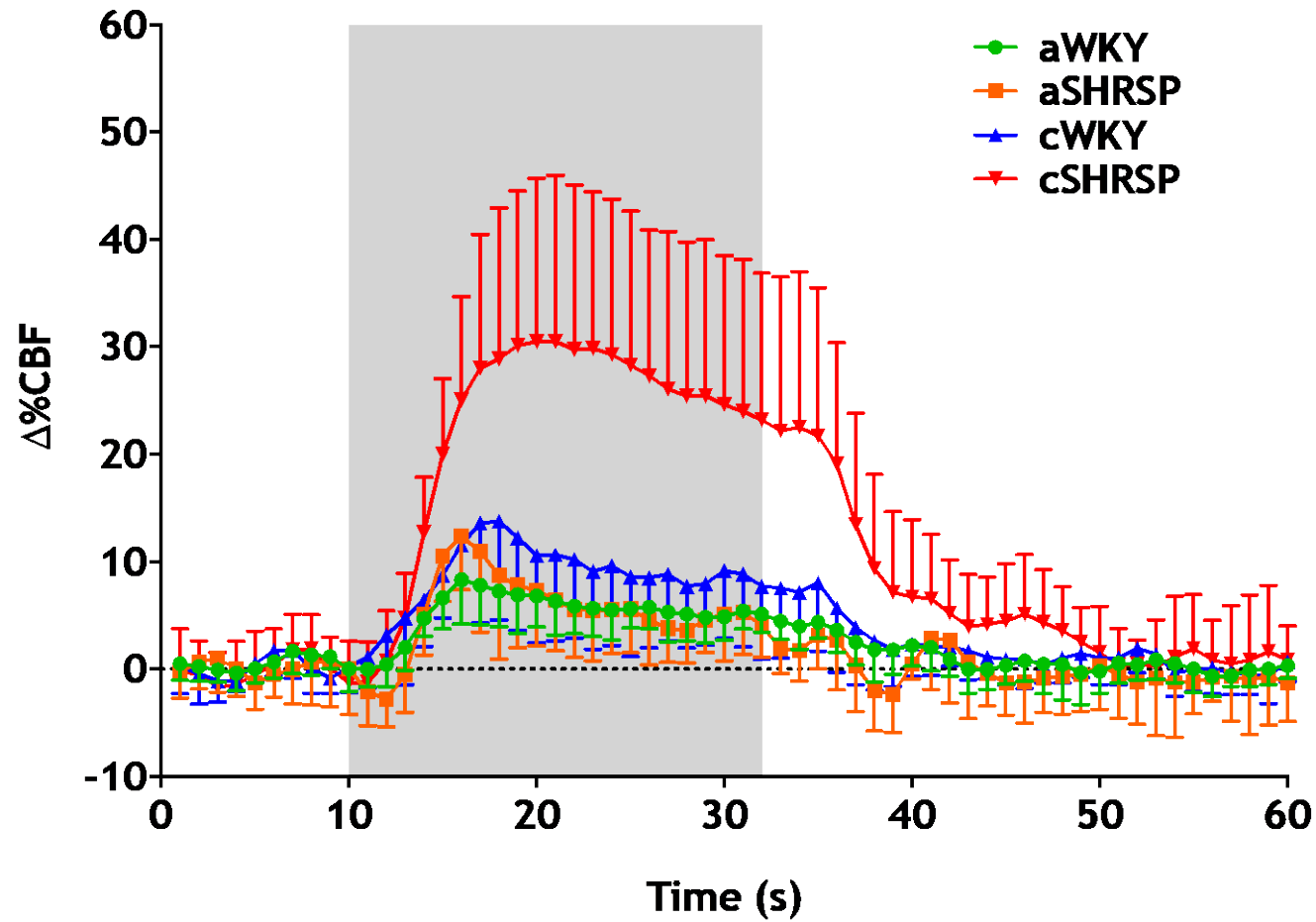


Figure 5.18: Contralateral S1FL area group-averaged %CBF time course for all experimental groups. Shaded area indicates stimulation. Data presented as mean \pm standard deviation.

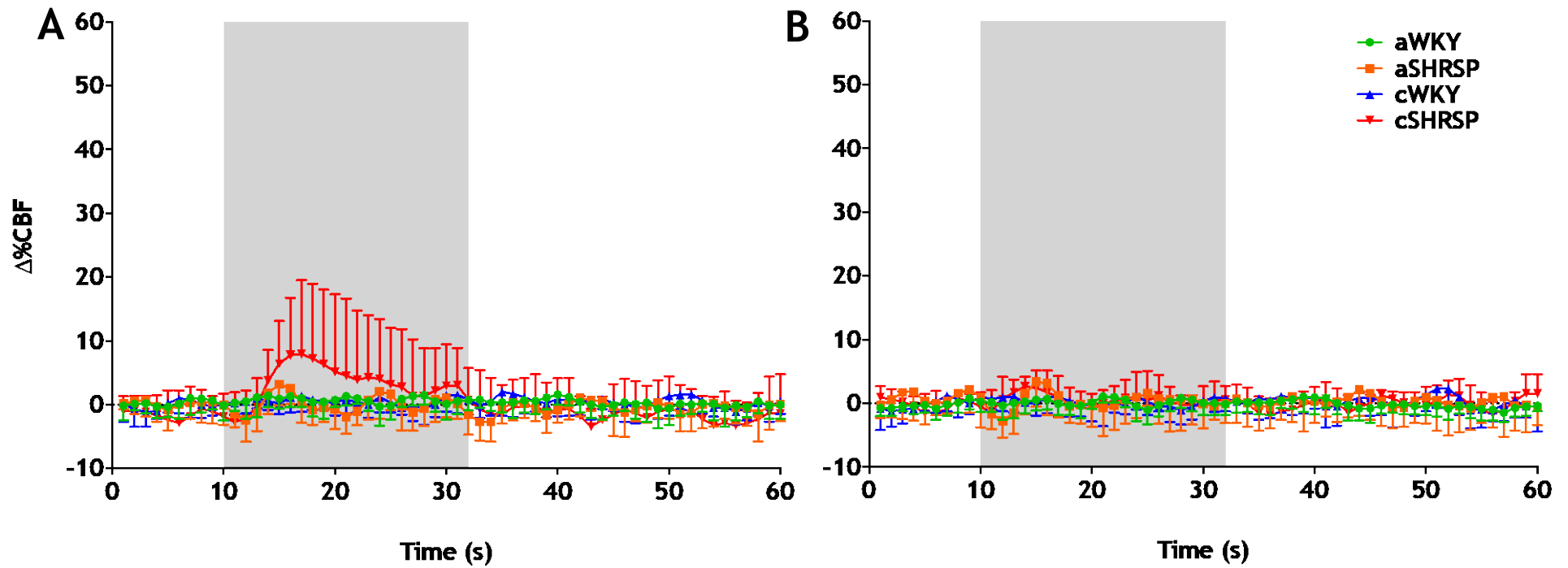


Figure 5.19: Group-averaged ΔCBF time courses for (A) ipsilateral S1FL and (B) ipsilateral visual cortex. Shaded area indicates stimulation. Data presented as mean \pm standard deviation.

When the characteristics of the stimulus-evoked CBF response in the contralateral S1FL area were assessed by two-way ANOVA, a significant effect of strain ($p=0.0009$) and age ($p=0.0003$) was observed on CBF peak values, but no interaction ($p=0.1470$). Generally, CBF responses with larger peaks were observed in chronic groups compared to younger groups and in SHRSPs compared to WKYs. Both aSHRSPs (13.9%) and cSHRSPs (32.7%) demonstrated higher peak CBF changes compared to their respective aWKY (9.4%) and cWKY (15.3%) counterparts. The largest group-average peak CBF change was observed in the cSHRSP group, being significantly higher than aWKY ($p<0.0001$), aSHRSP ($p=0.0042$) and cWKY ($p=0.0116$) groups. No significant differences were observed between any other experimental groups.

Similar findings were observed when assessing the integral of the CBF response. Two-way ANOVA revealed a significant effect of strain ($p=0.0093$), age ($p<0.0001$) and a significant interaction ($p=0.0017$). Group-averaged integrated CBF values were similar for aWKY (139.5%) and aSHRSPs (134.8%) indicating that CBF responses between these two acute groups were similar over the course of stimulation. Higher integrated CBF values were observed in the cWKY group (228.1%) compared to both acute groups, although the highest integrated CBF values, and hence largest CBF responses, were observed in the cSHRSP group (618.6%), being significantly larger than aWKY ($p<0.0001$), aSHRSP ($p<0.0001$) and cWKYs ($p<0.0020$).

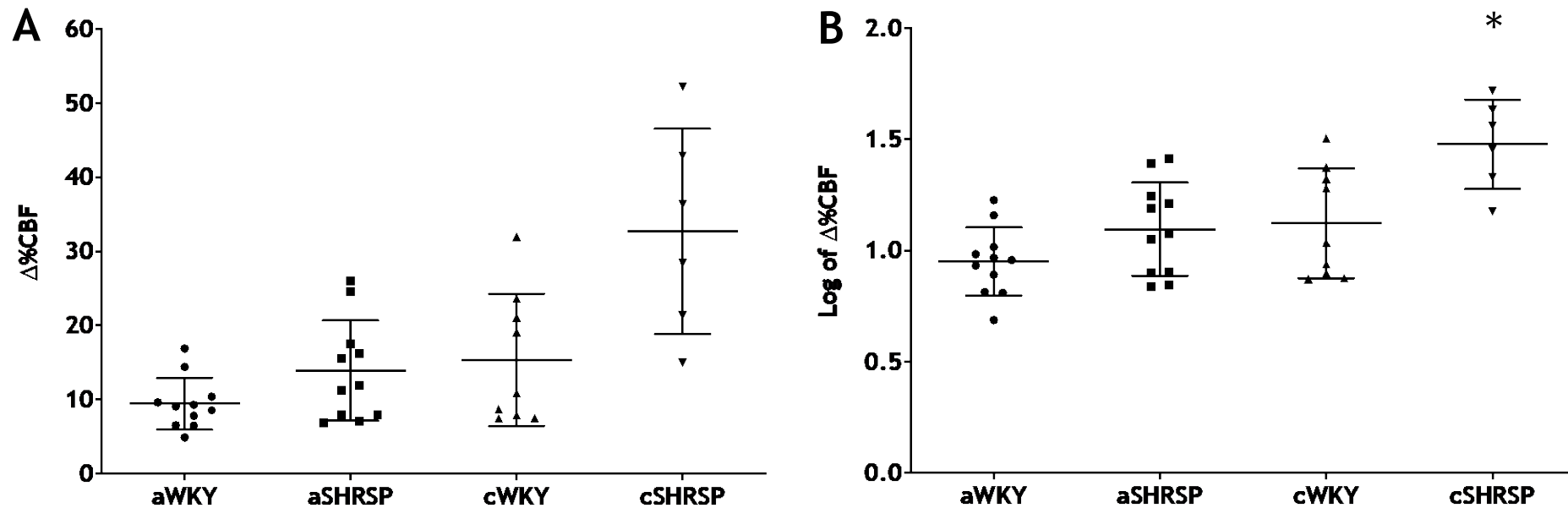


Figure 5.20: Peak %CBF in the contralateral S1FL area. A significant effect of strain ($p=0.0009$) and age ($p=0.0003$) were observed but no interaction ($p = 0.1407$; Two-way ANOVA). Larger %CBF peak values were evoked in cSHRSPs compared to aWKY ($p<0.0001$), aSHRSP ($p=0.0042$) and cWKY ($p=0.0116$). Adjusted p -values are indicated. Individual data points are shown with mean \pm standard deviation overlaid. Statistical analysis performed on log-transformed values only.

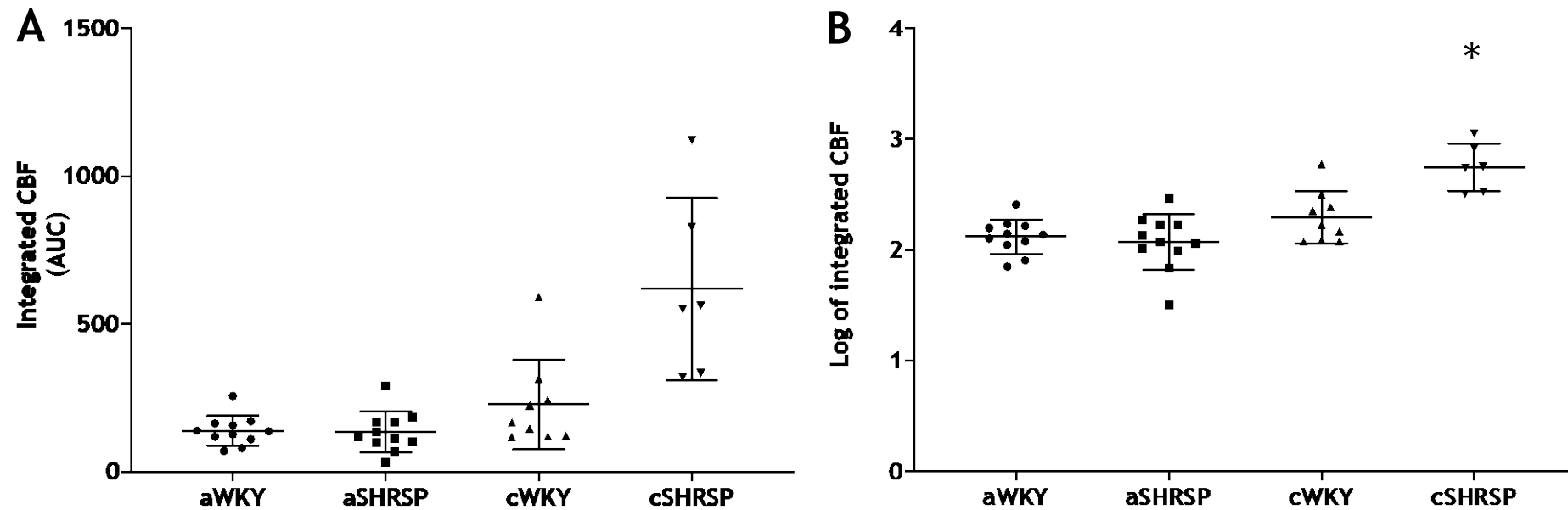


Figure 5.21: (A) Integrated CBF and (B) log of integrated CBF in the contralateral S1FL. Integrated CBF measurements violated the assumption of normal distribution, which was corrected by logarithmic transformation of the data. An effect of strain ($p=0.0093$), age ($p<0.0001$) and an interaction ($p=0.0017$; Two-way ANOVA) was observed. Integrated CBF values were significantly larger in cSHRSPs compared to aWKY ($P<0.0001$), aSHRSP ($p<0.0001$) and cWKY ($p=0.0020$). Adjusted p-values indicated. Individual data points shown with mean \pm standard deviation overlaid. Statistical analysis was performed on log-transformed values only. Non-transformed values shown for display purposes.

Ipsilateral S1FL and visual cortex areas were also monitored for non-specific CBF changes. Two-way ANOVA identified a significant effect of strain ($p=0.0370$) on peak $\% \Delta$ CBF in the ipsilateral S1FL area but no significant effect of age ($p=0.0987$) or any interaction between these variables (0.0620). For most animals, CBF fluctuated around baseline values in the ipsilateral S1FL area during stimulation, and therefore peak CBF values were generally low. However one cSHRSP demonstrated a large response, with a peak CBF value that was similar to responses seen in the contralateral S1FL area. Despite this observation, no significant pairwise comparisons were found when data was further analysed by a Tukey's multiple comparisons test. When assessing the integral of CBF responses in ipsilateral S1FL area, a significant interaction ($p=0.0397$) between age and strain was observed with cSHRSPs demonstrating numerically higher mean integrated CBF compared to all other experimental groups. This observation was again likely underpinned by the individual large response from the previously mentioned cSHRSP and the small size of this group. No significant pairwise comparisons were found when data were analysed using a Tukey's multiple comparisons test. CBF in the ipsilateral visual cortex was maintained at baseline levels for all experimental groups and no responses were observed during stimulation. No significant effect of strain, age or any interaction was observed for peak $\% \Delta$ CBF ($p=0.0737$, $p=0.1235$ and $p=0.2416$, respectively) or integrated CBF ($p=0.4023$, $p=0.9509$ and $p=0.9143$, respectively) in the ipsilateral visual cortex.

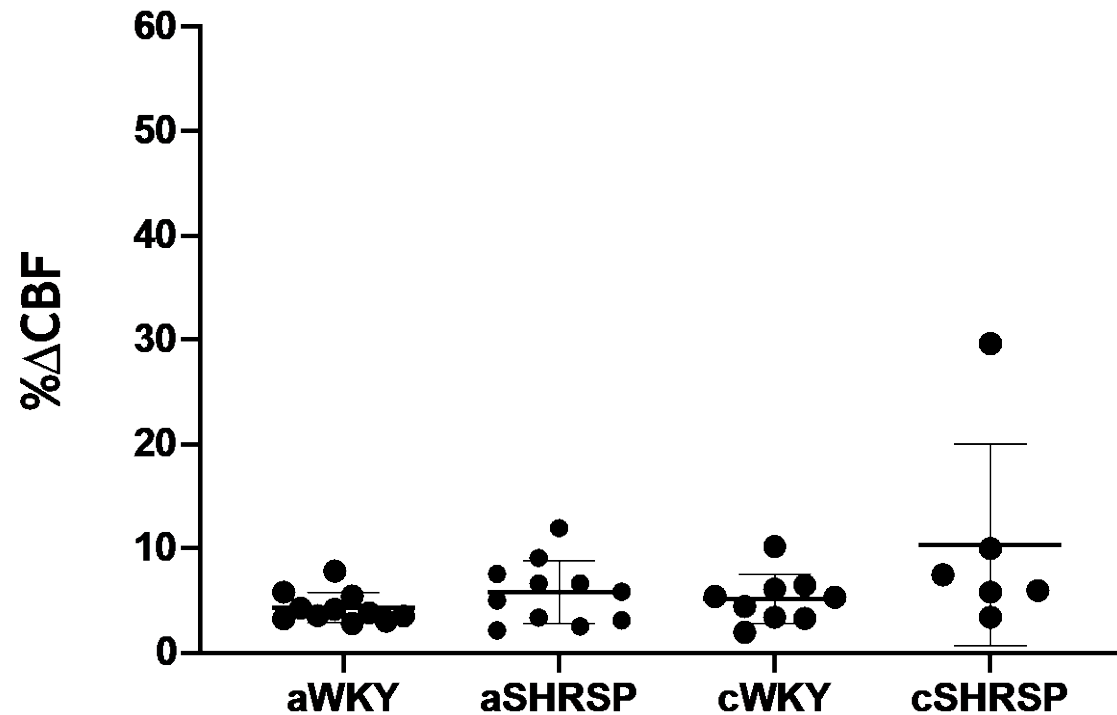


Figure 5.22 Peak % Δ CBF in the ipsilateral S1FL. Two-way ANOVA identified a significant effect of strain ($p=0.0370$) but no significant effect of age ($p=0.0987$) or any interaction between the two variables ($p=0.3620$). All animals demonstrated no relevant changes in peak % Δ CBF, with the exception of one cSHRSP that exhibited a large CBF response in the ipsilateral S1FL. No significant pairwise comparisons were observed. Individual data shown with mean \pm standard deviation overlaid.

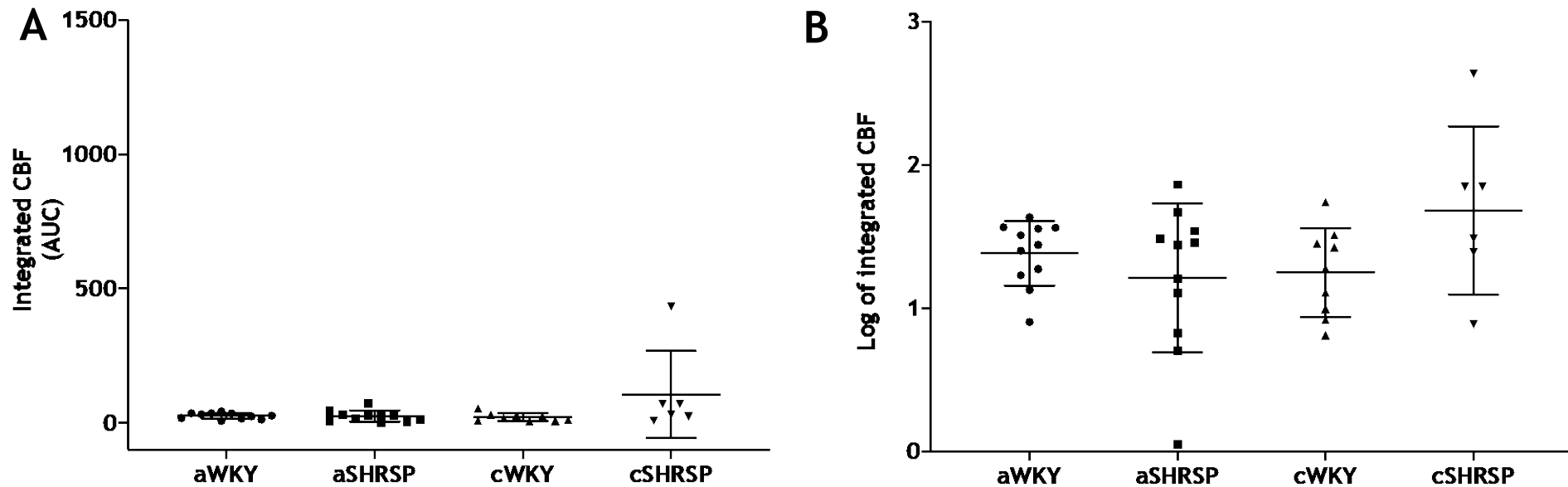


Figure 5.23: (A) Integrated CBF and (B) log of integrated CBF measurements in the ipsilateral S1FL. Integrated CBF measurements violated the assumption of normal distribution, which was corrected by logarithmic transformation of the data. Two-way ANOVA revealed a significant interaction ($p=0.0397$) but no significant effect of strain ($p=0.3558$) or age ($p=0.2406$). Most animals exhibited no relevant response in the ipsilateral S1FL and therefore small integrated CBF values were observed. One SHRSP exhibited a large CBF response in the ipsilateral S1FL. No significant pairwise comparisons were observed (Tukey's multiple comparisons test). Individual data shows with mean \pm standard deviation overlaid.

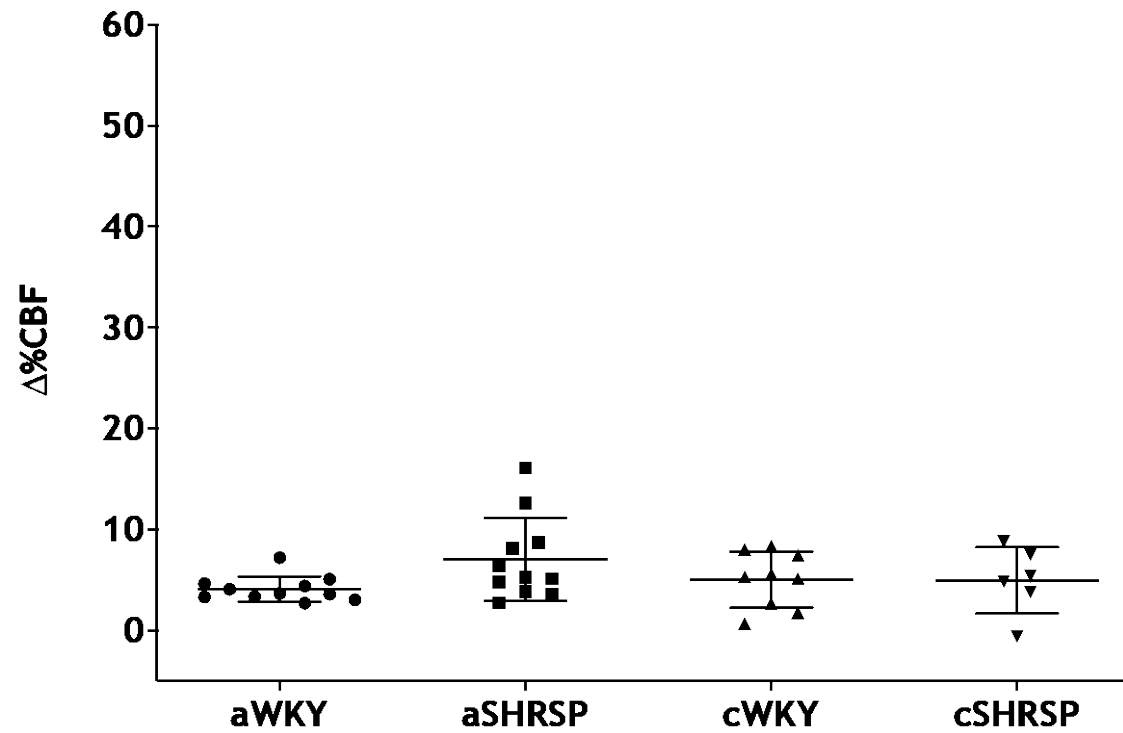


Figure 5.24: Peak $\Delta\%CBF$ in the ipsilateral visual cortex. Two-way ANOVA revealed no significant effect of strain ($p=0.0737$), age ($p=0.8242$) or any interaction between the two variables ($p=0.2416$). CBF activity was generally maintained around baseline with small fluctuations. Individual data points are shown with mean \pm standard deviation overlaid.

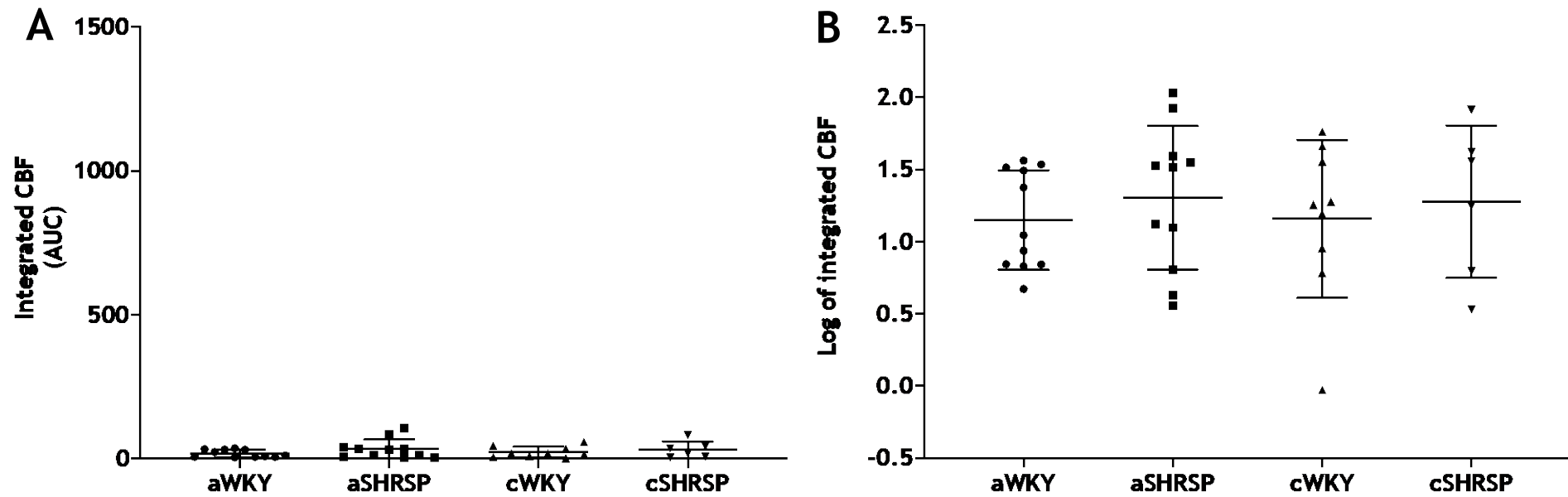


Figure 5.25: (A) Integrated CBF and (B) log of integrated CBF in the ipsilateral visual cortex. Integrated CBF measurements violated the assumption of normal distribution, which was corrected by logarithmic transformation of the data. Two-way ANOVA revealed no significant effect of strain ($p=0.4023$), age ($p=0.9509$) or any interaction between the two variables ($p=0.9143$). CBF activity was generally maintained at baseline levels with small fluctuations. Individual data points shown with mean \pm standard deviation overlaid.

5.4 Discussion

The studies in this chapter were performed with the aim to assess the ability of the hemodynamic response to inform on changes occurring in a rodent model of cerebral SVD, and assess whether these changes could be used to provide a biomarker of cerebrovascular health or as an indicator of therapeutic response. Furthermore we characterised the radiological features of these animals given that few studies have assessed such in aged SHRSPs.

5.4.1 Characterising WKY and SHRSPs

5.4.1.1 Animal Physiology

Generally, the assessed characteristics of WKYs and SHRSPs were as expected. SHRSPs weighed less than WKYs, a known difference between the two strains (Zanchi et al. 1997; Tarr 2012). SHRSPs were confirmed as hypertensive with a group-mean systolic blood pressure of 213.3 mmHg and 207.8 mmHg being observed for aSHRSPs and cSHRSPs, respectively. These observations are in agreement with literature values that reported elevated blood pressure of SHRSPs between 220–240 mmHg (Okamoto et al. 1974), marginally higher than the SHR, which generally demonstrates a systolic blood pressure between 180–200 mmHg (Okamoto and Aoki 1963; Dickhout and Lee 1998). Group-averaged systolic BP in cWKYs was also in agreement with literature values; in a plethysmography study an average systolic blood pressure of 114 mmHg was observed in normotensive rats (Olmstead et al. 1951). Younger aWKYs demonstrated marginally higher systolic blood pressure than older cWKYs when assessed by tail cuff plethysmography, with a group mean of 149.4 mmHg. A systolic blood pressure of 150 mmHg in the rat has previously been considered hypertensive (Okamoto and Aoki 1963), and therefore the younger aWKYs were marginally normotensive. Previous tail-cuff and telemetry studies in WKYs have observed mean systolic blood pressure values of 130 mmHg and 114 mmHg, respectively (Olmstead et al. 1951; Dickhout and Lee 1998), suggesting the blood pressure values in the current study were higher than normal. The observed higher systolic blood pressure in aWKYs could be due to stress-induced increases in blood pressure during tail cuff plethysmography. Although animals were acclimatised to the tail cuff procedure, it is possible that this was not enough to completely acclimatise animals and reduce stress-induced

elevations in systolic blood pressure. Older animals would have been handled more over time than younger animals, and therefore it is possible that older animals were more familiar with human interaction and less stressed by the tail cuff plethysmography procedure compared to younger animals. This may underpin the decrease in systolic blood pressure observed over time in the current study, as opposed to the gradual increase in BP that is generally known to occur with ageing (O'Rourke and Nichols 2005).

5.4.1.2 Brain volume

In contrast to previous studies in hypertensive patients and rats, the lateral ventricle volume of SHRSPs at both time points was significantly smaller than WKYs. Enlarged ventricles have previously been reported in older, hypertensive patients (Salerno et al. 1992; Strassburger et al. 1997). Furthermore, SHRs have demonstrated significantly larger lateral ventricle volumes compared to WKYs at 35 weeks of age (Kaiser et al. 2014). In that study, the group-averaged lateral ventricle volume in WKYs was approx. 50-60 mm³ which is similar to the volumes observed in our study for aWKYs (47.28 mm³) and cWKYs (67.56 mm³), suggesting that the ventricle volumes in SHRSPs were smaller than normal. It is unclear as to why the lateral ventricle volumes in SHRSPs were significantly smaller than WKYs in this study. However, it is worth noting that while the WKYs in the current study demonstrated similar values to those previously reported in the literature, the lateral ventricles of WKYs in the current study appeared noticeably dilated on the T₂-weighted images, especially in the cWKY group. WKYs were originally bred from the Wistar colony at Kyoto University. Both congenital spontaneous hydrocephalus and spontaneous ventriculomegaly have been observed to occur in the Wistar rat strain (Tu et al. 2014). Hydrocephalus in rats is characterised by a 'dome' shaped head and substantial dilation of the ventricles that notably compresses the surrounding tissue and subsequently leads to a decrease in cortical thickness (Olopade et al. 2012). Ventriculomegaly is characterised by mildly dilated ventricles (Tu et al. 2014). WKYs did not demonstrate a 'dome' head shape or notable compression of brain tissue and therefore it is unlikely that these animals developed spontaneous hydrocephalus. However, dilation of the lateral ventricles appeared similar that with previously reported spontaneous ventriculomegaly in Wistar rats (Tu et al. 2014). If the lateral ventricles of WKYs in the current

study were indeed similar to those seen in spontaneous ventriculomegaly, this may explain why SHRSP lateral ventricle volumes were significantly smaller. However, further investigation would be required to assess this observation.

5.4.1.3 T₂-weighted Imaging

In the current study, some of the animals that had suffered a stroke exhibited hyperintensity around the corpus callosum. In some instances, the corpus callosum appeared to have shifted and the hyperintense region appeared to follow the previous position of the white matter. WMHs are typically observed in the older and hypertensive populations and are an established characteristic of cerebral SVD (Fazekas et al. 1993; Dufouil et al. 2005; Schmidt et al. 2011; Wardlaw et al. 2013; Wardlaw et al. 2015). However, in human small vessel disease, white matter hyperintensities are generally hyperintense foci that appear in both hemispheres (Wardlaw et al. 2013). While some of the animals that had suffered a stroke demonstrated hyperintense areas in place of the corpus callosum, generally the hyperintense area was observed around the white matter and was limited to the affected hemisphere only. Therefore it is unlikely that we observed WMHs, as is generally defined in the clinical literature.

A previous MRI study assessing white matter in SHRSPs from the same colony used in the current study observed no signs of WMH in 10-month old animals (Brittain et al. 2013). In the current study, animals were generally older at scanning (approx. 12 months), however hyperintensities were only observed in 3 animals, all of which had suffered a stroke, as confirmed by MRI. In SHRSPs with no evidence of stroke in the current cohort, hyperintense areas were not observed. The SHRSP cohort examined by Britain et al. (2013) was also stroke-free, defined by the absence of inactivity and lethargy, hunched appearance, piloerection, uncoordinated movements, loss of weight and appetite, and confirmed by MRI. Therefore, it is likely that the WMHs observed in the current study are associated with the occurrence of stroke, likely owing to the reduction in blood flow that occurs with ischemia.

In cSHRSPs with cerebral infarcts, the infarcts in 4 animals were localised to the left hemisphere in the vicinity of the posterior/occipital cortex, while 1

cSHRSP exhibited an infarct in the right hemisphere. These consisted of a hyperintense area with evidence of old and recent haemorrhages. One animal also demonstrated evidence of small cortical infarcts within the striatum, consistent with the pathology of cerebral SVD (Wardlaw et al. 2013). A study of 1278 SHRSPs observed that cerebrovascular insults occurred at specified predilection sites, with the majority occurring within the cortex (69.8%), with the second greatest frequency occurring in the basal ganglia (24.5%; (Yamori et al. 1976). Of the infarcts occurring within the cortex, 33.7% occurred the anteromedial cortex, 6.0% occurred in the lateral cortex and 30.1% occurred in the posterior/occipital cortex, with these areas being supplied by the anterior, middle and posterior cerebral artery, respectively. Furthermore, cerebral infarction occurred more frequently in the left hemisphere compared to the right hemisphere. These findings are consistent with previous observations in the literature and therefore confirm that cerebrovascular infarction in SHRSPs generally occurs in cortical areas supplied by the cerebral arteries.

5.4.2 Stimulus-evoked BOLD and CBF responses

Patients with CAA have previously shown dampened BOLD responses in the visual cortex to visual stimuli (Dumas et al. 2012; Peca et al. 2013; van Opstal et al. 2017). Furthermore, patients with cerebral SVD who had suffered a lacunar stroke demonstrated smaller stimulus-evoked BOLD responses in the somatosensory cortex in response to a finger-tapping task (Pineiro et al. 2002). Blunted CBF responses have also been observed in hypertensive patients (Maeda et al. 1993; Jennings et al. 2005). However, in the current study, aSHRSPs and cSHRSPs exhibited significantly larger responses compared to both aWKYs and cWKYs, as assessed by peak BOLD and integral BOLD values. Stimulus-evoked CBF responses were also significantly larger in cSHRSPs compared to all other study groups, with aSHRSPs exhibiting similar responses as aWKYs and cWKYs. Arteriosclerosis, thickening of the vessel wall, narrowing of the arterial lumen, endothelial dysfunction and a loss of vessel reactivity have all been reported in SHRSPs (Weber et al. 2006; Bailey et al. 2011b; Li et al. 2018; Rajani et al. 2018), and therefore a similar reduction of stimulus-evoked BOLD and CBF responses was expected in the current study. The increased BOLD response in both SHRSP cohorts as well as the increased CBF response in cSHRSPs is therefore surprising. To our knowledge, no study has yet

examined the stimulus-evoked BOLD response to somatosensory stimulation in the SHRSP. While some studies have assessed vessel reactivity in SHRSPs, these have generally used vessel myography (Takemori et al. 2013; Wynne et al. 2018; Kagota et al. 2019). However, several studies have assessed the hemodynamic response in the SHR, the parental strain of the SHRSP. Hypercapnia-induced CBF and BOLD responses in 3-4 month old SHRs were observed to be significantly larger compared to normotensive WKYs (Kim et al. 2014). The authors attributed the lack of blunted BOLD and CBF responses in these hypertensive animals to the lack of hypertension-induced vascular remodelling at this early age. However, our observations suggest that this may not be the case as in the current study larger BOLD and CBF responses were observed in cSHRSPs, in which hypertension-induced vascular remodelling is established (Bailey et al. 2011). Furthermore, in a recent study, a significantly larger stimulus-evoked BOLD response was observed in 10-week old SHRs, and larger but non-significant responses in 40-week old SHRs, compared with age-matched WKYs (Li et al. 2021). Additionally, cerebrovascular reactivity was similar between 10-week old SHRs and WKYs but decreased in 40-week old SHRSPs compared to 40-week old WKYs, while stimulus-evoked CBF responses were significantly higher in SHRSPs in both groups, compared with WKYs. These observations are in opposition to those generally observed in the cerebral SVD and hypertensive patient populations and raise questions regarding the appropriateness of the SHRSP as a model of cerebral SVD for assessing cerebrovascular reactivity. While hypertension is generally associated with outward hypertrophic remodelling and thickening of the vessel wall, arterial distensibility has been observed to increase in SHRSPs up to 12 weeks old, compared to age-matched WKYs, when intra-arterial pressure is approx. 120-140 mmHg (Zanchi et al. 1997). However, when intra-arterial pressure is within the hypertensive range for these animals (180-200 mmHg), arterial distensibility is reduced compared to age-matched WKYs. Under the anaesthetic protocol in the current study, MABP was substantially decreased for SHRSPs during functional imaging, returning to normotensive values (approx. 100 mmHg). Therefore, it is possible that under these conditions, arterial distensibility was increased, which resulted in substantially larger CBF and BOLD responses to forelimb stimulation. Future studies are warranted to clarify the underlying mechanism.

Given that the SHRSP is also regarded as a model of hypertension, it is difficult to disentangle whether the changes in BOLD and CBF responses observed in the current study derive from the SVD pathology of this model or whether these may be attributable to hypertension alone. Such a distinction is likely difficult to ascertain given hypertension is an established risk factor for SVD and is typically comorbid with the disease (Khan et al. 2007; Abraham et al. 2016). However, the SHRSP is generally considered a viable model of human SVD disease (Bailey et al. 2011b) and is known to differ from the SHR (stroke-resistant). The differences between these two models likely underlie the stroke-proneness of the SHRSP and its use as a model of SVD. Therefore, future studies could assess both SHRSPs and SHRs to separate any effects that may be due to SVD or hypertension alone.

5.4.3 Variation in hemodynamic responses

While the standard deviation was similar between most study groups when assessing peak and integral BOLD and CBF response values, cSHRSPs exhibited substantially larger standard deviation, highlighting the variability of responses in this data set, which subsequently violated the assumption of homoscedasticity and required transformation of the data. A variety of factors can affect baseline CBF and thereby affect the stimulus-evoked BOLD/CBF response (Whittaker et al. 2016). PaCO₂ is one such factor (Cohen et al. 2002; Sicard and Duong 2005), however in the current study, it is unlikely that PaCO₂ underpinned the observed variation in responses since PaCO₂ was maintained within normal limits. We have also shown that under this anaesthetic protocol, the BOLD response is robust to changes in PaCO₂ even when the values fall outside the upper and lower normal limits (Chapter 3). Anaesthesia can also affect baseline CBF and thereby affect stimulus-evoked responses (Sicard et al. 2003; Franceschini et al. 2010). However, the dosage and administration of isoflurane and medetomidine was kept constant between animals, and therefore it is unlikely that depth of anaesthesia contributed to the observed variation in responses. Given that this variation was exhibited only by the cSHRSP cohort, it is possible that individual variation in disease severity, potentially due to individual differences in cerebrovascular reactivity, underlie these observations. Investigation of vessel structure and assessment of baseline

CBF may provide further insight into possible mechanisms underpinning the variation of responses observed in these animals.

5.4.4 Effect of age on BOLD and CBF responses

An effect of age was not observed on the stimulus-evoked BOLD response while a significant effect of age was observed on the stimulus-evoked CBF response, but no significant pairwise comparisons were found. However, cWKYs and cSHRSPs generally exhibited larger BOLD and CBF responses (as assessed by peak and integral values) compared to their younger counterparts, although this was more pronounced for the CBF responses. The lack of significant pairwise comparisons is likely underpinned by the large variability observed within our data and low sample sizes, particularly within the cSHRSP group.

5.4.5 Hypertension-induced neural alterations

Interestingly, aSHRSPs exhibited significantly larger BOLD responses compared to both WKY cohorts, however stimulus-evoked CBF responses were similar. The difference between these observations may be underpinned by the difference between these two techniques. LSCI measures CBF at the cortical surface while the BOLD signal is the result of the interaction between changes in CBF, CBV and $CMRO_2$, a marker of neural activity. While the stimulus-evoked CBF response in aSHRSPs was similar to that observed in WKY cohorts, the increased BOLD response suggests that $CMRO_2$ and hence the neural response to forelimb stimulation may be reduced in these animals. Indeed, chronic hypertension has been shown to alter neural activity and induce neuronal loss in human patients and a mouse model of Alzheimer's disease, respectively (Jennings and Zanstra 2009; Kruyer et al. 2015). A smaller increase in $CMRO_2$ to stimulation would result in reduced oxygen extraction from the blood and therefore a higher concentration of oxygenated haemoglobin would remain in the blood and result in a larger BOLD response. However, whether these observations in the current study are due to neuronal loss or due to altered neuronal activity is not known and further investigation is required.

5.4.6 Conclusion

In this chapter, we have shown that the SHRSPs from the University of Glasgow colony demonstrate many of the pathological features seen in human SVD. We have also shown that SHRSPs exhibit larger BOLD and CBF responses to forelimb stimulation compared to aged-matched WKYs. These observations are in contrast to that typically observed in older, hypertensive patients and in patients with SVD. This observation may be underpinned by the anaesthetic protocol employed in this study, which reduced MABP to within normotensive values and may have affected arterial distensibility. However, the observed changes in the stimulus-evoked BOLD and CBF responses were specific to SHRSPs, thereby suggesting altered hemodynamic responses may provide a biomarker of SVD. Given the difference between the direction of the change in our study and that reported in human SVD patients, further investigation is required to inform on these changes.

General Discussion

In this thesis, work was undertaken to assess the hemodynamic response in a rodent model of cerebral SVD. The SHRSP develops hypertension around 3 months of age and previous studies have shown that hypertension induces vascular remodelling which leads to a loss of vessel elasticity. Furthermore, dysfunction of the endothelium, which plays a key role in mediating the hemodynamic response, is impaired in both the SHRSP and patients with cerebral CVD (Rajani et al. 2018). The hemodynamic response in patients with cerebral SVD has previously demonstrated blunted stimulus-evoked BOLD responses and reduced cerebrovascular reactivity (Dumas et al. 2012; van Opstal et al. 2017). Interest is growing in using the hemodynamic response as a biomarker of endothelial function and marker of therapeutic impact. The assessment of cerebrovascular reactivity by measuring the BOLD response to a hypercapnic challenge has already been used as a primary endpoint in several clinical trials (Lavallée et al. 2009; NCT01821118; NCT03082014). However, no study has yet assessed the hemodynamic response in the SHRSP, a valid preclinical model of cerebral SVD. Therefore, the main study of this thesis aimed to assess the changes in the hemodynamic response in young and aged SHRSPs to confirm whether similar changes in the hemodynamic response exist and inform on its validity as a potential marker for therapeutic impact in this preclinical model. However, prior to this study, it was important to minimise or eliminate any other potential variables that may interfere with the BOLD signal prior to assessing the hemodynamic response in SHRSPs.

6.1 Carbon dioxide and capnography

CO₂ is one such factor that is known to affect the BOLD signal (Kety and Schmidt 1948; Brevard et al. 2003; Sicard and Duong 2005). In all studies described in this thesis, animals were anaesthetised and mechanically ventilated and therefore there was potential for the partial PaCO₂ to vary over the course of an experiment since the animals were not free breathing. Blood gas analysis provides an accurate but discrete measure of PaCO₂ and requires additional surgery which would not be required if a non-invasive measurement of PaCO₂ could be established. In human fMRI, side-stream end tidal capnography is typically used to sample a participant/patients expired air. Given that ETCO₂ is known to be 3-5 mmHg below PaCO₂, this provides a way to non-invasively assess PaCO₂ and ensure it remains within normal limits. However, acquiring reliable ETCO₂ from animals with small tidal volumes through long sampling lines is difficult due to several physical laws that govern the transport of a gas through a tube (Pascucci et al. 1989). This was subsequently confirmed in our study in which we observed large variations in the differences between ETCO₂ measures and PaCO₂. It was this variability that presented the issue as under some of the set ups, the range between the upper and lower limits was approximately 20 mmHg. Monitoring ETCO₂ under such circumstances could mean that for some measures the difference between PaCO₂ and ETCO₂ could be low and vary by a few mmHg but for others it could vary by 20 mmHg. Of course, it is unlikely that PaCO₂ would vary to this degree in such a short period of time however the variability in the ETCO₂ measure would make predicting the PaCO₂ difficult. Even if a single blood gas measurement was taken at the start of the experiment so that PaCO₂ was known, it would still be difficult to know when the PaCO₂ had increased or decreased given the large variation in the ETCO₂ measurements. Yet, we observed reduced variation between PaCO₂ and ETCO₂ when using the 1 m sampling line, compared to the 7 m line, and therefore it is likely that a further reduction in the sample line length may provide even narrower limits of agreement that could be used in a bench top experiment.

The monitoring of an anaesthetised animal's PaCO₂ is of particular importance during fMRI experiments given its vasodilatory properties and most studies

periodically sample blood from the tail or femoral artery for discrete blood gas analysis. Establishing a noninvasive and accurate method to monitor PaCO₂ could provide real-time measures and minimise any required invasive surgery however further investigation is required to optimise and assess the validity of side-stream capnography in small animals.

6.2 Assessment of stimulus parameters on BOLD, CBF and neural response.

The sequential assessment of BOLD, CBF and neural activity via separate fMRI, LSCI and electrophysiology studies provided an insight into how varying stimulus parameters affected these measures. This experiment was also required as forelimb stimulation had not previously been set up in our lab and given that we were using an anaesthetic protocol that is not commonly used, there was a need to characterise the effects of varying stimulation parameters and identify the optimal settings. We observed that the optimum parameters aligned with those that are commonly used in the literature relevant to our anaesthetic protocol i.e. those using medetomidine or low levels of isoflurane. However, it was also noted that due to the temporal instability of the BOLD signal under medetomidine anaesthesia and the lack of studies assessing the temporal evolution of the BOLD signal for our specific protocol, there may have been additional variation in our data. This observation highlights two issues; firstly, while the use of anaesthesia has many advantages for imaging preclinical animal models, it can introduce confounds into the data and therefore it is important to understand the effects of your anaesthetic of choice and minimise/eliminate any potential confounds as best as possible. Secondly, there is a wide variety of anaesthetic protocols in the literature that differ in type, dose and administration route. This makes it difficult to compare findings between studies and therefore, there is likely a need for some standardisation of protocols so that findings will more easily translate between studies.

Given that neural activity and CBF underlie the BOLD signal, assessing these measures in this study provided some insight into how neurovascular coupling may be affected under this anaesthetic protocol. However, the limitation with this study was that due to the lack of facilities to monitor the hemodynamic response and neural response simultaneously in the same animal, our findings

are only speculative. The ability to assess neural and hemodynamic changes simultaneously can indicate whether a change in the hemodynamic response arises due to a change in neural response or a change in the vascular response. Indeed, such a technique would have been informative in our SHRSP fMRI study (Chapter 5) to indicate the origin of the observed increased BOLD and CBF responses in the SHRSP compared with the WKY. While it is assumed that such observations are attributable to the vasculature, measuring the neural response could have confirmed that the neural component remained consistent, i.e. a larger BOLD / CBF response was not observed due to increase excitability of the neurons.

6.3 The hemodynamic response and SHRSPs

The increased hemodynamic response observed in the SHRSPs compared to WKYs was surprising given that this model has shown many similarities with human cerebral SVD pathology and assessments of the hemodynamic response in patients with cerebral SVD have generally shown blunted hemodynamic responses to stimulation (Pineiro et al. 2002; Dumas et al. 2012; Peca et al. 2013; van Opstal et al. 2017). As previously described, this observation may be due to increased vessel distensibility following a significant and sustained reduction in blood pressure. Additionally, baseline CBF is known to affect the resultant size of the stimulus-evoked response and therefore, if baseline CBF was lower in these animals due to hypertension induced vascular remodelling and increased arterial stiffness, it is possible that an increased BOLD response could be observed. During the scanning session in this study, diffusion weighted imaging were acquired, in addition to RARE and FLASH scans prior to and following intravenous administration of ferumoxytol, an ultra small superparamagnetic iron oxide agent. The analysis of these scans could have informed on baseline CBV and on vessel size index as previously described (Boehm-Sturm et al. 2013; Kim et al. 2013), which may provide some insight into the results we have observed. However, due to time constraints, this analysis could not be performed. Yet, it is worth noting that our observations are consistent with other studies that have also observed an increased stimulus-evoked BOLD response in the parent SHR strain, compared with WKYs (Kim et al. 2014; Li et al. 2021). Thus, evidence is accumulating to suggest that

increased BOLD responses are observed in these animals, which could subsequently lead us to question whether the SHRSP is an appropriate model for assessing cerebrovascular reactivity giving that its response appears the opposite of that observed in the human condition. Future studies should aim to clarify the mechanisms underlying this observation and confirm whether such may arise artificially due to the use of anaesthesia in these preclinical models. Such studies could assess the hemodynamic response in this model under other anaesthetics that do not drastically affect blood pressure, or even in awake animals to confirm whether these may underlie our observations. Until such clarification is achieved, it will likely be difficult to use the stimulus-evoked BOLD response as a marker of therapeutic response in this preclinical model owing to the current difficulty in reconciling endothelial dysfunction with an increased hemodynamic response.

6.4 The use of the hemodynamic response as a biomarker of cerebrovascular health and therapeutic response

Endothelial cells comprise the luminal surface of blood vessels and in addition to maintaining the integrity of the BBB, they play an active, functional role in propagating vasodilatory signals along the vasculature to dilate upstream vessels and amplify the hemodynamic response. Endothelial dysfunction, as well as dampened stimulus-evoked BOLD responses in the visual and somatosensory cortices have been observed in SHRSPs and patients with cerebral SVD (Pineiro et al. 2002; Dumas et al. 2012; Peca et al. 2013; van Opstal et al. 2017; Rajani et al. 2018). Furthermore, disruption of the endothelium results in the failure of neural activation induced vasodilation to propagate beyond the local area of activity and attenuates the amplitude and temporal dynamics of the hemodynamic response (Chen et al. 2014).

Collectively, these observations indicate a key role for endothelial cells in mediating the hemodynamic response and thereby support the potential for the hemodynamic response to provide a biomarker of endothelial function.

Few studies have investigated CVR in patients with cerebral SVD. However, in the few reported studies, not only was a reduction in CVR observed, but most studies also reported an association between reduced CVR and pathological changes, in particular WMHs. One study observed that decreased CVR in an ROI

around the carotid and basilar arteries was significantly associated with an increased number of WMHs in patients from the Dutch cross-sectional CADASIL study (Liem et al. 2009). Impaired CVR has also been associated with subtle changes in the tissue integrity of normal-appearing white matter (NAWM), as evidenced by a reduction in fractional anisotropy, CBF, CBV and increased diffusivity (Sam et al. 2016a). Furthermore, lower CVR values were observed in NAWM that later progressed to a WMH, thus indicating an association between cerebrovascular regulation and development of WMHs (Sam et al. 2016b). An association between a reduced stimulus-evoked BOLD response in the visual cortex, higher white matter lesion volume and an increased number of microbleeds was also observed in patients with CAA (Peca et al. 2013). Collectively, these observations suggest there is value in assessing the hemodynamic response in the study of SVD as such studies provide support for the key role of endothelial dysfunction in disease pathology and thus identify a potential therapeutic target. Indeed, SHRSPs treated with simvastatin or perindopril demonstrated reduced endothelial cell proliferation (an indication of endothelial dysfunction), significantly increased mature tight junctions and reduced myelin rarefaction (Rajani et al. 2018). Given that these drugs have differing mechanisms of action and that these changes were observed independent of changes in blood pressure, the role of endothelial dysfunction as a key mechanism underlying white matter lesions in cerebral SVD is further supported and thus a promising therapeutic target.

The use of MRI in cerebral SVD is already established given its role in aiding the diagnosis of the disease through the evaluation of structural brain images such as T₂-weighted and FLAIR images. While other neuroimaging modalities can detect some pathological changes to support a diagnosis of SVD, such as computed tomography, MRI is the key and preferred neuroimaging modality given its higher sensitivity and specificity (Heiss 2018). Therefore, it is not unreasonable to assume that in addition to the current MRI protocols already being used, others such as those assessing cerebrovascular reactivity could also make their way into clinical practice. These could potentially form a standard battery of MRI assessments that provide a more comprehensive overview of the patient's condition than that provided by analysis of structural images alone. The association between reduced CVR and microstructural changes in NAWM (e.g. FA, MD), and the observation that such changes precede the formation of

WMHs suggests that the assessment of CVR may identify tissue at risk in patients with cerebral SVD. Furthermore, monitoring the hemodynamic response of specific areas of known decreased CVR, such as the visual or somatosensory cortices, could be used to assess the effect of therapeutic intervention on endothelial function, given the critical role of the endothelial in mediating the hemodynamic response.

While current evidence is promising it is also limited given the infrequency of such assessments in the SVD patient population. Therefore, more studies are required to confirm such findings. Furthermore, there is a need to standardise the approach for assessing CVR in the patient population. Of the currently available studies assessing CVR in patients with cerebral SVD, several different stimuli have been used such as breath-holding, hyperventilation, inspired CO₂ challenges, pharmacological stimuli (e.g. acetazolamide) and task-based stimulation. Of all these methods, inspired CO₂ is likely the easiest to implement and requires no task on the part of the patient. It could be argued that task-based assessments (i.e. somatosensory or visual) may be limited by their reliance on neural activity in response to a stimulus to evoke the cerebrovascular response. If over the course of the disease, the relevant neural pathways were injured, a reduced hemodynamic response to stimulation may result from the reduced neural response owing to injury and therefore the hemodynamic response would not be representative of endothelial function. However, a CO₂ challenge exerts its effect directly on the vasculature, dilating the vessels in the absence of any task-based stimuli. Therefore, it is not subject to any potential confound owing to reduced neural activity. Previous studies in patients with possible CCA-related disease have observed that neural responses in the visual cortex remain unaffected despite blunted stimulus-evoked BOLD responses to visual stimuli (Peca et al. 2013). However, it is not known whether neural responses remain intact in different patient populations of cerebral SVD or whether they may be affected with increasing disease burden and progression. Future studies should clarify whether such a confound exists, but it is likely that both task-based and hypercapnic approaches will have value in the study and monitoring of pre-clinical and clinical populations.

Reference list

- Abdullah, K.M. et al. 2020. Do cerebral microbleeds affect cognition in patients with symptomatic small vessel disease? *Egyptian Journal of Neurology, Psychiatry and Neurosurgery* 56(1), p. 7. Available at: <https://ejnnp.springeropen.com/articles/10.1186/s41983-019-0144-1> [Accessed: 14 April 2021].
- Abernethy, W.. et al. 1993. Microvascular Density of the Human Paraventricular Nucleus Decreases with Aging but Not Hypertension. *Experimental Neurology* 121, pp. 270-274.
- Abraham, H.M.A. et al. 2016. Cardiovascular risk factors and small vessel disease of the brain: Blood pressure, white matter lesions, and functional decline in older persons. *Journal of Cerebral Blood Flow and Metabolism* 36(1), pp. 132-142. Available at: <http://www.ncbi.nlm.nih.gov/pubmed/26036933> [Accessed: 29 March 2020].
- Aksenov, D.P. et al. 2015. Effects of Anesthesia on BOLD Signal and Neuronal Activity in the Somatosensory Cortex. *Journal of Cerebral Blood Flow & Metabolism* 35(11), pp. 1819-1826. Available at: <http://journals.sagepub.com/doi/10.1038/jcbfm.2015.130>.
- Alarcon-Martinez, L. et al. 2018. Capillary pericytes express α -smooth muscle actin, which requires prevention of filamentous-actin depolymerization for detection. *eLife* 7. doi: 10.7554/eLife.34861.
- Alba, C. et al. 2004. Ultrastructural and quantitative age-related changes in capillaries of the dorsal lateral geniculate nucleus. *Brain Research Bulletin* 64(2), pp. 145-153. doi: 10.1016/j.brainresbull.2004.06.006.
- Ances, B. et al. 2009. Effects of Aging on Cerebral Blood Flow, Oxygen Metabolism, and Blood Oxygenation Level Dependent Responses to Visual Stimulation Beau. *Human Brain Mapping* 30(4), pp. 1120-1132. doi: 10.1038/jid.2014.371.
- Anderson, J.M. and Van Itallie, C.M. 2009. Physiology and function of the tight junction. *Cold Spring Harbor perspectives in biology* 1(2). doi: 10.1101/cshperspect.a002584.

- Angenstein, F. et al. 2010. The current functional state of local neuronal circuits controls the magnitude of a BOLD response to incoming stimuli. *NeuroImage* 50(4), pp. 1364-1375. Available at: <http://dx.doi.org/10.1016/j.neuroimage.2010.01.070>.
- Arena, F. et al. 2019. Gadolinium presence, MRI hyperintensities, and glucose uptake in the hypoperfused rat brain after repeated administrations of gadodiamide. *Neuroradiology* 61(2), pp. 163-173. Available at: <https://doi.org/10.1007/s00234-018-2120-3> [Accessed: 18 April 2021].
- Aribisala, B.S. et al. 2013. Brain atrophy associations with white matter lesions in the ageing brain: The Lothian Birth Cohort 1936. *European Radiology* 23(4), pp. 1084-1092. doi: 10.1007/s00330-012-2677-x.
- Armstead, W.M. 2016. Cerebral Blood Flow Autoregulation and Dysautoregulation. *Anesthesiology Clinics* 34(3), pp. 465-477. doi: 10.1016/j.anclin.2016.04.002.
- Armulik, A. et al. 2010. Pericytes regulate the blood-brain barrier. *Nature* 468(7323), pp. 557-561. doi: 10.1038/nature09522.
- Attems, J. et al. 2011. Review: Sporadic cerebral amyloid angiopathy. *Neuropathology and Applied Neurobiology* 37(1), pp. 75-93. Available at: <https://pubmed.ncbi.nlm.nih.gov/20946241/> [Accessed: 18 April 2021].
- Atwi, S. et al. 2018. Attention-related brain activation is altered in older adults with white matter hyperintensities using multi-echo fMRI. *Frontiers in Neuroscience* 12(OCT). Available at: </pmc/articles/PMC6200839/> [Accessed: 11 April 2021].
- Austin, V.C. et al. 2005. Confounding effects of anesthesia on functional activation in rodent brain: A study of halothane and α -chloralose anesthesia. *NeuroImage* 24(1), pp. 92-100. doi: 10.1016/j.neuroimage.2004.08.011.
- Ayata, C. 2010. CADASIL: Experimental insights from animal models. In: *Stroke*. NIH Public Access, p. S129. Available at: </pmc/articles/PMC2953736/> [Accessed: 18 April 2021].
- Bailey, E.L. et al. 2009. Potential animal models of lacunar stroke: a systematic review. *Stroke* 40(6). doi: 10.1161/STROKEAHA.108.528430.

- Bailey, E.L. et al. 2011a. Cerebral small vessel endothelial structural changes predate hypertension in stroke-prone spontaneously hypertensive rats : a blinded , controlled immunohistochemical study of 5- to 21-week-old rats. *Neuropathology and Applied Neurobiology* 37, pp. 711-726. doi: 10.1111/j.1365-2990.2011.01170.x.
- Bailey, E.L. et al. 2011b. Is the spontaneously hypertensive stroke prone rat a pertinent model of sub cortical ischemic stroke? A systematic review. *International Journal of Stroke* 6(5), pp. 434-444. doi: 10.1111/j.1747-4949.2011.00659.x.
- Bailey, E.L. et al. 2018. Effects of dietary salt on gene and protein expression in brain tissue of a model of sporadic small vessel disease. *Clinical Science* 132, pp. 1315-1328. Available at: <https://doi.org/10.1042/CS20171572> [Accessed: 14 April 2021].
- Balestrino, M. and Somjen, G.G. 1988. Concentration of carbon dioxide, interstitial pH and synaptic transmission in hippocampal formation of the rat. *The Journal of Physiology* 396(1), pp. 247-266. doi: 10.1113/jphysiol.1988.sp016961.
- Bamford, J. et al. 1988. A prospective study of acute cerebrovascular disease in the community: the Oxfordshire Community Stroke Project 1981-86 1. Methodology, demography and incident cases of first-ever stroke. *Journal of Neurology, Neurosurgery and Psychiatry* 51(11), pp. 1373-1380. Available at: <http://www.ncbi.nlm.nih.gov/pubmed/3266234> [Accessed: 29 March 2020].
- Baumbach, G.L. and Heistad, D.D. 1988. Cerebral Circulation in Chronic Arterial Hypertension. *Hypertension* 12(2), pp. 89-95.
- Bell, R.D. et al. 2010. Pericytes Control Key Neurovascular Functions and Neuronal Phenotype in the Adult Brain and during Brain Aging. *Neuron* 68(3), pp. 409-427. Available at: <http://www.ncbi.nlm.nih.gov/pubmed/21040844> [Accessed: 26 March 2020].
- Blair, G.W. et al. 2015. Magnetic resonance imaging for assessment of cerebrovascular reactivity in cerebral small vessel disease: A systematic review. *Journal of Cerebral Blood Flow and Metabolism* 36(5), pp. 833-841. Available at: </pmc/articles/PMC4853842/> [Accessed: 14 April 2021].

Bland, J.M. and Altman, D.G. 1999. Measuring agreement in method comparison studies. *Statistical methods in medical research* 8(2), pp. 135-160. doi: 10.1191/096228099673819272.

Bland, J.M. and Altman, D.G. 2007. Agreement between methods of measurement with multiple observations per individual. *Journal of Biopharmaceutical Statistics* 17(4), pp. 571-582. doi: 10.1080/10543400701329422.

Block, F.E. and McDonald, J.S. 1992. Sidestream versus mainstream carbon dioxide analyzers. *Journal of Clinical Monitoring* 8(2), pp. 139-141. Available at: <http://www.ncbi.nlm.nih.gov/pubmed/1583550> [Accessed: 28 March 2020].

Body, S.C. et al. 2000. Dual-plateau capnogram caused by cracked sample filter [10]. *Anesthesia and Analgesia* 90(1), pp. 233-234. doi: 10.1097/00000539-200001000-00061.

Boehm-Sturm, P. et al. 2013. Vascular changes after stroke in the rat: a longitudinal study using optimized magnetic resonance imaging. *Contrast Media & Molecular Imaging* 8(5), pp. 383-392. Available at: <http://doi.wiley.com/10.1002/cmml.1534> [Accessed: 30 March 2020].

Braeuninger, S. and Kleinschnitz, C. 2009. Rodent models of focal cerebral ischemia: procedural pitfalls and translational problems. *Experimental and Translational Stroke Medicine* 1, pp. 1-11. Available at: <http://www.etsmjournal.com/content/1/1/8> [Accessed: 29 March 2020].

Brevard, M.E. et al. 2003. Changes in MRI signal intensity during hypercapnic challenge under conscious and anesthetized conditions. *Magnetic Resonance Imaging* 21(9), pp. 995-1001. doi: 10.1016/S0730-725X(03)00204-2.

Brinker, G. et al. 1999. Simultaneous recording of evoked potentials and T2*-weighted MR images during somatosensory stimulation of rat. *Magnetic resonance in medicine* 41(3), pp. 469-73. Available at: <http://www.ncbi.nlm.nih.gov/pubmed/10204868>.

Brisset, M. et al. 2013. Large-vessel correlates of cerebral small-vessel disease. *Neurology* 80(7), pp. 662-669. doi: 10.1212/WNL.0b013e318281ccc2.

Brittain, J.F. et al. 2013. An MRI-histological study of white matter in stroke-free SHRSP. *Journal of cerebral blood flow and metabolism : official journal of the International Society of Cerebral Blood Flow and Metabolism* 33(5), pp. 760-3. Available at: <http://dx.doi.org/10.1038/jcbfm.2013.14>.

Bruhn, H. et al. 2001. Modulation of cerebral blood oxygenation by indomethacin: MRI at rest and functional brain activation. *Journal of Magnetic Resonance Imaging* 13(3), pp. 325-334. Available at: <http://doi.wiley.com/10.1002/jmri.1047> [Accessed: 23 February 2020].

Burns, E.M. et al. 1981. Changes with age in cerebral capillary morphology. *Neurobiology of Aging* 2(4), pp. 285-291. doi: 10.1016/0197-4580(81)90037-3.

Buxton, R.B. and Frank, L.R. 1997. A model for the coupling between cerebral blood flow and oxygen metabolism during neural stimulation. *Journal of cerebral blood flow and metabolism : official journal of the International Society of Cerebral Blood Flow and Metabolism* 17(1), pp. 64-72. Available at: <http://www.ncbi.nlm.nih.gov/pubmed/8978388> [Accessed: 10 March 2020].

Camus, S. et al. 2015. Why bother using non-human primate models of cognitive disorders in translational research? *Neurobiology of Learning and Memory* 124, pp. 123-129. doi: 10.1016/j.nlm.2015.06.012.

Chabriat, H. et al. 2009. *CADASIL*. Available at: www.thelancet.com/neurology [Accessed: 18 April 2021].

Chan, K.. L. et al. 2003. Mainstream vs. sidestream capnometry for prediction of arterial carbon dioxide tension during supine craniotomy. *Anaesthesia* 58(2), pp. 149-155. Available at: <http://www.embase.com/search/results?subaction=viewrecord&from=export&id=L36284743%0Ahttp://dx.doi.org/10.1046/j.1365-2044.2003.03035.x>.

Charidimou, A. et al. 2016. The concept of sporadic cerebral small vessel disease: A road map on key definitions and current concepts. *International Journal of Stroke* 11(1), pp. 6-18. Available at: <http://journals.sagepub.com/doi/10.1177/1747493015607485> [Accessed: 18 April 2021].

Chen, B.R. et al. 2014. A Critical Role for the Vascular Endothelium in

Functional Neurovascular Coupling in the Brain. *Am Heart Assoc* 3(3). doi: 10.1161/JAHA.114.000787.

Choi, B.R. et al. 2016. Characterization of White Matter Injury in a Rat Model of Chronic Cerebral Hypoperfusion. *Stroke* 47(2), pp. 542-547. doi: 10.1161/STROKEAHA.115.011679.

Chue, C.H. et al. 1993. The possible role of lysosomal enzymes in the pathogenesis of hypertensive cerebral lesions in spontaneously hypertensive rats. *Acta Neuropathologica* 85(4), pp. 383-389. doi: 10.1007/BF00334448.

Cohen, E.R. et al. 2002. Effect of Basal Conditions on the Magnitude and Dynamics of the Hemodynamic Response. *Mind* 10(1), pp. 57180-57180.

Cordonnier, C. et al. 2007. Spontaneous brain microbleeds: systematic review, subgroup analyses and standards for study design and reporting. 130(Pt 8), pp. 1988-2003. Available at: <http://www.ncbi.nlm.nih.gov/pubmed/17322562> [Accessed: 29 March 2020].

Corfield, D.R. et al. 2001. Does hypercapnia-induced cerebral vasodilation modulate the hemodynamic response to neural activation? *NeuroImage* 13(6), pp. 1207-1211. doi: 10.1006/nimg.2001.0760.

Coyle, P. 1987. Dorsal cerebral collaterals of stroke-prone spontaneously hypertensive rats (SHRSP) and Wistar Kyoto rats (WKY). *The Anatomical Record* 218(1), pp. 40-44. Available at: <https://doi.org/10.1002/ar.1092180108>.

Debette, S. and Markus, H.S. 2010. The clinical importance of white matter hyperintensities on brain magnetic resonance imaging: Systematic review and meta-analysis. *BMJ (Online)* 341(7767), p. 288. doi: 10.1136/bmj.c3666.

DeGirolami, U. et al. 1984. Selective Necrosis and Total Necrosis in Focal Cerebral Ischemia. Neuropathologic Observations on Experimental Middle Cerebral Artery Occlusion in the Macaque Monkey. *Journal of Neuropathology & Experimental Neurology* 43(1), pp. 57-71. Available at: <https://academic.oup.com/jnen/article-lookup/doi/10.1097/00005072-198401000-00005> [Accessed: 29 March 2020].

Detre, J.A. et al. 1998. Signal averaged laser Doppler measurements of activation-flow coupling in the rat forepaw somatosensory cortex. *Brain*

Research 796(1-2), pp. 91-98. doi: 10.1016/S0006-8993(98)00322-9.

Devor, A. et al. 2011. 'Overshoot' of O₂ is required to maintain baseline tissue oxygenation at locations distal to blood vessels. *Journal of Neuroscience* 31(38), pp. 13676-13681. doi: 10.1523/JNEUROSCI.1968-11.2011.

Di, S. and Barth, D.S. 1991. Topographic analysis of field potentials in rat vibrissa/barrel cortex. *Brain Research* 546(1), pp. 106-112. doi: 10.1016/0006-8993(91)91164-V.

Dickhout, J.G. and Lee, R.M.K.W. 1998. Blood pressure and heart rate development in young spontaneously hypertensive rats. *American Journal of Physiology - Heart and Circulatory Physiology* 274(3 43-3), pp. 794-800. doi: 10.1152/ajpheart.1998.274.3.h794.

Diehl, K.H. et al. 2001. A good practice guide to the administration of substances and removal of blood, including routes and volumes. *Journal of Applied Toxicology* 21(1), pp. 15-23. doi: 10.1002/jat.727.

Dietrich, H.H. et al. 1996. Local and conducted vasomotor responses in isolated rat cerebral arterioles. *American Journal of Physiology - Heart and Circulatory Physiology* 271(3 40-3). doi: 10.1152/ajpheart.1996.271.3.h1109.

Doubal, F.N. et al. 2010. Enlarged Perivascular Spaces on MRI Are a Feature of Cerebral Small Vessel Disease. *Stroke* 41(3), pp. 450-454. doi: 10.1161/STROKEAHA.109.564914.

Du, C. et al. 2009. Differential effects of anesthetics on cocaine's pharmacokinetic and pharmacodynamic effects in brain. *European Journal of Neuroscience* 30(8), pp. 1565-1575. Available at: <http://www.ncbi.nlm.nih.gov/pubmed/19821842> [Accessed: 8 March 2020].

Dufouil, C. et al. 2005. Effects of blood pressure lowering on cerebral white matter hyperintensities in patients with stroke: The PROGRESS (Perindopril Protection Against Recurrent Stroke Study) Magnetic Resonance Imaging Substudy. *Circulation* 112(11), pp. 1644-1650. doi: 10.1161/CIRCULATIONAHA.104.501163.

Dumas, A. et al. 2012. Functional magnetic resonance imaging detection of vascular reactivity in cerebral amyloid angiopathy. *Annals of Neurology* 72(1),

pp. 76-81. Available at: <https://pubmed.ncbi.nlm.nih.gov/22829269/> [Accessed: 11 April 2021].

Dunn, A.K. et al. 2005. Spatial extent of oxygen metabolism and hemodynamic changes during functional activation of the rat somatosensory cortex. *NeuroImage* 27(2), pp. 279-290. Available at: www.elsevier.com/locate/ynimg.

Durduran, T. et al. 2004. Spatiotemporal Quantification of Cerebral Blood Flow During Functional Activation in Rat Somatosensory Cortex Using Laser-Speckle Flowmetry. *Journal of Cerebral Blood Flow and Metabolism* 24, pp. 518-525. doi: 10.1097/01.WCB.0000119967.74298.15.

Edvinsson, L. 1982. Sympathetic control of cerebral circulation. *Trends in Neurosciences* 5(C), pp. 425-429. doi: 10.1016/0166-2236(82)90232-6.

Eger, E.I. 2nd 1984. The pharmacology of isoflurane. *British journal of anaesthesia* 56 Suppl 1, pp. 71S-99S.

Epstein, R.A. et al. 1980. Determinants of distortions in CO₂ catheter sampling systems: A mathematical model. *Respiration Physiology* 41(1), pp. 127-136. doi: 10.1016/0034-5687(80)90028-6.

Fang, X.H. et al. 2012. Incidence and survival of symptomatic lacunar infarction in a Beijing population: A 6-year prospective study. *European Journal of Neurology* 19(8), pp. 1114-1120. doi: 10.1111/j.1468-1331.2012.03709.x.

Fazekas, F. et al. 1993. Pathologic correlates of incidental MRI white matter signal hyperintensities. *Neurology* 43(9), pp. 1683-1689. doi: 10.1212/wnl.43.9.1683.

Fenstermacher, J. et al. 1988. Structural and Functional Variations in Capillary Systems within the Brain. *Annals of the New York Academy of Sciences* 529(1), pp. 21-30. Available at: <http://doi.wiley.com/10.1111/j.1749-6632.1988.tb51416.x> [Accessed: 28 February 2020].

Finsterer, J. et al. 2019. Update on hereditary, autosomal dominant cathepsin-A-related arteriopathy with strokes and leukoencephalopathy (CARASAL). *Acta Neurologica Belgica* 119(3), pp. 299-303. Available at: <https://pubmed.ncbi.nlm.nih.gov/31177426/> [Accessed: 18 April 2021].

- Fisher, C.M. 1965. Lacunes: Small, deep cerebral infarcts. *Neurology* 15, pp. 774-84.
- Fisher, C.M. 1979. Capsular Infarcts The Underlying Vascular Lesions. *Archives of neurology* 36, pp. 65-73. Available at: <https://jamanetwork.com/> [Accessed: 29 March 2020].
- Fox, P.T. and Raichle, M.E. 1986. *Focal physiological uncoupling of cerebral blood flow and oxidative metabolism during somatosensory stimulation in human subjects (positron emission tomography)*.
- Franceschini, M.A. et al. 2008. Coupling between somatosensory evoked potentials and hemodynamic response in the rat. *NeuroImage* 41(2), pp. 189-203. doi: 10.1016/j.neuroimage.2008.02.061.
- Franceschini, M.A. et al. 2010. The effect of different anesthetics on neurovascular coupling. *NeuroImage* 51(4), pp. 1367-1377. Available at: <http://dx.doi.org/10.1016/j.neuroimage.2010.03.060>.
- Fredriksson, K. et al. 1987. Blood-brain barrier leakage and brain edema in stroke-prone spontaneously hypertensive rats. *Acta Neuropathologica* 74(3), pp. 259-268. Available at: <http://www.springerlink.com/index/q890k22564339862.pdf>.
- Fredriksson, K. et al. 1988. Cerebral microangiopathy in stroke-prone spontaneously hypertensive rats. An immunohistochemical and ultrastructural study. *Acta neuropathologica* 75(3), pp. 241-252. doi: 10.1007/bf00690532.
- Frisoni, G.B. et al. 2007. The effect of white matter lesions on cognition in the elderly - Small but detectable. *Nature Clinical Practice Neurology* 3(11), pp. 620-627. doi: 10.1038/ncpneuro0638.
- From, R.P. and Scamman, F.L. 1988. Ventilatory Frequency Influences Accuracy of End-Tidal CO₂ Measurements Analysis of Seven Capnometers. *Anesthesia & Analgesia* 67(9), p. 884-886. doi: 10.1213/00000539-198809000-00016.
- Furspan, P.B. and Bohr, D.F. 1990. Calcium sensitivity of Ca²⁺-activated K⁺ channels in spontaneously hypertensive stroke-prone rats. *Hypertension (Dallas, Tex. : 1979)* 15(2 Suppl), pp. I97-101. doi:

10.1161/01.hyp.15.2_suppl.i97.

Furspan, P.B. and Webb, R.C. 1993. Decreased ATP sensitivity of a K⁺ channel and enhanced vascular smooth muscle relaxation in genetically hypertensive rats. *Journal of hypertension* 11(10), p. 1067–1072. Available at: <https://doi.org/10.1097/00004872-199310000-00010>.

Furuta, A. et al. 1991. Medullary arteries in aging and dementia. *Stroke* 22(4), pp. 442-446. doi: 10.1161/01.STR.22.4.442.

Garrett, K.M. and Gan, J. 1998. Enhancement of γ -Aminobutyric Acid A Receptor Activity by α -Chloralose. *Journal of Pharmacology and Experimental Therapeutics* 285(2), pp. 680 LP - 686. Available at: <http://jpet.aspetjournals.org/content/285/2/680.abstract>.

Giau, V. Van et al. 2019. Genetic factors of cerebral small vessel disease and their potential clinical outcome. *International Journal of Molecular Sciences* 20(17). Available at: [/pmc/articles/PMC6747336/](https://pubmed.ncbi.nlm.nih.gov/35444444/) [Accessed: 18 April 2021].

Goldmann, E.E. 1909. *Die äussere und innere Sekretion des gesunden Organismus im Lichte der "vitalen Färbung": Mit 15 farb. lithogr. Tafeln.*

Goldmann, E.E. 1913. Vitalfärbung am zentralnervensystem. *Abhandl Konigl preuss Akad Wiss* 1, pp. 1-60.

Gordon, G.R.J. et al. 2008. Brain metabolism dictates the polarity of astrocyte control over arterioles. *Nature* 456(7223), pp. 745-750. doi: 10.1038/nature07525.

Göttler, J. et al. 2019. Reduced blood oxygenation level dependent connectivity is related to hypoperfusion in Alzheimer's disease. *Journal of Cerebral Blood Flow and Metabolism* 39(7), pp. 1314-1325. doi: 10.1177/0271678X18759182.

Govindpani, K. et al. 2019. Vascular Dysfunction in Alzheimer's Disease: A Prelude to the Pathological Process or a Consequence of It? *Journal of Clinical Medicine* 8(5), p. 651. doi: 10.3390/jcm8050651.

Greicius, M.D. et al. 2004. Default-mode network activity distinguishes Alzheimer's disease from healthy aging: Evidence from functional MRI.

Proceedings of the National Academy of Sciences of the United States of America 101(13), pp. 4637-4642. doi: 10.1073/pnas.0308627101.

Groeschel, S. et al. 2006. Virchow-Robin spaces on magnetic resonance images: Normative data, their dilatation, and a review of the literature. *Neuroradiology* 48(10), pp. 745-754. doi: 10.1007/s00234-006-0112-1.

Gyngell, M.L. et al. 1996. Variation of functional MRI signal in response to frequency of somatosensory stimulation in ??-chloralose anesthetized rats. *Magnetic Resonance in Medicine* 36(1), pp. 13-15. doi: 10.1002/mrm.1910360104.

Hainsworth, A.H. et al. 2012. Pre-clinical models of human cerebral small vessel disease: Utility for clinical application. *Journal of the Neurological Sciences* 322(1-2), pp. 237-240. doi: 10.1016/j.jns.2012.05.046.

Hainsworth, A.H. and Markus, H.S. 2008. Do in vivo experimental models reflect human cerebral small vessel disease? A systematic review. *Journal of cerebral blood flow and metabolism : official journal of the International Society of Cerebral Blood Flow and Metabolism* 28(12), pp. 1877-1891. doi: 10.1038/jcbfm.2008.91.

Hamner, J.W. et al. 2010. Sympathetic control of the cerebral vasculature in humans. *Stroke* 41(1), pp. 102-9. Available at: <http://www.ncbi.nlm.nih.gov/pubmed/20007920> [Accessed: 21 February 2020].

Hamner, J.W. et al. 2012. Cholinergic control of the cerebral vasculature in humans. *The Journal of Physiology* 590, pp. 6343-6352. doi: 10.1113/jphysiol.2012.245100.

Hamner, J.W. and Tan, C.O. 2014. Relative contributions of sympathetic, cholinergic, and myogenic mechanisms to cerebral autoregulation. *Stroke* 45(6), pp. 1771-1777. Available at: <https://www.ahajournals.org/doi/10.1161/STROKEAHA.114.005293> [Accessed: 21 February 2020].

Han, H.C. 2012. Twisted blood vessels: Symptoms, etiology and biomechanical mechanisms. *Journal of Vascular Research* 49(3), pp. 185-197. doi:

10.1159/000335123.

Hara, K. et al. 2009. Association of HTRA1 Mutations and Familial Ischemic Cerebral Small-Vessel Disease. *New England Journal of Medicine* 360(17), pp. 1729-1739. Available at: <https://pubmed.ncbi.nlm.nih.gov/19387015/> [Accessed: 18 April 2021].

He, Z. et al. 1999. Experimental model of small deep infarcts involving the hypothalamus in rats: Changes in body temperature and postural reflex. *Stroke* 30(12), pp. 2743-2751. doi: 10.1161/01.STR.30.12.2743.

Heiss, W.-D. 2018. *Neuroimaging in Cerebral Small Vessel Disease*. Available at: www.jneurology.com/Neuromedicine [Accessed: 17 April 2021].

Heistad, D.D. and Baumbach, G.L. 1992. Cerebral vascular changes during chronic hypertension: Good guys and bad guys. *Journal of Hypertension* 10(7), pp. S71-S75. doi: 10.1097/00004872-199212000-00008.

Hendrich, K.S. et al. 2001. Cerebral perfusion during anesthesia with fentanyl, isoflurane, or pentobarbital in normal rats studied by arterial spin-labeled MRI. *Magnetic Resonance in Medicine* 46(1), pp. 202-206. Available at: <http://doi.wiley.com/10.1002/mrm.1178> [Accessed: 8 March 2020].

Herzig, M.C. et al. 2004. Aβ is targeted to the vasculature in a mouse model of hereditary cerebral hemorrhage with amyloidosis. *Nature Neuroscience* 7(9), pp. 954-960. Available at: <http://www.nature.com/natureneuroscience> [Accessed: 18 April 2021].

Hesselmann, V. et al. 2001. Age related signal decrease in functional magnetic resonance imaging during motor stimulation in humans. *Neuroscience Letters* 308(3), pp. 141-144. doi: 10.1016/S0304-3940(01)01920-6.

Hill, R.A. et al. 2015. Regional Blood Flow in the Normal and Ischemic Brain Is Controlled by Arteriolar Smooth Muscle Cell Contractility and Not by Capillary Pericytes. *Neuron* 87(1), pp. 95-110. doi: 10.1016/j.neuron.2015.06.001.

Hoge, R.D. et al. 1999. Investigation of BOLD signal dependence on CBF and CMRO₂: the Deoxyhemoglobin Dilution Model. *Magn. Reson. Med.* 42(5), pp. 849-863.

Hollyer, T. 2016. *MRI indices of functional recovery following intracerebral implantation of a human neural stem cell line in a pre-clinical model of ischaemic stroke.*

Hom, S. et al. 2007. Comparative changes in the blood-brain barrier and cerebral infarction of SHR and WKY rats. *American Journal of Physiology-Regulatory, Integrative and Comparative Physiology* 292(5), pp. R1881-R1892. Available at: <https://www.physiology.org/doi/10.1152/ajpregu.00761.2005> [Accessed: 17 April 2021].

Horvath, I. et al. 1994. Role of nitric oxide in regulating cerebrocortical oxygen consumption and blood flow during hypercapnia. *Journal of Cerebral Blood Flow and Metabolism* 14(3), pp. 503-509. Available at: <http://www.ncbi.nlm.nih.gov/pubmed/8163593> [Accessed: 8 March 2020].

Hosford, P.S. and Gourine, A. V. 2019. What is the key mediator of the neurovascular coupling response? *Neuroscience and Biobehavioral Reviews* 96, pp. 174-181. doi: 10.1016/j.neubiorev.2018.11.011.

Hossmann, K. -A 1994. Viability thresholds and the penumbra of focal ischemia. *Annals of Neurology* 36(4), pp. 557-565. Available at: <http://doi.wiley.com/10.1002/ana.410360404> [Accessed: 21 February 2020].

Howarth, C. et al. 2012. Updated energy budgets for neural computation in the neocortex and cerebellum. *Journal of Cerebral Blood Flow and Metabolism* 32(7), pp. 1222-1232. doi: 10.1038/jcbfm.2012.35.

Hurford, R. et al. 2014. MRI-visible perivascular spaces: Relationship to cognition and small vessel disease MRI markers in ischaemic stroke and TIA. *Journal of Neurology, Neurosurgery and Psychiatry* 85(5), pp. 522-525. doi: 10.1136/jnnp-2013-305815.

Huttmann, S.E. et al. 2014. Techniques for the Measurement and Monitoring of Carbon Dioxide in the Blood. *Ann Am Thorac Soc* 11(4), pp. 645-652. Available at: www.atsjournals.org [Accessed: 28 March 2020].

Hyder, F. et al. 1998. *A model for the regulation of cerebral oxygen delivery.* Available at: <http://www.jap.org> [Accessed: 10 March 2020].

Iadecola, C. et al. 1997. Local and propagated vascular responses evoked by

- focal synaptic activity in cerebellar cortex. *Journal of Neurophysiology* 78(2), pp. 651-659. doi: 10.1152/jn.1997.78.2.651.
- Iadecola, C. 2017. The Neurovascular Unit Coming of Age: A Journey through Neurovascular Coupling in Health and Disease. *Neuron* 96(1), pp. 17-42. doi: 10.1016/j.neuron.2017.07.030.
- Iida, H. et al. 1998. Isoflurane and sevoflurane induce vasodilation of cerebral vessels via ATP-sensitive K⁺ channel activation. *Anesthesiology* 89(4), pp. 954-960. Available at: <http://www.ncbi.nlm.nih.gov/pubmed/9778013> [Accessed: 8 March 2020].
- Intagliata, S. and Rizzo, A. 2018. *Physiology, Lung Dead Space*. StatPearls Publishing. Available at: <http://www.ncbi.nlm.nih.gov/pubmed/29494107> [Accessed: 28 March 2020].
- Ito, H. et al. 2002. Effect of aging on cerebral vascular response to PaCO₂ changes in humans as measured by positron emission tomography. *Journal of Cerebral Blood Flow and Metabolism* 22(8), pp. 997-1003. doi: 10.1097/00004647-200208000-00011.
- Jackson, C.A. et al. 2010. Differing risk factor profiles of ischemic stroke subtypes: Evidence for a distinct lacunar arteriopathy? *Stroke* 41(4), pp. 624-629. Available at: <http://www.ncbi.nlm.nih.gov/pubmed/20150553> [Accessed: 30 March 2020].
- Jaffe, M.B. 2002. Mainstream or Sidestream Capnography? *Respiroics* , pp. 1-14.
- Jeffrey-Gauthier, R. et al. 2013. Neurovascular coupling during nociceptive processing in the primary somatosensory cortex of the rat. *Pain* 154(8), pp. 1434-1441. Available at: <http://dx.doi.org/10.1016/j.pain.2013.04.042>.
- Jellema, T. et al. 2004. Sequential activation of microcircuits underlying somatosensory-evoked potentials in rat neocortex. *Neuroscience* 129(2), pp. 283-295. doi: 10.1016/j.neuroscience.2004.07.046.
- Jennings, J.R. et al. 2005. Reduced cerebral blood flow response and compensation among patients with untreated hypertension. *Neurology* 64(8), pp. 1358 LP - 1365. Available at:

<http://n.neurology.org/content/64/8/1358.abstract>.

Jennings, J.R. and Zanstra, Y. 2009. Is the brain the essential in hypertension? *NeuroImage* 47(3), pp. 914-921. doi: 10.1016/j.neuroimage.2009.04.072.

Jiang, H.X. et al. 1992. Age related alterations in the response of the pial arterioles to adenosine in the rat. *Mechanisms of Ageing and Development* 65(2-3), pp. 257-276. doi: 10.1016/0047-6374(92)90040-K.

Jiménez-Balado, J. et al. 2019. Cognitive Impact of Cerebral Small Vessel Disease Changes in Patients With Hypertension. *Hypertension (Dallas, Tex. : 1979)* 73(2), pp. 342-349. Available at: <http://www.ncbi.nlm.nih.gov/pubmed/30606062> [Accessed: 29 March 2020].

Jones, M. et al. 2005. The effect of hypercapnia on the neural and hemodynamic responses to somatosensory stimulation. *NeuroImage* 27(3), pp. 609-623. Available at: <http://www.ncbi.nlm.nih.gov/pubmed/15978844> [Accessed: 8 March 2020].

Joutel, A. et al. 2010. Cerebrovascular dysfunction and microcirculation rarefaction precede white matter lesions in a mouse genetic model of cerebral ischemic small vessel disease. *Journal of Clinical Investigation* 120(2), pp. 433-445. Available at: <https://pubmed.ncbi.nlm.nih.gov/20071773/> [Accessed: 18 April 2021].

Jung, K.H. et al. 2021. Heterogeneity of Cerebral White Matter Lesions and Clinical Correlates in Older Adults. *Stroke* 52(2), pp. 620-630. Available at: <https://www.ahajournals.org/doi/suppl/10.1161/STROKEAHA.120.031641>. [Accessed: 18 April 2021].

Kagota, S. et al. 2019. Angiotensin II Type 1 Receptor Antagonist Azilsartan Restores Vascular Reactivity Through a Perivascular Adipose Tissue-Independent Mechanism in Rats with Metabolic Syndrome. *Cardiovascular Drugs and Therapy* 33(5), pp. 501-509. Available at: <https://pubmed.ncbi.nlm.nih.gov/31420755/> [Accessed: 20 April 2021].

Kaiser, D. et al. 2014. Spontaneous white matter damage, cognitive decline and neuroinflammation in middle-aged hypertensive rats: An animal model of early-stage cerebral small vessel disease. *Acta Neuropathologica*

Communications 2(1). doi: 10.1186/s40478-014-0169-8.

Kastrup, a et al. 1999. Regional variability of cerebral blood oxygenation response to hypercapnia. *NeuroImage* 10(6), pp. 675-681. doi: 10.1006/nimg.1999.0505.

Kawamura, J. et al. 1993. Leuko-araiosis and cerebral perfusion in normal aging. *Experimental Aging Research* 19(3), pp. 225-240. Available at: <https://doi.org/10.1080/03610739308253935>.

Keilholz, S.D. et al. 2004. Functional MRI of the rodent somatosensory pathway using multislice echo planar imaging. *Magnetic Resonance in Medicine* 52(1), pp. 89-99. doi: 10.1002/mrm.20114.

Kemna, L.J. and Posse, S. 2001. Effect of respiratory CO₂ changes on the temporal dynamics of the hemodynamic response in functional MR imaging. *NeuroImage* 14(3), pp. 642-649. doi: 10.1006/nimg.2001.0859.

Kemper, T. et al. 1999. Microinfarction as a result of hypertension in a primate model of cerebrovascular disease. *Acta Neuropathologica* 98(3), pp. 295-303. Available at: <http://www.ncbi.nlm.nih.gov/pubmed/10483788> [Accessed: 29 March 2020].

Kemper, T.L. et al. 2001. Neuropathology of progressive cognitive decline in chronically hypertensive rhesus monkeys. *Acta Neuropathologica* 101(2), pp. 145-153. doi: 10.1007/s004010000278.

Kety, S.S. 1950. Circulation and metabolism of the human brain in health and disease. *The American Journal of Medicine* 8(2), pp. 205-217. doi: 10.1016/0002-9343(50)90363-9.

Kety, S.S. and Schmidt, C.F. 1948. The Effects of Altered Arterial Tensions of Carbon Dioxide and Oxygen on Cerebral Blood Flow and Cerebral Oxygen Consumption of Normal Young Men. *The Journal of clinical investigation* 27(4), pp. 484-492. doi: 10.1172/JCI101995.

Khan, U. et al. 2007. Risk factor profile of cerebral small vessel disease and its subtypes. *Journal of Neurology, Neurosurgery and Psychiatry* 78(7), pp. 702-706. doi: 10.1136/jnnp.2006.103549.

- Kim, K.W. et al. 2019. Multimodal imaging analyses in patients with genetic and sporadic forms of small vessel disease. *Scientific Reports* 9(1). Available at: <https://pubmed.ncbi.nlm.nih.gov/30692550/> [Accessed: 18 April 2021].
- Kim, S.G. et al. 2013. Cerebral blood volume MRI with intravascular superparamagnetic iron oxide nanoparticles. *NMR in Biomedicine* 26(8), pp. 949-962. doi: 10.1002/nbm.2885.
- Kim, T. et al. 2010. Frequency-dependent neural activity, CBF, and BOLD fMRI to somatosensory stimuli in isoflurane-anesthetized rats. *NeuroImage* 52(1), pp. 224-233. Available at: <http://dx.doi.org/10.1016/j.neuroimage.2010.03.064>.
- Kim, T. et al. 2014. Regional cerebral blood flow and arterial blood volume and their reactivity to hypercapnia in hypertensive and normotensive rats. *Journal of Cerebral Blood Flow and Metabolism* 34(3), pp. 408-414. Available at: <http://dx.doi.org/10.1038/jcbfm.2013.197>.
- Kitamura, A. et al. 2012. Selective white matter abnormalities in a novel rat model of vascular dementia. *Neurobiology of Aging* 33(5), pp. 1012.e25-1012.e35. Available at: <http://www.ncbi.nlm.nih.gov/pubmed/22133276> [Accessed: 30 March 2020].
- Kitazono, T. et al. 1995a. Enhanced responses of the basilar artery to activation of endothelin-B receptors in stroke-prone spontaneously hypertensive rats. *Hypertension (Dallas, Tex. : 1979)* 25(4 Pt 1), pp. 490-494. doi: 10.1161/01.hyp.25.4.490.
- Kitazono, T. et al. 1995b. Role of potassium channels in cerebral blood vessels. *Stroke* 26(9), pp. 1713-1723. doi: 10.1161/01.STR.26.9.1713.
- Kliefoth, A.B. et al. 1979. Depression of cerebral oxygen utilization by hypercapnia in the rhesus monkey. *Journal of Neurochemistry* 32(2), pp. 661-663. Available at: <http://doi.wiley.com/10.1111/j.1471-4159.1979.tb00404.x> [Accessed: 8 March 2020].
- Knot, H.J. et al. 1996. Extracellular K⁺-induced hyperpolarizations and dilatations of rat coronary and cerebral arteries involve inward rectifier K⁺ channels. *Journal of Physiology* 492(2), pp. 419-430. Available at:

<http://www.ncbi.nlm.nih.gov/pubmed/9019539> [Accessed: 23 February 2020].

Knox, C.A. et al. 1980. Effects of aging on the structural and permeability characteristics of cerebrovasculature in normotensive and hypertensive strains of rats. *Acta Neuropathologica* 51(1), pp. 1-13. doi: 10.1007/BF00688844.

Kontos, H.A. et al. 1977. Analysis of vasoactivity of local ph, pCO₂ and bicarbonate on pial vessels. *Stroke* 8(3), pp. 358-360. doi: 10.1161/01.STR.8.3.358.

Kooij, G. et al. 2012. The Role of ATP-Binding Cassette Transporters in Neuro-Inflammation: Relevance for Bioactive Lipids. *Frontiers in Pharmacology* 3, p. 74. Available at: <http://journal.frontiersin.org/article/10.3389/fphar.2012.00074/abstract> [Accessed: 28 February 2020].

Kortelainen, J. et al. 2016. The effect of anaesthesia on somatosensory evoked potential measurement in a rat model. *Laboratory Animals* 50(1), pp. 63-66. doi: 10.1177/0023677215589514.

Krejza, J. et al. 1999. Transcranial Color Doppler Sonography Arteries in of Basal Cerebral I 82 Healthy Subjects: Age and SexYariability and NormalReference Values for Blood Flow Parameters. *American Journal of Roentgenology* (January), pp. 213-218.

Kruyer, A. et al. 2015. Chronic hypertension leads to neurodegeneration in the TgSwDI mouse model of Alzheimer's disease. *Hypertension* 66(1), pp. 175-182. Available at: <http://www.ncbi.nlm.nih.gov/pubmed/25941345> [Accessed: 29 March 2020].

Kublik, E. et al. 2001. Identification of principal components in cortical evoked potentials by brief surface cooling. *Clinical Neurophysiology* 112(9), pp. 1720-1725. doi: 10.1016/S1388-2457(01)00603-4.

Kulics, A.T. and Cauller, L.J. 1986. Cerebral cortical somatosensory evoked responses, multiple unit activity and current source-densities: their interrelationships and significance to somatic sensation as revealed by stimulation of the awake monkey's hand. *Experimental Brain Research* 62(1), pp. 46-60. doi: 10.1007/BF00237402.

Kynast, J. et al. 2018. White matter hyperintensities associated with small vessel disease impair social cognition beside attention and memory. *Journal of Cerebral Blood Flow and Metabolism* 38(6), pp. 996-1009. doi: 10.1177/0271678X17719380.

de la Torre, J.C. et al. 1992. Chronic cerebrovascular insufficiency induces dementia-like deficits in aged rats. *Brain research* 582(2), pp. 186-95. Available at: <http://www.ncbi.nlm.nih.gov/pubmed/1327402> [Accessed: 29 March 2020].

Lacroix, A. et al. 2015. COX-2-derived prostaglandin E2 produced by pyramidal neurons contributes to neurovascular coupling in the rodent cerebral cortex. *Journal of Neuroscience* 35(34), pp. 11791-11810. doi: 10.1523/JNEUROSCI.0651-15.2015.

Lahti, K.M. et al. 1998. Imaging brain activity in conscious animals using functional MRI. *Journal of neuroscience methods* 82(1), pp. 75-83. doi: 10.1016/S0165-0270(98)00037-5.

Lammie, G.A. et al. 1997. Nonhypertensive cerebral small-vessel disease: An autopsy study. *Stroke* 28(11), pp. 2222-2229. Available at: <https://pubmed.ncbi.nlm.nih.gov/9368569/> [Accessed: 18 April 2021].

Larsen, M. et al. 1997. Isoflurane increases the uptake of glutamate in synaptosomes from rat cerebral cortex. *British Journal of Anaesthesia* 78(1), pp. 55-59. doi: 10.1093/bja/78.1.55.

Larsen, M. and Langmoen, I.A. 1998. The effect of volatile anaesthetics on synaptic release and uptake of glutamate. *Toxicology Letters* 100-101, pp. 59-64. doi: 10.1016/S0378-4274(98)00165-9.

Lassen, N.A. and Agnoli, A. 1972. The upper limit of autoregulation of cerebral blood flow - on the pathogenesis of hypertensive encephalopathy. *Scandinavian Journal of Clinical and Laboratory Investigation* 30(2), pp. 113-116. doi: 10.3109/00365517209081099.

Lavallée, P.C. et al. 2009. Placebo-controlled trial of high-dose atorvastatin in patients with severe cerebral small vessel disease. *Stroke* 40(5), pp. 1721-1728. Available at: <http://stroke.ahajournals.org> [Accessed: 19 April 2021].

Lees, P. 1972. Pharmacology and toxicology of alpha chloralose: a review. *Veterinary Record* 91(14), pp. 330 LP - 333. Available at:
<http://veterinaryrecord.bmj.com/content/91/14/330.abstract>.

Van Leijsen, E.M.C. et al. 2018. Progression of white matter hyperintensities preceded by heterogeneous decline of microstructural integrity. *Stroke* 49(6), pp. 1386-1393. Available at:
<http://stroke.ahajournals.org/lookup/suppl/doi:10.1161/STROKEAHA>.
[Accessed: 18 April 2021].

Leithner, C. et al. 2010. Pharmacological uncoupling of activation induced increases in CBF and CMRO₂. *Journal of cerebral blood flow and metabolism : official journal of the International Society of Cerebral Blood Flow and Metabolism* 30(2), pp. 311-322. Available at:
<http://www.ncbi.nlm.nih.gov/pubmed/19794398> [Accessed: 23 February 2020].

Leoni, R.F. et al. 2017. Cerebral blood flow and vasoreactivity in aging: An arterial spin labeling study. *Brazilian Journal of Medical and Biological Research* 50(4), pp. 1-9. doi: 10.1590/1414-431X20175670.

Lewis, S.M. et al. 2005. Logarithmic transformation for high-field BOLD fMRI data. *Experimental Brain Research* 165(4), pp. 447-453. doi: 10.1007/s00221-005-2336-4.

Li, Q. et al. 2018. Cerebral Small Vessel Disease. *Cell Transplantation* 27(12), pp. 1711-1722. doi: 10.1177/0963689718795148.

Li, T.Q. et al. 1999. Functional MRI of human brain during breath holding by BOLD and FAIR techniques. *NeuroImage* 9(2), pp. 243-249. doi: 10.1006/nimg.1998.0399.

Li, Y. et al. 2021. MRI study of cerebral blood flow, vascular reactivity, and vascular coupling in systemic hypertension. *Brain Research* 1753. Available at:
<https://pubmed.ncbi.nlm.nih.gov/33358732/> [Accessed: 19 April 2021].

Liem, M.K. et al. 2009. Cerebrovascular reactivity is a main determinant of white matter hyperintensity progression in CADASIL. *American Journal of Neuroradiology* 30(6), pp. 1244-1247. Available at: www.ajnr.org [Accessed: 17

April 2021].

Lim, H.K. et al. 2014. Regional amyloid burden and intrinsic connectivity networks in cognitively normal elderly subjects. *Brain* 137(12), pp. 3327-3338. Available at: <https://academic.oup.com/brain/article-abstract/137/12/3327/2847124> [Accessed: 26 March 2020].

Lindauer, U. et al. 1999. Nitric oxide: A modulator, but not a mediator, of neurovascular coupling in rat somatosensory cortex. *American Journal of Physiology - Heart and Circulatory Physiology* 277(2 46-2). doi: 10.1152/ajpheart.1999.277.2.h799.

Lindauer, U. et al. 2010. Neurovascular coupling in rat brain operates independent of hemoglobin deoxygenation. *Journal of Cerebral Blood Flow and Metabolism* 30(4), pp. 757-768. doi: 10.1038/jcbfm.2009.259.

Liu, Z.M. et al. 2004. Imaging oxygen consumption in forepaw somatosensory stimulation in rats under isoflurane anesthesia. *Magnetic Resonance in Medicine* 52(2), pp. 277-285. doi: 10.1002/mrm.20148.

Logothetis, N.K. et al. 2001. Neurophysiological investigation of the basis of the fMRI signal. *Nature* 412(6843), pp. 150-157. doi: 10.1038/35084005.

Lu, H. et al. 2012. Rat brains also have a default mode network. *Proceedings of the National Academy of Sciences* 109(10), pp. 3979-3984. Available at: <http://www.pnas.org/cgi/doi/10.1073/pnas.1200506109>.

Ma, J. et al. 1996. Regional cerebral blood flow response to vibrissal stimulation in mice lacking type I NOS gene expression. *The American journal of physiology* 270(3 Pt 2), pp. H1085-90. Available at: <http://www.ncbi.nlm.nih.gov/pubmed/8780207> [Accessed: 23 February 2020].

MacKenzie, E.T. et al. 1976. Effects of acutely induced hypertension in cats on pial arteriolar caliber, local cerebral blood flow, and the blood brain barrier. *Circulation Research* 39(1), pp. 33-41. doi: 10.1161/01.RES.39.1.33.

MacLulich, A.M.J. et al. 2004. Enlarged perivascular spaces are associated with cognitive function in healthy elderly men. *Journal of Neurology, Neurosurgery and Psychiatry* 75(11), pp. 1519-1523. doi: 10.1136/jnnp.2003.030858.

Macrae, I. 2011. Preclinical stroke research - advantages and disadvantages of the most common rodent models of focal ischaemia. *British Journal of Pharmacology* 164(4), pp. 1062-1078. Available at: <http://doi.wiley.com/10.1111/j.1476-5381.2011.01398.x> [Accessed: 29 March 2020].

Maeda, H. et al. 1993. Reactivity of cerebral blood flow to carbon dioxide in various types of ischemic cerebrovascular disease: Evaluation by the transcranial doppler method. *Stroke* 24(5), pp. 670-675. doi: 10.1161/01.STR.24.5.670.

Mangiarua, E.I. and Lee, R.M.K.W. 1992. Morphometric study of cerebral arteries from spontaneously hypertensive and stroke-prone spontaneously hypertensive rats. *Journal of hypertension* 10(10), pp. 1183-1190. doi: 10.1097/00004872-199210000-00011.

Mariappan, R. et al. 2015. Cerebrovascular reactivity to carbon dioxide under anesthesia: a qualitative systematic review. *Journal of neurosurgical anesthesiology* 27(2), pp. 123-135. doi: 10.1097/ANA.0000000000000092.

Marshall, M. 2004. Capnography in dogs. *Compendium* (October), pp. 761-778.

Masamoto, K. et al. 2007. Relationship between neural, vascular, and BOLD signals in isoflurane-anesthetized rat somatosensory cortex. *Cerebral Cortex* 17(4), pp. 942-950. doi: 10.1093/cercor/bhl005.

Masamoto, K. et al. 2009. Dose-dependent Effect of Isoflurane on Neurovascular Coupling in Rat Cerebral Cortex. *European Journal of Neuroscience* 30(2), pp. 242-250. Available at: <https://www.ncbi.nlm.nih.gov/pmc/articles/PMC3624763/pdf/nihms412728.pdf>.

Masamoto, K. and Kanno, I. 2012. Anesthesia and the quantitative evaluation of neurovascular coupling. *Journal of Cerebral Blood Flow and Metabolism* 32(7), pp. 1233-1247. Available at: <http://www.ncbi.nlm.nih.gov/pubmed/22510601> <http://www.ncbi.nlm.nih.gov/pmc/articles/PMC3390804/pdf/jcbfm201250a.pdf>.

Masawa, N. et al. 1994. Morphometry of structural preservation of tunica

media in aged and hypertensive human intracerebral arteries. *Stroke* 25(1), pp. 122-127. doi: 10.1161/01.STR.25.1.122.

Matsuura, T. and Kanno, I. 2001. Quantitative and temporal relationship between local cerebral blood flow and neuronal activation induced by somatosensory stimulation in rats. *Neuroscience Research* 40(3), pp. 281-290. doi: 10.1016/S0168-0102(01)00236-X.

Mayhan, W.G. et al. 1990. Effects of aging on responses of cerebral arterioles. *American Journal of Physiology-Heart and Circulatory Physiology* 258(4), pp. H1138-H1143. Available at: <https://doi.org/10.1152/ajpheart.1990.258.4.H1138>.

McElhone, K. et al. 2006. A review of health related quality of life in systemic lupus erythematosus. *Lupus* 15(10), pp. 633-643. doi: 10.1177/0961203306071710.

Meng, L. and Gelb, A.W. 2015. Regulation of cerebral autoregulation by carbon dioxide. *Anesthesiology* 122(1), pp. 196-205. Available at: <http://www.ncbi.nlm.nih.gov/pubmed/25401418> [Accessed: 21 February 2020].

Metea, M.R. and Newman, E.A. 2006. Glial cells dilate and constrict blood vessels: A mechanism of neurovascular coupling. *Journal of Neuroscience* 26(11), pp. 2862-2870. doi: 10.1523/JNEUROSCI.4048-05.2006.

Miao, J. et al. 2005. Cerebral microvascular amyloid β protein deposition induces vascular degeneration and neuroinflammation in transgenic mice expressing human vasculotropic mutant amyloid β precursor protein. *American Journal of Pathology* 167(2), pp. 505-515. doi: 10.1016/S0002-9440(10)62993-8.

Minami, M. et al. 1985. Changes in ambulation and drinking behavior related to stroke in stroke-prone spontaneously hypertensive rats. *Stroke* 16(1), pp. 44-48. doi: 10.1161/01.str.16.1.44.

Moody, D.M. et al. 1997. Cerebral microvascular alterations in aging, leukoaraiosis, and Alzheimer's disease. *Annals of the New York Academy of Sciences* 826, pp. 103-116. doi: 10.1111/j.1749-6632.1997.tb48464.x.

- Moss, M.B. and Jonak, E. 2007. Cerebrovascular disease and dementia: A primate model of hypertension and cognition. *Alzheimer's and Dementia* 3(2 SUPPL.), pp. S6-15. Available at: <http://www.ncbi.nlm.nih.gov/pubmed/19595977> [Accessed: 29 March 2020].
- Mosso, A. 1880. Sulla circolazione del cervello dell'uomo. *Atti della R. Accademia dei Lincei* 5, pp. 237-358.
- Mulvany, M.J. 1999. Vascular remodelling of resistance vessels: Can we define this? *Cardiovascular Research* 41(1), pp. 9-13. Available at: [https://academic.oup.com/circvasres/article-lookup/doi/10.1016/S0008-6363\(98\)00289-2](https://academic.oup.com/circvasres/article-lookup/doi/10.1016/S0008-6363(98)00289-2) [Accessed: 27 March 2020].
- Nagasawa, S. et al. 1979. Mechanical properties of human cerebral arteries. Part 1: Effects of age and vascular smooth muscle activation. *Surgical neurology* 12(4), p. 297–304. Available at: <http://europepmc.org/abstract/MED/524244>.
- Nakajima, S. et al. 2008. Loss of CO₂-induced distensibility in cerebral arteries with chronic hypertension or vasospasm after subarachnoid hemorrhage. *The Kobe journal of medical sciences* 53(6), pp. 317-326.
- Nakao, Y. et al. 2001. Effects of anesthesia on functional activation of cerebral blood flow and metabolism. *Proceedings of the National Academy of Sciences of the United States of America* 98(13), pp. 7593-7598. Available at: <http://www.ncbi.nlm.nih.gov/pubmed/11390971> [Accessed: 8 March 2020].
- Nasrallah, F.A. et al. 2015. Dependence of BOLD signal fluctuation on arterial blood CO₂ and O₂: Implication for resting-state functional connectivity. *NeuroImage* 117, pp. 29-39. Available at: <http://dx.doi.org/10.1016/j.neuroimage.2015.05.035>.
- NCT01821118 [no date]. Study Evaluating the Safety, Tolerability and Efficacy of PF-04360365 in Adults With Probable Cerebral Amyloid Angiopathy - Full Text View - ClinicalTrials.gov. Available at: <https://clinicaltrials.gov/ct2/show/NCT01821118?term=reactivity&cond=small+vessel+disease&draw=2&rank=9> [Accessed: 19 April 2021].
- NCT03082014 [no date]. Effects of Amlodipine and Other Blood Pressure

Lowering Agents on Microvascular Function - Full Text View - ClinicalTrials.gov.

Available at:

<https://clinicaltrials.gov/ct2/show/NCT03082014?term=reactivity&cond=small+vessel+disease&draw=2&rank=2> [Accessed: 19 April 2021].

Ndung'u, M. et al. 2012. Cerebral amyloid B(42) deposits and microvascular pathology in ageing baboons. *Neuropathology and Applied Neurobiology* 38(5), pp. 487-499. Available at: <http://www.ncbi.nlm.nih.gov/pubmed/22126319> [Accessed: 29 March 2020].

Nelson, J.W. et al. 2021. The gut microbiome contributes to blood-brain barrier disruption in spontaneously hypertensive stroke prone rats. *FASEB journal : official publication of the Federation of American Societies for Experimental Biology* 35(2), p. e21201. doi: 10.1096/fj.202001117R.

Ngai, A.C. et al. 1999. Frequency-dependent changes in cerebral blood flow and evoked potentials during somatosensory stimulation in the rat. *Brain Research* 837(1-2), pp. 221-228. doi: 10.1016/S0006-8993(99)01649-2.

Di Nicolantonio, R. and Silvapulle, M.J. 1988. BLOOD PRESSURE, SALT APPETITE AND MORTALITY OF GENETICALLY HYPERTENSIVE AND NORMOTENSIVE RATS MAINTAINED ON HIGH AND LOW SALT DIETS FROM WEANING. *Clinical and Experimental Pharmacology and Physiology* 15(10), pp. 741-751. Available at: <https://doi.org/10.1111/j.1440-1681.1988.tb01014.x>.

Nilsson, B. and Siesjö, B.K. 1976. A Method for Determining Blood Flow and Oxygen Consumption in the Rat Brain. *Acta Physiologica Scandinavica* 96(1), pp. 72-82. Available at: <http://www.ncbi.nlm.nih.gov/pubmed/1251748> [Accessed: 8 March 2020].

NINDS 2001. Final Report of the Stroke Progress Review Group.

Niwa, K. et al. 2000. AB1-40-related reduction in functional hyperemia in mouse neocortex during somatosensory activation. *Proceedings of the National Academy of Sciences of the United States of America* 97(17), pp. 9735-9740. Available at: <http://www.ncbi.nlm.nih.gov/pubmed/10944232> [Accessed: 26 March 2020].

Niwa, K. et al. 2001. AB-peptides enhance vasoconstriction in cerebral

circulation. *American Journal of Physiology - Heart and Circulatory Physiology* 281(6 50-6). doi: 10.1152/ajpheart.2001.281.6.h2417.

Niwa, K. et al. 2002. Alterations in cerebral blood flow and glucose utilization in mice overexpressing the amyloid precursor protein. *Neurobiology of Disease* 9(1), pp. 61-68. Available at: <http://www.ncbi.nlm.nih.gov/pubmed/11848685> [Accessed: 26 March 2020].

Nordborg, C. et al. 1985. The morphometry of consecutive segments in cerebral arteries of normotensive and spontaneously hypertensive rats. *Stroke* 16(2), pp. 313-320. Available at: <https://doi.org/10.1161/01.STR.16.2.313>.

O'Regan, M. 2005. Adenosine and the regulation of cerebral blood flow. *Neurological research* 27(2), pp. 175-181. doi: 10.1179/016164105X21931.

O'Rourke, M.F. and Nichols, W.W. 2005. Aortic diameter, aortic stiffness, and wave reflection increase with age and isolated systolic hypertension. *Hypertension* 45(4 SUPPL.), pp. 652-658. doi: 10.1161/01.HYP.0000153793.84859.b8.

Ogawa, S. et al. 1990. *Brain magnetic resonance imaging with contrast dependent on blood oxygenation (cerebral blood flow/brain metabolism/oxygenation)*.

Okamoto, K. et al. 1974. *Establishment of the stroke-prone spontaneously hypertensive rat (SHRSP)*.

Okamoto, K. and Aoki, K. 1963. Development of a strain of Spontaneously Hypertensive Rats. *Japanese Circulation Journal* 27(43), pp. 282-293. Available at: <http://www.mendeley.com/research/geology-volcanic-history-eruptive-style-yakedake-volcano-group-central-japan/>.

Oldendorf, W.H. et al. 1977. The large apparent work capability of the blood-brain barrier: A study of the mitochondrial content of capillary endothelial cells in brain and other tissues of the rat. *Annals of Neurology* 1(5), pp. 409-417. Available at: <http://doi.wiley.com/10.1002/ana.410010502> [Accessed: 28 February 2020].

Olmstead, F. et al. 1951. Blood pressure in the unaesthetized rat. *Circulation* 111, pp. 727-730.

- Olopade, F.E. et al. 2012. The relationship between ventricular dilatation, neuropathological and neurobehavioural changes in hydrocephalic rats. *Fluids and Barriers of the CNS* 9(1), pp. 1-10. doi: 10.1186/2045-8118-9-19.
- van Opstal, A.M. et al. 2017. Cerebrovascular function in presymptomatic and symptomatic individuals with hereditary cerebral amyloid angiopathy: a case-control study. *The Lancet Neurology* 16(2), pp. 115-122. doi: 10.1016/S1474-4422(16)30346-5.
- Paasonen, J. et al. 2018. Functional connectivity under six anesthesia protocols and the awake condition in rat brain. *NeuroImage* 172(January), pp. 9-20. doi: 10.1016/j.neuroimage.2018.01.014.
- Pantoni, L. 2010. Cerebral small vessel disease: from pathogenesis and clinical characteristics to therapeutic challenges. *The Lancet Neurology* 9(7), pp. 689-701. doi: 10.1016/S1474-4422(10)70104-6.
- Pardridge, W.M. et al. 1985. Human Blood–Brain Barrier Insulin Receptor. *Journal of Neurochemistry* 44(6), pp. 1771-1778. Available at: <http://www.ncbi.nlm.nih.gov/pubmed/2859355> [Accessed: 28 February 2020].
- Pardridge, W.M. et al. 1990. Brain-type glucose transporter (GLUT-1) is selectively localized to the blood-brain barrier: Studies with quantitative Western blotting and in situ hybridization. *Journal of Biological Chemistry* 265(29), pp. 18035-18040.
- Pardridge, W.M. and Oldendorf, W.H. 1975. Kinetic analysis of blood-brain barrier transport of amino acids. *BBA - Biomembranes* 401(1), pp. 128-136. Available at: <http://www.ncbi.nlm.nih.gov/pubmed/1148286> [Accessed: 28 February 2020].
- Pascucci, R.C. et al. 1989. Comparison of a sidestream and mainstream capnometer in infants. *Critical Care Medicine* 17(6), pp. 560-562. doi: 10.1097/00003246-198906000-00016.
- Pauling, L. and Coryell, C.D. 1936. The Magnetic Properties and Structure of Hemoglobin, Oxyhemoglobin and Carbonmonoxyhemoglobin. *Proceedings of the National Academy of Sciences* 22(4), pp. 210-216. doi: 10.1073/pnas.22.4.210.

- Paulson, O.B. and Newman, E.A. 1987. Does the release of potassium from astrocyte endfeet regulate cerebral blood flow? *Science* 237(4817), pp. 896-898. Available at: <http://www.ncbi.nlm.nih.gov/pubmed/3616619> [Accessed: 23 February 2020].
- Pawela, C.P. et al. 2008. Modeling of region-specific fMRI BOLD neurovascular response functions in rat brain reveals residual differences that correlate with the differences in regional evoked potentials. *NeuroImage* 41(2), pp. 525-534. doi: 10.1016/j.neuroimage.2008.02.022.
- Pawela, C.P. et al. 2009. A protocol for use of medetomidine anesthesia in rats for extended studies using task-induced BOLD contrast and resting-state functional connectivity. *NeuroImage* 46(4), pp. 1137-1147. Available at: <http://dx.doi.org/10.1016/j.neuroimage.2009.03.004>.
- Paxinos, G. and Watson, C. 1998. *The Rat Brain In Stereotaxix Coordinates*. doi: 10.1017/CBO9781107415324.004.
- Peca, S. et al. 2013. Neurovascular decoupling is associated with severity of cerebral amyloid angiopathy. *Neurology* 81(19), pp. 1659-1665. Available at: <https://n.neurology.org/content/81/19/1659> [Accessed: 11 April 2021].
- Peeters, R.R. et al. 2001. Comparing BOLD fMRI signal changes in the awake and anesthetized rat during electrical forepaw stimulation. *Magnetic Resonance Imaging* 19(6), pp. 821-826. doi: 10.1016/S0730-725X(01)00391-5.
- Peng, X. et al. 2002. Suppression of cortical functional hyperemia to vibrissal stimulation in the rat by epoxygenase inhibitors. *American Journal of Physiology - Heart and Circulatory Physiology* 283(5 52-5). doi: 10.1152/ajpheart.01130.2000.
- Peng, X. et al. 2004. Dependency of cortical functional hyperemia to forepaw stimulation on epoxygenase and nitric oxide synthase activities in rats. *Journal of cerebral blood flow and metabolism : official journal of the International Society of Cerebral Blood Flow and Metabolism* 24(5), pp. 509-17. Available at: <http://www.ncbi.nlm.nih.gov/pubmed/15129182> [Accessed: 23 February 2020].
- Peterson, E.C. et al. 2011. Regulation of Cerebral Blood Flow. *International*

Journal of Vascular Medicine 2011. doi: 10.1155/2011/823525.

Phillips, S.J. and Whisnant, J.P. 1992. Hypertension and the Brain. *Archives of Internal Medicine* 152(5), pp. 938-945. doi: 10.1001/archinte.1992.00400170028006.

Pineiro, R. et al. 2002. Altered hemodynamic responses in patients after subcortical stroke measured by functional MRI. *Stroke* 33(1), pp. 103-109. doi: 10.1161/hs0102.100482.

Pires, P.W. et al. 2013. The effects of hypertension on the nervous system. *American Journal of Physiology - Heart and Circulatory Physiology* 304(12), pp. H1598-H1614. doi: 10.1152/ajpheart.00490.2012.

Posse, S. et al. 1997. Regional dynamic signal changes during controlled hyperventilation assessed with blood oxygen level-dependent functional MR imaging. *American Journal of Neuroradiology* 18(9), pp. 1763-1770.

Posse, S. et al. 2001. Effect of graded hypo- and hypercapnia on fMRI contrast in visual cortex: Quantification of T² changes by multiecho EPI. *Magnetic Resonance in Medicine* 46(2), pp. 264-271. doi: 10.1002/mrm.1187.

Potter, G.M. et al. 2015. Cerebral Perivascular Spaces Visible on Magnetic Resonance Imaging: Development of a Qualitative Rating Scale and its Observer Reliability. *Cerebrovascular Diseases* 39(3-4), pp. 224-231. Available at: <https://www.karger.com/Article/FullText/375153> [Accessed: 14 April 2021].

Powers, W.J. et al. 1996. Effect of stepped hypoglycemia on regional cerebral blood flow response to physiological brain activation. *American Journal of Physiology - Heart and Circulatory Physiology* 270(2 39-2). doi: 10.1152/ajpheart.1996.270.2.h554.

Pulsinelli, W.A. and Buchan, A.M. 1988. The four-vessel occlusion rat model: Method for complete occlusion of vertebral arteries and control of collateral circulation. *Stroke* 19(7), pp. 913-914. Available at: <http://ahajournals.org> [Accessed: 29 March 2020].

Quick, S. et al. 2021. A Vessel for Change: Endothelial Dysfunction in Cerebral Small Vessel Disease. *Trends in Neurosciences* 44(4), pp. 289-305. Available at: <https://doi.org/10.1016/j.tins.2020.11.003> [Accessed: 14 April 2021].

- Rademakers, R. et al. 2012. Mutations in the colony stimulating factor 1 receptor (CSF1R) gene cause hereditary diffuse leukoencephalopathy with spheroids. *Nature Genetics* 44(2), pp. 200-205. Available at: <https://pubmed.ncbi.nlm.nih.gov/22197934/> [Accessed: 18 April 2021].
- Rajani, R.M. et al. 2018. Reversal of endothelial dysfunction reduces white matter vulnerability in cerebral small vessel disease in rats. *Science Translational Medicine* 10(448), p. 9507. Available at: <http://stm.sciencemag.org/> [Accessed: 13 April 2021].
- Revesz, T. et al. 2002. Sporadic and familial cerebral amyloid angiopathies. In: *Brain Pathology*. International Society of Neuropathology, pp. 343-357. doi: 10.1111/j.1750-3639.2002.tb00449.x.
- Richards, C.D. 2002. Anaesthetic modulation of synaptic transmission in the mammalian CNS. *British Journal of Anaesthesia* 89(1), pp. 79-90. Available at: <http://dx.doi.org/10.1093/bja/aef162>.
- Rost, N.S. et al. 2010. White matter hyperintensity volume is increased in small vessel stroke subtypes. *Neurology* 75(19), pp. 1670-1677. doi: 10.1212/WNL.0b013e3181fc279a.
- Rostrup, E. et al. 1994. Functional MRI of CO₂ induced increase in cerebral perfusion. *NMR in biomedicine* 7(1-2), pp. 29-34.
- Roy, C. and Sherrington, C. 1890. On the regulation of the blood-supply of the brain. *Journal of Physiology* 11, pp. 85-158.
- Royle, G. et al. 2006. Functional imaging with Laser Speckle Contrast Analysis: Vascular compartment analysis and correlation with Laser Doppler Flowmetry and somatosensory evoked potentials. *Brain Research* 1121(1), pp. 95-103. doi: 10.1016/j.brainres.2006.08.125.
- Sagare, A.P. et al. 2013. Pericyte loss influences Alzheimer-like neurodegeneration in mice. *Nature Communications* 4. doi: 10.1038/ncomms3932.
- Sagawa, K. and Guyton, A.C. 1961. Pressure-flow relationships in isolated canine cerebral circulation. *The American journal of physiology* 200, pp. 711-714. doi: 10.1152/ajplegacy.1961.200.4.711.

Saji, N. et al. 2016. Cerebral Small Vessel Disease and Arterial Stiffness: Tsunami Effect in the Brain? *Pulse* 3(3-4), pp. 182-189. doi: 10.1159/000443614.

Salerno, J.A. et al. 1992. Brain Atrophy in Hypertension. *Hypertension* 20(3), pp. 340-348.

Salvadores, N. et al. 2017. Chronic cerebral hypoperfusion alters amyloid- β peptide pools leading to cerebral amyloid angiopathy, microinfarcts and haemorrhages in Tg-SwDI mice. *Clinical Science* 131(16), pp. 2109-2123. Available at: <http://portlandpress.com/clinsci/article-pdf/131/16/2109/445747/cs-2017-0962.pdf> [Accessed: 18 April 2021].

Sam, K. et al. 2016a. Development of White Matter Hyperintensity Is Preceded by Reduced Cerebrovascular Reactivity. *Annals of Neurology* 80(2), pp. 277-285. Available at: <https://pubmed.ncbi.nlm.nih.gov/27352039/> [Accessed: 11 April 2021].

Sam, K. et al. 2016b. Impaired dynamic cerebrovascular response to hypercapnia predicts development of white matter hyperintensities. *NeuroImage: Clinical* 11, pp. 796-801. Available at: </pmc/articles/PMC4917393/> [Accessed: 11 April 2021].

Samuelsson, M. et al. 1996. Functional outcome in patients with lacunar infarction. *Stroke* 27(5), pp. 842-846. doi: 10.1161/01.STR.27.5.842.

Sándor, P. 1999. Nervous control of the cerebrovascular system: Doubts and facts. *Neurochemistry International* 35(3), pp. 237-259. doi: 10.1016/S0197-0186(99)00067-4.

Sandstrom, D.J. 2004. Isoflurane depresses glutamate release by reducing neuronal excitability at the *Drosophila* neuromuscular junction. *Journal of Physiology* 558(2), pp. 489-502. doi: 10.1113/jphysiol.2004.065748.

Sanganahalli, B.G. et al. 2008. Frequency-dependent tactile responses in rat brain measured by functional MRI. *NMR in Biomedicine* 21(4), pp. 410-416. doi: 10.1002/nbm.1259.

Scammen, F.L. and Fishbaugh, B.S. 1986. Frequency Response of Long Mass-spectrometer Sampling Catheters. *Anaesthesia* (65), pp. 422-425.

- Schieber, R.A. et al. 1985. Accuracy of expiratory carbon dioxide measurements using the coaxial and circle breathing circuits in small subjects. *Journal of Clinical Monitoring* 1(3), pp. 149-155. doi: 10.1007/BF02832254.
- Schmidt, R. et al. 2011. Heterogeneity in age-related white matter changes. *Acta Neuropathologica* 122(2), pp. 171-185. doi: 10.1007/s00401-011-0851-x.
- Sedlakova, R. et al. 1999. Ultrastructure of the blood-brain barrier in the rabbit. *Journal of Submicroscopic Cytology and Pathology* 31(1), pp. 149-161.
- Segal, S.S. 2015. Integration and modulation of intercellular signaling underlying blood flow control. *Journal of Vascular Research* 52(2), pp. 136-157. doi: 10.1159/000439112.
- Shang, J. et al. 2019. Chronic cerebral hypoperfusion alters amyloid- β transport related proteins in the cortical blood vessels of Alzheimer's disease model mouse. *Brain Research* 1723, p. 146379. doi: 10.1016/j.brainres.2019.146379.
- Shi, Y. and Wardlaw, J.M. 2016. Update on cerebral small vessel disease: A dynamic whole-brain disease. *Stroke and Vascular Neurology* 1(3), pp. 83-92. Available at: <http://svn.bmj.com/> [Accessed: 13 April 2021].
- Shoamanesh, A. et al. 2011. Cerebral microbleeds: Histopathological correlation of neuroimaging. *Cerebrovascular Diseases* 32(6), pp. 528-534. Available at: <https://pubmed.ncbi.nlm.nih.gov/22104448/> [Accessed: 18 April 2021].
- Sicard, K. et al. 2003. Regional Cerebral Blood Flow and BOLD Responses in Conscious and Anesthetized Rats under Basal and Hypercapnic Conditions: Implications for Functional MRI Studies. *Journal of Cerebral Blood Flow & Metabolism* 23(4), pp. 472-481. Available at: <http://jcb.sagepub.com/lookup/doi/10.1097/01.WCB.0000054755.93668.20>.
- Sicard, K.M. and Duong, T.Q. 2005. Effects of hypoxia, hyperoxia, and hypercapnia on baseline and stimulus-evoked BOLD, CBF, and CMRO₂ in spontaneously breathing animals. *NeuroImage* 25(3), pp. 850-858. doi: 10.1016/j.neuroimage.2004.12.010.
- Silva, A.C. et al. 1999. Simultaneous Blood Oxygenation Level-Dependent and

Cerebral Blood Flow Functional Magnetic Resonance Imaging During Forepaw Stimulation in the Rat. *Journal of Cerebral Blood Flow & Metabolism* , pp. 871-879. Available at: <http://jcb.sagepub.com/lookup/doi/10.1097/00004647-199908000-00006>.

Silva, A.C. and Koretsky, A.P. 2002. *Laminar specificity of functional MRI onset times during somatosensory stimulation in rat*. Available at: www.pnas.org/cgi/doi/10.1073/pnas.222561899 [Accessed: 23 February 2020].

Sinclair, M.D. 2003. A review of the physiological effects of α 2-agonists related to the clinical use of medetomidine in small animal practice. *Canadian Veterinary Journal* 44(11), pp. 885-897.

Sirmpilatze, N. et al. 2019. Temporal stability of fMRI in medetomidine-anesthetized rats. *Scientific Reports* 9(1). Available at: [/pmc/articles/PMC6853937/](https://pubmed.ncbi.nlm.nih.gov/34811111/) [Accessed: 8 April 2021].

Sironi, L. et al. 2004. Analysis of pathological events at the onset of brain damage in stroke-prone rats: A proteomics and magnetic resonance imaging approach. *Journal of Neuroscience Research* 78(1), pp. 115-122. doi: 10.1002/jnr.20219.

Sleight, E. et al. 2021. Cerebrovascular Reactivity Measurement Using Magnetic Resonance Imaging: A Systematic Review. *Frontiers in Physiology* 12, p. 643468. Available at: [/pmc/articles/PMC7947694/](https://pubmed.ncbi.nlm.nih.gov/37111111/) [Accessed: 14 April 2021].

Smith, E.E. et al. 2012. Cerebral microinfarcts: The invisible lesions. *The Lancet Neurology* 11(3), pp. 272-282. Available at: <http://www.ncbi.nlm.nih.gov/pubmed/22341035> [Accessed: 29 March 2020].

Snowdon, D.A. 1997. Brain Infarction and the Clinical Expression of Alzheimer Disease_{title>The Nun Study}. *JAMA: The Journal of the American Medical Association* 277(10), p. 813. Available at: <https://jamanetwork.com/journals/jama/fullarticle/414570> [Accessed: 13 April 2021].

Sonntag, W.E. et al. 1997. Decreases in cerebral microvasculature with age are associated with the decline in growth hormone and insulin-like growth factor 1. *Endocrinology* 138(8), pp. 3515-20.

- Sorg, C. et al. 2007. Selective changes of resting-state networks in individuals at risk for Alzheimer's disease. *Proceedings of the National Academy of Sciences of the United States of America* 104(47), pp. 18760-18765. Available at: <http://www.ncbi.nlm.nih.gov/pubmed/18003904> [Accessed: 26 March 2020].
- Staba, R.J. et al. 2003. Effects of ventrobasal lesion and cortical cooling on fast oscillations (>200 Hz) in rat somatosensory cortex. *Journal of Neurophysiology* 89(5), pp. 2380-2388. doi: 10.1152/jn.01098.2002.
- Stefanovic, B. et al. 2006. The effect of global cerebral vasodilation on focal activation hemodynamics. *NeuroImage* 30(3), pp. 726-734. doi: 10.1016/j.neuroimage.2005.10.038.
- Steiner, A.R. et al. 2021. Systematic review: Anesthetic protocols and management as confounders in rodent blood oxygen level dependent functional magnetic resonance imaging (BOLD fMRI)-part B: Effects of anesthetic agents, doses and timing. *Animals* 11(1), pp. 1-34. Available at: <https://pubmed.ncbi.nlm.nih.gov/33467584/> [Accessed: 7 April 2021].
- Stienen, P.J. et al. 2004. Differences between primary somatosensory cortex- and vertex-derived somatosensory-evoked potentials in the rat. *Brain Research* 1030(2), pp. 256-266. doi: 10.1016/j.brainres.2004.10.014.
- Stillman, A.. et al. 1995. Functional MRI of Brain during Breath Holding at 4T. *Magnetic Resonance Imaging* 13(6), pp. 893-897.
- Strandgaard, S. et al. 1974. Upper limit of autoregulation of cerebral blood flow in the baboon. *Circulation research* 34(4), pp. 435-440. doi: 10.1161/01.RES.34.4.435.
- Strassburger, T.L. et al. 1997. Interactive Effects of Age and Hypertension on Volumes of Brain Structures. *Stroke* 28(7), pp. 1410-1417. Available at: <https://doi.org/10.1161/01.STR.28.7.1410>.
- Stringer, M.S. et al. 2021. A Review of Translational Magnetic Resonance Imaging in Human and Rodent Experimental Models of Small Vessel Disease. *Translational Stroke Research* 12(1), pp. 15-30. Available at: </pmc/articles/PMC7803876/> [Accessed: 14 April 2021].

- De Strooper, B. and Karran, E. 2016. The Cellular Phase of Alzheimer's Disease. *Cell* 164(4), pp. 603-615. Available at: <http://www.ncbi.nlm.nih.gov/pubmed/26871627> [Accessed: 26 March 2020].
- Sudlow, C.L.M. and Warlow, C.P. 1997a. Comparable Studies of the Incidence of Stroke and its Pathological Types : Results From an International Collaboration. *Stroke* 28(3), pp. 491-499. Available at: <http://stroke.ahajournals.org/cgi/content/long/28/3/491> [Accessed: 15 May 2016].
- Sudlow, C.L.M. and Warlow, C.P. 1997b. Comparable studies of the incidence of stroke and its pathological types: Results from an international collaboration. *Stroke* 28(3), pp. 491-499. doi: 10.1161/01.STR.28.3.491.
- Takemori, K. et al. 2013. Effects of oxidative stress on vascular reactivity in the offspring of protein-restricted stroke-prone spontaneously hypertensive rats. *Bioscience, Biotechnology and Biochemistry* 77(8), pp. 1689-1693. Available at: <https://pubmed.ncbi.nlm.nih.gov/23924731/> [Accessed: 20 April 2021].
- Takiguchi, K. 1983. Experimental hypertension: Pathological study of the cerebrovascular lesions of stroke-prone spontaneously hypertensive rat (SHR-SP). *Acta Medica Nagasakiensia* 28(1-4), pp. 46-63.
- Talman, W.T. and Nitschke Dragon, D. 2007. Neuronal nitric oxide mediates cerebral vasodilatation during acute hypertension. *Brain Research* 1139(1), pp. 126-132. Available at: <http://www.ncbi.nlm.nih.gov/pubmed/17291465> [Accessed: 21 February 2020].
- Tamaki, K. et al. 1995. Effects of Aging and Chronic Hypertension on Cerebral Blood Flow and Cerebrovascular CO₂ Reactivity in the Rat. *Gerontology* 41(1), pp. 11-17. Available at: <https://www.karger.com/DOI/10.1159/000213657>.
- Tarr, D. 2012. *Imaging the effects of acute hyperglycaemia on early ischaemic injury using MRI in an experimental stroke model*. Available at: <http://search.ebscohost.com/login.aspx?direct=true&db=edsble&AN=ethos.016239024&site=eds-live>.
- Thomas, T. et al. 1996. B-Amyloid-mediated vasoactivity and vascular

endothelial damage. *Nature* 380(6570), pp. 168-171. Available at:
<http://www.ncbi.nlm.nih.gov/pubmed/8600393> [Accessed: 26 March 2020].

Thompson, L.E. et al. 1988. Sodium-calcium exchange in vascular smooth muscle of Wistar-Kyoto and stroke-prone spontaneously hypertensive rats. *Journal of hypertension. Supplement : official journal of the International Society of Hypertension* 6(4), pp. S160-2. doi: 10.1097/00004872-198812040-00047.

Thomsen, M.S. et al. 2017. Synthesis and deposition of basement membrane proteins by primary brain capillary endothelial cells in a murine model of the blood-brain barrier. *Journal of Neurochemistry* 140(5), pp. 741-754. Available at: <http://doi.wiley.com/10.1111/jnc.13747> [Accessed: 28 February 2020].

Todd, M.E. et al. 1983. The dimensional characteristics of smooth muscle in rat blood vessels. A computer-assisted analysis. *Circulation Research* 53(3), pp. 319-331. doi: 10.1161/01.RES.53.3.319.

Tombaugh, G.C. and Sapolsky, R.M. 1990. Mild acidosis protects hippocampal neurons from injury induced by oxygen and glucose deprivation. *Brain research* 506(2), pp. 343-5. Available at:
<http://www.ncbi.nlm.nih.gov/pubmed/2154291> [Accessed: 8 March 2020].

Tripathi, M. and Pandey, M. 2000. Atypical 'tails-up' capnograph due to breach in the sampling tube of side-scream capnometer. *Journal of Clinical Monitoring and Computing* 16(1), pp. 17-20. doi: 10.1023/A:1009990210114.

Tsai, C.F. et al. 2013. Epidemiology of stroke and its subtypes in Chinese vs white populations. *Neurology* 81(3), pp. 264-272. Available at:
<https://n.neurology.org/content/81/3/264.short> [Accessed: 29 March 2020].

Tu, T.-W. et al. 2014a. Imaging of Spontaneous Ventriculomegaly and Vascular Malformations in Wistar rats: implications for Preclinical Research. *Journal of Neuropathology and Experimental Neurology* 73(12), pp. 1152-1165. Available at:
<https://www.ncbi.nlm.nih.gov/pmc/articles/PMC3624763/pdf/nihms412728.pdf>.

Tu, T.-W.W. et al. 2014b. Imaging of spontaneous ventriculomegaly and

- vascular malformations in Wistar rats: Implications for preclinical research. *Journal of Neuropathology and Experimental Neurology* 73(12), pp. 1152-1165. Available at: <https://www.ncbi.nlm.nih.gov/pmc/articles/PMC3624763/pdf/nihms412728.pdf>.
- Uchida, S. et al. 2017. Systemic blood pressure alters cortical blood flow and neurovascular coupling during nociceptive processing in the primary somatosensory cortex of the rat. *Neuroscience* 343, pp. 250-259. doi: 10.1016/j.neuroscience.2016.12.014.
- Ueki, M. et al. 1992. Effect of alpha-chloralose, halothane, pentobarbital and nitrous oxide anesthesia on metabolic coupling in somatosensory cortex of rat. *Acta Anaesthesiologica Scandinavica* 36(4), pp. 318-322. doi: 10.1111/j.1399-6576.1992.tb03474.x.
- Uludag, K. et al. 2004. Coupling of cerebral blood flow and oxygen consumption during physiological activation and deactivation measured with fMRI. *NeuroImage* 23(1), pp. 148-155. doi: 10.1016/j.neuroimage.2004.05.013.
- Ureshi, M. et al. 2004. Stimulus frequency dependence of the linear relationship between local cerebral blood flow and field potential evoked by activation of rat somatosensory cortex. *Neuroscience Research* 48(2), pp. 147-153. doi: 10.1016/j.neures.2003.10.014.
- Ureshi, M. et al. 2005. Nonlinear correlation between field potential and local cerebral blood flow in rat somatosensory cortex evoked by changing the stimulus current. *Neuroscience Research* 51(2), pp. 139-145. doi: 10.1016/j.neures.2004.10.008.
- Ushiwata, I. and Ushiki, T. 1990. Cytoarchitecture of the smooth muscles and pericytes of rat cerebral blood vessels. *Journal of Neurosurgery* 73(1), pp. 82-90. Available at: <https://thejns.org/view/journals/j-neurosurg/73/1/article-p82.xml>.
- Verdura, E. et al. 2015. Heterozygous HTRA1 mutations are associated with autosomal dominant cerebral small vessel disease. *Brain* 138(8), pp. 2347-2358. Available at: <https://pubmed.ncbi.nlm.nih.gov/26063658/> [Accessed: 18 April 2021].

Vermeer, S.E. et al. 2003. Silent Brain Infarcts and the Risk of Dementia and Cognitive Decline. *New England Journal of Medicine* 348(13), pp. 1215-1222. Available at: <https://pubmed.ncbi.nlm.nih.gov/12660385/> [Accessed: 13 April 2021].

Vermeer, S.E. et al. 2007. Silent brain infarcts: a systematic review. *Lancet Neurology* 6(7), pp. 611-619. doi: 10.1016/S1474-4422(07)70170-9.

Vinters, H. V. 2015. Emerging Concepts in Alzheimer's Disease. *Annual Review of Pathology: Mechanisms of Disease* 10(1), pp. 291-319. Available at: <http://www.ncbi.nlm.nih.gov/pubmed/25387055> [Accessed: 26 March 2020].

Wadi, L.C. et al. 2020. Mechanisms of Cerebral Microbleeds. *Journal of Neuropathology & Experimental Neurology* 79(10), pp. 1093-1099. Available at: <https://academic.oup.com/jnen/article/79/10/1093/5905874> [Accessed: 18 April 2021].

Wardlaw, J.M. 2005. What causes lacunar stroke? *Journal of Neurology, Neurosurgery and Psychiatry* 76(5), pp. 617-619. doi: 10.1136/jnnp.2004.039982.

Wardlaw, J.M. et al. 2013. Mechanisms of sporadic cerebral small vessel disease: Insights from neuroimaging. *The Lancet Neurology* 12(5), pp. 483-497. doi: 10.1016/S1474-4422(13)70060-7.

Wardlaw, J.M. et al. 2015. What are white matter hyperintensities made of? Relevance to vascular cognitive impairment. *Journal of the American Heart Association* 4(6), p. 001140. doi: 10.1161/JAHA.114.001140.

Weber, R. et al. 2006. A fully noninvasive and robust experimental protocol for longitudinal fMRI studies in the rat. *NeuroImage* 29(4), pp. 1303-1310. doi: 10.1016/j.neuroimage.2005.08.028.

Weckesser, M. et al. 1999. Functional imaging of the visual cortex with bold-contrast MRI: Hyperventilation decreases signal response. *Magnetic Resonance in Medicine* 41(1), pp. 213-216. doi: 10.1002/(SICI)1522-2594(199901)41:1<213::AID-MRM31>3.0.CO;2-S.

White, R.P. et al. 2000. *Effect of inhibition of nitric oxide synthase on dynamic cerebral autoregulation in humans.*

- Whittaker, J.R. et al. 2016. The absolute CBF response to activation is preserved during elevated perfusion: Implications for neurovascular coupling measures. *NeuroImage* 125, pp. 198-207. Available at: <http://dx.doi.org/10.1016/j.neuroimage.2015.10.023>.
- Wise, R.G. et al. 2004. Resting fluctuations in arterial carbon dioxide induce significant low frequency variations in BOLD signal. *NeuroImage* 21(4), pp. 1652-1664. Available at: <https://www.sciencedirect.com/science/article/pii/S1053811903007663#BIB6> [Accessed: 26 February 2020].
- Wolf, T. et al. 1997. Excessive oxygen or glucose supply does not alter the blood flow response to somatosensory stimulation or spreading depression in rats. *Brain Research* 761(2), pp. 290-299. Available at: <http://www.ncbi.nlm.nih.gov/pubmed/9252028> [Accessed: 22 February 2020].
- Wong, E.C. and Bandettini, P.A. 1997. A hypercapnia-based normalization method for improved spatial localization of human brain activation with fMRI. *NMR in Biomedicine* 10(4-5), pp. 197-203. Available at: <http://www.ncbi.nlm.nih.gov/pubmed/9430348> <http://www.ncbi.nlm.nih.gov/sites/entrez?db=pubmed&TermToSearch=9430348&Cmd=ShowDetailView>.
- Wuerfel, J. et al. 2008. Perivascular spaces--MRI marker of inflammatory activity in the brain? *Brain : a journal of neurology* 131(Pt 9), pp. 2332-40. Available at: <http://www.ncbi.nlm.nih.gov/pubmed/18676439> [Accessed: 30 March 2020].
- Wynne, B.M. et al. 2018. Mesenteric arteries from stroke-prone spontaneously hypertensive rats exhibit an increase in nitric-oxide-dependent vasorelaxation. *Canadian Journal of Physiology and Pharmacology* 96(8), pp. 719-727. Available at: <https://pubmed.ncbi.nlm.nih.gov/29430946/> [Accessed: 20 April 2021].
- Xu, W.H. 2014. Large artery: An important target for cerebral small vessel diseases. *Annals of Translational Medicine* 2(8). doi: 10.3978/j.issn.2305-5839.2014.08.10.
- Yamamoto, M. et al. 1980. Aging and Cerebral Vasodilator Responses to Hypercarbia: Responses in Normal Aging and in Persons With Risk Factors for Stroke. *Archives of Neurology* 37(8), pp. 489-496. Available at:

<https://doi.org/10.1001/archneur.1980.00500570037005>.

Yamori, Y. et al. 1976. Pathogenetic Similarity of Strokes in Stroke-Prone Spontaneously Hypertensive Rats and Humans. *Stroke* 7(1), pp. 46-53.

Yang, G. et al. 2003. Attenuation of activity-induced increases in cerebellar blood flow in mice lacking neuronal nitric oxide synthase. *American Journal of Physiology - Heart and Circulatory Physiology* 285(1 54-1), pp. H298-304. Available at: <http://www.ncbi.nlm.nih.gov/pubmed/12623792> [Accessed: 23 February 2020].

Zanchi, A. et al. 1997. Age-related changes of the mechanical properties of the carotid artery in spontaneously hypertensive rats. *Journal of Hypertension* 15(12), pp. 1415-1422. doi: 10.1097/00004872-199715120-00008.

Zappe, A.C. et al. 2008. The influence of moderate hypercapnia on neural activity in the anesthetized nonhuman primate. *Cerebral Cortex* 18(11), pp. 2666-2673. doi: 10.1093/cercor/bhn023.

Zhang, F. et al. 1997. *Increased Susceptibility to Ischemic Brain Damage in Transgenic Mice Overexpressing the Amyloid Precursor Protein.*

Zhang, R. et al. 2004. Inhibition of nitric oxide synthase does not alter dynamic cerebral autoregulation in humans. *Am J Physiol Heart Circ Physiol* 286, pp. 863-869. Available at: <http://ajpheart.physiology.org/> [Accessed: 21 February 2020].

Zhao, F. et al. 2008. BOLD study of stimulation-induced neural activity and resting-state connectivity in medetomidine-sedated rat. *NeuroImage* 39(1), pp. 248-260. doi: 10.1016/j.neuroimage.2007.07.063.

Zhou, X. et al. 2020. Altered Brain Function in Cerebral Small Vessel Disease Patients With Gait Disorders: A Resting-State Functional MRI Study. *Frontiers in Aging Neuroscience* 12, p. 234. Available at: <https://www.frontiersin.org/article/10.3389/fnagi.2020.00234/full> [Accessed: 11 April 2021].

van Zijl, P.C.M. et al. 2012. The BOLD post-stimulus undershoot, one of the most debated issues in fMRI. *NeuroImage* 62(2), pp. 1092-1102. doi: 10.1016/j.neuroimage.2012.01.029.

Zupan, J. et al. 2006. End-Tidal CO₂ Excretion Waveform and Error with Gas Sampling Line Leak. *Anesthesia & Analgesia* 67(6), pp. 579-581. doi: 10.1213/00000539-198806000-00015.